UNIVERSIDAD NACIONAL AUTÓNOMA DE MÉXICO
PROGRAMA DE MAESTRÍA Y DOCTORADO EN INGENIERÍA
INGENIERÍA ELÉCTRICA – CONTROL

CONTROL AND MONITORING FOR A CLASS OF CHEMICAL TUBULAR REACTORS

TESIS
QUE PARA OPTAR POR EL GRADO DE:
DOCTOR EN INGENIERÍA

PRESENTA:
HUGO ANDRÉS FRANCO DE LOS REYES

TUTOR PRINCIPAL
DR. JESÚS ÁLVAREZ CALDERÓN, UAM-I
COMITÉ TUTOR
DR. JESÚS ÁLVAREZ CALDERÓN, UAM-I
DR. JAIME ALBERTO MORENO PÉREZ, INSTITUTO DE INGENIERÍA
DR. LUIS AGUSTÍN ÁLVAREZ ICAZA-LONGORIA, INSTITUTO DE INGENIERÍA

CIUDAD UNIVERSITARIA, CIUDAD DE MÉXICO, MARZO 2022

JURADO ASIGNADO:

Presidente: Dr. Jaime Alberto Moreno Pérez

Secretario: Dr. Luis Agustín Álvarez Icaza-Longoria

1 er. Vocal: Dr. Jesús Álvarez Calderón

2 do. Vocal: Dr. Paul Rolando Maya Ortiz

3 er. Vocal: Dr. Alexander Schaum

La tesis se realizó en el Instituto de Ingeniería perteneciente al Posgrado de Ingeniería, UNAM

TUTOR DE TESIS:

Dr. Jesús Álvarez Calderón

HUGO ANDRÉS FRANCO DE LOS REYES

CONTROL AND MONITORING FOR A CLASS OF CHEMICAL TUBULAR REACTORS

CONTROL AND MONITORING FOR A CLASS OF CHEMICAL TUBULAR REACTORS

HUGO ANDRÉS FRANCO DE LOS REYES

Doctorado en Ingeniería Eléctrica campo Control

Septiembre 2021 – classicthesis v4.6

Para Lourdes, Diego, Sonia, Aaragon, Emiliano, Viviana, Petra y Cirila.

ABSTRACT

The application-oriented MIMO control-estimation design problem for an important class spatially distributed tubular reactors is addressed in an integral design approach, including early and late lumping implementations. First, the saturated output feedback control and state estimation problem for the tubular reactor class is considered following an efficient early lumping approach. On the basis of a finite dimensional model obtained from the application of the so-called efficient modeling approach for tubular reactors, passivity and detectability solvability properties, in terms of the number of sensors and their locations, are identified, and then a saturated output feedback controller is build as the combination of a saturated passive state feedback control law and a geometric observer. Closed-loop robust stability is ensured in terms of sensor locations, control saturation limits and gains. For application-oriented purposes, the advanced output feedback controller is realized, by model redesign, as a set of decentralized PI controller with antiwindup scheme and a decoupled pointwise-like observer, with low computational load, for state estimation purposes. The design is accompanied with structural and gain tuning to set the actuator and sensor configuration, the sensor locations, the control limits and the gains of the control-estimation scheme. Simulation results shown the effectiveness of the proposed control-estimation scheme.

In the next part of the study, within a late lumping approach, a second control-estimation system, which considers unconstrained control, is build by combining a nonlinear control with two terms: (i) a pointwise temperature driven stabilizing control term, based on a sensor location dependent output linearizing property, and (ii) a section-wise control term, inspired in inventory control ideas and feedback passivtion by output selection; and a distributed pointwise observer. The exponential stability of the closed-loop origin is ensured in terms of sensor location and control gains. The control-estimation system implementation is done by performing an efficient late lumping step, by recalling the efficient modeling approach, to draw a low implementable algorithm. The implementation scheme is accompanied with sensor and actuator configuration, sensor locations and gains. The performance of this second control-estimation system is assessed with numerical simulations.

In the final part of the study, first, a comparative simulation-based study between the obtained closed-loop robust performance with the two proposed control-estimation schemes and a third control-monitoring system constructed by combining an existing adaptive controller that produce a distributed control action and the same pointwise observer used in the proposed schemes. It is shown that the proposed algorithms present best or similar behavior than its adaptive counterpart. Then, in an exploratory an informal way, the construction of each control-estimation system,

initially done in an early or late lumping approach, are performed following the opposite approach, late or early, with the appropriate theoretical tools for analysis and synthesis. The obtained results suggests that both control-estimation schemes can be derived following the early or late lumping settings to end up with exactly the same implementable algorithm. As closure, it is shown with simulations that the combination of the controllers of the two proposed control-estimation schemes produces closed-loop behavior improvement.

PUBLICATIONS

Derived from the work presented in this thesis, the following academic production has been presented in national and international conferences and journals, similar ideas and figures as the ones in this study may be found on those works:

[FA] Hugo Andrés Franco–de los Reyes and Jesus Alvarez. "Saturated–output feedback control and state estimation of a class of exothermic tubular reactors (in review process), 2021." In: *Journal of Process Control, submited* ().

[Bad+20] Ulises Badillo–Hernández, Jesús Álvarez, Hugo A. Franco–De los Reyes, and Luis A. Álvarez–Icaza. "Nonlinear output feedback–feedforward control of tubular gasification reactors." In: *IFAC–PapersOnLine*. Vol. 53. 2. Elsevier B.V., Jan. 2020, pp. 7789–7794. DOI: `10.1016/j.ifacol.2020.12.1869`.

[Fra+20] Hugo A. Franco–de los Reyes, Alexander Schaum, Thomas Meurer, and Jesus Alvarez. "Stabilization of an unstable tubular reactor by nonlinear passive output feedback control." In: *Journal of Process Control* 93 (2020), pp. 83–96. ISSN: 09591524. DOI: `10.1016/j.jprocont.2020.07.005`. URL: `https://doi.org/10.1016/j.jprocont.2020.07.005`.

[Fra+19a] Hugo A. Franco–de los Reyes, Alexander Schaum, Thomas Meurer, and Jesús Alvarez. "Nonlinear passive control of a class of coupled partial differential equation models." In: *Proceedings of the National Conference on Automatic Control, Mexico*. 2019, pp. 477–482.

[Fra+19b] Hugo A. Franco–De Los Reyes, Alexander Schaum, Thomas Meurer, and Jesus Alvarez. "Nonlinear feedback control of a class of semilinear parabolic PDEs." In: *Proceedings of the IEEE Conference on Decision and Control* 2019–Decem.Cdc (2019), pp. 4023–4028. ISSN: 07431546. DOI: `10.1109/CDC40024.2019.9029734`.

[Fra+19c] Hugo A. Franco–de los Reyes, Alexander Schaum, Thomas Meurer, and Jesus Alvarez. "Passivity–based output–feedback control for a class of 1–D semilinear PDE models." In: *2019 16th International Conference on Electrical Engineering, Computing Science and Automatic Control, CCE 2019* (2019). DOI: `10.1109/ICEEE.2019.8884530`.

[CFA18] Luis A Contreras, Hugo A. Franco–de los Reyes, and Jesús Alvarez. "Estimación robusta de los estados de un tren de tres reactores químicos exotérmicos." In: *Memorias del Congreso Nacional de Control Automático*. San Luis Potosí, 2018, pp. 213–218.

[CFÁ18] Luis A. Contreras, Hugo A. Franco–de los Reyes, and Jesús Álvarez. “Saturated output–feedback nonlinear control of a 3–continuous exothermic reactor train.” In: *IFAC–PapersOnLine* 51.13 (2018), pp. 425–430. ISSN: 24058963. DOI: 10.1016/j.ifacol.2018.07.316.

[FA18] Hugo A. Franco–de los Reyes and Jesús Alvarez. “Anti–windup scheme for PI temperature control of an open–loop unstable chemical reactor.” In: *IFAC–PapersOnLine* 51.4 (2018), pp. 491–496. ISSN: 24058963. DOI: 10.1016/j.ifacol.2018.06.143.

[FA17] Hugo A. Franco–de los Reyes and Jesús Alvarez. “Saturated linear PI control of a class of exothermic tubular reactors.” In: *Proceedings of the Natinonal Conference on Automatic Control*. Monterrey, Nuevo León, México: AMCA, 2017, pp. 347–352.

ACKNOWLEDGMENTS

The author would like to thank the continuous assistance and support, and the inspiring discussions with Dr. Jesús Álvarez alongside my scholar period.

Special thanks to Dr. Alexander Schaum, Professor Thomas Meurer and Pascal Jerono for their guidance and fruitful talks and collaboration during my academic staying at the Chair of Automation and Control of the Engineering Faculty at Kiel University, Kiel, Germany.

Furthermore, the author thanks all members of my advisory committee, Dr. Jesús Álvarez Calderón, Dr. Jaime Alberto Moreno Pérez and Dr. Luis Álvarez-Icaza Longoria, and all members of the academic panel of my doctorate dissertation, the previous three plus Dr. Alexander Schaum and Dr. Paul Rolando Maya Ortiz, for their continuous evaluation of my research work and academic activities. Their ideas, suggestions and criticism helped me to improve the process of writing this thesis work.

This work was made with great efforts inspired and powered by the love and tenderness provided by a large list of relatives and friends. The author thanks Lourdes, Susana, Sonia and Diego for being always there, the accomplishment of this thesis work is your success too. Tanks to all members of La Imposible for all the hope, joyfulness and deliciousness given. Special thanks to Viviana, Petra y Cirila, the daily inspiration of the author, all the love for the three of you.

Finally, the author gratefully appreciate all facilities and financial support provided by the Instituto de Ingeniería, Universidad Nacional Autónoma de México, and Consejo Nacional de Ciencia y Tecnología.

CONTENTS

ACRONYMS

AOF-PWO Adaptive Output Feedback controller-Pointwise Observer

AW Anti-Windup

EMPC Economic Model Predictive Control

CE Control-Estimation

CES Control-Estimation System

FD Finite Differences

IOBM Input-Output Bifurcation Map

ISS Input-to-State Stability

LIOF Linear-Inventory-like control

LIOF-PWO Linear-Inventory-like control-Pointwise Observer

MIMO Multiple Input Multiple Output

MPC Model Predictive Control

ODE Ordinary Differential Equation

OF-GO Output Feedback control with Geometric Observer

PI Proportional-Integral

PIAW Proportional-Integral control with Anti Windup scheme

PIAW-PWO PI control with AW scheme-Pointwise Observer

PIIAW-PWO Proportional-Integral-Inventory control with Anti Windup scheme-Pointwise Observer

PID Proportional-Integral-Derivative

PDE Partial Differential Equation

SF State Feedback controller

SISO Single Input-Single Output

Part I

ABOUT THIS STUDY

This is an introductory preview of this thesis work. Here the technological relevance and motivation of the tubular reactor control-estimation problem is identified and put in perspective with the related literature to highlight the pertinence of the proposed methodology. Then, the problem is technically stated and the methodological scope of this study is established. The contributions of the present study are highlighted. A case study which will be used througout the entire work for illustration of theoretical developments is presented. Finally, some useful theoretical tools and the efficient modeling approach that underlie the whole work are summarized.

1 INTRODUCTION

1.1 MOTIVATION

Along the years, tubular reactors have been widely employed on chemical industries as one of the most important operating units. Several raw material are treated on tubular reactors to produce precursors for other processes or terminated chemical products such as ethylene, ethanol and ammonia [57]. Other applications of tubular reactors include waste water treatment [65] and bioprocesses [46].

The physical phenomena involved in the dynamic behavior of exothermic jacketed tubular reactors are: (i) diffusive-convective mass and heat transport, (ii) heat conduction with the cooling jacket, and (iii) exothermic chemical reactions which is the mechanism that convert reactants into products and generates an excess of heat. These transport and reaction phenomena, modeled by Partial Differential Equations (PDEs), interact in a complex manner to produce a rich nonlinear dynamic behavior that includes multiple (stable and unstable) steady-states, limit cycling, chaos, parameter sensitivity, among others [129; 130; 131; 71].

According to the previous ideas, the tubular reactor Control-Estimation (CE) problem is a difficult task that demands precise and robust Control-Estimation Systems (CESs) to satisfy operational (product quality, reliable functioning, etc.) and supervisory (for setpoint adjustment, fault detection and isolation, etc.) requirements, as well as physical constraints (such as limited control action). In what follows, the motivation of the present study from the industrial and research points of view are established.

1.1.1 *Industrial practice perspective*

In most industries, tubular reactors are usually stabilized (around a nominal steady-state that satisfy production requirements) with Proportional-Integral (PI) controllers [88; 119; 70; 42; 121]. PI control has low cost, reliable functioning, and acceptance by practitioners, but its implementation requires experience, insight, and testing [119; 89]. The industrial design of PI controllers for tubular reactors with limited control action: (i) is based on a lumped Ordinary Differential Equation (ODE) input/output model (at least for testing purposes), (ii) requires an adequate selection of the number of sensors and actuators and their locations to achieve reliable closed-loop behavior, and (iii) use a proper (*ad-hoc*) Anti-Windup (AW) scheme for saturation handling [132].

For industrial monitoring purposes, the (extended) Kalman Filter [95] and data driven techniques [90] are widely employed to perform state estimation to assess control performance (for retuning or adjustment of setpoints), as well as fault detection and isolation [90]. These estimation algorithms [45; 46]: (i) are constructed and/or implemented on the basis of lumped ODE models, and (ii) require an adequate selection of the number of sensors and their locations to achieve reliable performance.

According to the current state of industrial control practice and new trends raised up by the industrial paradigm *Industry 4.0* [90], the main interests of industry on control topics are Proportional-Integral-Derivative (PID) control and Model Predictive Control (MPC) (the unique advanced technique accepted in industry). Furthermore, it is agreed that PID control is of upmost relevance and ubiquitous, and its performance enhancement is relevant for industries. Nevertheless, it has been reported [88; 90] that most of the industrial PID loops are poorly tuned, implying low plant performance, so that in some cases open-loop control is preferred. PID control and MPC coexist in factories in a hierarchical structure with three layers: (i) an upper large-term optimization (over months or years) which consider economic requirements and resource constraints, (ii) an intermediate mid-term optimization (over weeks, days) driven by MPC algorithms that computes setpoints, and (iii) a bottom short-term control decision layer composed by PID controllers (that use the setpoints computed by the MPCs in the previous layer) to drive field equipment (valves and pumps).

Accordingly, the ubiquity of PID control will remain, with monitoring for performance assessment as an important ally. Thus, the areas of improvement for industrial CES in tubular reactors are: (i) the design of reliable, robust, and simple output feedback controllers similar to PID ones, (ii) new and more efficient PID tuning and retuning for different operating conditions and uncertain systems, (iii) the consideration of structural tuning or retuning to enhance control performance (sensor and actuator configuration as design degree of freedom), and (iv) regarding estimation, the design of computationally efficient and robust algorithms.

1.1.2 *Academic research perspective*

In academic research studies, usually the solution to the CE problem of tubular reactors is performed using advanced model-based techniques [109; 24; 72; 73; 39; 83; 36; 104; 38]. Basically, two different approaches are followed, the so-called *early lumping* and *late lumping*. On the one hand, the early lumping approach (first discretize then design and implant) yields a ready to implement CES according to the mature control theory for ODE systems, but most designs lack reliability assurance via PDE model-based closed-loop stability. On the other hand, at the cost of more mathematical complexity, the late lumping approach (first design, then discretize and implant) retains throughout control design the reactor physics inherent to the PDE model, and formal closed-loop stability conditions can be drawn for certain classes of distributed control systems.

In the early lumping approach, the first design step is to construct a lumped ODE model that approximates, accurately enough, the dynamic behavior of the PDE tubular reactor model, either by spatial discretization or model reduction techniques [36]. Then, model-based design is employed to come up with the CE algorithm, assurance of closed-loop functioning and performed assessment. The implantation is straightforward since the design is done in a lumped model. Usually, in the early lumping step, efficient models are drawn to describe local transient behavior, but not much attention is given to the dynamic behavior beyond locality (ignoring the possibility of generation of spurious steady-states) [22].

Contrarily, in the late lumping approach, the PDE model is used for the design of the CES based on the properties of the distributed dynamics [93]. Reliable functioning is ensured for the infinite dimensional closed-loop system. At the implementation step (which does not receive much attention), usually high dimensional finite-difference lumped ODE models or low dimensional orthogonal collocation methods are used. The fact that this may lead to unduly computational load and even generation of spurious steady-states or extraneous attractors is usually neglected.

An important conclusion of the above discussion is that each approach, early or late, may present problems at the design or implementation stage, if the inherent problems of the opposite approach are ignored. For instance, in the early or late lumping design of CES for tubular reactors, usually both approaches overlook a key applicability subject: the extent of spatial lumping in the light of on-line computational load, which reflects number of ODEs and their ill-conditioning, and the generation of spurious dynamic behaviors [22].

In both, early and late lumping approaches, several advanced control and estimation techniques have been proposed and combined to design CESs for tubular reactors. Among these techniques, passivity-based control (studies only in control [9; 110; 140; 141; 142]), and MPC [50; 49; 48; 82] are two techniques that have received much attention. Important advances have been presented in both areas, nevertheless, most of these control and/or estimation designs are too complex in comparison with the standard and widely employed industrial PID control and data driven estimation techniques, and thus usually are not considered relevant for industrial deployment.

The preceding considerations motivate the aims of this study, the improvement of industrial PI control and estimation algorithms using an advanced and application-oriented model-based approach. The design must have: (i) criteria for selection of the number of sensors and their locations, (ii) assurance of robust closed-loop functioning, (iii) simple tuning guidelines, (iv) simplicity, as much as possible, in terms of linearity, and dynamic coupling, and (v) an efficient lumping implementation. For this end, the open-loop dynamics of the system will be exploited: the interplay between stabilizing mechanisms (mass and heat transport, heat conduction, and mass consumption phenomena) with destabilizing ones (heat production by reaction).

Both paths, early and late lumping, will be considered. The former one will be employed first since it enables a clear way to use powerful and well-known CE design techniques for lumped systems, including robust closed-loop stability for the lumped tubular reactor model. Then, the late lumping approach will be used to construct, on the basis of the tubular reactor PDE model, a similar CE algorithm as well as assurance of closed-loop stability.

1.2 METHODOLOGICAL APPROACH

According to the preceding discussion, in this work the aim is to design CES which preserves some well known properties of industrial-like control and estimators algorithms, such as, simplicity, simple tuning guidelines, low computational load. Also, the designed CES must have reliable performance with assurance of closed-loop robust stability in the presence of exogenous disturbances and uncertain conditions (in the sense of practical stability). Furthermore, the design must be accompanied with criteria for the selection of sensors and/or actuators and control limits. This complex objective will be reached by following a constructive control [118] approach in a three-step methodological procedure: (i) starting with the construction of a Multiple Input Multiple Output (MIMO) CES for an unstable tubular reactor within an early lumping approach, then (ii) a second MIMO CES will be constructed in the late lumping framework for an unstable tubular reactor, (iii) finally, the implications of each design for its opposite will be explored.

In the first step, using an efficient modeling approach for tubular reactor modeled by PDEs [22], a low order finite-dimensional lumped model will be obtained. Then, using a nonlinear constructive control approach, a MIMO output feedback controller for joint state stabilization and estimation will be constructed with geometric techniques. The assurance of closed-loop robust and reliable functioning will be established within a practical stability framework based on structural and Input-to-State Stability (ISS). The implementation must be, as possible as it could be, similar to what is used in industry, i. e., PI control and simple estimation schemes.

In the second step, the tubular reactor CE problem is faced within the late-lumping approach. Using constructive ideas, the transport and reaction dynamic mechanisms will be analyzed to identify how this interaction produce destabilizing or stabilizing effect along space yielding to the identification of sensible regions in which the sensors must be placed. Then, using this measurements a MIMO controller will be constructed to stabilize an (open-loop) unstable profile pair and an additional control term for behavior improvement will be drawn with inventory control ideas. An estimator, with innovation mechanism as simple as possible, will be used later for output feedback control and estimation purposes. The stability will be assured with the help of functional analysis. Following the efficient modeling approach, a reliable late lumping method will be used to implement the control-estimation system.

In the last step, a methodological question arise: for the particular tubular reactor class, there is a chance that constructing a control estimation system using the early and late lumping approaches leads to the same implementation result? The answer to this question will be explored. The implications and connections between the two proposed CES, constructed within an early or late lumping methodology, will be explored in the opposite, late or early lumping approach, respectively.

1.3 STATE OF THE ART

As mentioned before, the CE problem of tubular reactor has been tackled with two strategies: the early and late lumping methods. Several review papers can be found in the literature [109; 24; 72; 73; 39; 83; 36; 104; 38] in which the issues of modeling, model reduction, PDE dynamics analysis, and estimation and control synthesis for general distributed parameter systems, and chemical engineering problems in particular, including tubular reactors. The next revision to the state of the art is based on the available tubular reactor CE found on the above review papers and other references therein. Special attention is given to the following issues: (i) the discretization or model approximation scheme used for implementation (knowing that for early lumping this is the first step of the design, and that in late lumping is the latest one), (ii) the type of the employed control and estimation techniques, (iii) the method to select the number of sensors and their locations, (iv) the consideration of control saturation in the controller design, and (iv) the assurance of robust closed-loop stability.

1.3.1 *Early lumping approach*

The early lumping approach was the first natural step for the design of CE schemes for distributed parameter systems. This is so because, the available analysis and synthesis techniques for lumped ODE models were very matured compared with the current state of development of theory for systems modeled by PDEs. Two main approaches exists for model-based CES design purposes: (i) obtain a reduced state-space ODE model, and (ii) obtain a reduced model with considers only input/output interactions for the measured variables. In the present review only the first case is considered.

One of the very first strategies used on the CE problem of tubular reactors was the use of Finite Differences (FD) to obtain a lumped model and then linearize it around an steady-state of interest. This is the case of Pell and Aris in [105], where a least square estimation algorithm and an optimizing control are constructed. The authors consider the limiting case in which the FD approximation converge to the infinitesimal case so that the proposed control and estimation system is continuous in space. The methodology is illustrated with a tubular reactor with stochastic disturbances.

The works of Amundson and co-workers in the 60's and 70's decades [15], where a mathematical perspective of several chemical engineering problems is given, include a large collections of studies on stability, estimation and control of tubular reactors where mostly orthogonal collocation is used to obtain lumped ODE models.

In the 70's and 80's decades, a bunch of theoretical and experimental studies on control of fixed-bed, homogeneous and heterogeneous tubular reactors were developed. Some of these works are collected and resemble in the review papers by Jørgensen [72] and Jørgensen and Jensen [73]. At that time, most studies were based on discretized or approximated models where FD or weighted residuals (orthogonal collocation being the most popular) techniques were employed. Then, linearized models computed around an steady-state of interest (possibly open-loop unstable), were employed for CE synthesis. Regarding the estimation task, Kalman Filtering, Luenberger observers, and least square estimation schemes were employed. For control synthesis, several approaches have been employed, such as pole placement, LQ, LQG, optimal control, self-tuning regulators, adaptive control, internal model control, modal control, and frequency domain-based designs, among others.

With the development of new lumping methods and advanced nonlinear CE techniques, further studies, that draw lumped nonlinear tubular reactor ODE models, were developed during the late 80's and early 90's. The works of Balas, Daoutidis and Christofides [24; 36] were based on Galerkin methods (a special case of the method of proper orthogonal collocation) and its combination with approximated inertial manifolds to obtain a nonlinear model reduction technique. On the basis of this lumped ODE models, different CESs were developed by combining linear and nonlinear Luenberger observers for state estimation with controllers coming from application of differential geometric (partial) feedback linearization, robust control by Lyapunov redesign, and nonlinear optimal control design techniques.

Recent studies on CESs designs for tubular reactors includes: orthogonal collocation for model reduction and the combination of a linear Luenberger observer with adaptive linearizing control [47] or Kalman filtering for estimation purposes combined with MPC [5]. It is worth noting the big effort of Christofides and co-workers in the use of nonlinear Galerkin methods (combined with approximated inertial manifolds) for the construction of Luenberger and static estimators which are combined with several control techniques: (i) robust Lyapunov-redesign control [37; 2], (ii) geometric feedback linearizing control [17; 18; 20], (iii) MPC [50; 49; 48], (iv) Economic Model Predictive Control (EMPC) [82], and (v) adaptive control [107].

Other approaches combines infinite power series ansatz for model reduction with Luenberger estimation and flatness-based feedforward and geometric feedback control [91], FD discretization methods for the design of CES based on open-loop observers and geometric control [137; 138], and nonlinear geometric estimation with passivity-based control [99; Bad+20]. Recent studies includes: (i) nonlinear discretizing schemes such as weighting essentially non-oscillatory schemes, particle filtering for state estimation and MPC [63], and (ii) orthogonal collocation for model reduction, Kalman filtering for state estimation and nonlinear MPC [74].

Most of the above mentioned CE studies follows an application-oriented approach and contribute with important results, nevertheless, according to the late lumping approach, inherited from the use of lumped models, the distributed nature of the system is not completely exploited or taken into account in the design procedure. As mentioned in [30], the reliable functioning of the designed control estimation system in terms of practical stability and state reconstruction convergence it is not independent on the model reduction technique and may be affected by a non adequate lumping. For instance, it is well recognized that some discretization schemes such as FD, finite element or orthogonal collocation (possibly on finite differences or elements), if are not properly employed, may lead to generation of spurious steady-states, limit cycling,and high frequency oscillatory behavior. Furthermore, spill-over effects may produce unstable closed-loop dynamics [61].

1.3.2 *Late lumping approach*

With the development of suitable theory for the analysis of PDE systems, the late lumping approach emerged, in the late 80's, as an appealing method for the analysis and design of CE algorithms for tubular reactors, this having the advantage that closed-loop reliable functioning can be assured for the real dynamics of the distributed system under consideration.

CES designs for tubular reactors, includes, for the control part, several techniques such as flatness-based, modal, backstepping, optimizing, adaptive, sliding mode, and MPC control designs [92; 124; 134; 135; 102; 46]. The state estimation task is usually performed with distributed linear or nonlinear Luenberger observers, Kalman Filters or other techniques such as least square estimation and asymptotic or interval observers. The studies listed below are presented here because: (i) the proposed control-estimation methodology is of methodological interest, and/or (ii) special attention is given to the implementation step.

One of the first designed CESs is the one proposed by Windes and Ray [134; 135], in which a robust CE scheme, that also considers online yield optimization based on the temperature hotspot measurements, is constructed as the combination of: (i) a distributed least squares-based state estimation, (ii) a parameter estimation scheme, (iii) a cascaded control for wall temperature with a digital PI control with rate constraints in the outer loop and a PID in the inner loop, and (iv) an optimizing scheme for the computation of the hotspot setpoint. The implementation is pursued using orthogonal collocation.

Dochain [46] propose a CES for chemical and biological tubular reactors where an asymptotic observer (which using reaction invariant manifolds avoids the need to know the reaction rate function), driven by the temperature profile measurement, is combined with an adaptive linearizing control law. For implementation purposes, guidelines for the use of orthogonal collocation or FD on a coarse grid are given.

A CES based on sliding mode control is proposed in [102], the design considers a discontinuous feedback controller driven by a full state (or reduced order) observer with a discontinuous correction term. The design is applied to an open-loop unstable tubular reactor. It is assumed that the system is of minimum phase, the measured output is the entire temperature profile, and the control input is the jacket temperature. The implementation of the controller is performed using backwards FD over a fine mesh with a large number interior points.

In [124], on the basis of a boundary measurement at the end of the reactor and boundary control at the inlet, a linear backstepping infinite dimensional observer-based output feedback controller is constructed, and applied to a, rather academic, tubular reactor example.

In [92], flatness-based feedforward and feedback control are combined to design a CES. Formal power series and summability methods are used to approximate the system dynamics and for the design of the infinite dimensional feedforward term. Then, the feedback term (a PID controller) and a Luenberger observer are designed on the basis of a truncation of the formal power series introduced in the first step of the design. Reliable closed-loop performance is ensured and the proposed control-estimation system is applied to an unstable tubular reactor with boundary measurements and controls. The closed-loop system is simulated by using the power series expansion for the implementation of the controller while the system is simulated with a high order spatial discretization based on the method of lines.

Recently, a new late lumping approach [139; 77; 78], propose the use of the linearized PDE tubular reactor model is converted into a continuous-space-discrete-time model by means of the Cayley-Tustin transform. Then, a discrete-time Luenberger observer is designed and combined, to construct an output feedback controller, with different MPCs, which account for control and state constraints as well as closed-loop stability. The implementation is based on the discrete-time model obtained by the Cayley-Tustin transform and spatial discretization with an Euler scheme.

Passivity-based control is a design technique which is particular case of dissipativity which considers as supply rate the inner product between the vector of inputs and outputs that must be of the same dimension [31]. Passivity is a concept that comes from electrical and mechanical system [103] and has been extended for general nonlinear abstract systems [126]. Since the energy approach of passivity-based control does not suit well the variables commonly employed in distributed chemical processes, the extension of this technique has been done using a thermodynamic representation of process systems [9; 110; 140; 141; 142]. Nevertheless, the concept of feedback passivation has not been interpreted within a chemical engineering framework in terms of transport, conduction and reaction phenomena in tubular reactors.

From the previous review, it is identified that several tubular reactor CE studies have been proposed, the extension of several control and estimation techniques originated for finite-dimensional systems are employed. In other cases, analysis and synthesis techniques explicitly constructed for infinite dimensional systems are considered. Undoubtedly these studies represent important contributions to the field, however, the late lumping designs usually neglect, with few exceptions, the relevance of efficient implementation schemes and the fact that the proposed CES ar too complex to be considered in an industrial practice setting.

1.3.3 *Sensors and actuators*

In most of the preceding studies, the vector of measured outputs is a set of pointwise temperatures at fixed axial locations. Regarding actuators, usually inlet flows or the cooling jacket are considered. As it must be pointed out in [67], while experimental tubular reactors have plenty of sensors and actuators because usually they are highly instrumented, in industrial applications usually only few fixed sensors and actuators are available. Thus, it is important to design robust and reliable control-estimation systems that use a limited quantity of measured outputs and control inputs.

When the actuator and sensor configuration is a design degrees of freedom for CE purposes, several configuration design techniques can be found in the literature. For the selection of sensors and their locations, usually model-based or data driven optimization techniques are applied (see, e. g., [108] for a detailed review on both methods). For instance, in model-based procedures on can find: (i) the maximization of local (about a prescribed steady-state operation) standard or Gramian observability or detectability measures [62; 133; 29; 8; 7; 120], and (ii) nonlinear optimization [20; 19]. In the area of data-driven optimization [127; 98; 108] present approaches in which different sensitivity measures constructed with simulation data are optimized to determine the sensor locations. Regarding actuators, the most used technique is to employ optimization algorithms which minimize performance indexes that penalize control effort with explicit dependency on the actuator location [16; 20; 19].

The above mentioned studies establish systematic procedures, based on optimization algorithms, that give sensor and actuator configurations that ensures adequate CE performance in relation with the related penalty function. Nevertheless, the location of sensors and/or actuators within a model-based comprehensive approach related to the physical phenomena that take place has not been fully explored, furthermore, the connection between advanced sensor placement techniques and the industrial sensitivity criterion have not been connected in a formal manner.

1.3.4 *Constrained control of tubular reactors*

It is well known that the limited capacity of actuators must be considered for the design of constrained control schemes due to the fact that control saturation may lead to poor closed-loop performance. For instance, in finite-dimensional open-loop unstable chemical processes it has been shown that control saturation may lead to unstable closed-loop functioning if control limits are not selected properly [35; 10; 11].

In industrial settings, when saturated PI control is considered, a common drawback is the generation of windup effects due to accumulation of regulation error in the integral term. This issue is addressed with ad-hoc techniques such as: conditional integration, back calculation, and autonomous reset schemes, as well as combination of them [132]. Other techniques includes observer-based designs [66].

In the context of advanced control, saturation is usually handled with optimal nonlinear control, using the Sontag formula, or in MPC designs, as constraints in the optimal control problem setting [3; 1; 4; 49; 5; 82; 63]. Another approach is the one used in [94] where finite time transition between steady-states with limited control actuation is solved as a constrained two-point boundary value problem.

Besides the preceding studies propose controllers for tubular reactors that ensure robust stability in the presence of control and state constraints, in all these approaches the control limits are fixed and not considered as a design degree of freedom. Furthermore, the possibility of having undesired closed-loop steady-states due to the combination of control saturation and open-loop instability are simply ignored.

1.3.5 *Comments regarding the state of the art*

From the previous review to the available, industrial and academic research, literature on CES, sensor and actuator configuration strategies, and constrained control for tubular reactors, the following areas of opportunity have been identified:

- The improvement of industrial CES designs on: (i) control tuning and retuning for operation in wide regions of the state space, (ii) model-based estimation for performance monitoring purposes, (iii) systematization of selection of sensor locations, and (iv) actuator saturation handling.

- The early or late lumping must be performed in a robust fashion to obtain reliable models for model-based design or implementation purposes, that avoids spurious transient and static behaviors and present efficient computational load.

- Regarding the late lumping approach, beyond MPC, most of the proposed designs are too complex to be considered for implantation in industrial control of tubular reactors, thus advanced model-based design must lead to robust and efficient controllers with simple implementation schemes.

- Passivity-based control, asides from the thermodynamics framework, has not been interpreted within a physical perspective for control design.
- The structural tuning, i.e., consideration of sensor and actuators as design degrees of freedom for the CE problem, can be further exploited for performance enhancement within a passivity-based framework.
- Selection of control limits as design degree of freedom has not been explored, furthermore, the avoidance of appearances of undesired closed-loop transient or static behaviors due to the combination of open-loop multiplicity and control saturation have not been analyzed in tubular reactors studies.

1.4 CONTRIBUTIONS

In the light of the previously identified issues, the main contributions on the design of CES of the present study are:

- The construction, from an early lumping perspective, of a MIMO CES for a multi–jacket unstable tubular reactor as the combination of a saturated robust passive nonlinear stabilizing controller and a nonlinear geometric estimator which can be implemented as an industrial PI controller with saturation handling via a back calculation scheme with a decoupled robustly convergent estimator. The design is accompanied with simple tuning and implementation guidelines with criteria for the selection of sensor location and control limits, and assurance of robust and reliable closed-loop functioning.
- In a late lumping approach, a second MIMO CES is constructed as an observer-based output feedback control for a multi–jacket possibly open-loop unstable tubular reactor. The scheme is composed by: (i) a stabilizing MIMO state-feedback control, (ii) a supplementary inventory-like passive state-feedback component for behavior improvement. The output feedback controller is implemented with the use of a pointwise observer, leading to a control design with: (i) a closed-loop stability condition in terms of the sensor set and control gains, (ii) an application-oriented control gain-measurement tuning procedure, and (iii) reduced on-line computational load via efficient late lumping.
- The exploration of connections and implications of each of the preceding CESs with its opposite lumping approach. An answer to the question: for the particular class of chemical tubular reactor class under study, is it possible to arise to the same implementation system going from the early and late lumping approaches?

The above problems, that can be considered as three methodological steps, are tackled within a constructive control framework [118]: instead of using generic CE design techniques for nonlinear systems, the exploitation of the specific characteristics of the considered reactor class will be employed throughout the CE design procedure. Different theoretical and practical tools will be used throughout design steps, from the off-line development to the on-line implementation, such as linear and nonlinear finite and infinite dimensional dynamics [76; 118; 39; 38], chemical reactor engineering sciences [57; 64], bifurcation theory [71], passivity-based control [118; 31], realization theory [122], PID [132], inventory [88; 119; 110], and lumping techniques [22].

Methodologically speaking, the early and late lumping approaches are used for CE design within an efficient modeling [22] and application-oriented framework leading to: (i) the use of several model variants for off-line developments and on-line implementation, (ii) procedures for sensor/actuator selection, and gain and control limits tuning, and (iii) assurance of robust stability, in the sense of ISS.

The efficient modeling approach recommends the use of FD or finite elements instead of orthogonal collocations due to the fact that the former method preserves the physical interactions of transport and reaction phenomena. The efficient modeling approach provides a systematic procedure to obtain a finite-dimensional model that avoids spurious transient and static behaviors and ensures efficient computational load in the light of typical parameter uncertainty and discretization errors [22].

In the first methodological step, using the FD and the efficient modeling approach, a lumped model will be obtained and then used, within a constructive control spirit [118], to identify passivity and detectability properties to draw a CES composed by a saturated passive nonlinear state feedback controller and a geometric observer. Closed-loop robust and reliable functioning, in the presence of parasitic dynamics, is established in terms of sensor location, control limits and gains. It is shown that the controller can be implemented as an industrial PI controller with an AW term of back calculation type [132] and decoupled from a estimator with low computational load.

In the second step, the CE problem is solved with a late lumping strategy. A MIMO CES, with unconstrained control, is constructed to modify the natural interplay (open-loop destabilizing) between transport and reaction dynamic mechanisms at key spatial locations, so that the target steady-state becomes stable. The controller is supplemented with an additional inventory-like control term for performance improvement. A pointwise state estimator [115] is used for output feedback control and estimation purposes. Following the efficient modeling approach, the CES is implemented with late lumping with low computational load. Closed-loop stability, in terms of sensor locations and gains, is assured for the distributed model .

In the last step, the two proposed CESs are put in perspective between them and compared with existing CE algorithms. The extension of the early and late lumping design strategies to their opposites, late or early, is explored in an informal manner.

1.5 SUMMARY

Based on the respective industrial and academic research states of the art, the considered tubular reactor joint CE problem has been motivated and justified. The methodological approach which will be followed has been motivated in general terms, and the main contributions have been announced.

2 CONTROL ESTIMATION PROBLEM

In this chapter, the Multiple Input Multiple Output (MIMO) Control-Estimation (CE) problem for a class of exothermic chemical tubular reactors with a coolant jacket with multiple sections and multiple sensors is formulated. The cases of unconstrained and constrained control action are considered. To introduce the problem, first, the tubular reactor model is introduced and its open-loop dynamics are briefly described. Then, the CE problem is technically stated. This is followed by a detailed delineation of the methodological strategy employed throughout the entire study. Finally, a case study that will be used for illustration of theoretical developments is introduced.

2.1 THE REACTOR CLASS

Consider the jacketed tubular reactor (with volume V, cross area A, perimeter P, and length L) depicted in Figure 2.1, where a reactant (fed at constant flow rate Q, concentration $C_e(t_a)$, and temperature $T_e(t_a)$) is converted into product through an exothermic reaction $R(C,T)$. The reactor is cooled with a multi–jacket subdivided in q subsections, all of the same size $\frac{L}{q}$, with region of actuation $\left[\frac{L(i-1)}{q}, \frac{Li}{q}\right]$, $i = 1, \ldots, q$, and individual per jacket temperature $T_{c,i}(t_a)$, $i = 1, \ldots, q$. Each section of the reactor is equipped with one temperature sensor at location l_i, thus the set of temperature outputs is $T(l_i, t_a)$, $i = 1, \ldots, q$.

The state of the tubular reactor is defined as the pair

$$\{C(l,t_a),\, T(l,t_a)\}, \quad 0 \leq l \leq L,\, t_a > 0, \tag{2.1a}$$

composed by the distributed concentration $C(l,t_a)$ and temperature $T(l,t_a)$ profiles which vary along the spatial and temporal coordinates $l \in [0,L]$ and $t_a \in \mathbb{R}$, respectively. Under standard assumptions [57], the corresponding dynamics are obtained from the mass and heat balances described by the following pair of parabolic Partial Differential Equations (PDEs):

$$\partial_{t_a} C(l,t_a) = D_m \partial_l^2 c(l,t_a) - v_Q \partial_l C(l,t_a) - R(C(l,t_a), T(l,t_a)), \tag{2.1b}$$

$$\begin{aligned}\partial_{t_a} T(l,t_a) = {} & D_h \partial_l^2 T(l,t_a) - v_Q \partial_l T(l,t_a) + \Theta R(C(l,t_a), T(l,t_a)) - \\ & - H(T(l,t_a) - T_c(l,t_a)),\end{aligned} \tag{2.1c}$$

$$D_m \partial_l C(0,t_a) = v_Q (C(0,t_a) - C_e(t_a)), \qquad \partial_l C(L,t_a) = 0, \tag{2.1d}$$

$$D_h \partial_l T(0,t_a) = v_Q (T(0,t_a) - T_e(t_a)), \qquad \partial_l T(L,t_a) = 0, \tag{2.1e}$$

$$C(l,0) = C_0(l), \tag{2.1f}$$

$$T(l,0) = T_0(l). \tag{2.1g}$$

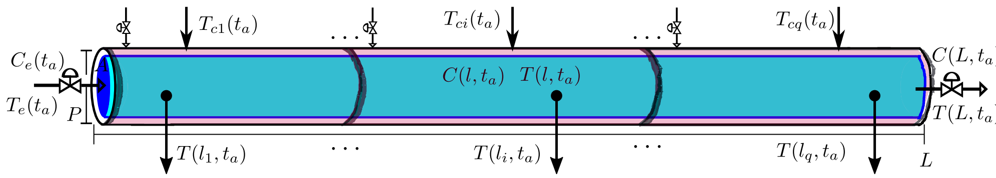

Figure 2.1: Tubular reactor and its control monitoring scheme

In (2.1), (2.1b) [or (2.1c)] is the mass (or heat) balance with boundary (2.1d) [or (2.1e)] and initial (2.1f) [or (2.1g)] conditions. The constant axial velocity is defined as $v_Q = \frac{Q}{A}$, D_m (or D_h) is the mass (or heat) dispersion number. The parameters $H = \frac{U_h P}{\rho c_p}$ and $G = \frac{(-\Delta H_R)}{\rho_\Theta c_p}$, are defined in terms of the heat transfer coefficient U_h, heat of reaction $-\Delta H_r$, and density (or specific heat capacity) of the reacting mixture ρ_G (or c_p). $R[C(l,t_a), T(l,t_a)]$ is the reaction rate function which is defined pointwise over the axial position and is assumed to be monotonically increasing on the concentration and bounded with respect to its arguments.

The jacket temperature $T_c(l,t_a)$ is given as

$$T_c(l,t_a) = \sum_{i=1}^{q} B_i(l) T_{c,i}(t_a), \tag{2.1h}$$

where B_i, $i = 1,\ldots,q$ is the characteristic function of the i-th actuator, and is given by

$$B_i(l) = \begin{cases} 1 & \text{if } l \in \mathcal{R}_i \\ 0 & \text{else} \end{cases}, \; i = 1,\ldots,1, \quad \mathcal{R}_i = \begin{cases} \left(\frac{L(i-1)}{q}, \frac{iL}{q}\right] & \text{if } 1 \le i \le q-1 \\ \left[\frac{L(i-1)}{q}, L\right) & \text{if } i = q \end{cases}, \tag{2.1i}$$

where $\mathcal{R}_i$, $i = 1,\ldots,q$ are the fixed regions of actuation of each jacket section with length dependent on the number of jacket sections q. The set of temperature measurements is defined as

$$T_{m,i}(t_a) := T_{m,i}(l_i,t_a), \quad l_i \in \mathcal{R}_i, \quad i = 1,\ldots,q. \tag{2.1j}$$

Since the operational aim is to produce a high yield, the controlled output is defined as the outlet concentration $C(L,t_a)$. The exogenous inputs are the inlet concentration $C_e(t_a)$ and the inlet temperature $T_e(t_a)$.

Due to physical restrictions, the exogenous inputs are bounded as follows

$$0 \le C_e(t_a) \le C_e^+, \quad T_e^- \le T_e(t_a) \le T_e^+, \tag{2.2a}$$

where $(\cdot)^-$ [or $(\cdot)^+$] is the lower (or upper) limit of $(\cdot)$. The jacket temperatures satisfy the bounds

$$T_c^- \le T_{c,i}(l,t_a) \le T_c^+, \quad i = 1,\ldots,q. \tag{2.2b}$$

Consequently, by mass and energy conservation (2nd law of thermodynamics), reactor-jacket heat exchange directionality (1st law of thermodynamics) and the continuity of the reaction rate function, the concentration and temperature profiles are bounded as:

$$0 \le C(l,t_a) \le C_e^+, \quad \min\{T_e^-, T_c^-\} \le T(l,t_a) \le \max\{T_e^+, T_c^+\} + T_a, \tag{2.2c}$$

where $T_a = G\bar{C}_e$ is the adiabatic temperature rise referred to the nominal concentration $\bar{C}_e$. Here $\bar{(\cdot)}$ denotes the nominal value of $(\cdot)$.

For given nominal values of flow $\bar{Q}$, feed concentration $\bar{C}_e$ (or temperature $\bar{\tau}_e$), and nominal jacket temperature profile $\bar{T}_c(l) = \sum_{i=1}^{q} B_i(l)\bar{T}_{c,i}$ and $\bar{T}_{c,i} = \bar{T}_c$, $i = 1,\ldots,q$, the concentration and temperature profile pair at steady-state $\left\{\bar{C}(l),\ \bar{T}(l)\right\},\quad 0 \le l \le L$ is the solution to the Ordinary Differential Equation (ODE) boundary value problem

$$\begin{aligned}
D_m\frac{\mathrm{d}^2\bar{C}(l)}{\mathrm{d}l^2} - v_Q\frac{\mathrm{d}\bar{C}(l)}{\mathrm{d}l} - R(\bar{C}(l),\bar{T}(l)) &= 0,\\
D_h\frac{\mathrm{d}^2\bar{T}(l)}{\mathrm{d}l^2} - v_Q\frac{\mathrm{d}\bar{T}(l)}{\mathrm{d}l} + GR(\bar{C}(l),\bar{T}(l)) - H(\bar{T}(l) - \bar{T}_c(l)) &= 0,\\
D_m\frac{\mathrm{d}C(0)}{\mathrm{d}l} = \bar{v}_Q(\bar{C}(0) - \bar{C}_e), \quad D_h\frac{\mathrm{d}T(0)}{\mathrm{d}l} &= \bar{v}_Q(\bar{T}(0) - \bar{T}_e),\\
\frac{\mathrm{d}C(L)}{\mathrm{d}l} = 0, \quad \frac{\mathrm{d}T(L)}{\mathrm{d}l} &= 0.
\end{aligned}$$

For simplification of notation, consider the following scaling coordinate change for the independent time and space variables

$$t = \frac{v_Q}{L}t_a, \quad s = \frac{l}{L}. \tag{2.3a}$$

Define the dimensionless concentrations referred to the nominal inlet one:

$$c(s,t) = \frac{C\left(Ls, \frac{L}{v_Q}t\right)}{\bar{C}_e}, \quad c_e(t) = \frac{C_e\left(\frac{L}{v_Q}t\right)}{\bar{C}_e}, \tag{2.3b}$$

as well as the dimensionless temperatures referred to the adiabatic temperature rise:

$$\tau(s,t) = \frac{T\left(Ls, \frac{L}{v_Q}t\right)}{T_a}, \quad \tau_e(t) = \frac{T_e\left(\frac{L}{v_Q}t\right)}{T_a}, \quad \tau_c(s,t) = \frac{T_c\left(Ls, \frac{L}{v_Q}t\right)}{T_a}. \tag{2.3c}$$

From the substitution of the dimensionless variables (2.3) on (2.1h), the dimensionless control input is defined as

$$\tau_c(s,t) = \sum_{i=1}^{q}\beta_i(s)\tau_{c,i}(t), \quad \boldsymbol{\tau}_c(t) = \begin{bmatrix}\tau_{c,1}(t)\\ \vdots \\ \tau_{c,q}(t)\end{bmatrix}, \tag{2.4a}$$

where the characteristic functions of the actuators $\beta_i(s)$, $i = 1, \dots q$ are defined as

$$\beta_i(s) = \begin{cases} 1 & \text{if } s \in \mathscr{R}_i \\ 0 & \text{else} \end{cases}, \quad i = 1, \dots, q, \quad \mathscr{R}_i = \begin{cases} \left(\frac{i-1}{q}, \frac{i}{q}\right] & \text{if } 1 \le i \le q-1 \\ \left[\frac{i-1}{q}, 1\right) & \text{if } i = q \end{cases}, \tag{2.4b}$$

Proceeding in a similar manner, the vector of measured outputs is defined as

$$\tau_{m,i} = \int_0^1 \delta_i(s)\tau(s,t)\mathrm{d}s, \quad i = 1 \dots, 1, \quad \boldsymbol{\tau}_m(t) = \begin{bmatrix} \tau_{m,1}(t) \\ \vdots \\ \tau_{m,q}(t) \end{bmatrix}, \tag{2.5a}$$

where the sensor characteristic functions $\delta_i(s) = \delta(s - \varsigma_i)$ are Dirac delta functions at the sensor locations ς_i. The latter ones are grouped in the sensor location set $\boldsymbol{\varsigma}$ defined as

$$\boldsymbol{\varsigma} = \{\varsigma_i \in \mathcal{R}_i \subset (0,1), \quad i = 1, \dots, q\}. \tag{2.5b}$$

Finally, the controlled output is

$$c_o(t) := c(1,t). \tag{2.6}$$

With the previous definitions, the dimensionless reactor model is described as

$$\partial_t c(s,t) = \frac{1}{Pe_m}\partial_s^2 c(s,t) - \partial_s c(s,t) - r(c(s,t), \tau(s,t)), \tag{2.7a}$$

$$\begin{aligned} \partial_t \tau(s,t) = {} & \frac{1}{Pe_h}\partial_s^2 \tau(s,t) - \partial_s \tau(s,t) - \upsilon\tau(s,t) + r(c(s,t), \tau(s,t)) - \\ & - \upsilon \sum_{i=1}^{q} \beta_i(s)\tau_{c,i}(t), \end{aligned} \tag{2.7b}$$

$$\frac{1}{Pe_m}\partial_s c(0,t) = c(0,t) - c_e(t), \qquad \partial_s c(1,t) = 0, \tag{2.7c}$$

$$\frac{1}{Pe_h}\partial_s \tau(0,t) = \tau(0,t) - \tau_e(t), \qquad \partial_s \tau(1,t) = 0, \tag{2.7d}$$

$$c(s,0) = c_0(s), \tag{2.7e}$$

$$\tau(s,0) = \tau_0(s), \tag{2.7f}$$

$$\tau_{m,i}(t) = \int_0^1 \delta_i(s)\tau(s,t)\mathrm{d}s, \quad i = 1, \dots, q, \qquad c_z(t) = c(1,t), \tag{2.7g}$$

where $c(s,t)$ [or $\tau(s,t)$] is the concentration (or temperature) state profile, the exogenous inputs are: the inlet concentration (or temperature) $c_e(t)$ [or $\tau_e(t)$]. The reaction rate function and the related parameters in dimensionless form are given by

$$r(c,\tau) = \frac{LR(\bar{C}_e c, T_a \tau)}{\bar{v}_Q \bar{C}_e}, \quad Pe_m = \frac{Lv_Q}{D_m}, \quad Pe_h = \frac{Lv_Q}{D_h}, \quad \upsilon = \frac{LH}{v_Q},$$

Pe_m, Pe_h, are the mass and heat Peclet numbers while v is the heat exchange number.

From the mass and heat conservation restrictions given by (2.2), the dimensionless variables involved in (2.7) are defined over bounded set as established next:

$$c_e(t) \in [0, c_e^+], \quad \tau_e(t) \in [\tau_e^-, \tau_e^+], \tag{2.8a}$$

for the exogenous inputs. For the concentration and temperature profiles:

$$c(s,t) \in [0, c_e^+] := \mathscr{C} \quad \tau(s,t) \in [\tau^-, \tau^+] := \mathscr{T}, \tag{2.8b}$$

and the control input

$$\tau_{c,i}(t) \in [\tau_c^-, \tau_c^+] := \mathscr{T}_c, \quad i = 1, \ldots, q. \tag{2.8c}$$

From (2.8b) the state profiles are defined over the product set $\mathscr{X}$:

$$[c(s,t)\, \tau(s,t)]^T \in \mathscr{X} = \mathscr{C} \times \mathscr{T}. \tag{2.8d}$$

The corresponding steady-state profiles $[\bar{c}(s,t)\, \bar{\tau}(s,t)]^T$, for given nominal feed concentration $\bar{c}_e$ (or temperature $\bar{\tau}_e$) and jacket temperature profile $\bar{\tau}_c(s,t) = \bar{\tau}_c \sum_{i=1}^{q} \beta_i(s)$, are the solution to the two point boundary value problem

$$\begin{aligned}
\frac{1}{Pe_m}\frac{\mathrm{d}^2\bar{c}(s)}{\mathrm{d}s^2} - \frac{\mathrm{d}\bar{c}(s)}{\mathrm{d}s} - r(\bar{c}(s), \bar{\tau}(s)) = 0,\\
\frac{1}{Pe_h}\frac{\mathrm{d}^2\bar{\tau}(s)}{\mathrm{d}s^2} - \frac{\mathrm{d}\bar{\tau}(s)}{\mathrm{d}s} - v\bar{\tau}(s,t) + r(\bar{c}(s), \bar{\tau}(s)) + v\bar{\tau}_c \sum_{i=1}^{q} \beta_i(s) = 0,\\
\frac{1}{Pe_m}\frac{\mathrm{d}c(0)}{\mathrm{d}s} = \bar{c}(0) - \bar{c}_e, \quad \frac{1}{Pe_h}\frac{\mathrm{d}\tau(0)}{\mathrm{d}s} = \bar{\tau}(0) - \bar{\tau}_e,\\
\frac{\mathrm{d}c(1)}{\mathrm{d}s} = 0, \quad \frac{\mathrm{d}\tau(1)}{\mathrm{d}s} = 0.
\end{aligned}$$

The associated steady-state outputs are given by

$$\bar{\tau}_{m,i} = \int_0^1 \delta_i(s)\bar{\tau}(s)\mathrm{d}s, \quad i = 1, \ldots, q, \qquad \bar{c}_o = \bar{c}(1).$$

2.2 OPEN-LOOP DYNAMICS

In this section, the open-loop dynamics, in terms of limit sets (steady-states and limit cycles) of the tubular reactor class (2.7) are characterized.

2.2.1 *Nominal distributed dynamics and limit sets*

Henceforth, the explicit dependency on the spatial (s) and time (t) independent variables will be omitted for brevity and written only when needed for clarity purposes. Define the temperature and concentration profiles and exogenous inputs vectors:

$$\chi = \begin{bmatrix} \chi_1 \\ \chi_2 \end{bmatrix} = \begin{bmatrix} c(s,t) \\ \tau(s,t) \end{bmatrix}, \quad \chi_e = \begin{bmatrix} \chi_{1,e} \\ \chi_{2,e} \end{bmatrix} = \begin{bmatrix} c_e(t) \\ \tau_e(t) \end{bmatrix}.$$

Thus, the reactor dynamics can be rewritten in compact form as

$$\partial_t \chi = \mathscr{F}(\chi) + \mathscr{G}(\chi) + \mathscr{B}_c \boldsymbol{\tau}_c, \tag{2.9a}$$

$$\mathscr{B}_b(\chi, \chi_e) = \mathbf{0}, \tag{2.9b}$$

$$\chi(0) = \chi_0, \tag{2.9c}$$

$$\boldsymbol{\tau}_m = \int_0^1 \mathscr{H}_m \chi \mathrm{d}s, \qquad c_o = \mathscr{H}_o \chi(1,t), \tag{2.9d}$$

where $\boldsymbol{\tau}_c$, $\boldsymbol{\tau}_m$, and c_o are defined in (2.6), (2.4), (2.5a), respectively. The functions $\mathscr{F}$, $\mathscr{G}$, and $\mathscr{B}c$ are

$$\mathscr{F}(\chi) = \boldsymbol{Pe}^{-1}\partial_s^2 \chi - \partial_s \chi - v \boldsymbol{g}_1 \chi, \quad \boldsymbol{Pe} = \begin{bmatrix} Pe_m & 0 \\ 0 & Pe_h \end{bmatrix}, \quad \boldsymbol{g}_1 = \begin{bmatrix} 0 \\ 1 \end{bmatrix},$$

$$\mathscr{G}(\chi) = \begin{bmatrix} -\rho(\chi) \\ \rho(\chi), \end{bmatrix}, \quad \mathscr{B}_b(\chi, \chi_e) = \begin{bmatrix} \boldsymbol{Pe}^{-1}\partial_s \chi(0,t) - \chi(0,t) + \chi_e(t) \\ \partial_s \chi(1,t) \end{bmatrix}.$$

The input and output maps are given by

$$\mathscr{B}_c = v \boldsymbol{g}_1 \boldsymbol{\beta}, \quad \boldsymbol{\beta} = \begin{bmatrix} \beta_1 \\ \vdots \\ \beta_q \end{bmatrix}^T, \quad \mathscr{H}_m = \boldsymbol{g}_1^T \delta, \quad \delta = \begin{bmatrix} \delta_1 \\ \vdots \\ \delta_q \end{bmatrix}, \quad \mathscr{H}_o = \begin{bmatrix} 1 \\ 0 \end{bmatrix}.$$

By virtue of the boundedness and continuity of the reaction rate function $\boldsymbol{r}$ (see [136]), for given initial state-input data $(\chi_0, \chi_e, \boldsymbol{\tau}_c)$, the Partial Differential Equation (PDE) model (2.9) has a unique solution motion χ with unique output signal $\boldsymbol{\tau}_m$, i. e.,

$$\chi(t) = \mathrm{t}_\chi(t, \chi_0, \chi_e, \boldsymbol{\tau}_c), \quad \boldsymbol{\tau}_m(t) = \int_0^1 \mathscr{H}_m \mathrm{t}_\chi(t, \chi_0, \chi_e, \boldsymbol{\tau}_c) \mathrm{d}s.$$

For constant input data $(\bar{\chi}_e, \bar{\boldsymbol{\tau}}_c)$, the motion χ reaches exponentially a stable steady-state $\bar{\chi}$ or a limit cycle $\bar{\chi}(t)$, i. e.,

$$(\chi_e, \boldsymbol{\tau}_c) = (\bar{\chi}_e, \bar{\boldsymbol{\tau}}_c), \quad \chi_0 \notin \mathscr{S} = \mathscr{S}_s \cup \mathscr{S}_l \Rightarrow \chi(t) \to \bar{\chi} \in \mathscr{S}_s \text{ or } \bar{\chi}(t) \in \mathscr{S}_l$$

where

$$\mathscr{S}_s = \{\bar{\chi}_1, \ldots, \bar{\chi}_{n_s}\}, \qquad \mathscr{S}_l = \left\{\bar{\chi}_1(t), \ldots, \bar{\chi}_{n_l}(t)\right\}, \tag{2.10}$$

$\mathscr{S}_s$ (or $\mathscr{S}_l$) is the set of n_s (or n_l) steady-states (or limit cycles).

2.3 PROBLEM

The CE problem consist in designing, a decentralized model-based on-line Control-Estimation System (CES) (depicted in Figure 2.2) composed by an output feedback MIMO controller and an estimator. The CES has the form

$$\dot{\boldsymbol{\theta}} = \boldsymbol{\Gamma}(\boldsymbol{\theta}, \boldsymbol{\tau}_m, \boldsymbol{\chi}_e, \boldsymbol{p}, \mathfrak{S}_q, \boldsymbol{K}_\theta), \quad \boldsymbol{\theta}(0) = \boldsymbol{\theta}_0, \tag{2.11a}$$

$$\hat{\boldsymbol{\chi}} = \boldsymbol{\Omega}(\boldsymbol{\theta}, \mathfrak{S}_q), \tag{2.11b}$$

$$\boldsymbol{\tau}_c = \boldsymbol{\mu}_s(\boldsymbol{\theta}, \boldsymbol{\tau}_m, \boldsymbol{\chi}_e, \boldsymbol{p}, \boldsymbol{K}_\theta, \mathfrak{S}_q), \quad \tau_{c,i} \in \mathscr{T}_c, \tag{2.11c}$$

Driven by output $\boldsymbol{\tau}_m$ and exogenous input $\boldsymbol{\chi}_e$ (if available) measurements, the dynamic CES, which use a tubular reactor model $\boldsymbol{\Gamma}$ with internal state $\boldsymbol{\theta}$ and parameters $\boldsymbol{p}$, produce the state estimate $\hat{\boldsymbol{\chi}}$ and the control action $\boldsymbol{\tau}_c$, each one given by the output maps $\boldsymbol{\Omega}$ and $\boldsymbol{\mu}_s$, respectively. The vector of gains $\boldsymbol{K}_\theta$ and the CES structure $\mathfrak{S}_q$ are given as

$$\boldsymbol{K}_\theta = (\boldsymbol{K}_c, \boldsymbol{K}_e), \quad \mathfrak{S}_q = (n_\theta, q, \boldsymbol{\varsigma}, \mathscr{T}_c). \tag{2.11d}$$

$\boldsymbol{K}_\theta$ contains control $\boldsymbol{K}_c$ and estimator $\boldsymbol{K}_e$ gains. In $\mathfrak{S}_q$, n_θ is the finite dimension of the CES, q is the number of coolant jacket sections and sensors, $\boldsymbol{\varsigma}$ is the sensor location set (2.5b), and $\mathscr{T}_c = [\tau_c^-, \tau_c^+]$, defined in (2.8c), is the admissible size of i-th control action, $i = 1, \ldots, q$. In (2.11c), the symbol $\boldsymbol{\mu}_s$ denotes component-wise saturation, with limits (τ_c^-, τ_c^+), of each entry of the control output map $\boldsymbol{\mu}$ $(i = 1, \ldots, q)$:

$$\boldsymbol{\mu}_s(\cdot) := \mathrm{sat}_{\tau_c^-}^{\tau_c^+}[\boldsymbol{\mu}(\cdot)] = \begin{bmatrix} \mathrm{sat}_{\tau_c^-}^{\tau_c^+}[\mu_1(\cdot)] \\ \vdots \\ \mathrm{sat}_{\tau_c^-}^{\tau_c^+}[\mu_q(\cdot)] \end{bmatrix}, \ \mathrm{sat}_{\tau_c^-}^{\tau_c^+}[\mu_i(\cdot)] \begin{cases} \tau_c^+ & \text{if } \mu_i(\cdot) > \tau_c^+ \\ \mu_i(\cdot) & \text{if } \tau_c^- < \mu_i(\cdot) < \tau_c^+ \\ \tau_c^- & \text{if } \tau_c^- < \mu_i(\cdot) \end{cases},$$

In agreement with [67], since industrial tubular reactors are operated with a low amount of sensors and actuators, in this study only the cases for $q = 1, 2, 3$ will be considered for the design of the MIMO CES (2.11).

The CES (2.11) must: (i) adjust with saturated output-feedback control $\boldsymbol{\mu}_s$ the coolant temperature vector $\boldsymbol{\tau}_c$ to attain closed-loop robust stability and output regulation about a prescribed (possibly open-loop unstable) steady-state-outputs pair $(\bar{\boldsymbol{\chi}}, \bar{\boldsymbol{\tau}}_m, \bar{c}_o)$ which ensures high yield ($\bar{c}_o \approx 0$), (ii) provide a robustly convergent estimate $\hat{\boldsymbol{\chi}}$ of the concentration-temperature profile $\boldsymbol{\chi}$, and (iii) satisfy a trade-off between convergence speed, control effort, computational efficiency and complexity.

Despite the finite dimension of CES (2.11), for implementation purposes, its design may be done following either the early or late lumping approaches. In both cases, the lumping step will be performed using the efficient modeling approach [22].

It must be pointed out that in this study only the control input $\boldsymbol{\tau}_c$ is considered for design, in the understanding that it corresponds with the master component of a typical cascade control configuration. The design of the slave component is a straightforward task [34] that is omitted in the study.

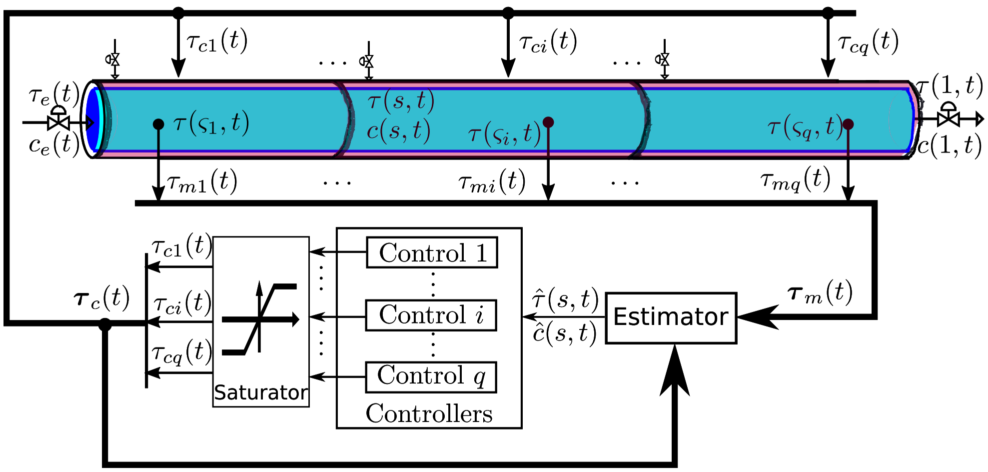

Figure 2.2: Multi–jacket tubular reactor with a MIMO CES and constrained control action.

2.4 METHODOLOGICAL APPROACH

The problem is solved within a constructive [118] and application-oriented framework for process control design [116]. The aim is to obtain a CES, for the considered class of open-loop unstable tubular reactors, similar to what is use in industrial practice supplemented with the benefits of model-based design: assurance of robust stability and formal criteria for the selection of the structure of the CES. Three methodological steps will be considered for the solution of the CE problem. In a first step, within the early lumping approach, a MIMO CES, with constrained control, will be designed by exploiting passivity and detectability properties and realization theory to obtain a CES composed by a PI control decoupled from the estimator. This design is appealing for industrial practice since it is a well-known structure. In a second step, an advanced MIMO CES, with unconstrained control, will be constructed within a late lumping approach by the exploitation of constructive and inventory control ideas. In the final step, the implications of each design in the opposite perspective, late or early lumping, will be explored.

Specifically, in the first methodological step, a CES design will be performed on the basis of a lumped model obtained from the application of the efficient modeling approach [22]. Using this model, the CES will be constructed as the combination of a passive controller and a geometric observer. The solvability properties will be established in terms of the sensor location and control limits by using the concepts of zero dynamics and closed-loop detectability of the Single Input-Single Output (SISO) case that are inherited to the MIMO setting. The closed-loop stability will be ensured within a practical stability framework. Finally, by using concepts from realization theory and the inseparability principle of Skelton [123], the CES will be realized as a decoupled PI controller with AWs protection and a pointwise-like observer.

In the second step, within a late lumping approach, an advanced CES system is designed by exploiting the interplay between the stabilizing heat transport and destabilizing heat generation mechanisms. This is done by studying the system as an Lur'e interconnection: stability conditions for the linear dynamics as first established and then modified to account for the nonlinear effects of the reaction rate function. An additional control component, drawn with the relationship between heat inventory control and passivity for distributed systems, leads to the control component of the CES. A pointwise observer is considered for output feedback control and estimation purposes. Closed-loop stability conditions in terms of the structure of the CES and gains are characterized together with structural-gain tuning guidelines.

The proposed CES are put in perspective with their industrial counterparts and other advanced CES, including the comparison of the proposed sensor location criteria with the usually employed in industry, and simulation-based comparison of closed-loop performance with an adaptive output feedback controller coupled with a pointwise observer. Finally, the extension of the first CES, designed within an early lumping strategy, is explored in the infinite dimensional setting. Then, the extension of the second CES, constructed in the late lumping framework, is explored in the early lumping case. The performance of the proposed CESs is compared and the benefits of each one are identified and combined to obtain a mixed CES which combines the two design methodologies.

2.5 CASE STUDY

Without restricting the approach, the theoretical developments and the functioning of the proposed CES will be illustrated and tested with a representative bistable reactor example [129; 130; 131] that has been employed in previous studies with advanced model-based nonlinear feedback stabilizing control [102; 30; Fra+20; FA].

A first order chemical reaction is considered

$$r(c,\tau) = c e^{b_r - \frac{a_r}{\tau}}, \quad a_r = \frac{E_a}{R_g T_a}, \quad b_r = \ln Da, \tag{2.12}$$

where E_a is the activation energy, R_g is the ideal gases constant, T_a is the adiabatic temperature rise, and Da is the Damkohler number. The tubular reactor dimensionless parameters and nominal input values are given in Table 2.1.

The application of a standard FD PDE solver with $N = N_{pde} = 200$, yields that the reactor example has a three-steady-state set (2.10) and no limit cycles, i. e.,

$$\hat{\mathscr{S}}(N_{pde,\boldsymbol{p}}) = \hat{\mathscr{S}}_s(N_{pde}, \boldsymbol{p}) = \left\{\bar{\chi}_{N,E}, \bar{\chi}_N, \bar{\chi}_{N,I}\right\}, \quad \hat{\mathscr{S}}_l(N_{pde}, \boldsymbol{p}) = \emptyset.$$

The three steady-states are presented in Figure 2.3: an extinction-ignition stable steady-state pair $\{\bar{\chi}_{N,E}, \bar{\chi}_{N,I}\}$ with an unstable saddle $\bar{\chi}_N$ in between. This example captures basic nonlinear characteristics of important industrial reactors with reported

PARAMETER	VALUE	UNCERTAINTY
Pe_m	5	± 10 %
Pe_h	5	± 10 %
v	1	± 5 %
a	50	± 3 %
b	23.719	± 3 %
INPUT	VALUE	DOMAIN
$\bar{c}_e$	1	[0.5, 1.5]
$\bar{\tau}_e$	2	[1.5, 2.5]
$\bar{\tau}_c$	1.5	[0.7, 2.3]

Table 2.1: Nominal parameters and inputs for the case study.

experimental data, like the bistable biomass gasification [22; 44], and the ammonia synthesis with abnormal behavior in close to bifurcation operation condition [97].

The dynamic behavior of the tubular reactor is shown in Figure 2.4, in the presented two simulations[1], the state profiles are initialized around the unstable steady-state, each simulation considers a different basin of attraction. For the initial profile on the upper temperature basin of attraction, see Figure 2.4a, the states are pushed away from the unstable saddle to the ignition steady-state. In case of the lower temperature basin of attraction, in Figure 2.4b, the states are repelled by the unstable saddle and settle down in the extinction steady-state.

The operational goal of the tubular reactor is to ensure high yield while keeping the hotspot temperature profile far from dangerous high values, accordingly, the unstable target steady state $\bar{\chi}_N$ is selected for closed-loop operation since it has high conversion $(\chi_1(1,t) \approx 0.15)$ and the associated temperature profiles has a hotspot with acceptable temperature out of dangerous operation (in comparison with the ignition stable steady-state with high yield but dangerous temperature profile).

2.6 SUMMARY

In this chapter, the class of tubular reactors under study, the general CE problem, the methodological approach, and a case study that will be used throughout the present study have been stated. The considered tubular reactor class and the corresponding spatially distributed model were first presented. Then the CE problem that will be

1 All simulations performed in this thesis work will be executed with Matlab ODE integrator ode45 on an Intel© Core™ i7-6500U CPU with 2.50 GHz × 2 personal computer with Linux Mint 19.3 operative system.

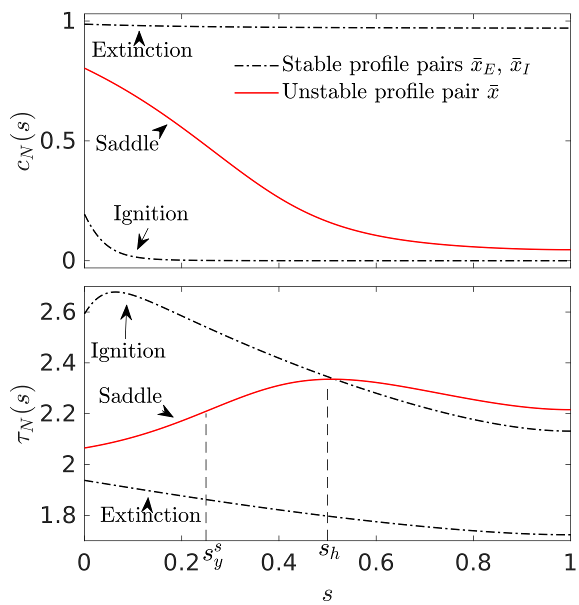

Figure 2.3: Reactor case exmple: concentration-temperature interpolated steady-states profile pair with FD PDE solver-type of order $N_{pde} = 200$; (i) stable exctinction (or ignition) steady-state $\bar{\chi}_{N,E}$ (or $\bar{\chi}_{N,I}$) (black plots), and (ii) unstable saddle steady-state $\bar{\chi}_N$ (red plots). For the unstable steady state, the typical sensor location for industrial SISO PI control, based on the sensitivity criterion, is indicated at $s_y^s \approx 0.25$, and the hotspot at $s_h \approx 0.5$.

solved was formulated. The methodological approach that will be followed throughout the rest of the work was introduced in detail, including the formulation of three methodological steps employed to solve the CE problem. Finally, a case study, to illustrate theoretical developments, was presented: a representative tubular reactor with a first order chemical reaction and Arrhenius temperature dependency.

The proposed three-step methodology for the solution of the MIMO CE problem splits the analysis and synthesis procedures in three objects of study: (i) the CE problem of a multi–jacket tubular reactor with saturated control using an efficiently discretized lumped model, (ii) the version of the problem with unconstrained control and to infinite-dimensional tubular reactor model with an efficient late lumping implementation, and (iii) the implications of each of the previous designs using the opposite (late or early) lumping approach. All designs must be accompanied with assurance of robust stability, criteria for the structural (i. e., sensor and actuator configuration and control limits) and gain tuning, and an efficient implementation. All this will be accomplished within an application-oriented perspective.

It must be pointed out that each of these problems constitutes an important field of actual studies in the chemical process engineering sciences and offers an interesting contribution with respect to the preceding literature

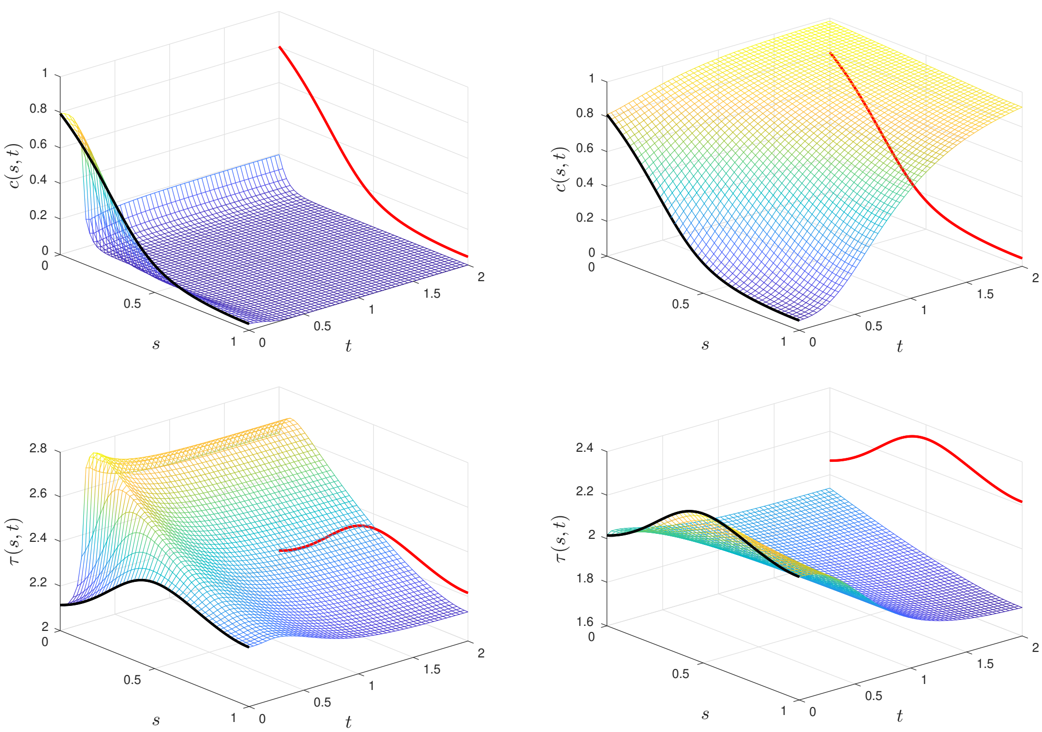

(a) Initial profile pair on basin of attraction of the ignition steady-state.

(b) Initial profile pair on basin of attraction of the ignition steady-state.

Figure 2.4: Open-loop transient behavior of the case study with initial profile pair around the unstable steady-state. The initial profile pair is in black solid thick lines, while the unstable saddle steady-state is shown in red solid thick lines.

3 PRELIMINARIES: ROBUST STABILITY FRAMEWORK AND EFFICIENT MODELING APPROACH

In this chapter, the stability notion and the efficient modeling approach, ingredients that underlain the present study, are recalled from the literature. First, the robust stability concept, i. e., practical stability in the sense of exponential Input-to-State Stability (ISS) [125] is established for finite and infinite dimensional systems defined in suitable spaces. The above mentioned concepts are introduced for certain class of nonlinear systems and then particularized for nonlinear models usually employed to describe the behavior od chemical reactors, this includes system composed by linear and nonlinear components and interconnected systems. Then, a brief description of the employed efficient modeling approach [22] is given, including methodological concepts and a detailed explanation of the algorithm and the application of the method to the case example.

3.1 ROBUST STABILITY FRAMEWORK

Industrial tubular reactors are subjected to uncertainties and fluctuating exogenous input disturbances. Thus, and adequate concept of stability suited for this setting is in order. Furthermore, a stability concept easy to apply and with physical meaning must be considered. A suited definition of stability that match the requirements previously described is the one of *practical stability*: Input-to-State Stability (ISS) [125; 75] over a finite domain of interest in which the variables of the tubular reactor have physical sense. In short words, practical stability means [80]: *steady-state exponential stability when no disturbances are present, and ultimately boundedness around steady-state with admissible size excursions in the presence of exogenous disturbances of admissible size*.

To illustrate the concepts introduced on this chapter, consider the following dynamic nonautonomous system of finite or infinite dimension, that without loss of generality has the origin as steady-state (possibly non unique), and is subjected to parameter errors $\tilde{\boldsymbol{p}}$, exogenous time varying input vector $\boldsymbol{d}$, output measurement uncertainty $\tilde{\boldsymbol{y}}$, and controlled output uncertainty $\tilde{z}(t)$:

$$\dot{\boldsymbol{x}}(t) = \boldsymbol{f}_1(\boldsymbol{x}(t), \boldsymbol{p} + \tilde{\boldsymbol{p}}, \boldsymbol{d}(t), \boldsymbol{u}(t)), \qquad \boldsymbol{x}(0) = \boldsymbol{x}_0, \tag{3.1a}$$

$$\boldsymbol{y}(t) = \boldsymbol{C}_y \boldsymbol{x}(t) + \tilde{\boldsymbol{y}}(t), \quad z(t) = \boldsymbol{C}_z x(t) + \tilde{z}(t), \tag{3.1b}$$

where

$$\boldsymbol{f}_1(\boldsymbol{0}, \boldsymbol{p}, \boldsymbol{0}, \boldsymbol{0}) = \boldsymbol{0}. \tag{3.1c}$$

The state $\boldsymbol{x} \in \mathscr{X}$ (possibly distributed in space) is a vector that contains the concentration and temperature profiles in deviation from a steady-state of interest and is defined in a suitable state-space X (an euclidian or L^2 space), $\boldsymbol{d} \in \mathfrak{D} \subset \mathbb{R}^2$ is the vector of exogenous inputs, $\boldsymbol{u} \in \mathscr{U} \in \mathbb{R}^q$ is the control input vector, $\boldsymbol{p}$ is the vector of nominal parameters, $\boldsymbol{y} \in \mathbb{R}^q$ is the measured output vector, and z is the controlled output. Consider that the set of admissible initial conditions, errors and disturbances satisfy the bounds

$$\|\boldsymbol{x}_0\|_X \leq \delta_{x0}, \quad \|\boldsymbol{p}\| \leq \delta_p, \quad \|\boldsymbol{d}(t)\| \leq \varepsilon_d(t), \quad \|\tilde{\boldsymbol{u}}(t)\| \leq \varepsilon_u(t), \tag{3.2a}$$

where the majorizing functions $\varepsilon_d(t) > 0$ and $\varepsilon_u(t) > 0$ satisfy

$$\sup_{t\geq 0} \varepsilon_d(t) \leq \varepsilon_d^+, \qquad \sup_{t>0} \leq \varepsilon_u^+. \tag{3.2b}$$

The definition of *robust stability* [125], that underlies the present study is stated next.

Definition 3.1. *Robust stability*.
System (3.1a), defined in the set $\mathfrak{X} = \{\boldsymbol{x} \in \mathscr{X} \mid \|\boldsymbol{x}\| \leq r_x\}$ and subjected to bounded initial state, errors and inputs, according to (3.2) is said to be locally robustly (exponentially) stable if it has the origin as the unique steady-state, and satisfy the bounding expression

$$\|\boldsymbol{x}_0\|_{\mathscr{X}} \leq \delta_x, \|\boldsymbol{d}(t)\|_{\sup} \leq \varepsilon_d^+, \|\boldsymbol{u}(t)\|_{\sup} \leq \varepsilon_u^+ \Rightarrow \|\boldsymbol{x}(t)\| \leq a_x \mathrm{e}^{-\nu_x t}\delta_x + \varepsilon_x, \tag{3.3}$$

where $\varepsilon_x =: a_x\delta_x + b_p\delta_p + b_d\varepsilon_d^+ + b_u\varepsilon_u^+ > 0$. If r_x is the radius set of X the result is nonlocal.

Note that (3.3) implies local ISS for system (3.1a): the origin is exponentially stable under nominal conditions (without disturbances) and ultimately bounded with admissible ultimate bound dependent on the size of admissible disturbances.

Definition 3.1 applies for systems composed by nominal $\boldsymbol{f}$ and disturbance $\boldsymbol{g}$ terms:

$$\dot{\boldsymbol{x}} = \boldsymbol{f}(\boldsymbol{x}) + \boldsymbol{g}(\boldsymbol{x}; \tilde{\boldsymbol{p}}, \boldsymbol{d}, \boldsymbol{u}), \quad \boldsymbol{x}(0) = \boldsymbol{x}_0, \tag{3.4a}$$

where $\boldsymbol{f}$ and $\boldsymbol{g}$, which accounts for the effect of uncertainties are given by:

$$\boldsymbol{f}(\boldsymbol{x}) = \boldsymbol{f}_1(\boldsymbol{x}, \boldsymbol{p}, \boldsymbol{0}, \boldsymbol{0}), \quad \boldsymbol{g}(\boldsymbol{x}; \tilde{\boldsymbol{p}}, \boldsymbol{d}, \boldsymbol{u}) = \boldsymbol{f}_1(\boldsymbol{x}, \boldsymbol{p} + \tilde{\boldsymbol{p}}, \boldsymbol{d}, \boldsymbol{u}) - \boldsymbol{f}_1(\boldsymbol{x}, \boldsymbol{p}, \boldsymbol{0}, \boldsymbol{0}), \tag{3.4b}$$

and $\boldsymbol{g}$ satisfy the Lipschitz bound

$$\|\boldsymbol{g}(\boldsymbol{x}, \tilde{\boldsymbol{p}}, \boldsymbol{d}, \boldsymbol{u})\| \leq L_x^g \|\boldsymbol{x}\| + L_p^g \|\tilde{\boldsymbol{p}}\| + L_d^g \|\boldsymbol{d}\| + l_u^g \|\boldsymbol{u}\|. \tag{3.4c}$$

Assuming that the nominal system, (3.4a) with $\boldsymbol{g} = \boldsymbol{0}$, is exponentially stable, then, by the converse Lyapunov theorems [76], there exist a quadratic Lyapunov functional $V(\boldsymbol{x}) : \mathfrak{X} \subset \mathscr{X} \to \mathbb{R}$ that satisfy the following bounds on $\boldsymbol{x} \in \mathfrak{X}$

$$c_1 \|\boldsymbol{x}\|^2 \leq V(\boldsymbol{x}) \leq c_2 \|\boldsymbol{x}\|^2, \quad \partial_{\boldsymbol{x}} V \boldsymbol{f}(\boldsymbol{x}) \leq -c_3 \|\boldsymbol{x}\|^2, \quad \|\partial_{\boldsymbol{x}} V\| \leq c_4 \|\boldsymbol{x}\|. \tag{3.5a}$$

and the state of the nominal system is bounded as

$$\|\boldsymbol{x}\| \leq a_x \mathrm{e}^{-\lambda_x t} \|\boldsymbol{x}_0\|, \quad a_x = \sqrt{\frac{c_2}{c_1}}, \quad \lambda_x = \frac{1}{2}\frac{c_3}{c_2}. \tag{3.5b}$$

With the previous result and the employment of the comparison method (see [76, Subsections 9.2 and 9.3]) the robust stability of the perturbed system (3.4) can be established according to the following result.

Lemma 3.1. ***Robust stability of perturbed systems****. Proof in Section a.1*
Let $\boldsymbol{x} = \mathbf{0}$ be an exponentially stable equilibrium point of the nominal system, (3.4a) with $\boldsymbol{g} = \mathbf{0}$, defined in the set $\mathfrak{X} = \{\boldsymbol{x} \in \mathscr{X} \mid \|\boldsymbol{x}\| \leq r_x\}$ where r_x is the set radius of $\mathfrak{X}$ (or $\mathscr{X}$). Let $V(\boldsymbol{x})$ be a Lyapunov function of the nominal system that satisfies (3.5a) in $\mathfrak{X}$ (or in $\mathscr{X}$). Suppose that the exogenous inputs and parameter error satisfy (3.2), and the perturbation term $\boldsymbol{g}(\boldsymbol{x}, \tilde{\boldsymbol{p}}, \boldsymbol{d}, \boldsymbol{u})$ satisfies (3.4c). Provided that

$$\nu_x = \lambda_x - \frac{c_4 L_x^g}{c_1} > 0, \tag{3.6a}$$

and $\boldsymbol{x}_0$ and b_p, b_d, b_u satisfy

$$\|x_0\| \leq \frac{r_x}{a_x} \Rightarrow \delta_{x0} \leq \frac{r_x}{a_x}, \quad b_p\delta_p + b_d\varepsilon_d^+ + b_u\varepsilon_u^+ := \varepsilon_x \leq r_x, \tag{3.6b}$$

where

$$\frac{a_x}{\nu_x}\left(L_p^g, L_d^g, L_u^g\right) := \left(b_p, b_d, b_u\right). \tag{3.6c}$$

Then, the state of the perturbed system (3.4) satisfies (3.3) locally on $\mathfrak{X}$ (or nonlocally on $\mathscr{X}$).

Lemma 3.1 gives sufficient conditions to characterize the robust stability property used in this study. A straightforward result is the exponential stability of the origin in the presence of vanishing disturbances. This is established next.

Corollary 3.1. *Let $\boldsymbol{x} = \mathbf{0}$ be an exponentially stable equilibrium point of the nominal system (3.4) with $\boldsymbol{g} = \mathbf{0}$ defined in the state-space $\mathfrak{X} = \{\boldsymbol{x} \in \mathscr{X} \mid \|\boldsymbol{x}\| \leq r_x\}$ where r_x is the radius set of $\mathfrak{X}$ (or $\mathscr{X}$). Let $V(\boldsymbol{x})$ be a Lyapunov functional of the nominal system that satisfies (3.5a) in $\mathfrak{X}$ (or $\mathscr{X}$). Suppose that the bounding conditions in (3.2) are met with satisfied*

$$\lim_{t\to\infty} \varepsilon_d(t) = 0, \quad \lim_{t\to\infty} \varepsilon_u(t) = 0, \tag{3.7}$$

and the perturbation term $\boldsymbol{g}(\boldsymbol{x}, \tilde{\boldsymbol{p}}, \boldsymbol{d}, \boldsymbol{u})$ is Lipschitz bounded as in (3.4c). Then the origin of (3.4) is a locally (or nonlocally) exponentially stable steady-state over $\mathfrak{X}$ (or $\mathscr{X}$).

Several classes of chemical reactors, including the discretized models of tubular ones, are modeled as finite dimensional systems composed by a linear part, associated to transport phenomena and a nonlinear one due to chemical reaction. When this is the case, (3.4) is composed by a linear nominal part and a nonlinear Lipschitz bounded perturbation term $\boldsymbol{g}$, i. e.,

$$\dot{\boldsymbol{x}} = \boldsymbol{A}\boldsymbol{x} + \boldsymbol{g}(\boldsymbol{x}, \tilde{\boldsymbol{p}}, \boldsymbol{d}, \boldsymbol{u}), \quad \boldsymbol{x}(0) = \boldsymbol{x}_0, \tag{3.8a}$$

where $\boldsymbol{A}$ is a Hurwitz matrix. Then, there exist a Lyapunov function for the nominal part of the system (i. e., $\boldsymbol{g} = \boldsymbol{0}$)

$$V = \boldsymbol{x}^T\boldsymbol{P}\boldsymbol{x}, \quad \boldsymbol{P} = \boldsymbol{P}^T > 0. \tag{3.8b}$$

where the matrix $\boldsymbol{P}$ satisfies the Lyapunov inequality

$$\boldsymbol{A}^T\boldsymbol{P} + \boldsymbol{P}\boldsymbol{A} + 2\zeta\boldsymbol{P} < \boldsymbol{0}, \quad \zeta < |\lambda_A{}^*|, \quad \lambda_A{}^* = \max_{\lambda_n \in \sigma(\boldsymbol{A})} \{\mathrm{Re}(\lambda_n)\}, \quad a_P = \frac{\lambda_P{}^*}{\lambda_{P*}}, \tag{3.8c}$$

where $\lambda_{P*} = \min_{\lambda_n \in \sigma(\boldsymbol{P})}\{\lambda_n\}$ and $\lambda_P{}^* = \max_{\lambda_n \in \sigma(\boldsymbol{P})}\{\lambda_n(\boldsymbol{P})\}$. Then, the constants in (3.5a) are replaced with

$$c_1 = \lambda_{P*}, \quad c_2 = \lambda_P{}^*, \quad c_3 = -2\zeta\lambda_P{}^*, \quad c_4 = 2\lambda_P{}^*, \tag{3.8d}$$

Accordingly, the following result can be established.

Corollary 3.2. *Proof in Section a.2. Let $\boldsymbol{x} = \boldsymbol{0}$ be an exponentially stable equilibrium point of the nominal linear system, (3.8a) with $\boldsymbol{g} = \boldsymbol{0}$, defined in the set $\mathfrak{X} = \{\boldsymbol{x} \in \mathscr{X} \mid \|\boldsymbol{x}\| \leq r_x\}$ where r_x is the radius set of $\mathfrak{X}$ (or in $\mathscr{X}$). Let $V(\boldsymbol{x})$ be the quadratic Lyapunov function of the nominal system that satisfies (3.8c)-(3.8d) in $\mathfrak{X}$ (or in $\mathscr{X}$). Suppose that the bounding conditions (3.2) and the Lipschitz bound (3.4c) of the perturbation term $\boldsymbol{g}(\boldsymbol{x}, \tilde{\boldsymbol{p}}, \boldsymbol{d}, \boldsymbol{u})$ are all satisfied. Provided that $\boldsymbol{x}_0$ and b_p, b_d, b_u satisfy (3.6b), then if*

$$\nu_x = \zeta - a_x L_x^g > 0, \quad a_x = a_P, \tag{3.9}$$

then, the solutions of the perturbed system (3.4) satisfies (3.3) locally in $\mathfrak{X}$ (or nonlocally in $\mathscr{X}$) with ν_x and (b_p, b_d, b_u) given as in (3.6c).

If the constant $a_P = \frac{\lambda_P{}^*}{\lambda_{P*}}$ is overestimated, an alternative is to use the bound of the transition matrix related to the linear part of the system (3.8a):

$$\left\|\mathrm{e}^{\boldsymbol{A}t}\right\| \leq a_A \mathrm{e}^{-\lambda_A{}^* t} = a_A \mathrm{e}^{-|\lambda_A{}^*|t}, \quad -\lambda_A{}^* = \max_{\lambda_n \in \sigma(\boldsymbol{A})} \{\mathrm{Re}(\lambda_n)\}, \tag{3.10}$$

where $a_A > 0$, and $-\lambda_A{}^*$ is maximum real part of the eigenvalues λ_n in the spectrum $\sigma(\boldsymbol{A})$ of matrix $\boldsymbol{A}$.

In this case, the robust stability is characterized by the following result.

Corollary 3.3. *Proof in Section a.2. Consider the perturbed system (3.8a) with state $\boldsymbol{x} \in \mathfrak{X} = \{\boldsymbol{x} \in \mathscr{X} \mid \|\boldsymbol{x}\| \leq r_x\}$ where r_x is the radius set of $\mathfrak{X}$ (or $\mathscr{X}$), Hurwitz matrix $\boldsymbol{A}$ that satisfies (3.10), $\boldsymbol{g}$ that satisfies (3.4c), and the exogenous inputs satisfying (3.2b). If the condition*

$$\nu_x = |\lambda_A{}^*| - a_x L_x^g > 0, \quad a_x = a_A, \tag{3.11}$$

is met, then the equilibrium of (3.8a) is locally (or nonlocally) robustly stable and satisfy (3.3) over $\mathfrak{X}$ (or $\mathscr{X}$) with decaying rate ν_x, and constant a_x and (b_p, b_d, b_u) given as in (3.6c).

The finite dimensional approximation of the model of a tubular reactor is composed by two or more sets of ODEs, each of these sets corresponds to a state profile. These models can be written as interconnected subsystems composed by linear and nonlinear components. In what follows, two useful stability results for this class of system are introduced. The first one is an alternative form to use the integral bounds used in the proof of Lemma 3.1, while the second one gives conditions for the robust stability of the origin of two interconnected robustly stable subsystems of the form

$$\dot{\boldsymbol{x}}_1 = \boldsymbol{f}_1(\boldsymbol{x}_1) + \boldsymbol{g}_1(\boldsymbol{x}_1, \boldsymbol{x}_2; \tilde{\boldsymbol{p}}_1, \boldsymbol{d}_1, \boldsymbol{u}_1), \quad \boldsymbol{x}_1(0) = \boldsymbol{x}_{10}, \tag{3.12a}$$

$$\dot{\boldsymbol{x}}_2 = \boldsymbol{f}_2(\boldsymbol{x}_2) + \boldsymbol{g}_2(\boldsymbol{x}_1, \boldsymbol{x}_2; \tilde{\boldsymbol{p}}_2, \boldsymbol{d}_2, \boldsymbol{u}_2), \quad \boldsymbol{x}_1(0) = \boldsymbol{x}_{20}. \tag{3.12b}$$

Each nominal subsystem has its origin exponentially stable and each $\boldsymbol{g}_i$ is Lipschitz bounded with respect to its arguments as in (3.4c). Additionally, when $\boldsymbol{g}_1(\boldsymbol{x}_1, \boldsymbol{0}; \tilde{\boldsymbol{p}}_1, \boldsymbol{d}_1, \boldsymbol{u}_1)$ and $\boldsymbol{g}_2(\boldsymbol{0}, \boldsymbol{x}_2; \tilde{\boldsymbol{p}}_2, \boldsymbol{d}_2, \boldsymbol{u}_2)$ are at play, their origins remain robustly stable and satisfies (3.3) with parameters $\{(\zeta_j, a_{Pj})(\text{ or } \lambda_{A_j}{}^*, a_{Aj}), b_{pj}, b_{dj}, b_{uj}\}$, $j = 1, 2$, respectively. From the application of Corollary 3.2 (or 3.3), each subsystem satisfy

$$\nu_{xj} = \zeta_{xj} - a_{Pj} L_{x_j}^{g_j} > 0, \quad (\text{ or } \nu_{xj} = |\lambda_{A_j}{}^*| - a_{Aj} L_{x_j}^{g_j} > 0), \quad j = 1, 2. \tag{3.13}$$

The following lemma and theorem establish conditions for robust stability of the interconnected system with state $\boldsymbol{x} = \left[\boldsymbol{x}_1^T \; \boldsymbol{x}_2^T\right]^T$.

Lemma 3.2. *Proof in Section a.3.1 Inequalities* (a.2) *and* (3.3) *are, respectively, equivalent to the following differential inequalities:*

$$\|\boldsymbol{x}\| \leq \Xi, \quad \dot{\Xi} = -\nu_x \Xi + a_x \left(L_p^g \delta_p + L_d^g \varepsilon_d(t) + L_u^g \varepsilon_u\right), \quad \Xi(0) = a_x \|\boldsymbol{x}_0\|, \tag{3.14a}$$

$$\|\boldsymbol{x}\| \leq \Xi, \quad \dot{\Xi} \leq -\nu_x \Xi + a_x \left(L_p^g \delta_p + L_d^g \varepsilon_d^+ + L_u^g \varepsilon_u^+\right), \quad \Xi(0) = a_x \|\boldsymbol{x}_0\|. \tag{3.14b}$$

Note that from the inequalities in (3.14) and the use of the comparison lemma, the inequalities (a.2) and (3.3) can be obtained.

Proposition 3.1. ***ISS Small Gain Theorem for interconnections****. Proof in Section a.3.2 Consider the interconnected system* (3.12). *Assume that without the interconnection each subsystem is loacally (or not locally) exponentially stable in the nominal case, and each perturbed subsystem is locally (or nonlocally) robustly stable and satisfies* (3.13). *Then, the interconnection is locally (or not locally) robustly stable if*

$$\nu_{x1}\nu_{x2} - a_{x1}a_{x2}L_1^g L_2^g > 0, \tag{3.15}$$

and the state of the interconnection satisfies (3.3) *with parameters* λ_x, a_x *and* b_p, b_d *and* b_u.

The previous results are some of the theoretical tools that will be used to analyze the open and closed-loop stability properties of the tubular reactor model in finite or infinite dimension. These mathematical tools will be combined with physical insight to interpret within and engineering perspective the mechanisms at play in the tubular reactor dynamics. The gained insight will be exploited to design Control-Estimation Systems (CESs) for the considered class of tubular reactors.

3.2 EFFICIENT MODELING APPROACH FOR TUBULAR REACTORS

Industrial tubular reactors are stabilized with Single Input-Single Output (SISO) Proportional-Integral (PI) temperature control and monitored with data driven techniques [70; 121; 89; 100; 108]. Thus, the consideration of advanced early and late lumping CESs rises design-maintenance cost and reliability concerns because its implementation requires the on-line integration of a large number of nonlinear Ordinary Differential Equations (ODEs).

According to [22], on one hand, several lumping techniques for the modeling of tubular reactor with steady-state multiplicity have been used. For instance, global and local orthogonal collocation on finite elements for two-profile reactors, and local (from first to fourth order) Finite Differences (FD) for multiple-profile reactors. Usually, this methods requires moderate to large discretization orden N_{pde} and only reproduce local behaviors. On the other hand, the cell modeling approach [41; 40; 84]: (i) questions the use of a discretization order N_{pde} because it leads to unduly ill-conditioning and computational load by overmodeling in the light of parameter uncertainty and the breaking down of the pseudo-continuity assumption for the modeling of distributed reactors at particle and/or eddy scale, (ii) recommends as low order the reactor length-to-eddy/particle scale quotient, (iii) lacks criteria to preclude limit set alteration by overlumping, and (iv) has been recently supplemented with a procedure to choose the discretization order [22], by combining numerical continuation-based bifurcation [43; 87] and error propagation [69] analyses.

3.2.1 *Discrete lumped model*

The efficient modeling approach [22] recommends the use of a spatial discretization scheme with FD or finite element methods because the natural interaction between neighbor spatial locations of transport phenomena is retained. Accordingly, and without loss of generality, a lumped model is obtained next by the application of a FD scheme to the spatially distributed model (2.7).

The spatial coordinate $s \in [0, 1]$ is discretized over a homogeneous mesh $\mathcal{S}$ with size grid Δs, N interior points and two boundaries ones:

$$s_k \in \mathcal{S} = 0, \ldots, k\Delta s, \ldots, 1, \quad k = 1, \ldots, N+1, \quad \Delta s = \frac{1}{(N+1)}. \tag{3.16}$$

The approximation of the state profiles $\chi_1(s,t)$, $\chi_2(s,t)$ at the discretization points is given by the sequences $\chi_{j,k}$, $j = 1, 2$, $k = 0, \ldots, N+1$:

$$\chi_{j,k}(t) = \chi_j(s_k, t),\ j = 1, 2. \tag{3.17a}$$

are the corresponding discretized concentration and temperature steady-state profiles. The first and second spatial derivatives are approximated with first backward and second central finite differences, i. e.,

$$\partial_s \chi_j(s_k, t) \approx \frac{\chi_{j,k}(t) - \chi_{j,k-1}(t)}{\Delta s}, \quad \partial_s^2 \chi_j(s_k, t) \approx \frac{\chi_{j,k+1}(t) - 2\chi_{j,k}(t) + \chi_{j,k-1}(t)}{\Delta s^2}, \tag{3.17b}$$

with substitution of $\chi_{j,0}$ for $k = 1$ and $\chi_{j,N+1}$ for $k = N$ by using the boundary conditions, at $k = 0$ (or $k = N + 1$) first forward (or backward) FD were used.

To draw the lumped model, define the state variables $\boldsymbol{x}_j$, $j = 1, 2$ (with the origin shifted to the discretized target steady-state $\bar{\chi}$ for closed-loop operation), as well as the deviated (from nominal values $(\boldsymbol{d}, \boldsymbol{u})$) exogenous and control input vectors:

$$\boldsymbol{x}_j = \begin{bmatrix} \chi_{j,1} - \bar{\chi}_{j,1} \\ \vdots \\ \chi_{j,N} - \bar{\chi}_{j,N} \end{bmatrix}, \quad \boldsymbol{d} = \begin{bmatrix} \chi_{1,e} - \bar{\chi}_{1,e} \\ \chi_{2,e} - \bar{\chi}_{2,e} \end{bmatrix}, \quad \boldsymbol{u} = \begin{bmatrix} \tau_{c,1} - \bar{\tau}_{c,1} \\ \vdots \\ \tau_c - \bar{\tau}_c \end{bmatrix}.$$

The sensor location set, over the discretization mesh $\mathcal{S}$ can be redefined as

$$\varsigma = \{\varsigma_i = s_{m_i} \in \mathcal{R}_i \subset \mathcal{S}, \quad i = 1, \ldots, q\}, \tag{3.18a}$$

where $m_i \in \mathcal{R}_i$ are the mesh points in which temperature measurement are taken, and the jacket section intervals are redefined as

$$\mathcal{R}_i = \left[s_{\frac{(i-1)N}{q}+1}, s_{\frac{iN}{q}}\right), \, i = 1, \ldots, q-1, \quad \mathcal{R}_q = \left[s_{\frac{(q-i)N}{q}+1}, s_N\right]. \tag{3.18b}$$

Thus, the measured output vector is written as

$$\boldsymbol{y} = \begin{bmatrix} \chi_{2,m_1}(\varsigma_1, t) - \bar{\chi}_{2,m_1}(\varsigma_1, t) \\ \vdots \\ \chi_{2,m_q}(\varsigma_q, t) - \bar{\chi}_{2,m_q}(\varsigma_q, t) \end{bmatrix} = \begin{bmatrix} \chi_{2,m_1}(s_{m_1}, t) - \bar{\chi}_{2,m_1}(s_{m_1}, t) \\ \vdots \\ \chi_{2,m_q}(s_{m_q}, t) - \bar{\chi}_{2,m_q}(s_{m_k}, t) \end{bmatrix}.$$

Finally, the controlled output is given as

$$z = \chi_{2,N} - \bar{\chi}_{2,N}.$$

With the previous definitions, the lumped reactor dynamics in state-space form are

$$\dot{\boldsymbol{x}}_1 = \boldsymbol{A}_1\boldsymbol{x}_1 - \boldsymbol{\psi}(\boldsymbol{x}_1, \boldsymbol{x}_2) + \boldsymbol{B}_{d,1}d_1, \qquad \boldsymbol{x}_1(0) = \boldsymbol{x}_{10}, \tag{3.19a}$$
$$\dot{\boldsymbol{x}}_2 = \boldsymbol{A}_2\boldsymbol{x}_2 + \boldsymbol{\psi}(\boldsymbol{x}_1, \boldsymbol{x}_2) + \boldsymbol{B}_{d,2}d_2 + \boldsymbol{B}_{u,2}\boldsymbol{u}, \qquad \boldsymbol{x}_2(0) = \boldsymbol{x}_{20}, \tag{3.19b}$$
$$\boldsymbol{y} = \boldsymbol{C}_{y,2}\boldsymbol{x}_2, \quad z = \boldsymbol{C}_{z,1}\boldsymbol{x}_1. \tag{3.19c}$$

The states of the systems evolve in the sets $\boldsymbol{x}_j \in X_j$, $j = 1, 2$ where each X_j is a bounded and compact set in the euclidian space $\mathbb{R}^N$. Each component of the control input vector is defined in the bounded set U, and the exogenous input vector $\boldsymbol{d}$ is defined also in a bounded and compact set D.

The system and boundary condition matrices are

$$\boldsymbol{A}_j = \begin{bmatrix} -\mathrm{d}_j & \mathrm{c}_j & & & & & & & & & \\ \mathrm{b}_j & -\mathrm{a}_j & \mathrm{c}_j & & & & & & & & \\ & \mathrm{b}_j & \ddots & \ddots & & & & & & & \\ & & \ddots & \ddots & \mathrm{c}_j & & & & & & \\ & & & \mathrm{b}_j & \mathrm{a}_j & \mathrm{c}_j & & & & & \\ & & & & \mathrm{b}_j & \mathrm{a}_j & \mathrm{c}_j & & & & \\ & & & & & \mathrm{b}_j & \mathrm{a}_j & \mathrm{c}_j & & & \\ & & & & & & \mathrm{b}_j & \ddots & \ddots & & \\ & & & & & & & \ddots & \ddots & \mathrm{c}_j & \\ & & & & & & & & \mathrm{b}_j & -\mathrm{a}_j & \mathrm{c}_j \\ & & & & & & & & & \mathrm{b}_j & -\mathrm{d}_j \end{bmatrix}, \quad \boldsymbol{B}_{d,j} = \begin{bmatrix} \frac{1}{\Delta s} \\ 0 \\ \vdots \\ 0 \end{bmatrix},$$

for $j = 1, 2$ with entries defined as

$$\begin{aligned} \mathrm{a}_1 &= -\frac{2 + Pe_m \Delta s}{Pe_m \Delta s^2}, & \mathrm{b}_1 &= \frac{1 + Pe_m \Delta_s}{Pe_m \Delta s^2}, & \mathrm{c}_1 &= \frac{1}{Pe_m \Delta s^2}, & \mathrm{d}_1 &= \mathrm{a}_1 + \mathrm{c}_1, \\ \mathrm{a}_2 &= -\frac{2 + Pe_h \Delta s + Pe_h v \Delta s^2}{Pe_h \Delta s^2}, & \mathrm{b}_2 &= \frac{1 + Pe_h \Delta_s}{Pe_h \Delta s^2}, & \mathrm{c}_2 &= \frac{1}{Pe_h \Delta s^2}, & \mathrm{d}_2 &= \mathrm{a}_2 + \mathrm{c}_2. \end{aligned}$$

The nonlinear function and its entries are

$$\boldsymbol{\psi}(\boldsymbol{x}_1, \boldsymbol{x}_2) = \begin{bmatrix} \psi_1(\boldsymbol{x}_{1,1}, \boldsymbol{x}_{2,1}) \\ \vdots \\ \psi_N(\boldsymbol{x}_{1,N}, \boldsymbol{x}_{2,N}) \end{bmatrix} = \begin{bmatrix} r(\boldsymbol{x}_{1,1} + \bar{\chi}_{1,1}, \boldsymbol{x}_{2,1} + \bar{\chi}_{2,1}) - r(\bar{\chi}_{1,1}, \bar{\chi}_{2,1}) \\ \vdots \\ r(\boldsymbol{x}_{1,N} + \bar{\chi}_{1,N}, \boldsymbol{x}_{2,N} + \bar{\chi}_{2,N}) - r(\bar{\chi}_{1,N}, \bar{\chi}_{2,N}) \end{bmatrix} \tag{3.20}$$

for $k = 1, \dots, N$. The input and output matrices are

$$\boldsymbol{B}_{u,2} = v \begin{bmatrix} \boldsymbol{b}_1 & \dots & \boldsymbol{b}_q \end{bmatrix}, \quad \boldsymbol{C}_{y,2} = \begin{bmatrix} \boldsymbol{c}_1 \\ \vdots \\ \boldsymbol{c}_q \end{bmatrix}, \quad \boldsymbol{C}_{z,1} = \begin{bmatrix} 0 & \dots & 0 & 1 \end{bmatrix},$$

where $\boldsymbol{b}_i \in \mathbb{R}^{1,N}$, and $\boldsymbol{c}_i \in \mathbb{R}^{N,1}$ are column and row vectors, respectively, defined as

$$\boldsymbol{b}_i = \begin{cases} 1 & \text{if } s_k \in \mathcal{R}_i \\ 0 & \text{else} \end{cases}, \quad \boldsymbol{c}_i = \begin{cases} 1 & \text{if } s_k = s_{,i} \\ 0 & \text{else} \end{cases}, \quad k = 1, \dots, N, \quad i = 1, \dots, q.$$

The following assumption is considered for the lumped nonlinear function $\boldsymbol{\psi}$.

Assumption 3.1. *The reaction rate function $\boldsymbol{\psi}$ is assumed to be monotonically increasing with respect to the concentration vector $\boldsymbol{x}_1$, it vanishes only at the origin and satisfies a Lipschitz bounding condition i.e.,*

$$\boldsymbol{\psi}(\mathbf{0},\mathbf{0}) = \mathbf{0}, \quad \|\boldsymbol{\psi}(\boldsymbol{x}_1,\boldsymbol{x}_2)\| \leq L^{\psi}_{x_1}\|\boldsymbol{x}_1\| + L^{\psi}_{x_2}\|\boldsymbol{x}\|_2\,, \tag{3.21}$$

where $L^{\psi}_{x_j}$, $j = 1, 2$ are local Lipschitz constants that depend on the state-space in which model (3.19) is defined, and $\|(\cdot)\|$ is the euclidian norm in the space X_j.

In compact form, the reactor dynamics can be written as

$$\dot{\boldsymbol{x}} = \boldsymbol{A}\boldsymbol{x} + \boldsymbol{B}_d\boldsymbol{d} + \boldsymbol{\Psi}(\boldsymbol{x}) + \boldsymbol{B}_u\boldsymbol{u}, \quad \boldsymbol{x}(0) = \boldsymbol{x}_0, \tag{3.22a}$$

$$\boldsymbol{y} = \boldsymbol{C}_y\boldsymbol{x}, \quad z = \boldsymbol{C}_z\boldsymbol{x}, \quad \chi_N = \boldsymbol{\mathcal{I}}(\boldsymbol{x}), \tag{3.22b}$$

where $\boldsymbol{x} = \begin{bmatrix}\boldsymbol{x}_1 & \boldsymbol{x}_2\end{bmatrix}^T \in \mathbb{R}^{2N}$ is the state, and χ_N is an approximated profile pair computed through the interpolation scheme $\boldsymbol{\mathcal{I}}$. The related matrices are

$$\boldsymbol{A} = \begin{bmatrix}\boldsymbol{A}_1 & \mathbf{0}\\ \mathbf{0} & \boldsymbol{A}_2\end{bmatrix}, \quad \boldsymbol{B}_u = \begin{bmatrix}\mathbf{0}\\ \boldsymbol{B}_{u,2}\end{bmatrix}, \quad \boldsymbol{C}_y = \begin{bmatrix}\mathbf{0} & \boldsymbol{C}_{y,2}\end{bmatrix}, \quad \boldsymbol{C}_z = \begin{bmatrix}\boldsymbol{C}_{z,1} & \mathbf{0}\end{bmatrix}, \quad \boldsymbol{B}_d = \begin{bmatrix}\boldsymbol{B}_{d,1}\\ \boldsymbol{B}_{d,2}\end{bmatrix},$$

and the nonlinear function is defined as $\mathbf{Psi}(\boldsymbol{x}) = \begin{bmatrix}-\boldsymbol{\psi}(\boldsymbol{x}_1,\boldsymbol{x}_2) & \boldsymbol{\psi}(\boldsymbol{x}_2,\boldsymbol{x}_2)\end{bmatrix}^T$.

For given initial state-input data $(\boldsymbol{x}_0, \boldsymbol{d}(t), \boldsymbol{u}(t))$, the ODE model (3.22) has a unique solution motion $\boldsymbol{x}$ with unique output signal $\boldsymbol{y}$, i.e.,

$$\boldsymbol{x}(t) = \mathrm{t}_x(t, \boldsymbol{x}_0, \boldsymbol{d}, \boldsymbol{u}), \quad \boldsymbol{y}(t) = \boldsymbol{C}_y\mathrm{t}_\chi(t, x0, \boldsymbol{d}, \boldsymbol{u}).$$

For vanishing input trajectories $(\boldsymbol{d}(t), \boldsymbol{u}(t))$, the motion $\boldsymbol{x}$ reaches exponentially a stable steady-state $\bar{\boldsymbol{x}}$ or a limit cycle $\bar{\boldsymbol{x}}(t)$, i.e.,

$$(\boldsymbol{d}(t), \boldsymbol{u}(t)) \to (\mathbf{0},\mathbf{0}), \quad \boldsymbol{x}_0 \notin \mathbb{S} = \mathbb{S}_s \cup \mathbb{S}_l \;\Rightarrow\; \boldsymbol{x}(t) \to \bar{\boldsymbol{x}} \in S_s \text{ or } \bar{\boldsymbol{x}}(t) \in S_l$$

where $\mathbb{S}_s$ (or $\mathbb{S}_l$) is the set of n_s (or n_l) steady-states (or limit cycles) (the origin $\boldsymbol{x} = 0$ is included in the set $\mathbb{S}_s$):

$$\mathbb{S}_s = \{\bar{\boldsymbol{x}}_1, \ldots, \bar{\boldsymbol{x}}_{n_s}\}\,, \quad \mathbb{S}_l = \{\bar{\boldsymbol{x}}_1(t), \ldots, \bar{\boldsymbol{x}}_{n_l}(t)\}\,. \tag{3.23}$$

By the convergence of the FD discretization scheme (3.16) [86], as $N \to \infty$ the state motion χ_N (or the limit set $\mathbb{S}$) of the lumped model (3.19) becomes, in the sense of the L^2 (or a suitable set) norm, the one of the distributed model:

$$\lim_{N\to\infty} \chi_N(t) = \chi(t), \quad (\text{or } \lim_{N\to\infty} \mathbb{S} = \mathscr{S}). \tag{3.24}$$

3.2.2 *Discretization order selection procedure*

The efficient modeling approach for tubular reactors is a systematic procedure to select the discretization order of a lumped model that approximates the dynamic behavior of a PDE model of interest, and overcomes unduly computational load. The aim is to determine the smallest integer N that ensures a robust (with respect to discretization order) quantitative description, up to kinetics-transport parameter uncertainty. The detailed algorithm is in [22] and here an adapted version (for the class of tubular reactors at hand) is briefly described.

The method compares two set metrics to determine the discretization order of (3.22): (i) the parametric error ε_p, computed with the transient and static responses of the reference model (3.22) with N_{pde} and typical parameter uncertainty $\tilde{\boldsymbol{p}}$, and (ii) the discretization error ε_d computed with nominal parameters $\boldsymbol{p}$ and for $N \in (N^-, N_{pde})$. The algorithm start at N^- where spurious static behavior is avoided and stops at N_e where the discretization error is comparable with the parametric one, i.e., $\varepsilon_p \approx \varepsilon_d$. The complete algorithm is presented in detail next.

As in [22], define the discretization order interval

$$\mathcal{N} = [N^-, \ldots, N_{pde}], \quad N^* + 1, \tag{3.25}$$

where the model (3.22) is structurally stable over $\mathcal{N}$ [79], in the sense that $\mathbb{S}$ is topologically invariant with respect to order change in $\mathcal{N}$. The order N_{pde} (from 100 to 400 for the considered reactor class) is the one of a standard FD PDE solver, the order N^- is determined by the ultimate bifurcation order N^*. Denote by

$$\hat{\mathbb{S}} \approx \mathbb{S}(N, \boldsymbol{p}), \quad N \in \mathcal{N}, \tag{3.26}$$

the numerically computed limit set $\mathbb{S}$, and define the sizes (in suitable norm) of: (i) the parameter error (induced in $\mathbb{S}$ by typical transport-kinetics parameter errors $\tilde{\boldsymbol{p}}$)

$$\epsilon_p(N_{pde}, \tilde{\boldsymbol{p}}) = \left\|\hat{\mathbb{S}}(N_{pde}, \boldsymbol{p} + \tilde{\boldsymbol{p}}, t) - \hat{\mathbb{S}}(N_{pde}, \boldsymbol{p}, t)\right\|_{\mathbb{S}}, \quad \epsilon_p(N_{pde}, \mathbf{0}) = 0, \tag{3.27a}$$

and (ii) the N_{pde}-to-N discretization error (with parameter $\boldsymbol{p}$)

$$\varepsilon_d(N, N_{pde}) = \left\|\hat{\mathbb{S}}(N, \boldsymbol{p}, t) - \hat{\mathbb{S}}(N_{pde}, \boldsymbol{p}, t)\right\|_{S}, \quad \epsilon_d(N_{pde}, N_{pde}) = 0, \tag{3.27b}$$

of the N_{pde}-to-N discretization error with nominal parameter $\boldsymbol{p}$. The norm set $\|(\cdot)\|_{\mathbb{S}}$ measures de distance between limit sets (see Appendix b).

Definition 3.2. *Discretization order [22]*
The efficient discretization order is the least integer N that satisfies

$$N_e = \min_{N \in \mathcal{N}} \ni \varepsilon_d(N, N_{pde}) \approx\lessapprox \varepsilon_p(N_{pde}, \tilde{\boldsymbol{p}}), \quad N_e \in \mathcal{N} \tag{3.28}$$

where the discretization error size is less or comparable with the parametric error size.

According to [22], the efficient discretization order N_e (3.28) is computed by the following algorithm: (i) the parametric error line (in the discretization-error plane $\mathscr{E}$: $N vs \varepsilon$)

$$\mathscr{C}_d = \left\{(N, \epsilon) \in \mathscr{E} \,|\, \epsilon = \epsilon_d(N, N_{pde})\right\}, \tag{3.29a}$$

build with error propagation analysis, (ii) the parametric error curve

$$\mathscr{C}_p = \left\{(N, \epsilon) \in \mathscr{E} \,|\, \epsilon = \epsilon_p(N_{pde}, \tilde{\boldsymbol{p}})\right\} \tag{3.29b}$$

computed with N-continuation from $N = 1$, (iii) the reliable discretization order

$$N^- > N^* + 1 \tag{3.29c}$$

on the basis of the N-bifurcation graph (3.26), (iv) the efficient discretization order N_e(3.28) from the intersection

$$[N_e, \epsilon_p(N_{pde}, \tilde{\boldsymbol{p}})] = \mathscr{C}_p \cap \mathscr{C}_d \subset \mathscr{E} = \mathcal{N} \times \mathbb{R}, \tag{3.29d}$$

of the curve $\mathscr{C}_d$ (3.29a) with the line $\mathscr{C}_p$ (3.29b), and (v) the corresponding ODE model dimension

$$n_e = 2N_e \tag{3.29e}$$

since the state of the discretized models use n_e ODEs for each state profile (concentration and temperature).

The preceding computationally intensive determination of the efficient discretization order N_e, which includes PDE solver-like high order N_{pde}, is part of the *a priori* (before implementation) stage of the proposed CES design methodology. The efficient discretization order N_e will be employed in: (i) the off-lime determination of the sensor locations and control limits of Chapter 4, and (ii) the online implementation of the proposed CESs of Chapter 4 and Chapter 5.

3.2.3 *Application to the case study*

The application ot the procedure Section 3.2.2 to the case study defined in Section 2.5 yields the efficient ODE discretization order

$$N_e = 20 \ni [N_e, \epsilon_p(N_{pde}, \tilde{\boldsymbol{p}})] = \mathscr{C}_d \cap \mathscr{C}_p, \tag{3.30}$$

determined, as shown in Figure 3.1, by the intersection (3.28), in the order-error plane $\mathscr{E}$, of the error discretization curve $\mathscr{C}_d$ (3.29a) with parametric line $\mathscr{C}_p$ (3.29b). The errors sizes ϵ_d and ϵ_p were computed with the open-loop response to the deviated initial state $(\chi_{10}, \bar{\chi}_{20}) = (0.9\bar{\chi}_{1,N}, 1.5\bar{\chi}_{2,N})$.

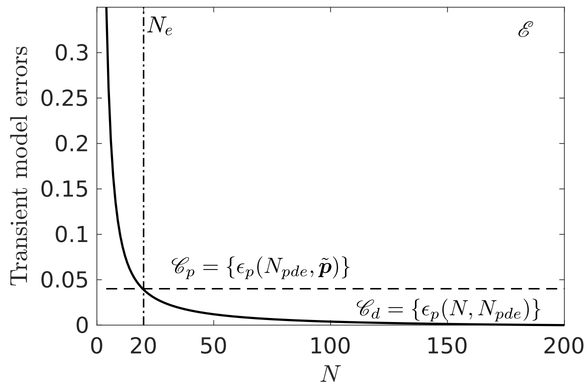

Figure 3.1: Determination of the efficient discretization order $N_e = 20$ by the intersection of the curve $\mathscr{C}_d$ (3.29a) with parametric error line $\mathscr{C}_p$ (3.29b).

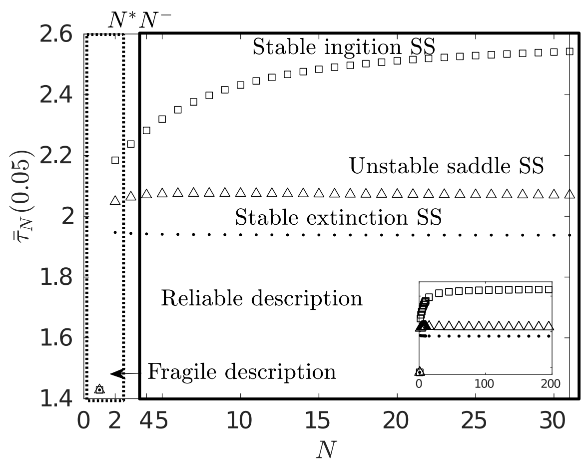

Figure 3.2: Open-loop bifurcation diagram (steady-state temperature $\bar{\tau}_N(0.1)$ vs N) $\hat{\mathbb{S}}(N, \boldsymbol{p}) = \mathbb{S}_s(N, \boldsymbol{p})$ (3.23): (i) interval $\mathcal{N} = [4, \ldots, 30]$ of robust bistability, (ii) bifurcation order $N^* = 3$, and (iii) interval [1,2] of spurious monostability.

In Figure 3.2 is presented the limit set bifurcation graph $\hat{\mathbb{S}}$ associated with the execution of Step 2 in Section 3.2.2, showing that the efficient discretization order N_e of Figure 3.1 is in the interval $\mathcal{N}$ (3.25) where the lumped model (3.22) with order N is robust with respect to order change, i. e.,

$$N_e = 20 \in \mathcal{N} = [N^-, \ldots, N_{pde}], \quad N^- = N^* + 1 = 4, \quad N^*, \quad N_{pde} = 200, \quad (3.31)$$

where $N^* = 3$ is the bifurcation order, in the sense that the discretization order is robustly (structurally stable) mono (or bi) stable for $N >$ (or $<$) N^*, with order change from $N^* = 3$ to $N^* - 1 = 2$ the model becomes monostable: the stable ignition-unstable steady-state pair $\{\bar{\chi}_N, \bar{\chi}_{N,I}\}$ vanishes while the stable extinction $\bar{\chi}_{N,E}$ remains.

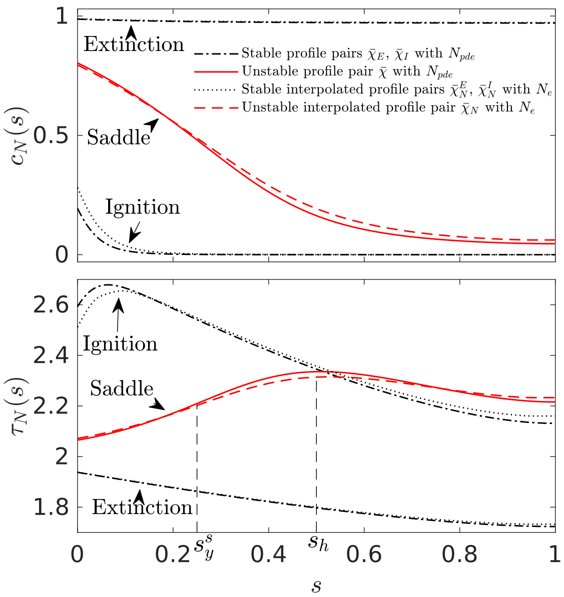

Figure 3.3: Stable (black plots) and unstable (dashed red plots) concentration (c_N) and temperature (τ_N) interpolated steady-state profile pairs $\bar{\chi}_N = \mathcal{I}(\bar{x})$ computed with FD PDE solver ($N = N_{pde} = 200$) (dashed-dotted lines for stable profiles and continuous lines for the unstable one) and efficient ($N = N_e = 20$) (dotted lines for the stable profiles and dashed lines for the unstable one) order. The stable

Accordingly, the reactor model (3.22) is of dimension $n_r = 2N_e = 40$ and is discretized over a mesh (3.16) with 20 equidistant interior points with discretization size step of $\Delta s = \frac{1}{N_e+1} = \frac{1}{21}$. The three steady-states of the efficient model, (3.22) with order $N_e = 20$, are presented in Figure 3.3 , including comparison against the steady-state profiles obtained (Figure 2.3) with PDE solver-like order $N_{pde} = 200$.

The previous results indicates that the off-line developments of Chapter 4 will be done using an efficient low dimensional model, ($N_r = 40$) that overcomes: (i) the low computational load of a large dimensional one (using $N_{pde} = 200$ of standard FD-based PDE solvers), and (ii) the inherent ill-conditioning of low dimensional models (obtained with orthogonal collocations or finite elements). Furthermore, the on-line implementations of the designed CESs on Chapter 4 and Chapter 5 will be performed on the basis of a low order model avoiding on-line computational load.

3.3 SUMMARY

In this chapter, the robust stability concept that will be employed for stability analysis on finite and infinite dimensions has been introduced. Also, the efficient modeling approach developed in [22] has been introduced and adapted to class of tubular reactor on the study to obtain an efficient lumping scheme.

The stability concept that has been introduces, and called robust stability, is the one of practical stability in an ISS framework: a system that has the robust stability property posses, under nominal conditions, an exponentially stable origin, and in the presence of parameter and modeling bounded errors, and exogenous fluctuating bounded inputs, the system has its state ultimately bounded with bounding size depending on the size of the exponential rate of convergence of the nominal system, and the size of the disturbances. The robust stability property was technically stated and useful lemmas and theorems were established. This set of mathematical tools will be employed along the rest of the study to characterize (or determine) open-loop (or closed-loop) stability properties.

The considered efficient modeling approach and the related numerical procedure were described. This algorithm yields a tubular reactor lumped model, that can be used for early lumping design or late lumping implementation, that captures the main dynamic behavior and physical properties of the distributed model and avoids computational burden while ensuring the preclusion of spurious static and dynamic behaviors. This method will be of great importance for the remaining of the present study since it will enable the off-line developments of Chapter 4 for the construction of a computationally efficient CES, and the on-line implementations of the two proposed CESs designed in Chapter 4 and Chapter 5.

Part II

EARLY LUMPING APPROACH

In this part of the thesis work, a control-estimation system is designed by employing an early lumping approach. First, the so-called efficient modeling approach is used to obtain a low order finite-difference lumped model for control-estimation design and implementation purposes. On the basis of this model, an advanced constrained control-estimation system is build on the basis of two solvability properties characterized in terms of the number of sensors and their locations: passivity and closed-loop detectability. The closed-loop stability is established with small gains arguments, in terms of sensor locations, control limits and gains. At the implementation step, the control-estimation system is realized as a set of decentralized PI controllers with antiwindup protection and a decoupled observer for the estimation task. The efficiency and robustness of the control-estimation algorithm is assessed by an extensive simulation study.

4

CONTROL-ESTIMATION SYSTEM DESIGN: EARLY LUMPING APPROACH

In this chapter the solution to the joint Control-Estimation (CE) problem delineated in Part i and stated in Chapter 2 (Section 2.3) is solved within an early lumping approach by using the efficiently discretized lumped model (3.22) (Section 3.2.1) with model order $n_e = 2N_e$ (3.28) (Section 3.2.2) delineated in Section 3.2.

Using an application-oriented perspective, a Control-Estimation System (CES) will be constructed as the combination of a passive saturated state feedback controller and a geometric estimator, with passivity and closed-loop detectability as solvability conditions. Then through model redesign this CES will be realized as a decoupled Proportional-Integral (PI) controller with back-calculation type Anti-Windup (AW) protector and a closed-loop pointwise-like estimator driven by point measurements. The design will be accompanied with robust stability assurance, and criteria for the selection of sensor-actuator configuration, sensor locations and control limits.

4.1 EARLY LUMPING CONTROL-ESTIMATION PROBLEM SETTING

Applying the efficient modeling approach presented in Section 3.2, the corresponding state space model in deviation form from the target (open-loop unstable) steady-state for closed-loop operation is given as

$$\dot{\boldsymbol{x}}_1 = \boldsymbol{A}_1\boldsymbol{x}_1 - \boldsymbol{\psi}(\boldsymbol{x}_1, \boldsymbol{x}_2) + \boldsymbol{B}_{d,1}d_1, \qquad \boldsymbol{x}_1(0) = \boldsymbol{x}_{10}, \tag{4.1a}$$

$$\dot{\boldsymbol{x}}_2 = \boldsymbol{A}_2\boldsymbol{x}_2 + \boldsymbol{\psi}(\boldsymbol{x}_1, \boldsymbol{x}_2) + \boldsymbol{B}_{d,2}d_2 + \boldsymbol{B}_{u,2}\boldsymbol{u}, \qquad \boldsymbol{x}_2(0) = \boldsymbol{x}_{20}, \tag{4.1b}$$

$$\boldsymbol{y} = \boldsymbol{C}_{y,2}\boldsymbol{x}_2, \quad z = \boldsymbol{C}_{z,1}\boldsymbol{x}_1, \quad \chi_n = \boldsymbol{\mathcal{I}}(\boldsymbol{x}_1, \boldsymbol{x}_2), \tag{4.1c}$$

with states $\boldsymbol{x}_j \in X_j$, $j = 1, 2$ in the bounded and compact sets, exogenous inputs d_j, $j = 1, 2$, control input $\boldsymbol{u}$, with bounded entries $u_i \in U$, measured $\boldsymbol{y}$ and controlled z outputs, and approximated concentration-temperature profiles $\boldsymbol{\mathcal{I}}$.

Considering that all mathematical models are only approximation from real physical phenomena, the model mismatch between reality and a Ordinary Differential Equation (ODE) used for modeling purposes can be represented with a parasitic dynamics coupled with the mathematical model. These parasitic dynamics accounts for: (i) fast unmodeled dynamics, due to assumptions made for model simplification, such as eddy, turbulence and radiation phenomena, (ii) approximation error due to lumping,

and (iii) noise-like sensor and actuator errors. Accordingly, the *lumped actual reactor model*, written in compact form,is given as

$$\dot{\boldsymbol{x}} = \boldsymbol{A}\boldsymbol{x} + \boldsymbol{G}\boldsymbol{\psi}(\boldsymbol{x}) + \boldsymbol{B}_d\boldsymbol{d} + \boldsymbol{B}_u\boldsymbol{u} + \boldsymbol{e}(\boldsymbol{x},\boldsymbol{d},\boldsymbol{u};\boldsymbol{\pi},\tilde{\boldsymbol{p}}), \qquad \boldsymbol{x}(0) = \boldsymbol{x}_0, \tag{4.2a}$$

$$\dot{\boldsymbol{\pi}} = \boldsymbol{\Pi}(\boldsymbol{x},\boldsymbol{d},\boldsymbol{u};\boldsymbol{\pi},\boldsymbol{w}), \qquad \boldsymbol{\pi}(0) = \boldsymbol{\pi}_0, \tag{4.2b}$$

$$\boldsymbol{y} = \boldsymbol{C}_y\boldsymbol{x} + \tilde{\boldsymbol{h}}_y(\boldsymbol{\pi}), \quad z = \boldsymbol{C}_z\boldsymbol{x} + \tilde{\boldsymbol{h}}_z(\boldsymbol{\pi}), \quad \chi_N = \mathcal{J}(\boldsymbol{x}), \tag{4.2c}$$

where ($\boldsymbol{I}_{a\times b}$ (or $\boldsymbol{0}_{a\times b}$) is an identity (or a zero) matrix of dimension $a \times b$)

$$\boldsymbol{A} = \begin{bmatrix} \boldsymbol{A}_1 & \boldsymbol{0}_{N_e\times N_e} \\ \boldsymbol{0}_{N_e\times N_e} & \boldsymbol{A}_2 \end{bmatrix}, \quad \boldsymbol{G} = \begin{bmatrix} \boldsymbol{I}_{N_e\times N_e} \\ -\boldsymbol{I}_{N_e\times N_e} \end{bmatrix}, \quad \boldsymbol{B}_u = \begin{bmatrix} \boldsymbol{0}_{N_e\times q} \\ \boldsymbol{B}_{u,2} \end{bmatrix}, \quad \boldsymbol{B}_d = \begin{bmatrix} \boldsymbol{B}_{d,1} \\ \boldsymbol{B}_{d,2} \end{bmatrix},$$

$$\boldsymbol{C}_y = \begin{bmatrix} \boldsymbol{0}_{q\times N_e} & \boldsymbol{C}_{y,2} \end{bmatrix}, \quad \boldsymbol{C}_z = \begin{bmatrix} \boldsymbol{C}_{z,1} & \boldsymbol{0}_{1\times N_e} \end{bmatrix}.$$

The parasitic dynamics (4.2b), with state $\boldsymbol{\pi}$ and excited by the fluctuating input $\boldsymbol{w}$, are: (i) assumed robustly stable in the sense of Definition 3.1, i. e., they satisfy a bound of the type (3.3) which can be written in differential form by using Lemma 3.2:

$$\|\boldsymbol{\pi}(t)\| \leq s_\pi(t) : \dot{s}_\pi = -\lambda_\pi s_\pi + l_w^\Pi \varepsilon_w(t), \quad s_\pi(0) = s_x(0) = a_\pi \|\boldsymbol{\pi}_0\|, \tag{4.3}$$

and (ii) coupled to the reactor dynamics by the term $\boldsymbol{e}$, $\boldsymbol{h}_y$ and $\boldsymbol{h}_z$.

The CE problem treated in this chapter, is to design the CES (2.11), so that the closed-loop system, the application of (2.11) with saturated entry-wise control component (i. e., $u_i \in U_c \subset U$) to the actual reactor dynamics (4.2), is robustly stable. Note that the control set $U_c \subset U$ is a degree of freedom. The design will be performed within the early lumping approach, based on the nominal model (4.1) and the stability and control functioning assessment will be performed with model (4.2).

4.2 OPEN-LOOP DYNAMICS

Here, the open-loop dynamics of the discrete reactor model (4.1) are analyzed with emphasis on the understanding and identification, within a physical and engineering perspective, of the main dynamic mechanism that contribute to the stabilization or destabilization of the reactor dynamics around each steady-state. First the steady-state multiplicity is characterized with bifurcation analysis, then the open-loop dynamics are studied as the interconnection of two Lur'e subsystems, finally the zero dynamics are characterized in the normal form and in original coordinate.

4.2.1 *Partitioned coordinate*

For the upcoming theoretical developments, a state partition useful for static and zero dynamics analyses is introduced next. First, the dynamics are described in this coordinate and then the related statics are analyzed through bifurcation analysis that yields a useful method to analyze high dimensional statics.

4.2.1.1 *Partitioned dynamics*

Consider, the Multiple Input Multiple Output (MIMO) system (4.1), the next transformation accommodates the temperature state in not measured-measured coordinate:

$$\begin{bmatrix} \boldsymbol{x}_{2,n} \\ \boldsymbol{x}_{2,m} \end{bmatrix} = \begin{bmatrix} \boldsymbol{C}_n \\ \boldsymbol{C}_{y,2} \end{bmatrix} \boldsymbol{x}_2, \quad \boldsymbol{x}_2 = \begin{bmatrix} \boldsymbol{C}_n^T & \boldsymbol{C}_{y,2}^T \end{bmatrix} \begin{bmatrix} \boldsymbol{x}_{2,n} \\ \boldsymbol{x}_{2,m} \end{bmatrix} = \boldsymbol{C}_n^T \boldsymbol{x}_{2,n} + \boldsymbol{C}_{y,2}^T \boldsymbol{x}_{2,m}, \quad \boldsymbol{M} = \begin{bmatrix} \boldsymbol{C}_n \\ \boldsymbol{C}_{y,2} \end{bmatrix},$$

where $\boldsymbol{x}_{2,n} \in \mathbb{R}^q$ (or $\boldsymbol{x}_{2,m} \in \mathbb{R}^{N-q}$)is the unmeasured (or measured) state. The square matrix $\boldsymbol{M} \in \mathbb{R}^N$ is an identity permutation matrix that satisfies $\boldsymbol{M}^{-1} = \boldsymbol{M}^T$.

Considering the above state partition, the reactor dynamics are written as

$$\begin{aligned}
\dot{\boldsymbol{x}}_1 &= \boldsymbol{A}_1 \boldsymbol{x}_1 + \boldsymbol{B}_{d,1} d_1 - \boldsymbol{\psi}_{n,m}(\boldsymbol{x}_1, \boldsymbol{x}_{2,n}, \boldsymbol{x}_{2,m}), & \boldsymbol{x}_1(0) &= \boldsymbol{x}_{10}, && \text{(4.4a)}\\
\dot{\boldsymbol{x}}_{2,n} &= \boldsymbol{A}_2^{n,n} \boldsymbol{x}_{2,n} + \boldsymbol{A}_2^{n,m} \boldsymbol{x}_{2,m} + \boldsymbol{B}_{d,2}^n d_2 + \boldsymbol{\psi}_n(\boldsymbol{x}_1, \boldsymbol{x}_{2,n}) + \boldsymbol{B}_{u,2}^n \boldsymbol{u}, & \boldsymbol{x}_{2,n}(0) &= \boldsymbol{x}_{2n0}, && \text{(4.4b)}\\
\dot{\boldsymbol{x}}_{2,m} &= \boldsymbol{A}_2^{m,m} \boldsymbol{x}_{2,m} + \boldsymbol{A}_2^{m,n} \boldsymbol{x}_{2,n} + \boldsymbol{B}_{d,2}^m d_2 + \boldsymbol{\psi}_m(\boldsymbol{x}_1, \boldsymbol{x}_{2,m}) + \boldsymbol{B}_{u,2}^m \boldsymbol{u}, & \boldsymbol{x}_{2,m}(0) &= \boldsymbol{x}_{2m0}, && \text{(4.4c)}\\
\boldsymbol{y} &= \boldsymbol{x}_{2,m}, \quad z = \boldsymbol{C}_{z,1} \boldsymbol{x}_1, &&&& \text{(4.4d)}
\end{aligned}$$

where the involved matrices $\boldsymbol{A}_2^{m,m} \in \mathbb{R}^{q,q}$, $\boldsymbol{A}_2^{m,n} \in \mathbb{R}^{q,N-q}$, $\boldsymbol{A}_2^{n,n} \in \mathbb{R}^{N-q,N-q}$, $\boldsymbol{A}_2^{n,m} \in \mathbb{R}^{N-q,q}$, $\boldsymbol{B}_{d,2}^m \in \mathbb{R}^q$, $\boldsymbol{B}_{d,2}^n \in \mathbb{R}^{N-q}$, $\boldsymbol{B}_{u,2}^m \in \mathbb{R}^{q,q}$, $\boldsymbol{B}_{u,2}^n \in \mathbb{R}^{N-q,q}$ are defined as

$$\begin{aligned}
&\boldsymbol{A}_2^{m,m} = \boldsymbol{C}_{y,2} \boldsymbol{A}_2 \boldsymbol{C}_{y,2}^T, \quad \boldsymbol{A}_2^{m,n} = \boldsymbol{C}_{y,2} \boldsymbol{A}_2 \boldsymbol{C}_n^T, \quad \boldsymbol{A}_2^{n,n} = \boldsymbol{C}_n \boldsymbol{A}_2 \boldsymbol{C}_n^T, \quad \boldsymbol{A}_2^{n,m} = \boldsymbol{C}_n \boldsymbol{A}_2 \boldsymbol{C}_{y,2}^T,\\
&\boldsymbol{B}_{d,2}^m = \boldsymbol{C}_{y,2} \boldsymbol{B}_{d,2}, \quad \boldsymbol{B}_{u,2}^m = \boldsymbol{C}_{y,2} \boldsymbol{B}_{u,2}, \quad \boldsymbol{B}_{d,2}^n = \boldsymbol{C}_n \boldsymbol{B}_{d,2}, \quad \boldsymbol{B}_{u,2}^n = \boldsymbol{C}_n \boldsymbol{B}_{u,2}.
\end{aligned}$$

Specifically, the control input matrices $\boldsymbol{B}_{u,2}^m$ and $\boldsymbol{B}_{u,2}^n$ are defined as

$$\boldsymbol{B}_{u,2}^m = v \boldsymbol{I}_{q \times q}, \quad \boldsymbol{B}_{u,2}^n = v \begin{bmatrix} \boldsymbol{b}_1^n & \dots & \boldsymbol{b}_q^n \end{bmatrix}, \quad \boldsymbol{b}_i^n = \begin{cases} 1 & \text{if } s_k \in \mathcal{R}_i \\ 0 & \text{else} \end{cases}, \tag{4.4e}$$

for $k = 1, \dots, N-q, \quad i = 1, \dots, q$ and $\boldsymbol{b}_i^n \in \mathbb{R}^{1 \times q}$ are column vectors.

The nonlinear terms $\boldsymbol{\psi}_{n,m} : \mathbb{R}^N \times \mathbb{R}^N \to \mathbb{R}^N$, $\boldsymbol{\psi}_m : \mathbb{R}^q \times \mathbb{R}^q \to \mathbb{R}^q$, and $\boldsymbol{\psi}_n : \mathbb{R}^{N-q} \times \mathbb{R}^{N-q} \to \mathbb{R}^{N-q}$ are given as

$$\begin{aligned}
\boldsymbol{\psi}_{n,m}(\boldsymbol{x}_1, \boldsymbol{x}_{2,m}, \boldsymbol{x}_{2,n}) &= \boldsymbol{\psi}(\boldsymbol{x}_1, \boldsymbol{C}_{y,2}^T \boldsymbol{x}_{2,m} + \boldsymbol{C}_n^T \boldsymbol{x}_{2,n}),\\
\boldsymbol{\psi}_m(\boldsymbol{x}_1, \boldsymbol{x}_{2,m}) &= \boldsymbol{C}_{y,2} \boldsymbol{\psi}(\boldsymbol{x}_1, \boldsymbol{C}_{y,2}^T \boldsymbol{x}_{2,m} + \boldsymbol{C}_n^T \boldsymbol{x}_{2,n})\\
\boldsymbol{\psi}_n(\boldsymbol{x}_1, \boldsymbol{x}_{2,n}) &= \boldsymbol{C}_n \boldsymbol{\psi}(\boldsymbol{x}_1, \boldsymbol{C}_{y,2}^T \boldsymbol{x}_{2,m} + \boldsymbol{C}_n^T \boldsymbol{x}_{2,n})
\end{aligned}$$

The above defined matrices and functions correspond to permutations and partitions of the original ones. Additionally, the nonlinear functions $\boldsymbol{\varphi}_{n,m}$, $\boldsymbol{\psi}_n$ and $\boldsymbol{\psi}_m$ satisfy the following local Lipschitz bounds (where $\|(\cdot)\|$ denotes Euclidian norm)

$$\begin{aligned}
\left\| \boldsymbol{\varphi}_{n,m}(\boldsymbol{x}_1, \boldsymbol{x}_{2,n}, \boldsymbol{x}_{2,m}) \right\| &\le L_{x_1}^{\varphi_n,m} \|\boldsymbol{x}_1\| \, L_{x_{2,n}}^{\varphi_n,m} \|\boldsymbol{x}_{2,n}\| + L_{x_{2,m}}^{\varphi_{n,m}} \|\boldsymbol{x}_{2,m}\| \ \forall \boldsymbol{x}_1, && \text{(4.5a)}\\
\|\boldsymbol{\psi}_m(\boldsymbol{x}_1, \boldsymbol{x}_{2,m})\| &\le L_{x_1}^{\psi_m} \|\boldsymbol{x}_1\| + L_{x_{2,m}}^{\psi_m} \|\boldsymbol{x}_{2,m}\|, && \text{(4.5b)}\\
\|\boldsymbol{\psi}_n(\boldsymbol{x}_1, \boldsymbol{x}_{2,n})\| &\le L_{x_1}^{\psi_n} \|\boldsymbol{x}_1\| + L_{x_{2,n}}^{\psi_n} \|\boldsymbol{x}_{2,n}\|. && \text{(4.5c)}
\end{aligned}$$

In compact form the rector dynamics are written as

$$\begin{aligned}
\dot{\boldsymbol{x}}_1 &= \boldsymbol{f}_1(\boldsymbol{x}_1, \boldsymbol{x}_{2,n}, d_1), & \boldsymbol{x}_1(0) &= \boldsymbol{x}_{10},\\
\dot{\boldsymbol{x}}_{2,n} &= \boldsymbol{f}_{2,n}(\boldsymbol{x}_1, \boldsymbol{x}_{2,n}, \boldsymbol{x}_{2,m}, d_2) + \boldsymbol{B}_{u,2}^{n}\boldsymbol{u}, & \boldsymbol{x}_{2,n}(0) &= \boldsymbol{x}_{2n0},\\
\dot{\boldsymbol{x}}_{2,m} &= \boldsymbol{f}_{2,m}(\boldsymbol{x}_1, \boldsymbol{x}_{2,n}, \boldsymbol{x}_{2,m}, d_2) + \boldsymbol{B}_{u,2}^{m}\boldsymbol{u}, & \boldsymbol{x}_{2,m}(0) &= \boldsymbol{x}_{2m0},
\end{aligned}$$

where

$$\begin{aligned}
\boldsymbol{f}_1(\boldsymbol{x}_1, \boldsymbol{x}_{2,n}, \boldsymbol{x}_{d,m}) &= \boldsymbol{A}_1 + \boldsymbol{B}_{d,1}d_1 - \boldsymbol{\varphi}_{n,m}(\boldsymbol{x}_1, \boldsymbol{x}_{2,n}, \boldsymbol{x}_{2,m}),\\
\boldsymbol{f}_{2,n}(\boldsymbol{x}_1, \boldsymbol{x}_{2,n}, \boldsymbol{x}_{2,m}, d_2) &= \boldsymbol{A}_2^{n,n}\boldsymbol{x}_{2,n} + \boldsymbol{A}_2^{n,m}\boldsymbol{x}_{2,m} + \boldsymbol{B}_{d,2}^{n}d_2 + \boldsymbol{\psi}_n(\boldsymbol{x}_1, \boldsymbol{x}_{2,n}),\\
\boldsymbol{f}_{2,m}(\boldsymbol{x}_1, \boldsymbol{x}_{2,n}, \boldsymbol{x}_{2,m}, d_2) &= \boldsymbol{A}_2^{m,m}\boldsymbol{x}_{2,m} + \boldsymbol{A}_2^{m,n}\boldsymbol{x}_{2,n} + \boldsymbol{B}_{d,2}^{m}d_2 + \boldsymbol{\psi}_m(\boldsymbol{x}_1, \boldsymbol{x}_{2,m}).
\end{aligned}$$

4.2.1.2 *Steady-state multiplicity: a bifurcation analysis*

Consider the open-loop statics in explicit form under nominal conditions, i. e., $\boldsymbol{d} = \boldsymbol{0}$

$$\boldsymbol{0} = \boldsymbol{f}_1(\bar{\boldsymbol{x}}_1, \bar{\boldsymbol{x}}_{2,n}, \bar{\boldsymbol{x}}_{2,m}, 0), \tag{4.6}$$

$$\boldsymbol{0} = \boldsymbol{f}_{2,n}(\bar{\boldsymbol{x}}_1, \bar{\boldsymbol{x}}_{2,n}, \bar{\boldsymbol{x}}_{2,m}, 0) + \boldsymbol{B}_{u,2}^{n}\bar{\boldsymbol{u}}, \tag{4.7}$$

$$\boldsymbol{0} = \boldsymbol{f}_{2,m}(\bar{\boldsymbol{x}}_1, \bar{\boldsymbol{x}}_{2,n}, \bar{\boldsymbol{x}}_{2,m}, 0) + \boldsymbol{B}_{u,2}^{m}\bar{\boldsymbol{u}}, \tag{4.8}$$

$$\bar{\boldsymbol{y}} = \bar{\boldsymbol{x}}_{2,m}, \quad \bar{z} = \boldsymbol{C}_{z,1}\bar{\boldsymbol{x}}_1. \tag{4.9}$$

From the first equation, the solution for the concentration vector is $\bar{\boldsymbol{x}}_1 = \mathfrak{f}_1(\bar{\boldsymbol{x}}_{2,n}, \bar{\boldsymbol{x}}_{2,m})$, and substitute in the second equation:

$$\boldsymbol{0} = \mathfrak{f}_{2,n}(\mathfrak{f}_1(\bar{\boldsymbol{x}}_{2,n}, \bar{\boldsymbol{x}}_{2,m}), \bar{\boldsymbol{x}}_{2,n}, \bar{\boldsymbol{x}}_{2,m}, 0) + \boldsymbol{B}_{u,2}^{n}\bar{\boldsymbol{u}}$$

solve for $\boldsymbol{x}_{2,n}$to get $\bar{\boldsymbol{x}}_{2,n} = \mathfrak{f}_{2,n}(\bar{\boldsymbol{x}}_{2,m}, \bar{\boldsymbol{u}})$ and substitute in $\boldsymbol{f}_{2,m}$:

$$\boldsymbol{0} = \boldsymbol{f}_{2,m}(\mathfrak{f}_1(\bar{\boldsymbol{x}}_{2,n}, \mathfrak{f}_{2,n}(\bar{\boldsymbol{x}}_{2,m}, \bar{\boldsymbol{u}}), \bar{\boldsymbol{x}}_{2,m}, 0) + \boldsymbol{B}_{u,2}^{m}\bar{\boldsymbol{u}} := \boldsymbol{\mathcal{F}}(\bar{\boldsymbol{y}}, \bar{\boldsymbol{u}}) \tag{4.10}$$

The above expression can be inverted for $\boldsymbol{y}$ to obtain and Input-Output Bifurcation Map (IOBM) to perform steady-state multiplicity analysis:

$$\bar{\boldsymbol{x}}_{2,m,l} = \boldsymbol{y}_l = \mathfrak{f}_u(\bar{\boldsymbol{u}}),\ \bar{\boldsymbol{x}}_{2,n,l} = \mathfrak{f}_{2,n}(\bar{\boldsymbol{x}}_{2,m,l}, \bar{\boldsymbol{u}}),\ \bar{\boldsymbol{x}}_{1,l} = \mathfrak{f}_1(\bar{\boldsymbol{x}}_{2,n,i}, \bar{\boldsymbol{x}}_{2,m,i}),\ l = 1, \ldots, n_s, \tag{4.11}$$

where $\mathfrak{f}_u$ is the solution of for the static value of the output of (4.10). From the above expressions, if $\bar{\boldsymbol{u}}$ is varied in a set of physical interest, an IOBM can be constructed to analyze how the steady-state set varies with $\bar{\boldsymbol{u}}$.

Furthermore, (4.10) may be inverted for $\bar{\boldsymbol{u}}$ to perform an input-multiplicity analysis: for given $\bar{\boldsymbol{y}}$, the IOBM (4.10) can be solved for $\bar{\boldsymbol{u}}_l$, $l = 1, \ldots, n_s$, and then using the expressions for the other two states the complete statics can be found:

$$\bar{\boldsymbol{u}}_l = \mathfrak{f}_y(\bar{\boldsymbol{y}}_l),\ \bar{\boldsymbol{x}}_{2,n,l} = \mathfrak{f}_{2,n}(\bar{\boldsymbol{x}}_{2,m,l}, \bar{\boldsymbol{u}}_l),\ \bar{\boldsymbol{x}}_1 = \mathfrak{f}_1(\bar{\boldsymbol{x}}_{2,n,l}, \bar{\boldsymbol{x}}_{2,m,l}), \quad l = 1, \ldots, n_s, \tag{4.12}$$

where $\mathfrak{f}_y$ is the solution of for the static value of the input of (4.10). From the above expressions, if $\bar{\boldsymbol{y}}$ is varied an IOBM can be constructed to analyze how the steady-state set and the corresponding value of the input vary with $\bar{\boldsymbol{y}}$.

In the above expression, $\mathfrak{f}_u$ and $\mathfrak{f}_y$ may not be solvable analytically but numerically. Furthermore, in the Single Input-Single Output (SISO) case, the previous analyses enable to generate IOBM with geometric representation that will be used for open-loop, zero dynamics, and closed-loop steady-state multiplicity analyses.

4.2.2 *Open-loop analysis*

The dynamics of the concentration-temperature dynamics can be interpreted as the interconnection of two Lur'e systems: a linear component in negative (or positive) feedback interconnection with a nonlinearity. This structure enables the stability analysis of each individual state by first studying the properties of the linear part and then the effect of the nonlinear reaction rate function.

For the purpose at hand, recall system (3.19) with $\boldsymbol{u} = \boldsymbol{0}$:

$$\dot{\boldsymbol{x}}_1 = \boldsymbol{A}_1\boldsymbol{x}_1 + \boldsymbol{B}_{d,1}d_1 - \boldsymbol{\psi}(\boldsymbol{x}_1, \boldsymbol{x}_2), \qquad \boldsymbol{x}_1(0) = \boldsymbol{x}_{10}, \tag{4.13a}$$

$$\dot{\boldsymbol{x}}_2 = \boldsymbol{A}_2\boldsymbol{x}_2 + \boldsymbol{B}_{d,2}d_2 + \boldsymbol{\psi}(\boldsymbol{x}_1, \boldsymbol{x}_2), \qquad \boldsymbol{x}_2(0) = \boldsymbol{x}_{20}. \tag{4.13b}$$

The concentration (or temperature) dynamics are composed by a linear stabilizing part, due to mass (or heat) transport, in negative (or positive) feedback interconnection with the term $\boldsymbol{\psi}$, that reflects the stabilizing (or destabilizing) capability of the sync (or source) effect of the consumption of reactant (or heat production) by the chemical reaction. Also, the function $\boldsymbol{\psi}$ couples the temperature and concentration dynamics.

In Appendix c, using a Gerschgorin circles [128], it is shown that matrices $\boldsymbol{A}_j$ are Hurwitz with dominant eigenvalues $\lambda_{A_j}{}^*$, $j = 1, 2$. When $\boldsymbol{\psi} = \boldsymbol{0}_{N_e\times 1}$ in (4.13), the application of Corollary 3.2 (or Corollary 3.2), leads to conclude that when $d_j(t) \neq 0$, each subsystem is robustly stable with parameters $\{\zeta_j, a_{P_j}, \frac{a_{xj}\|\boldsymbol{B}_{d,j}\|}{\zeta_j}\}$(or $\{|\lambda_{A_1}{}^*|, a_{A_j}, \frac{a_{xj}\|\boldsymbol{B}_{d,j}\|}{\lambda_{A_1}{}^*}\}$.

Once established the stability of the linear components of the concentration and temperature dynamics, what follows is to analyze the effect of the negative or positive interconnection, respectively, with the reaction rate function. This is analyzed next.

4.2.2.1 *Concentration dynamics*

For the purpose at hand, recall the open-loop dynamics (4.13), and note that the reaction rate function has decoupled entries from the concentration and temperature states, see (3.20). The function $\boldsymbol{\psi}(\boldsymbol{x}_1, \boldsymbol{x}_2)$ can be rewritten as follows

$$\boldsymbol{\psi}(\boldsymbol{x}_1, \boldsymbol{x}_2) = \boldsymbol{\varphi}_1(\boldsymbol{x}_1) + \boldsymbol{\varphi}_{12}(\boldsymbol{x}_1; \boldsymbol{x}_2), \tag{4.14a}$$

where

$$\boldsymbol{\varphi}_1(\boldsymbol{x}_1) := \boldsymbol{\psi}(\boldsymbol{x}_1, \boldsymbol{0}), \quad \boldsymbol{\varphi}_{12}(\boldsymbol{x}_1; \boldsymbol{x}_2) := \boldsymbol{\psi}(\boldsymbol{x}_1, \boldsymbol{x}_2) - \boldsymbol{\psi}(\boldsymbol{x}_1, \boldsymbol{0}). \tag{4.14b}$$

Due to the Lipschitz continuity of the reaction rate function $\boldsymbol{\psi}$, the entries of the function $\boldsymbol{\varphi}_1$ satisfy the following sector conditions

$$a_k x_{1,k}^2 \leq x_{1,k}\varphi_{1,k}(x_{1,k}) \leq b_k x_{1,k}^2, \quad k = 1, \ldots, N_e.$$

Using the above expression, it can be shown that for a matrix $\boldsymbol{P}_1 = \boldsymbol{P}_1^T > 0$ of appropriate dimensions, the following expression holds

$$(\boldsymbol{\varphi}_1(\boldsymbol{x}_1) - a\boldsymbol{x}_1)^T \boldsymbol{P}_1 (\boldsymbol{\varphi}_1(\boldsymbol{x}_1) - b\boldsymbol{x}_1) \leq 0,$$

with $a = \max_k\{a_k\}$ and $b = \max_k\{b_k\}$. Some algebraic manipulations yield to

$$\boldsymbol{x}_1^T \boldsymbol{P}\boldsymbol{\varphi}_1(\boldsymbol{x}_1) \geq c\boldsymbol{x}_1^T \boldsymbol{P}_1 \boldsymbol{x}_1 + d\boldsymbol{\varphi}_1^T(\boldsymbol{x}_1)\boldsymbol{P}_1\boldsymbol{\varphi}_1(\boldsymbol{x}_1), \quad c = \frac{ab}{a+b}, \quad d = \frac{1}{a+b}. \tag{4.15}$$

Furthermore, the function $\boldsymbol{\varphi}_{12}$ is, uniformly Lipschitz bounded with respect to $\boldsymbol{x}_2$:

$$\|\boldsymbol{\varphi}_{12}(\boldsymbol{x}_1;\boldsymbol{x}_2)\| = \|\boldsymbol{\psi}(\boldsymbol{x}_1,\boldsymbol{x}_2) - \boldsymbol{\psi}(\boldsymbol{x}_1,\boldsymbol{0})\| \leq L_{x_2}^{\varphi_{12}} \|\boldsymbol{x}_2\|. \tag{4.16}$$

With the previous preparations, the robust stability of the concentration dynamics is established next. First, the concentration dynamics (4.13a) is rewritten using (4.14a),

$$\dot{\boldsymbol{x}}_1 = \boldsymbol{A}_1\boldsymbol{x}_1 + \boldsymbol{B}_{d,1}d_1 - \boldsymbol{\varphi}_1(\boldsymbol{x}_1) - \boldsymbol{\varphi}_{12}(\boldsymbol{x}_1;\boldsymbol{x}_2), \quad \boldsymbol{x}_1(0) = \boldsymbol{x}_{10}.$$

For the purpose at hand, consider the Lyapunov function

$$V_1(\boldsymbol{x}_1) = \boldsymbol{x}_1^T\boldsymbol{P}_1\boldsymbol{x}_1, \quad \boldsymbol{P}_1 = \boldsymbol{P}_1^T > 0,$$

where $\boldsymbol{P}_1$ satisfy the Lyapunov equation (3.8c) and (3.8d) in $X_{1,r} = \{\boldsymbol{x}_1 \in X_1 \mid \|\boldsymbol{x}_1\| \leq r_{x,1}\}$ with parameters $\zeta_1 > |\lambda_{A_1}{}^*|$ and $a_{P_1} = \frac{\lambda_{P_1}{}^*}{\lambda_{P_1}{}_*}$. The time derivative along the trajectories of the concentration dynamics is

$$\begin{aligned}
\dot{V}_1 &= \boldsymbol{x}_1^T(\boldsymbol{A}_1^T\boldsymbol{P}_1 + \boldsymbol{P}_1\boldsymbol{A}_1)\boldsymbol{x}_1 + 2\boldsymbol{x}_1^T\boldsymbol{P}_1\boldsymbol{B}_{d,1}d_1 - 2\boldsymbol{x}_1^T\boldsymbol{P}_1\boldsymbol{\varphi}_1(\boldsymbol{x}_1) - 2\boldsymbol{x}_1^T\boldsymbol{P}_1\boldsymbol{\varphi}_{12}(\boldsymbol{x}_1;\boldsymbol{x}_2),\\
&= \boldsymbol{x}_1^T(\boldsymbol{A}_1^T\boldsymbol{P}_1 + \boldsymbol{P}_1\boldsymbol{A}_1)\boldsymbol{x}_1 + 2\boldsymbol{x}_1^T\boldsymbol{P}_1\boldsymbol{B}_{d,1}d_1 - 2c\boldsymbol{x}_1^T\boldsymbol{P}_1\boldsymbol{x}_1 - 2d\boldsymbol{\varphi}_1^T(\boldsymbol{x}_1)\boldsymbol{P}_1\boldsymbol{\varphi}_1(\boldsymbol{x}_1) -\\
&\quad - 2\boldsymbol{x}_1^T\boldsymbol{P}_1\boldsymbol{\varphi}_{12}(\boldsymbol{x}_1;\boldsymbol{x}_2),\\
&\leq -2(\zeta_1 + c)\boldsymbol{x}_1^T\boldsymbol{P}_1\boldsymbol{x}_1 + 2\boldsymbol{x}_1^T\boldsymbol{P}_1\boldsymbol{B}_{d,1}d_1 - 2\boldsymbol{x}_1^T\boldsymbol{P}_1\boldsymbol{\varphi}_{12}(\boldsymbol{x}_1;\boldsymbol{x}_2),
\end{aligned}$$

where (3.8c) and (4.15) have been used. Taking norms of the last two terms in the above inequality, and the use of the triangle inequality and the bound (4.16) yields

$$\dot{V}_1 \leq -2(\zeta_1 + \gamma)\boldsymbol{x}_1^T\boldsymbol{P}_1\boldsymbol{x}_1 + 2\lambda_{P_1}{}^* \|\boldsymbol{x}_1\| \left(\|\boldsymbol{B}_{d,1}\| |d_1(t)| + 2L_{x_2}^{\varphi_{12}} \|\boldsymbol{x}_2\|\right).$$

Proceed as in the proof of Corollary 3.2 (or Corollary 3.3), to get the estimate

$$\|\boldsymbol{x}_1(t)\| \leq a_1 \|\boldsymbol{x}_{10}\| \mathrm{e}^{-\nu_1 t} + a_1 \int_0^t \mathrm{e}^{-\nu_1(t-\mathrm{t})}(\|\boldsymbol{B}_{d,1}\| |d_1(\mathrm{t})| + L_{x_2}^{\varphi_{12}} \|\boldsymbol{x}_2(\mathrm{t})\|)\mathrm{dt}. \tag{4.17a}$$

where

$$\nu_1 = \zeta_1 + c, \quad a_1 = a_{P_1}. \tag{4.17b}$$

Considering the finite domains $\|\boldsymbol{x}_{10}\| \leq \delta_{10}$, $\sup_{t \geq t} \varepsilon_d(t) \leq \varepsilon_{d1}$, $\sup_{t \geq t} \|\boldsymbol{x}_2(t)\| \leq \varepsilon_{x2}$, the previous inequality is written as

$$\|\boldsymbol{x}_1(t)\| \leq a_1 \delta_{10} e^{-\nu_1 t} + b_{d_1} \varepsilon_{d1} + b_{x2} \varepsilon_{x2}.$$

If the following conditions are satisfied

$$\nu_1 > 0, \quad a_1 \delta_{10} \leq \varepsilon_{x1}, \quad b_{d_1} \varepsilon_{d1} + b_{x2} \varepsilon_{x2} \leq \varepsilon_{x1}, \tag{4.18}$$

the robust stability of the concentration dynamics with respect to the inlet concentration and the temperature state is ensured, with parameters $b_{d_1} = \frac{a_1 \|\boldsymbol{B}_{d,1}\|}{\nu_1}$, $b_d = \frac{a_1 L_{x_2}^{\varphi_{12}}}{\nu_1}$.

Using (3.10) instead of (3.8d), the parameters (4.17b) can be also defined as

$$\nu_1 = |\lambda_{A_1}{}^*| + c, \quad a_1 = a_{A_1}. \tag{4.19}$$

From a physical perspective, both transport and reaction phenomena contribute with stabilizing effects (as measured by $\nu_1 > 0$), and ensures the exponential stability of the origin $\boldsymbol{x}_1$ in $X_{1,r}$ when there is no exogenous inputs. If the origin is unique, then the robust stability is ensured nonlocally for the whole set X_1. Contrarily, if there is steady-state multiplicity, the stability result is local over $X_{1,r}$, and for temperature trajectories that violates the second condition in (4.18), the concentration trajectories are pushed away of the subset $X_{1,r}$, destroying the local robust stability property. Accordingly, from a control perspective, feedback must be used to produce bounded and vanishing temperature trajectories to drive the concentration profile to the origin.

4.2.2.2 *Temperature dynamics*

Consider the temperature dynamics (4.13b) with initial conditions, inlet temperature and bounded concentration trajectories defined over the finite domains $\|\boldsymbol{x}_{20}\| \leq \delta_{20}$, $\sup_{t \leq t} \varepsilon_{d2} \leq \varepsilon_{d2}^+$, and $\sup_{t \leq t} \|\boldsymbol{x}_1(t)\| \leq \varepsilon_{x1}$, and state defined in the set $X_{2,r} = \{\boldsymbol{x}_2 \in X_2 \mid \|\boldsymbol{x}_2\| \leq r_{x2}\}$. Furthermore, $\boldsymbol{\psi}$ satisfy the Lipschitz condition (3.21) with constants $L_{x_j}^{\psi}$, $j = 1, 2$. The application of Corollary 3.2 (or Corollary 3.3) yields to

$$\|\boldsymbol{x}_2(t)\| \leq a_2 \|\boldsymbol{x}_{20}\| e^{-\nu_2} + a_2 \int_0^t e^{-\nu_2(t-t)} \left(\|\boldsymbol{B}_{d,2}\| \varepsilon_{d2} + L_{x_1}^{\psi} \|\boldsymbol{x}_1\| \right) dt, \tag{4.20a}$$

where

$$\nu_2 = \zeta_2 - a_2 L_{x_2}^{\psi}, \quad a_2 = a_{P_2}, \quad (\text{ or } \nu_2 = |\lambda_{A_1}{}^*| - a_2 L_{x_2}^{\psi}, \quad a_2 = a_{A_2}),$$

or equivalently

$$\|\boldsymbol{x}_{20}\| \leq \delta_{20} \Rightarrow \|\boldsymbol{x}_2(t)\| \leq a_2 \|\boldsymbol{x}_{20}\| e^{-\nu_2 t} + b_{d2} \varepsilon_{2e}^+ + b_{x1} \varepsilon_{x1},$$

with $b_{d2} = \frac{a_2\|\boldsymbol{B}_{d,2}\|}{\nu_1}$, and $b_{x1} = \frac{a_2 L^{\psi}_{x_1}}{\nu_2}$. The above expressions state that the temperature dynamics are robustly stable in the finite domain $X_{2,r}$ if

$$\nu_2 > 0, \quad a_2\delta_{20} \leq \varepsilon_{x2}, \quad b_{d2}\varepsilon^{+}_{d,2} + b_{x1}\varepsilon_{x1} \leq \varepsilon_{x2}. \tag{4.21}$$

If the origin is not unique, the second and third conditions in (4.21) restrict the size of initial conditions and exogenous inputs so that temperature trajectories do not leave the set $X_{2,r}$. If the origin is unique, then nonlocal robust stability is ensured in X_2.

From a physical perspective, in case the origin is unstable since the inlet temperature and the concentration are exogenous bounded inputs that remain close to zero and satisfy the third condition in (4.21), the main destabilizing effect is the domination of the destabilizing dynamic mechanism, heat production, over the stabilizing ones, heat transport and exchange with the jacket. Accordingly, the control aim is to modify the interplay between stabilizing transport and destabilizing reaction phenomena so that the open-loop unstable origin becomes robustly stable.

4.2.2.3 *Interconnected dynamics*

Once stability conditions for the concentration and temperature dynamics have been drawn, the robust stability of the interconnection (4.13) is assured in the next result.

Proposition 4.1. ***Robust stability of the open-loop dynamics.***
Consider the reactor dynamics (4.13), with state $\boldsymbol{x} = [\boldsymbol{x}_1^T\, \boldsymbol{x}_2^T]^T \in X = \{X_{1,r} \times X_{2,r}\}$ (or $X = X_1 \times X_2$), and bounded exogenous input $\boldsymbol{d} = [d_1\, d_2]^T$. Assume that the concentration and temperature dynamics separately are robustly stable and that (4.17a), (4.18) (or (4.19)), (4.20), and (4.21) are satisfied. If the following condition is met

$$\nu_2 - \frac{a_1 a_2 L^{\varphi_{12}}_{x_2} L^{\psi}_{x_1}}{\nu_1} > 0, \tag{4.22}$$

then, if the origin is (or not) the unique steady-state then the interconnection is robustly stable nonlocally (or locally) in $X = X_1 \times X_2$ (or $X = \{X_{1,r} \times X_{2,r}\}$) and the state trajectories satisfy (3.3) with constants ν_x, a_x, and b_d.

Proof. Apply Lemma 3.1 to the system (4.13) to obtain (4.22) as requirement for robust stability. When this condition is met, then the state trajectories are bounded as

$$\|\boldsymbol{x}(t)\| \leq a_x \|\boldsymbol{x}_0\| \,\mathrm{e}^{-\lambda_x t} + a_x \int_0^t \mathrm{e}^{-\lambda_x(t-\mathrm{t})}\varepsilon_d(\mathrm{t})\mathrm{dt}. \tag{4.23}$$

After taking the maximum of $\varepsilon_d(t)$, the state trajectories satisfy (3.3) with

$$\lambda_x = \max_{\lambda_j \in \sigma(\boldsymbol{A}_s)} \{\mathrm{Re}(\lambda_j)\}, \quad j = 1, 2, \quad \boldsymbol{A}_s = \begin{bmatrix} -\nu_1 & a_1 L^{\varphi_{12}}_{x_2} \\ a_2 L^{\psi}_{x_1} & -\nu_2 \end{bmatrix}$$

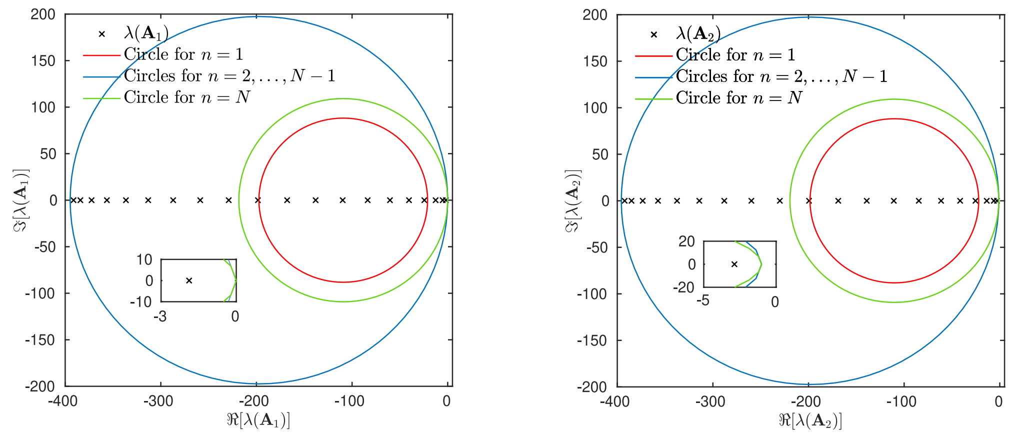

(a) Spectra of matrix A_1.

(b) Spectra of matrix A_2.

Figure 4.1: Eigenvalues and Gerghorin circles of matrices A_j, $j = 1, 2$ of the case example.

$$a_x = a_s(a_1 + a_2), \quad b_d = \frac{a_x \left\| \boldsymbol{B}_d \right\|}{\lambda_x}, \quad \boldsymbol{B}_d = \begin{bmatrix} a_1 \left\| \boldsymbol{B}_{d,1} \right\| & 0 \\ 0 & a_2 \left\| \boldsymbol{B}_{d,2} \right\| \end{bmatrix}.$$

□

From a physical perspective, in the inequality (4.22): the first term $\nu_2 =$ measures the destabilizing effect of the heat generation by reaction on the heat balance against stabilization by transport, and the second term measures destabilizing effects by interconnection between the concentration and temperature dynamics. Thus, the stability condition requires the stabilizing heat transport phenomenon to dominates the destabilizing heat generation and mass and heat interaction by chemical reaction. In case of instability, heat generation dominates the stabilizing effect of the heat transport so that the assumptions of Proposition 4.1 are not fulfilled. From a control perspective, the aim is to ensure that the heat generation is dominated by heat transport and additional heat removal induced by feedback.

4.2.3 *Case example: stability analysis*

Here, the previous stability analysis es applied to the case example introduced in Section 2.5 to analyze its stability property around the unstable steady-state.

Model 3.19 with the efficient discretization order $N_e = 20$, reaction rate function (2.12) and parameters and nominal input values given in Table 2.1 is considered. The spectrum of the matrices A_j, $j = 1, 2$ defined after 3.19 are presented in Figure 4.1 accompanied with the corresponding Gersghorin circles (see Appendix c). It can be seen that both matrices have only real eigenvalues and all of them are in the left half

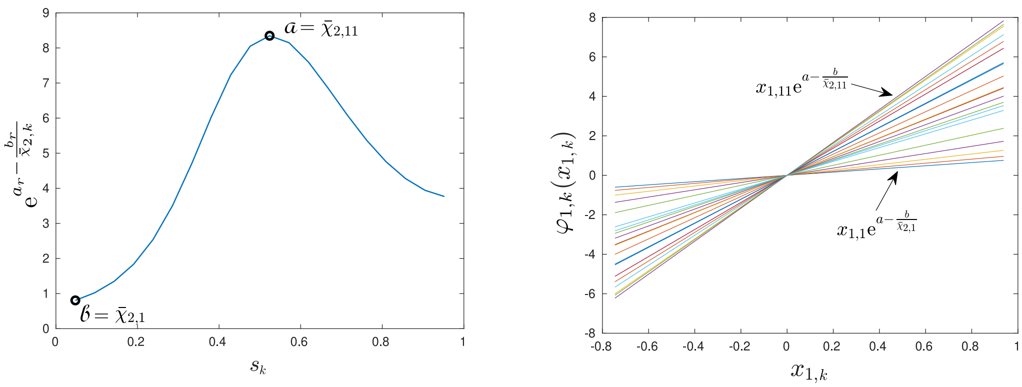

(a) Slopes $e^{a_r - \frac{b_r}{\bar{x}_{2,k}}}$, $k = 1, \ldots, 20$.

(b) Functions $\varphi_{1,k}(x_{1,k})$, $k = 1, \ldots, 20$.

Figure 4.2: Sector condition of the function $\boldsymbol{\varphi}_1(\boldsymbol{x}_1)$ in terms of its entries $\varphi_{1,k}(x_{1,k}) = x_{1,k}e^{a_r - \frac{b_r}{\bar{x}_{2,k}}}$.

of the complex plane. Thus, the maximum eigenvalues for each matrix are negative and given as

$$\lambda_{A_1}{}^* \approx -1.88, \quad \lambda_{A_2}{}^* \approx -2.88.$$

Picking $\zeta_1 = 1.00$ and $\zeta_2 = 2.00$, the solution of corresponding Lyapunov inequalities (3.8c) (solved using CVX a Matlab package for specifying and solving convex programs [60; 59]) yields to $\boldsymbol{P}_j$, $j = 1, 2$ with constants $a_1 \approx 2.50$ and $a_2 \approx 2.50$.

Considering (2.12), the entries of the nonlinearity $\boldsymbol{\psi}$ (3.20) are given as

$$\psi_k(x_{1,k}, x_{2,k}) = (x_{1,k} + \bar{x}_{1,k})e^{a - \frac{b}{x_{2,k} + \bar{x}_{2,k}}} - \bar{x}_{1,k}e^{a - \frac{b}{\bar{x}_{2,k}}}, \quad k = 1, \ldots, N,$$

then, the entries of the nonlinear functions $\boldsymbol{\varphi}(\boldsymbol{x}_1)$ and $\boldsymbol{\varphi}_{12}(\boldsymbol{x}_1, \boldsymbol{x}_2)$ are:

$$\varphi_{1,k}(x_{1,k}) = x_{1,k}e^{a_r - \frac{b_r}{\bar{x}_{2,k}}}, \quad \varphi_{12,k}(x_{1,k}, x_{2,k}) = (x_{1,k} + \bar{x}_{1,k})\left(e^{a_r - \frac{b_r}{x_{2,k} + \bar{x}_{2,k}}} - e^{a_r - \frac{b_r}{\bar{x}_{2,k}}}\right).$$

The evaluation of the sector condition of $\boldsymbol{\varphi}_1(\boldsymbol{x}_1)$ stated in (4.15), is straightforward since functions $\varphi_{1,k}(x_{1,k})$ are straight lines with slopes given by $e^{a_r - \frac{b_r}{\bar{x}_{2,k}}}$, shown in Figure 4.2. It can be seen that the sector bounds a and b are

$$a = \min\left\{e^{a_r - \frac{b_r}{\bar{x}_{2,k}}}\right\} = e^{a_r - \frac{b_r}{\bar{x}_{2,1}}} \approx 0.81, \quad b = \max\left\{e^{a_r - \frac{b_r}{\bar{x}_{2,n}}}\right\} = e^{a_r - \frac{b_r}{\bar{x}_{2,11}}} \approx 8.35, \quad (4.24)$$

which yields to the parameter $c \approx 0.74$.

The use of the mean value theorem rise that the Lipschitz constants of the function $\boldsymbol{\psi}(\boldsymbol{x}_1, \boldsymbol{x}_2)$can be computed as $L^{\psi}_{x_j} = \left\|\partial_{x_j}\boldsymbol{\psi}(\boldsymbol{x}_1, \boldsymbol{x}_2)\right\|$. Considering that

$$\partial_{x_1}\boldsymbol{\psi}(\boldsymbol{x}_1, \boldsymbol{x}_2) = \operatorname{diag}\left(\begin{bmatrix} e^{a_r - \frac{b_r}{x_{2,1} + \bar{x}_{2,1}}} & \ldots & e^{a_r - \frac{b_r}{x_{2,N} + \bar{x}_{2,N}}}\end{bmatrix}\right),$$
$$\partial_{x_2}\boldsymbol{\psi}(\boldsymbol{x}_1, \boldsymbol{x}_2) = \operatorname{diag}\left(\begin{bmatrix} b\frac{x_{1,1} + \bar{x}_{1,1}}{(x_{2,1} + \bar{x}_{2,1})^2}e^{a - \frac{b}{x_{2,1} + \bar{x}_{2,1}}} & \ldots & b\frac{x_{1,N} + \bar{x}_{1,N}}{(x_{2,N} + \bar{x}_{2,N})^2}e^{a - \frac{b}{x_{2,N} + \bar{x}_{2,N}}}\end{bmatrix}\right),$$

then the Lipschitz constants are

$$L_{x_1}^{\psi} = \max\left\{ \mathrm{e}^{a - \frac{b}{x_{2,k} + \bar{x}_{2,k}}} \right\}, \quad L_{x_2}^{\psi} = \max\left\{ b \frac{x_{1,k} + \bar{x}_{1,k}}{(x_{2,k} + \bar{x}_{2,k})^2} \mathrm{e}^{a - \frac{b}{x_{2,k} + \bar{x}_{2,k}}} \right\}.$$

The numeric evaluation of the above expressions in the sets X_1 and X_2, gives

$$L_{x_1}^{\psi} \approx 2.44, \quad L_{x_2}^{\psi} \approx 11.19.$$

The concentration subsystem is robustly stable in X_1 because

$$\nu_1 = \zeta_1 + \gamma \approx 1 + 0.74 \approx 1.74 > 0. \tag{4.25a}$$

The condition for stability of the temperature dynamics is not fulfilled:

$$\nu_2 = \zeta_2 - a_2 L_{x_2}^{\psi} \approx 2 - (2.50)(11.18) \approx -25.95 \not> 0. \tag{4.25b}$$

Accordingly, condition (4.21) is not fulfilled nor (3.12). Note that this do not proof the instability of the steady-state of interest (since the stated implications of Proposition 3.1 and Proposition 4.1 are just of sufficiency type). The instability of the unstable steady-state is confirmed by the evaluation of the linearization of the temperature dynamics around the corresponding steady-state: there is an eigenvalue with positive real part.

4.3 ZERO DYNAMICS AND SENSOR LOCATION CRITERION

Here, the robust stability of the MIMO zero dynamics of the reactor model (4.1) are studied in the normal form [32] and in original coordinate. The concept of the zero dynamics [76] is of upmost relevance for the present study since it plays an important role in the design of feedback control strategies. The SISO case, will be employed to characterize the steady-state multiplicity for the selection of sensor locations.

Recall the partitioned model (4.4). Since $\boldsymbol{y} = \boldsymbol{x}_{2,m}$, the vector of relative degrees for the control input-measured output vectors pair

$$\boldsymbol{rd}(\boldsymbol{u}, \boldsymbol{y}) = \begin{bmatrix} 1 & \dots & 1 \end{bmatrix} \tag{4.26}$$

is robustly well-defined if the matrix $\boldsymbol{B}_u^m$ is not singular. Condition that is met since $v > 0$: the coolant jacket is designed so that the heat extraction from inside the reactor to the jacket is always enable. Accordingly, the zero dynamics is of dimension $N - q$. In the following the stability of the zero dynamics is characterized.

4.3.1 *Normal form*

Consider the following dipheomorphism, well-defined in the state space X, which is presented in original concentration-temperature coordinate as well as concentration and partitioned temperature state:

$$\boldsymbol{T}\boldsymbol{x} = \left[\begin{array}{c} \boldsymbol{x}_1 \\ \boldsymbol{E}\boldsymbol{x}_2 \\ \hline \boldsymbol{C}_{y,2}\boldsymbol{x}_2 \end{array}\right] = \begin{bmatrix} \boldsymbol{I}_{N\times N} & \boldsymbol{0} & \boldsymbol{0} \\ \boldsymbol{0}_{N-q\times N} & \boldsymbol{E}\boldsymbol{C}_n^T & \boldsymbol{E}\boldsymbol{C}_{y,2}^T \\ \boldsymbol{0} & \boldsymbol{0} & \boldsymbol{I} \end{bmatrix} \begin{bmatrix} \boldsymbol{x}_1 \\ \boldsymbol{x}_{2,n} \\ \boldsymbol{x}_{2,m} \end{bmatrix} = \left[\begin{array}{c} \boldsymbol{\eta}_1 \\ \boldsymbol{\eta}_2 \\ \hline \boldsymbol{\xi} \end{array}\right] \tag{4.27}$$

where $\boldsymbol{E} \in \mathbb{R}^{N-q\times N}$ is defined such that the following expression holds

$$\boldsymbol{E}\boldsymbol{x}_2 = \begin{bmatrix} x_{2,n,1} - x_{2,n,2} \\ \vdots \\ x_{2,n,k} - x_{2,n,k+1} \\ \vdots \\ x_{2,n,N-q} - x_{2,n,1} \end{bmatrix}.$$

The inverse transformation is

$$\begin{bmatrix} \boldsymbol{x}_1 \\ \boldsymbol{x}_{2,n} \\ \boldsymbol{x}_{2,m} \end{bmatrix} = \begin{bmatrix} \boldsymbol{I}_{N\times N} & \boldsymbol{0} & \boldsymbol{0} \\ \boldsymbol{0}_{N\times N} & (\boldsymbol{E}\mathbb{C}_n^T)^{-1} & -(\boldsymbol{E}\boldsymbol{C}_n^T)^{-1}\boldsymbol{E}\boldsymbol{C}_{y,2}^T \\ \boldsymbol{0} & \boldsymbol{0} & \boldsymbol{I}_{q,q} \end{bmatrix} \begin{bmatrix} \boldsymbol{\eta}_1 \\ \boldsymbol{\eta}_2 \\ \boldsymbol{\xi} \end{bmatrix}.$$

The application of the transformation (4.27) to (4.4) yields the normal form

$$\begin{aligned} \dot{\boldsymbol{\eta}}_1 &= \boldsymbol{A}_1\boldsymbol{\eta}_1 + \boldsymbol{B}_{d,1}d_1 - \boldsymbol{\psi}_1^{\eta}(\boldsymbol{\eta}_1, \boldsymbol{\eta}_2, \boldsymbol{\xi}), & \boldsymbol{\eta}_1(0) &= \boldsymbol{\eta}_{10}, \\ \dot{\boldsymbol{\eta}}_2 &= \boldsymbol{A}_2^{\eta}\boldsymbol{\eta}_2 + \boldsymbol{A}_2^{\xi}\boldsymbol{\xi} + \boldsymbol{B}_{d,2}^{\eta}d_2 + \boldsymbol{\psi}_2^{\eta}(\boldsymbol{\eta}_1, \boldsymbol{\eta}_2, \boldsymbol{\xi}), & \boldsymbol{\eta}_2(0) &= \boldsymbol{\eta}_{20}, \\ \dot{\boldsymbol{\xi}} &= \boldsymbol{A}_2^{m,m}\boldsymbol{x}_{2,m} + \boldsymbol{A}_2^{m,n}\boldsymbol{x}_{2,n} + \boldsymbol{B}_{d,2}^{m}d_2 + \boldsymbol{\psi}_m(\boldsymbol{x}_1, \boldsymbol{x}_{2,m}) + \boldsymbol{B}_{u,2}^{m}\boldsymbol{u}, & \boldsymbol{\xi}(0) &= \boldsymbol{\xi}_0, \\ \boldsymbol{y} &= \boldsymbol{\xi}, \quad z = \boldsymbol{C}_{z,1}\boldsymbol{\eta}_1. \end{aligned}$$

Note that the internal state $\boldsymbol{\eta}_1$ is equal to the concentration state $\boldsymbol{x}_1$, while the state $\boldsymbol{\eta}_2$ is a linear combination of the unmeasured, $\boldsymbol{x}_{2,n}$, and measured, $\boldsymbol{x}_{2,m}$, temperatures. The external state $\boldsymbol{\xi}$ is the measured temperature $\boldsymbol{x}_{2,m}$ and is written in the original coordinates for convenience. The involved matrices and functions are:

$$\begin{aligned} &\boldsymbol{A}_2^{\eta} = 2\boldsymbol{E}\boldsymbol{A}_2\boldsymbol{C}_n^T(\boldsymbol{E}\boldsymbol{C}_n^T)^{-1}, \quad \boldsymbol{A}_2^{\xi} = 2\boldsymbol{E}\boldsymbol{A}_2(\boldsymbol{C}_{y,2}^T - \boldsymbol{C}_n^T(\boldsymbol{E}\boldsymbol{C}_n^T)^{-1}\boldsymbol{E}\boldsymbol{C}_{y,2}^T), \quad \boldsymbol{B}_{d,2}^{\eta} = 2\boldsymbol{E}\boldsymbol{B}_{d,2}, \\ &\quad \boldsymbol{\psi}_1^{\eta}(\boldsymbol{\eta}_1, \boldsymbol{\eta}_2, \boldsymbol{\xi}) = \boldsymbol{\psi}\left(\boldsymbol{\eta}_1, (\boldsymbol{E}\boldsymbol{C}_n^T)^{-1}\boldsymbol{\eta}_2 - (\boldsymbol{E}\boldsymbol{C}_{y,2}^T\boldsymbol{\xi}), \boldsymbol{\xi}\right), \\ &\quad \boldsymbol{\psi}_2^{\eta}(\boldsymbol{\eta}_1, \boldsymbol{\eta}_2, \boldsymbol{\xi}) = 2\boldsymbol{E}\boldsymbol{\psi}\left(\boldsymbol{\eta}_1, (\boldsymbol{E}\boldsymbol{C}_n^T)^{-1}\boldsymbol{\eta}_2 - (\boldsymbol{E}\boldsymbol{C}_{y,2}^T\boldsymbol{\xi}), \boldsymbol{\xi}\right) \end{aligned}$$

The employment of the same representation as in (4.14a) for the nonlinear function $\boldsymbol{\psi}_1^\eta$ with respect to its argument $\boldsymbol{\xi}$ and $\boldsymbol{\eta}_2$ (iteratively) and for the nonlinear function $\boldsymbol{\psi}_2^\eta$ with respect to arguments $\boldsymbol{\xi}$, yields the dynamic model

$$\dot{\boldsymbol{\eta}}_1 = \boldsymbol{A}_1\boldsymbol{\eta}_1 + \boldsymbol{B}_{d,1}d_1 - \boldsymbol{\varphi}_1^\eta(\boldsymbol{\eta}_1) - \boldsymbol{\varphi}_{12}^\eta(\boldsymbol{\eta}_1,\boldsymbol{\eta}_2) - \boldsymbol{\varphi}_1^\xi(\boldsymbol{\eta}_1,\boldsymbol{\eta}_2,\boldsymbol{\xi})\boldsymbol{\xi}, \quad \boldsymbol{\eta}_1(0) = \boldsymbol{\eta}_{10}, \tag{4.28a}$$
$$\dot{\boldsymbol{\eta}}_2 = \boldsymbol{A}_2^\eta\boldsymbol{\eta}_2 + \boldsymbol{A}_2^\xi\boldsymbol{\xi} + \boldsymbol{B}_{d,2}^\eta d_2 + \boldsymbol{\varphi}_2^\eta(\boldsymbol{\eta}_1,\boldsymbol{\eta}_2) + \boldsymbol{\varphi}_2^\xi(\boldsymbol{\eta}_1,\boldsymbol{\eta}_2,\boldsymbol{\xi})\boldsymbol{\xi}, \quad \boldsymbol{\eta}_2(0) = \boldsymbol{\eta}_{20}, \tag{4.28b}$$
$$\dot{\boldsymbol{\xi}} = \boldsymbol{A}_2^{m,m}\boldsymbol{x}_{2,m} + \boldsymbol{A}_2^{m,n}\boldsymbol{x}_{2,n} + \boldsymbol{B}_{d,2}^m d_2 + \boldsymbol{\psi}_m(\boldsymbol{x}_1,\boldsymbol{x}_{2,m}) + \boldsymbol{B}_{u,2}^m\boldsymbol{u}, \quad \boldsymbol{\xi}(0) = \boldsymbol{\xi}_0, \tag{4.28c}$$
$$\boldsymbol{y} = \boldsymbol{\xi}, \quad z = \boldsymbol{C}_{z,1}\boldsymbol{\eta}_1. \tag{4.28d}$$

In the above dynamics the matrices $\boldsymbol{A}_2^\eta$ and $\boldsymbol{A}_2^{m,m}$ are Hurwitz with dominant eigenvalues $\lambda_{A_2^\eta}{}^*$ and $\lambda_{A_2^{m,m}}{}^*$, respectively, and the nonlinearities are defined as

$$\begin{aligned}
\boldsymbol{\varphi}_1^\eta(\boldsymbol{\eta}_1) &= \boldsymbol{\psi}_1^\eta(\boldsymbol{\eta}_1,\mathbf{0},\mathbf{0}), \quad \boldsymbol{\varphi}_2^\eta(\boldsymbol{\eta}_1,\boldsymbol{\eta}_2) = \boldsymbol{\psi}_2^\eta(\boldsymbol{\eta}_1,\boldsymbol{\eta}_2,\mathbf{0}),\\
\boldsymbol{\varphi}_{12}^\eta(\boldsymbol{\eta}_1,\boldsymbol{\eta}_2) &= \boldsymbol{\psi}_1^\eta(\boldsymbol{\eta}_1,\boldsymbol{\eta}_2,\mathbf{0}) - \boldsymbol{\psi}_1^\eta(\boldsymbol{\eta}_1,\mathbf{0},\mathbf{0}),\\
\boldsymbol{\varphi}_j^\xi(\boldsymbol{\eta}_1,\boldsymbol{\eta}_2,\boldsymbol{\xi})\boldsymbol{\xi} &= \boldsymbol{\psi}_j^\eta(\boldsymbol{\eta}_1,\boldsymbol{\eta}_2,\boldsymbol{\xi}) - \boldsymbol{\psi}_j^\eta(\boldsymbol{\eta}_1,\boldsymbol{\eta}_2,\mathbf{0}) = \int_0^1 \partial_\xi\boldsymbol{\psi}_1^\eta(\boldsymbol{\eta}_1,\boldsymbol{\eta}_2,\nu\boldsymbol{\xi})\mathrm{d}\nu\boldsymbol{\xi}, \ j = 1,2.
\end{aligned}$$

In the last cases the mean value theorem has been used to rewrite the nonlinearities in a convenient form. In particular, since $\boldsymbol{\phi}_1^\eta(\boldsymbol{\eta}_1) = \boldsymbol{\phi}(\boldsymbol{x}_1)$, it satisfies the same sector condition (4.15). Additionally, the rest of the nonlinearities satisfy the bounds

$$\left\|\boldsymbol{\phi}_2^\eta(\boldsymbol{\eta}_1,\boldsymbol{\eta}_2)\right\| \le L_{\eta_1}^{\varphi_2^\eta}\|\boldsymbol{\eta}_1\| + L_{\eta_2}^{\varphi_2^\eta}\|\boldsymbol{\eta}_2\|, \quad \left\|\boldsymbol{\varphi}_i^\eta(\boldsymbol{\eta}_1,\boldsymbol{\eta}_2,\boldsymbol{\xi})\boldsymbol{\xi}\right\| \le L_\xi^{\varphi_i}\|\boldsymbol{\xi}\|, \quad i = 1,2. \tag{4.29}$$

In compact vector notation, the normal form is written as

$$\dot{\boldsymbol{\eta}} = \boldsymbol{A}_\eta\boldsymbol{\eta} + \boldsymbol{B}_d^\eta\boldsymbol{d} + \boldsymbol{\varphi}_\eta(\boldsymbol{\eta}) + \boldsymbol{F}(\boldsymbol{\eta},\boldsymbol{\xi})\boldsymbol{\xi}, \quad \boldsymbol{\eta}(0) = \boldsymbol{\eta}_0, \tag{4.30a}$$
$$\dot{\boldsymbol{\xi}} = \boldsymbol{A}_2^{m,m}\boldsymbol{x}_{2,m} + \boldsymbol{A}_2^{m,n}\boldsymbol{x}_{2,n} + \boldsymbol{B}_{d,2}^m d_2 + \boldsymbol{\psi}_m(\boldsymbol{x}_1,\boldsymbol{x}_{2,m}) + \boldsymbol{B}_{u,2}^m\boldsymbol{u}, \quad \boldsymbol{\xi}(0) = \boldsymbol{\xi}_0 \tag{4.30b}$$
$$\boldsymbol{y} = \boldsymbol{\xi}, \quad z = \boldsymbol{C}_{z,1}\boldsymbol{\eta}_1, \tag{4.30c}$$

where $\boldsymbol{\eta} = [\boldsymbol{\eta}_1\ \boldsymbol{\eta}_2]^T$. The involved matrices and functions are

$$\boldsymbol{A}_\eta = \begin{bmatrix} \boldsymbol{A}_1 & \mathbf{0} \\ \mathbf{0} & \boldsymbol{A}_2^\eta \end{bmatrix}, \quad \boldsymbol{\varphi}_\eta(\boldsymbol{\eta}) = \begin{bmatrix} -\boldsymbol{\varphi}_1^\eta(\boldsymbol{\eta}_1) - \boldsymbol{\varphi}_{1,2}^\eta(\boldsymbol{\eta}_1,\boldsymbol{\eta}_2) \\ \boldsymbol{\phi}_2^\eta(\boldsymbol{\eta}_1,\boldsymbol{\eta}_2) \end{bmatrix},$$

$$\boldsymbol{B}_d^\eta = \begin{bmatrix} \boldsymbol{B}_{d,1} \\ \boldsymbol{B}_{d,2}^\eta \end{bmatrix}, \quad \boldsymbol{F}(\boldsymbol{\eta},\boldsymbol{\xi}) = \begin{bmatrix} -\boldsymbol{\varphi}_1^\xi(\boldsymbol{\eta}_1,\boldsymbol{\eta}_2,\boldsymbol{\xi}) \\ \boldsymbol{A}_2^\xi + \boldsymbol{\varphi}_2^\xi(\boldsymbol{\eta}_1,\boldsymbol{\eta}_2,\boldsymbol{\xi}) \end{bmatrix}.$$

The zero dynamics, when $\boldsymbol{\xi} = \mathbf{0}$, are given by

$$\dot{\boldsymbol{\eta}} = \boldsymbol{A}_\eta\boldsymbol{\eta} + \boldsymbol{B}_d^\eta\boldsymbol{d} + \boldsymbol{\varphi}_\eta(\boldsymbol{\eta}), \quad \boldsymbol{\eta}(0) = \boldsymbol{\eta}_0, \tag{4.31}$$

with state $\boldsymbol{\eta} = [\boldsymbol{\eta}_1^T\ \boldsymbol{\eta}_2^T]^T \in X_\eta = X_{\eta 1} \times X_{\eta 2}$, bounded exogenous input $\boldsymbol{d}$ that satisfy (3.2b), and zero dynamics controller $\boldsymbol{\mu}_z : X_z \to U_z \subset \mathbb{R}$,

$$\boldsymbol{\mu}_z(\boldsymbol{x}_1,\boldsymbol{x}_{2,n},d_2) = -\boldsymbol{B}_u^{m\,-1}\left(\boldsymbol{A}_2^{m,n}\boldsymbol{x}_{2,n} + \boldsymbol{B}_{d,2}^m d_2 + \boldsymbol{\psi}_m(\boldsymbol{x}_1,\mathbf{0})\right). \tag{4.32}$$

X_z is the state set in which the internal dynamics evolves and U_z is the control set spanned by the zero dynamics control, and

$$X_{\eta 1} = \{\boldsymbol{\eta}_1 \in \mathbb{R}^N \mid \|\boldsymbol{\eta}_1\| \le \varepsilon_{\eta 1}\}, \qquad X_{\eta 2} = \{\boldsymbol{\eta}_2 \in \mathbb{R}^{N-q} \mid \|\boldsymbol{\eta}_2\| \le \varepsilon_{\eta 2}\},$$

In (4.31) considering $\boldsymbol{\xi}$, defined in a finite domain $\|\boldsymbol{\xi}\| \le \varepsilon_{\xi}$, as input, the state $\boldsymbol{\eta}_1 \in X_{\eta_1}$ is equivalent to the concentration dynamics in (4.13) with a different representation of the nonlinear reaction rate function, thus, it satisfy a similar condition as the one (4.17a). For the state $\boldsymbol{\eta}_2 \in X_{\eta 2}$, since matrix $\boldsymbol{A}_2^{\eta}$ is assumed to be Hurwitz (with $\lambda^*_{A_2^{\eta}}, a_{A_2^{\eta}}$, see (3.10), there exists a matrix $\boldsymbol{P}_\eta = \boldsymbol{P}_\eta^T > 0$ with associated parameters ζ_η, a_{P_η} that satisfy a Lyapunov inequality of the form (3.8c). The application of Corollary 3.2 or Corollary 3.3 establishes that if the following condition is met

$$\nu_\eta = \zeta_\eta - a_{P_\eta} L_{\eta 2}^{\varphi_2^\eta} > 0 \quad (\text{ or } \nu_\eta = |\lambda_{A_2^\eta}{}^*| - a_{A_2^\eta} L_{\eta 2}^{\varphi_2^\eta} > 0), \tag{4.33}$$

then the second internal state of the zero dynamics is robustly stable. Then, the robust stability of the zero dynamics (4.31) can be ensured with the application of Proposition 3.1.

Proposition 4.2. ***Robust stability of the zero dynamics***. *Proof in Section d.1.*
Consider the system (4.30) subjected to bounded inputs $\boldsymbol{d}(t)$ and $\boldsymbol{\xi}(t)$ that satisfies $\|\boldsymbol{\xi}\| \le \varepsilon_\xi$. Assume that the involved nonlinearities in (4.30) satisfy (4.29) locally in X_η. If the origin is the unique steady-state and the following condition is met (ν_1 given in (4.17b) (or (4.19)))

$$\nu_\eta - \frac{a_1 a_\eta L_{\eta 2}^{\varphi_{12}} L_{\eta 1}^{\varphi_2^\eta}}{\nu_1} > 0. \tag{4.34}$$

Then, the zero dynamics (4.31) are nonlocally robustly stable in X_η.

The previous results implies that the origin of the zero dynamics is: (i) exponentially stable when $\boldsymbol{\xi} = \mathbf{0}$ or $\boldsymbol{\xi} \to \mathbf{0}$, and ultimately bounded when $\|\boldsymbol{\xi}\| \le \varepsilon_\xi$.

4.3.2 *Original coordinate*

In original coordinate, the zero dynamics is defined in the set ($\boldsymbol{\mu}_\eta$ is defined in (4.32)):

$$X_z = \Big\{\boldsymbol{x}_1, \times \boldsymbol{x}_2 \in X \,|\, \boldsymbol{y} = \mathbf{0}, \quad \boldsymbol{\mu}_\eta(\boldsymbol{x}_1, \boldsymbol{x}_2, d_2) \in U_z\Big\}, \quad X_z \subset X,$$

where the state evolves according to the dynamic system

$$\dot{\boldsymbol{x}}_1 = \boldsymbol{A}_1 \boldsymbol{x}_1 + \boldsymbol{B}_{d,1} d_1 - \boldsymbol{\psi}_{n,m}(\boldsymbol{x}_1, \boldsymbol{x}_{2,n}, \mathbf{0}), \qquad \boldsymbol{x}_1(0) = \boldsymbol{x}_{10}, \tag{4.35a}$$

$$\dot{\boldsymbol{x}}_{2,n} = \boldsymbol{A}_2^{n,n} \boldsymbol{x}_{2,n} + \boldsymbol{B}_{d,2}^n d_2 + \boldsymbol{\psi}_n(\boldsymbol{x}_1, \boldsymbol{x}_{2,n}) + \boldsymbol{B}_u^n \boldsymbol{\mu}_z(\boldsymbol{x}_1, \boldsymbol{x}_{2,n}, d_2), \quad \boldsymbol{x}_{2,n}(0) = \boldsymbol{x}_{2n0}, \tag{4.35b}$$

where (4.14a) has been substituted in the concentration dynamics. For vanishing $\boldsymbol{x}_{2,m}$, the related system approaches the zero dynamics as $\boldsymbol{x}_{2,m} \to \mathbf{0}$. Accordingly, consider the following dynamic system

$$\begin{aligned}\dot{\boldsymbol{x}}_1 &= \boldsymbol{A}_1\boldsymbol{x}_1 + \boldsymbol{B}_{d,1}d_1 - \boldsymbol{\psi}_{n,m}(\boldsymbol{x}_1, \boldsymbol{x}_{2,n}, \boldsymbol{x}_{2,m}), && \boldsymbol{x}_1(0) = \boldsymbol{x}_{10}, && (4.36a)\\ \dot{\boldsymbol{x}}_{2,n} &= \boldsymbol{A}_2^{m,m}\boldsymbol{x}_{2,m} + \boldsymbol{A}_2^{m,n}\boldsymbol{x}_{2,n} + \boldsymbol{B}_{d,2}^{m}d_2 + \boldsymbol{\psi}_m(\boldsymbol{x}_1, \boldsymbol{x}_{2,m}) + \\ &\quad + \boldsymbol{B}_{u,2}^{n}\boldsymbol{\mu}_z(\boldsymbol{x}_1, \boldsymbol{x}_{2,n}, \boldsymbol{x}_{2,m}, d_2), && \boldsymbol{x}_{2,n}(0) = \boldsymbol{x}_{2n0}, && (4.36b)\end{aligned}$$

where

$$\boldsymbol{\mu}_z(\boldsymbol{x}_1, \boldsymbol{x}_{2,n}, \boldsymbol{x}_{2,m}, d_2) = -{\boldsymbol{B}_{u,2}^{m}}^{-1}\left(\boldsymbol{A}_2^{m,m}\boldsymbol{x}_{2,m} + \boldsymbol{A}_2^{m,n}\boldsymbol{x}_{2,n} + \boldsymbol{B}_{d,2}^{m}d_2 + \boldsymbol{\psi}_m(\boldsymbol{x}_1, \boldsymbol{x}_{2,m})\right).$$

The above system is equivalent to:

$$\begin{aligned}\dot{\boldsymbol{x}}_1 &= \boldsymbol{A}_1\boldsymbol{x}_1 + \boldsymbol{B}_{d,1}d_1 - \boldsymbol{\varphi}_1(\boldsymbol{x}_1) - \boldsymbol{\varphi}_{n,m}(\boldsymbol{x}_1, \boldsymbol{x}_{2,n}, \boldsymbol{x}_{2,m}), && \boldsymbol{x}_1(0) = \boldsymbol{x}_{10}, && (4.37a)\\ \dot{\boldsymbol{x}}_{2,n} &= \boldsymbol{A}_2^{z}\boldsymbol{x}_{2,n} + \boldsymbol{A}_2^{z,m}\boldsymbol{x}_{2,m} + \boldsymbol{B}_{d,2}^{z}d_2 + \boldsymbol{\psi}_z(\boldsymbol{x}_1, \boldsymbol{x}_{2,n}, \boldsymbol{x}_{2,m}), && \boldsymbol{x}_{2,n}(0) = \boldsymbol{x}_{2,n,0}, && (4.37b)\end{aligned}$$

where the involved matrices and nonlinearity are defined as

$$\begin{aligned}\boldsymbol{A}_2^{z} = \boldsymbol{A}_2^{n,n} - \boldsymbol{F}\boldsymbol{A}_2^{m,n}, \quad \boldsymbol{A}_2^{z,m} = \boldsymbol{A}_2^{n,m} - \boldsymbol{F}\boldsymbol{A}_2^{m,m}, \quad \boldsymbol{B}_{d,2}^{z} = \boldsymbol{B}_{d,2}^{n} - \boldsymbol{F}\boldsymbol{B}_{d,2}^{m},\\ \boldsymbol{\psi}_z(\boldsymbol{x}_1, \boldsymbol{x}_{2,n}, \boldsymbol{x}_{2,m}) = \boldsymbol{\psi}_n(\boldsymbol{x}_1, \boldsymbol{x}_{2,n}) - \boldsymbol{F}\boldsymbol{\psi}_m(\boldsymbol{x}_1, \boldsymbol{x}_{2,m}).\end{aligned}$$

In this case, the concentration remains the same as in (4.35), while the unmeasured temperature dynamics is composed by new dynamic elements constructed as combinations of unmeasured and measured matrices and functions through the feedback matrix $\boldsymbol{I} - \boldsymbol{F}$, where $\boldsymbol{F}$ is a diagonal block matrix defined as

$$\boldsymbol{F} = \boldsymbol{B}_u^{n}(\boldsymbol{B}_u^{m})^{-1} = \begin{cases} 1 & \text{if } s_k = \varsigma_i \text{ and } s_k \in \mathcal{R}_i \\ 0 & \text{else } s_k \neq \varsigma_i \text{ and } s_k \in \mathcal{R}_i \\ 0 & \text{else} \end{cases}, \; k = 1, \dots, N_e - 1, \; i = 1, \dots, q. \quad (4.38)$$

The structure of matrix $\boldsymbol{A}_2^{z}$ and the nonlinearities $\boldsymbol{\varphi}_{n,m}$, $\boldsymbol{\psi}_z$ is modified by the internal state feedback imposed by the MIMO zero dynamics controller (4.32), thus, the actuator-sensor configuration manifests its structure on matrix $\boldsymbol{F}$: the temperature dynamics are influenced by the corresponding control input depending on the jacket section and the corresponding sensor location.

The eigenvalues of zero dynamics matrix $\boldsymbol{A}_2^{z}$ are sensible to the considered number of jacket sections and sensors and their locations. Actually, matrix $\boldsymbol{A}_2^{z}$ is block diagonal, each block is of dimension $\frac{N}{q-1}$, and on each block matrix $-F$ injects, on the columns

$m_i - 1$ and m_i, the entries related to the unmeasured states on the zero dynamics control law (4.32). Each block has the following structure

$$
A^z_{2,i} = \begin{bmatrix}
-\mathrm{d}_j & \mathrm{c}_j & & & -\mathrm{b}_j & -\mathrm{c}_j & & & & \\
\mathrm{b}_j & -\mathrm{a}_j & \mathrm{c}_j & & -\mathrm{b}_j & -\mathrm{c}_j & & & & \\
& \mathrm{b}_j & \ddots & \ddots & -\mathrm{b}_j & -\mathrm{c}_j & & & & \\
& & \ddots & \ddots & \mathrm{c}_j - \mathrm{b}_j & -\mathrm{c}_j & & & & \\
& & & \mathrm{b}_j & -\mathrm{a}_j - \mathrm{b}_j & -\mathrm{c}_j & & & & \\
& & & & -\mathrm{b}_j & -\mathrm{a}_j - \mathrm{c}_j & \mathrm{c}_j & & & \\
& & & & -\mathrm{b}_j & \mathrm{b}_j - \mathrm{c}_j & \ddots & \ddots & & \\
& & & & -\mathrm{b}_j & -\mathrm{c}_j & \ddots & \ddots & \mathrm{c}_j & \\
& & & & -\mathrm{b}_j & -\mathrm{c}_j & & \mathrm{b}_j & -\mathrm{a}_j & \mathrm{c}_j \\
& & & & -\mathrm{b}_j & -\mathrm{c}_j & & & \mathrm{b}_j & -\mathrm{d}_j
\end{bmatrix}, \qquad (4.39)
$$

for $i = 1, \ldots q$ and $j = 1, 2$ with

$$
\mathrm{a}_1 = -\frac{1 + Pe_m \Delta s}{Pe_m \Delta s^2}, \quad \mathrm{b}_1 = \frac{1 + Pe_m \Delta_s}{Pe_m \Delta s^2}, \quad \mathrm{c}_1 = \frac{1}{Pe_m \Delta s^2}, \quad \mathrm{d}_1 = \mathrm{a}_1 + \mathrm{c}_1,
$$
$$
\mathrm{a}_2 = -\frac{2 + Pe_h \Delta s + Pe_h v \Delta s^2}{Pe_h \Delta s^2}, \quad \mathrm{b}_2 = \frac{1 + Pe_h \Delta_s}{Pe_h \Delta s^2}, \quad \mathrm{c}_2 = \frac{1}{Pe_h \Delta s^2}, \quad \mathrm{d}_2 = \mathrm{a}_2 + \mathrm{c}_2.
$$

Matrix A^z_2 is assumed to be Hurwitz with constants $(\lambda_{A^z_2}{}^*, a_{A^z_2})$ as in (3.10). Thus, there exist a symmetric matrix $P_z = P_z^T > 0$ that satisfy (3.8c) with (ζ_z, a_{P_z}).

The nonlinear reaction rate function $\varphi_{n,m}$ is almost the same as ψ but its entries are identified as unmeasured or unmeasured ones, this variation may change the related Lipschitz constants. The nonlinearity is given as

$$
\varphi_{n,m}(x_1, x_{2,n}, x_{2,m}) = \begin{bmatrix}
\psi_1(x_{1,1}, x_{2,1}) - \psi_{1,1}(0, x_{2,1}) \\
\vdots \\
\psi_i(x_{1,k}, x_{2,k}) - \psi_{1,k}(0, x_{2,k}) \\
\vdots \\
\psi_N(x_{1,N_e}, x_{2,N_e}) - \psi_{1,N_e}(0, x_{2,N_e})
\end{bmatrix}, \quad \begin{cases} k = m_i & \text{measured state} \\ k \neq m_i & \text{unmeasured state} \end{cases},
$$

where $k = 2, \ldots, N_e - 1$, $i = 1, \ldots, q$. Note that $\varphi_{n,m}$ can be also written as

$$
\varphi_{n,m}(x_1, x_{2,n}, x_{2,m}) = C_n^T \varphi_n(x_1, x_{2,n}) + C_y^T \varphi_m(x_1, x_{2,m}),
$$

where

$$
\varphi_j(x_1, x_{2,j}) = \psi_j(x_1, x_{2,j}) - \psi_j(x_1, \mathbf{0}), \quad j = n, m,
$$

and the functions $\boldsymbol{\psi}_n$ and $\boldsymbol{\psi}_m$ are defined after (4.4). Accordingly, the Lipschitz condition of $\boldsymbol{\varphi}_{n,m}$ with respect to the unmeasured-measured temperature states (uniformly in $\boldsymbol{x}_1$) can be computed with the Lipschitz constants of $\boldsymbol{\psi}_j$, $j = n, m$:

$$\left\| \boldsymbol{\varphi}_{n,m}(\boldsymbol{x}_1, \boldsymbol{x}_{2,n}, \boldsymbol{x}_{2,m}) \right\| \leq L_{x_{2,n}}^{\varphi_{n,m}} \|\boldsymbol{x}_{2,n}\| + L_{x_{2,m}}^{\varphi_{n,m}} \|\boldsymbol{x}_{2,m}\|, \quad L_{x_{2,n}}^{\varphi_{n,m}} = L_{x_{2,n}}^{\psi_n}, \; L_{x_{2,m}}^{\varphi_{n,m}} = L_{x_{2,m}}^{\psi_m}.$$

The effect of $\boldsymbol{F}$ on $\boldsymbol{\psi}_z$ is depends on the sensor-actuator configuration: for the i-th jacket section, the reaction rate of the unmeasured temperature states is subtracted by the reaction rate function of the i-th measured temperature state

$$\boldsymbol{\psi}_z(\boldsymbol{x}_1, \boldsymbol{x}_{2,n}, \boldsymbol{x}_{2,m}) = \left[\begin{array}{c} \psi_{n,1}(x_{1,n,1}, x_{2,n,1}) - \psi_{m,1}(x_{1,m,1}, x_{2,m,1}) \\ \vdots \\ \psi_{n,\frac{Ne}{q}}(x_{1,n,\frac{Ne}{q}}, x_{2,n,\frac{Ne}{q}}) - \psi_{m,1}(x_{1,m,1}, x_{2,m,1}) \\ \hline \psi_{n,\frac{Ne}{q}+1}(x_{1,n,\frac{Ne}{q}+1}, x_{2,n,\frac{Ne}{q}+1}) - \psi_{m,i}(x_{1,m,i}, x_{2,m,i}) \\ \vdots \\ \psi_{n,\frac{iNe}{q}}(x_{1,n,\frac{iNe}{q}}, x_{2,n,\frac{iNe}{q}}) - \psi_{m,i}(x_{1,m,i}, x_{2,m,i}) \\ \hline \psi_{n,\frac{iNe}{q}+1}(x_{1,n,\frac{iNe}{q}+1}, x_{2,n,\frac{iNe}{q}+1}) - \psi_{m,q}(x_{1,m,q}, x_{2,m,q}) \\ \vdots \\ \psi_{n,N_e}(x_{1,n,N_e}, x_{2,n,N_e}) - \psi_{m,q}(x_{1,m,q}, x_{2,m,q}) \end{array} \right] \tag{4.40}$$

Since the nonlinearity $\boldsymbol{\psi}$ is Lipschitz bounded with respect to its arguments, it is expected that the zero dynamics Lipschitz constants of the bounding condition

$$\|\boldsymbol{\psi}_z(\boldsymbol{x}_1, \boldsymbol{x}_{2,n}, \boldsymbol{x}_{2,m})\| \leq L_{x_1}^{\psi_z} \|\boldsymbol{x}_1\| + L_{x_{2,n}}^{\psi_z} \|\boldsymbol{x}_{2,n}\| + L_{x_{2,m}}^{\psi_z} \|\boldsymbol{x}_{2,m}\|,$$

are lower than the open-loop ones (4.5).

From the previous analysis it can be seen that both, the maximum real part of the eigenvalues of matrix $\boldsymbol{A}_2^z$ and the Lipschitz constants of the nonlinear function $\boldsymbol{\psi}_z$ are sensor location dependent, this fact will be exploited later for the construction of a criterion for the selection of the sensor locations.

Accordingly, considering that the measured temperature state is bounded as

$$\|\boldsymbol{x}_{2,m}\|_{sup} \leq \varepsilon_{2m}, \tag{4.41}$$

from the application of Corollary 3.2 (or Corollary 3.3), the unmeasured temperature dynamics are robustly stable if

$$\nu_z = \zeta_z - a_{P_z} L_{x_{2,n}}^{\psi_z} > 0 \quad (\text{ or } \nu_z = |\lambda_{A_2^z}{}^*| - a_{A_2^z} L_{x_{2,n}}^{\psi_z} > 0). \tag{4.42}$$

If the above condition is met, then the application of 3.1 yields to the following result on the robust stability of the zero dynamics in original coordinate.

Proposition 4.3. ***Robust stability of the zero dynamics*** *(4.35). Proof in Section d.2. Consider the system (4.37) subjected to bounded inputs $\boldsymbol{d}(t)$ and $\boldsymbol{x}_{2,m}(t)$ that satisfies (3.2b) and (4.41). Assume that the Lipschitz bounds (4.5) and (4.42) are satisfied in X_z. If the origin is unique and the next condition is met, (ν_1 is given in (4.17b) (or (4.19))),*

$$l_z := \nu_z - \frac{a_1 L_{x_{2,n}}^{\varphi_{n,m}} a_z L_{x_1}^{\psi_z}}{\nu_1} > 0. \tag{4.43}$$

Then, the zero dynamics (4.37) are nonlocally robustly stable in X_z.

Proposition 4.2 and Proposition 4.3 require the zero dynamics origin to be unique. Since the zero dynamics multiplicity varies with the sensor location set ς, a bifurcation analysis can be used to determine the feasible sensor set that ensures uniqueness of the origin and that. In a second step, the sensor locations must be chosen to maximize condition (4.43). These ideas will be used next to draw a sensor location criterion.

4.3.3 *Sensor location criterion*

Here, the zero dynamics static and dynamic properties will be analyzed to get a sensor location criterion. First, based on a bifurcation analysis the zero dynamics static multiplicity is characterized to identify the spatial subset in which the zero dynamics origin is unique. Then, the sensor location set is determined as the spatial positions in which the zero dynamics stability condition (4.43) is maximal.

4.3.3.1 *Multiplicity*

The dependency of the zero dynamic steady-state multiplicity on the sensor location set can be established using a variant of the bifurcation analysis presented in Section 4.2.1.2. For this aim, consider the statics of the zero dynamics in original-partitioned coordinate, nominal conditions and explicit representation of the nominal value of the related controller ($\bar{\boldsymbol{u}} = \boldsymbol{\mu}_z(\bar{\boldsymbol{x}}_1, \bar{\boldsymbol{x}}_{2,n})$):

$$\boldsymbol{0} = \boldsymbol{A}_1 \bar{\boldsymbol{x}}_1 - \boldsymbol{\varphi}_1(\bar{\boldsymbol{x}}_1) - \boldsymbol{\varphi}_{n,m}(\bar{\boldsymbol{x}}_1, \bar{\boldsymbol{x}}_{2,n}, \boldsymbol{0}), \tag{4.44}$$

$$\boldsymbol{0} = \boldsymbol{A}_2^{n,n} \bar{\boldsymbol{x}}_{2,n} + \boldsymbol{\psi}_n(\bar{\boldsymbol{x}}_1, \bar{\boldsymbol{x}}_{2,n}) + \boldsymbol{B}_{u,2}^{n} \bar{\boldsymbol{u}}. \tag{4.45}$$

Imposing the zero dynamics condition $\bar{\boldsymbol{y}} = \boldsymbol{0}$ on the input-multiplicity analysis in (4.12), the statics of the zero dynamics are given by the input multiplicity map

$$\bar{\boldsymbol{u}}_i = \mathfrak{f}_y(\boldsymbol{0}), \quad \bar{\boldsymbol{x}}_{2,n,i} = \mathfrak{f}_{2,n}(\bar{\boldsymbol{x}}_{2,m,i}, \bar{\boldsymbol{u}}_i), \quad \bar{\boldsymbol{x}}_1 = \mathfrak{f}_1(\bar{\boldsymbol{x}}_{2,n,i}, \bar{\boldsymbol{x}}_{2,m,i}), \quad i = 1, \ldots, n_s. \tag{4.46}$$

The solution for $\bar{\boldsymbol{u}} = \boldsymbol{0}_{N_e \times 1}$ will be always present but its uniqueness may change as the sensor location set ς varies. In the case of multiple solutions all of them satisfy the restriction of the zero output with different values of the static control input and static state solutions. Accordingly, the aim is to select ς so that the origin is unique.

For $q = 1$, a unique sensor with location $\varsigma_1 \in \mathcal{R}_1 = (0,1)$ and a unique homogeneous coolant jacket with domain $\mathcal{R}_1$, if the uniqueness of the origin is ensured, then it is inherited to the MIMO case since the additional sensors do not modify the statics. Accordingly, for the SISO case, the IOBM (4.46) becomes a scalar one $\mathfrak{f}_y$ that gives directly the values of u_l, $l = 1, \ldots, n_s$. In case $\bar{y} = 0$, then the input multiplicity, and the corresponding steady-states, can be geometrically characterized easily in a plane and the steady-states can be computed using the expressions in (4.46).

The above procedure can be performed sequentially for each possible sensor location $\varsigma_1 = s_{m_1} \in \mathcal{S} = \left[\frac{1}{\Delta s}, \frac{N}{\Delta s}\right]$, and can be represented in a bifurcation map that presents the steady-state multiplicity for each sensor location. This bifurcation analysis involves two continuation steps and is summarized in the following procedure that can be executed with a suitable software package such as MATCONT [43]:

Step 1: For $q = 1$, set $k = 1$ and $s_{m_1} = s_k$.

Step 2: Construct the IOBM (4.46) for s_{m_1}.

Step 3: Collect the steady-states related to the nominal case $\bar{u} = 0$.

Step 4: Plot the first steady-state value $\bar{x}_{1,1} \in X_{1,1}$ of the temperature sequence $\bar{\boldsymbol{x}}_1$ versus the sensor location $\varsigma_1 = s_{m_1}$ in the plane $\mathcal{S} \times X_{1,1}$.

Step 5: Set $k = k + 1$ and proceed again from Step 2, if $k = \frac{N}{\Delta s}$ the procedure ends.

From this numerical analysis, the region $\mathcal{S}_m \in \mathcal{S}$ in which a single sensor ensures the zero dynamics origin uniqueness is identified:

$$\mathcal{S}_m = \{s_{m_1} \in \mathcal{S} \,|\, (\boldsymbol{x}_1, \boldsymbol{x}_{2,n}) = (\mathbf{0}_N, \mathbf{0}_{N-1}) \text{ Is the unique steady-state}\}. \tag{4.47}$$

For $q = 2, 3$, the above condition must be fulfilled to ensure the uniqueness of the zero dynamics, and the specific location for $\varsigma_1 \in \mathcal{S}_m$ and $\varsigma_i = s_{m_i}$, $i = 2, 3$ must be established so that the dynamic condition (4.43) is maximized.

4.3.3.2 *Sensor locations determination*

To find a sensor location set that satisfies (4.47) and maximize l_z, define the hypersurface $\Gamma_z(\boldsymbol{\varsigma})$ as the geometric loci spanned by l_z for $\varsigma_i \in \mathcal{R}_i$ subjected to (4.47):

$$\Gamma_z(\boldsymbol{\varsigma}) = l_z(\boldsymbol{\varsigma}), \quad s.t. \quad \varsigma_{siso} \in \mathcal{S}_m, \tag{4.48a}$$

and denote as $\Gamma_z^+(\boldsymbol{\varsigma})$ the maximum value of the hypersurface $\Gamma_z(\boldsymbol{\varsigma})$, i. e.,

$$\Gamma_z^+(\boldsymbol{\varsigma}) = \max \Lambda_z^+(\boldsymbol{\varsigma}). \tag{4.48b}$$

Thus, the sensor location set is defined as

$$\boldsymbol{\varsigma} = \left\{\varsigma_{m_i} \in \mathcal{R}_i \subset \mathcal{S} \,|\Gamma_z(\boldsymbol{\varsigma}) = \Gamma_z^+(\boldsymbol{\varsigma})\right\}. \tag{4.48c}$$

The above condition ensures the selection of the sensor location set which produce the most robust and fastest zero dynamics which will benefit the closed-loop response of the controllers constructed in Section 4.4.2.

While condition (4.48) establishes a formal criterion to select the sensor location, it must be evaluated for the particular class of reactors and specific reaction rate function and parameters, i. e., it is needed to compute the maximum eigenvalues of the matrices $\boldsymbol{A}_1$ (see Appendix c) and $\boldsymbol{A}_2^z$, defined in (4.39), the sector condition (4.15) of the nonlinearity $\boldsymbol{\varphi}_1$ (4.14a) and the Lipschitz constants of the nonlinearities $\boldsymbol{\psi}_{n,m}$, given by $\boldsymbol{\varphi}_2 \in$ (4.14a) in unmeasured-measured coordinate, and $\boldsymbol{\psi}_z$, defined in (4.40).

From a geometric interpretation, for, $q = 1$, $\Gamma_z(\varsigma)$ is a curve, while for $q = 2, 3$ it corresponds to a surface and a hypersurface, respectively. Nevertheless, since in the MIMO cases the sensor $\varsigma \in \mathcal{S}_m$ must be fixed, the geometric representations can be replaced for a curve, for $q = 2$, and a surface, for $q = 3$. The application of the presented sensor location criterion is performed next for the case study.

4.3.3.3 *Application to the case example*

The application of the proposed sensor location procedure to the case study of Section 2.5: model (3.22) with parameters presented in Table 2.1, and efficient model order $n_e = 2N_e = 40$ (discretized over a mesh (3.16) with $N_e = 20$ equidistant, $\Delta s = \frac{1}{21}$, interior points) determined in (3.31) yields the sensor location bifurcation diagram of Figure 4.3.

Three main regions of behavior can be identified: (i) $\mathcal{S}_m = \left[\frac{1}{21}, \frac{6}{21}\right] \approx [0.48, 0.29]$ where the origin is unique, (ii) the bifurcation position $\varsigma_1 = s_7 = \frac{7}{21} \approx 0.33$, and (iii) $\mathcal{S}_b = \left[\frac{8}{21}, \frac{20}{21}\right] \approx [0.38, 0.95]$ of steady-state multiplicity. Thus, from the SISO case the restriction (4.47) is $s_{m_1} \in \mathcal{S}_m = \left[\frac{1}{21}, \frac{6}{21}\right] \approx [0.48, 0.29]$.

The next step is to compute the specific locations for the sensor set according to the geometric procedure in (4.48). The case study considers a first order Arrhenius temperature dependency reaction rate function given by (2.12). The alternative definition for $\nu_z = |\lambda_{A_2^z}{}^* - a_{A_2^z} L_{x_{2,n}}^{\psi_z}|$ is used in the definition of l_z (in (4.43)):

$$l_z = |\lambda_{A_2^z}{}^* - a_{A_2^z} L_{x_{2,n}}^{\psi_z}| - \frac{a_1 L_{x_{2,n}}^{\varphi_{n,m}} a_z L_{x_1}^{\psi_z}}{\nu_1} > 0. \tag{4.49}$$

The matrices $\boldsymbol{A}_j$, $j = 1, 2$ are defined after (3.19). The decaying rate $\nu_1 = \zeta_1 + c$ and the constant a_{P_1} of matrix $\boldsymbol{A}_1$ are characterized in (4.25). The rest of the parameters involved in the definition of (4.49) change with the number of jacket sections and sensors and their locations and thus are computed for each required case $q = 1, 2, 3$.

First, for $q = 1$, the evaluation of the sensor location-based stability condition for the SISO case with a unique jacket with domain $\mathcal{R}_1 = \mathcal{S}$ and a unique sensor at location ς_1 is shown in Figure 4.4a. It can be seen that l_z is positive in the region $s \in [0, 0.52]$ and contains the region of robust monostability $\mathcal{S}_m$ (see Figure 4.3). Furthermore, l_z reaches its maximum at $s_5 \approx 0.24$, thus, the sensor location must be placed at

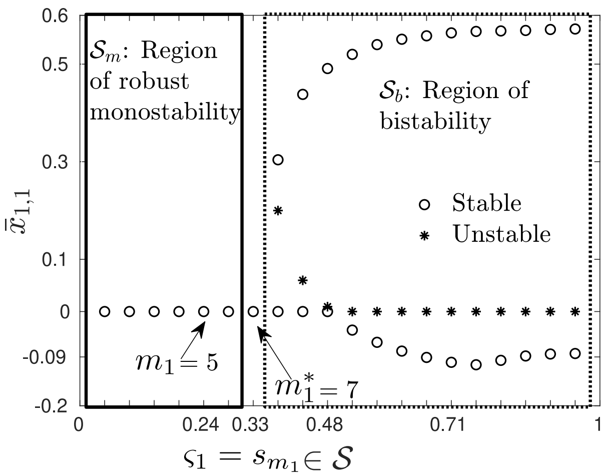

Figure 4.3: Dependency of the zero dynamics multiplicity on the sensor location ς_1 of the case study with efficient discretization order $N_e = 20$. The region of robust uniqueness of the origin is $\mathcal{S}_m = \left[\frac{1}{21}, \frac{6}{21}\right] \approx [0.48, 0.29]$, while the region of bistability is $\mathcal{S}_b = \left[\frac{8}{21}, \frac{20}{21}\right] \approx [0.38, 0.95]$.

$\varsigma_1 = s_{m_1} = s_5 \approx 0.24$, which ensures the fastest convergence of zero dynamics to the origin, the unique steady-state. The obtained sensor location match the one that is get with the industrial sensitivity criterion, before the hot spot where the temperature gradient is maximum [68; 100; 108], thus formalizes this heuristic recommendation.

For $q = 2, 3$, the sensor location $s_1 = s_{m_1} \approx 0.24$ is retained. For the case $q = 2$, with jacket sections domains $\mathcal{R}_1 \approx [0.05, 0.48]$ and $\mathcal{R}_2 \approx [0.52, 0.95]$, the evaluation of l_z in $\mathcal{R}_2$ is presented in Figure 4.4b, where it can be concluded that the second sensor location must be selected as $\varsigma_2 = s_{m_2} \approx 0.95$. Finally, for $q = 3$ with jacket section domains $\mathcal{R}_1 \approx [0.05, 0.29]$, $\mathcal{R}_2 = [0.33, 0.62]$, and $\mathcal{R}_3 = [0.67, 0.95]$, the evaluation of l_z in $\mathcal{R}_2 \times \mathcal{R}_3$, shown in Figure 4.4c, leads to $\varsigma_2 = s_{m_2} \approx 0.62$ and $\varsigma_3 = s_{m_3} \approx 0.95$.

Note that, in the 1-sensor case, the stability condition $l_z > 0$ is only ensured by locating the sensor at $\varsigma_1 \in [0, 0.52] \in \mathcal{S}_m$, and there are some regions in which the zero dynamics origin is non-unique and unstable in some cases. In the 2 and 3-sensor cases, the stability of the origin is ensured by the first sensor location, and condition l_z is enlarged, accordingly, it can be concluded that using a larger number of sensors the stability of the zero dynamics convergence is accelerated.

4.4 STATE FEEDBACK CONTROL

Passivity-based control [126; 31], originated in control of electrical and mechanical systems [103], where state variables are naturally connected with energy, is a well-known control technique that exploits the natural dissipativity of systems with the same number of inputs and outputs, to ensure robust stability in the presence of

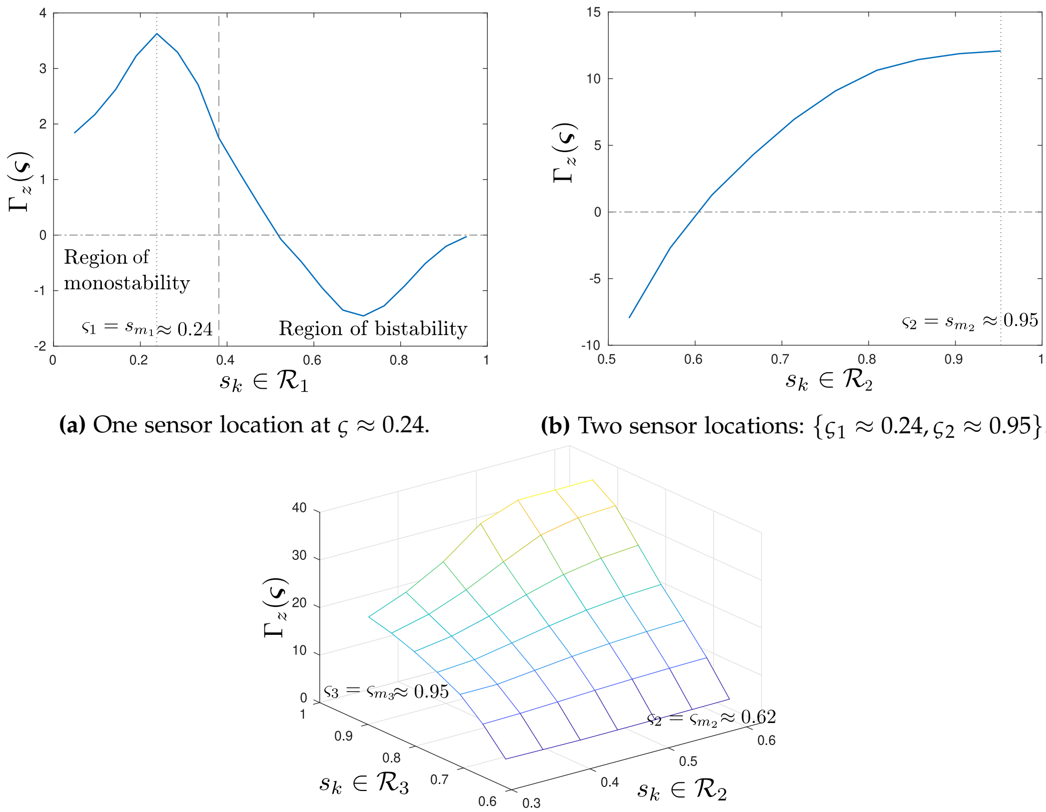

(a) One sensor location at $\varsigma \approx 0.24$.

(b) Two sensor locations: $\{\varsigma_1 \approx 0.24, \varsigma_2 \approx 0.95\}$.

(c) Three sensor locations: $\{\varsigma_1 \approx 0.24, \varsigma_2 \approx 0.62, \varsigma_2 \approx 0.95\}$.

Figure 4.4: Sensor location criterion: evaluation of the surface $\Gamma_z(\varsigma)$ (4.48).

parameter uncertainty and bounded disturbances. When a system is not passive in the open-loop, it can be passivated via feedback.

In the context of chemical processes, the direct generalization of passivity-based control within an energetic framework is not a straightforward task when irreversible chemical reactions are considered since the usual state variables are not directly connected with the energy of the system. Efforts have been made to combine a thermodynamics representation of chemical variables and Port-Hamiltonian modeling to link passivity-based control with thermodynamics [110; 9]. Nevertheless, in a more abstract framework it is possible to design passive controllers by feedback passivation.

In what follows, a passivity-based control design is constructed and interpreted with physical insight: the understanding of the stabilizing and destabilizing effects of the open-loop dynamic components enables the possibility to renders the closed-loop system robustly stable via passivity-based feedback control.

4.4.1 *Feedback passivation*

The required conditions for a system to be feedback equivalent to a passive system are [32]: (i) relative degree one, and (ii) weakly minimum phase, i. e., the origin of the zero dynamics must be stable in the sense of Lyapunov. In this study, the latter condition is replaced for robust stability of the zero dynamics origin.

In Section 4.3 it was shown that: (i) the vector of relative degrees (4.26) has only one-entries since by construction the matrix $\boldsymbol{B}_u^m$ is nonsingular (because i. e., $v > 0$, see (4.4e)) and (ii) the zero dynamics has the origin as unique robustly stable steady-state provided that the sensor location set $\boldsymbol{\varsigma}$ is selected as in (4.48), and Proposition 4.2 (or equivalently Proposition 4.3). These results are enables the following statement.

Proposition 4.4. ***Feedback equivalence to a passive system. Proof in Section d.3***
The reactor model (4.4) *is feedback passive if the following conditions are met*

(i) $v > 0$

(ii) $\boldsymbol{\varsigma} = \left\{\varsigma_{m_i} \in R_i \subset \mathcal{S} \,|\, \varsigma_{siso} \in \mathcal{S}_m,\ \text{and}\ \Lambda_z(\boldsymbol{\varsigma}) = \Lambda_z^+(\boldsymbol{\varsigma})\right\}$.

The definitions of $\mathcal{S}_m$ and $\Lambda_z(\boldsymbol{\varsigma})$ are given in (4.47) and (4.48), respectively. From the proof of this Proposition 4.4, the feedback control law that renders (4.4) passive is

$$\boldsymbol{u} = \boldsymbol{B}_u^{m\,-1}\bigg(- \boldsymbol{B}_{u,2}^{m\;\;-1}\left(\boldsymbol{A}_2^{m,m}\boldsymbol{x}_{2,m} + \boldsymbol{A}_2^{m,n}\boldsymbol{x}_{2,n} + \boldsymbol{B}_{d,2}^m d_2 + \boldsymbol{\psi}_m(\boldsymbol{x}_1, \boldsymbol{x}_{2,m})\right) + \\ + \left(\partial_\eta V_\eta(\boldsymbol{\eta})\boldsymbol{F}(\boldsymbol{\eta},\boldsymbol{\xi})\right)^T_{(\boldsymbol{\eta}^T,\boldsymbol{\xi}^T)^T = \boldsymbol{T}^{-1}(\boldsymbol{x})} - \boldsymbol{y}^T\boldsymbol{\kappa}_1(\boldsymbol{y}) - \boldsymbol{y}^T\boldsymbol{\kappa}_2(\boldsymbol{y})\bigg). \tag{4.50}$$

where $\boldsymbol{\kappa}_1$ and $\boldsymbol{\kappa}_2$ are static passive nonlinearities.

Note that the above nonlinear control law: (i) needs the explicit functionality of $\boldsymbol{F}(\boldsymbol{\eta},\boldsymbol{\xi})$ and the zero dynamics Lyapunov function, and (ii) is highly dependent on the system parameters. Accordingly, Proposition 4.4 only establishes the feedback passivity of system (3.22), but it is not used for implementation purposes. Next, a saturated state feedback control, that use some terms of (4.50), will be constructed.

4.4.2 *Saturated control*

The enforcement, on the reactor model (4.4), of the linear output regulation dynamics

$$\dot{\boldsymbol{y}} = -\boldsymbol{K}_c\boldsymbol{y}, \quad \boldsymbol{K}_c = \boldsymbol{K}_c^T > 0, \tag{4.51}$$

where $\boldsymbol{K}$ is a diagonal gain matrix, yields the output linearizing control law

$$\boldsymbol{u} = \boldsymbol{\mu}(\boldsymbol{x}_1, \boldsymbol{x}_{2,n}, \boldsymbol{x}_{2,m}, d_2), \tag{4.52a}$$

where

$$\boldsymbol{\mu}(\boldsymbol{x}_1, \boldsymbol{x}_{2,n}, \boldsymbol{x}_{2,m}, d_2) = -\boldsymbol{B}_{u,2}^{m\;\;-1}\left(\boldsymbol{A}_2^{m,m}\boldsymbol{x}_{2,m} + \boldsymbol{A}_2^{m,n}\boldsymbol{x}_{2,n} + \boldsymbol{B}_{d,2}^m d_2 + \boldsymbol{\psi}_m(\boldsymbol{x}_1, \boldsymbol{x}_{2,m}) + \boldsymbol{K}_c\boldsymbol{y}\right).$$

The preceding state feedback control law is a particular case of the passivating law (4.50) with $\boldsymbol{\kappa}_1(\boldsymbol{y}) + \boldsymbol{\kappa}_2(\boldsymbol{y}) = \boldsymbol{K}_c\boldsymbol{y}$, and the term related to the zero dynamics neglected.

The application of the above controller to the open-loop dynamics in the normal form (4.30) yields the cascaded closed-loop dynamics

$$\dot{\boldsymbol{\eta}} = \boldsymbol{A}_\eta\boldsymbol{\eta} + \boldsymbol{B}_d^\eta\boldsymbol{d} + \boldsymbol{\varphi}_\eta(\boldsymbol{\eta}) + \boldsymbol{F}(\boldsymbol{\eta},\boldsymbol{\xi})\boldsymbol{\xi}, \qquad \boldsymbol{\eta}(0) = \boldsymbol{\eta}_0, \tag{4.53a}$$

$$\dot{\boldsymbol{\xi}} = -\boldsymbol{K}_1\boldsymbol{\xi}, \qquad \boldsymbol{\xi}(0) = \boldsymbol{\xi}_0. \tag{4.53b}$$

By design the external dynamics converges exponentially to zero, and as a consequence of the robust stability of the internal dynamics with respect to $\boldsymbol{\xi}$, stated in Proposition 4.2, the closed-loop dynamics are robustly stable.

The control law (4.52) cancels out the stabilizing effects of heat convection and diffusion transport as well as heat conduction, $\boldsymbol{A}_2^{m,m}\boldsymbol{x}_{2,m}$ and the destabilizing effect of the reaction rate function $\boldsymbol{\psi}_m$, to impose a linear output regulation dynamics. To do so, the controller must know precisely the matrix $\boldsymbol{A}_2^{m,m}$ and the functionality of $\boldsymbol{\psi}_m$.

While the compensation of the reaction rate function is beneficial, the compensation of the stabilizing linear term is not a must and may be preferable to keep this stabilizing mechanism. Accordingly, an alternative control law is given by

$$\boldsymbol{u} = \boldsymbol{\mu}_2(\boldsymbol{x}_1, \boldsymbol{x}_{2,n}, \boldsymbol{x}_{2,m}, d_2), \tag{4.54a}$$

where

$$\boldsymbol{\mu}_2(\boldsymbol{x}_1, \boldsymbol{x}_{2,n}, \boldsymbol{x}_{2,m}, d_2) = -{\boldsymbol{B}_{u,2}^m}^{-1}\left(\boldsymbol{B}_{d,2}^m d_2 + \boldsymbol{\psi}_m(\boldsymbol{x}_1, \boldsymbol{x}_{2,m}) + \boldsymbol{K}_c\boldsymbol{y}\right), \quad \boldsymbol{K}_c = \boldsymbol{K}_c^T > 0,$$

which will be considered with late (or early) lumping in Chapter 5 (or Chapter 6).

Due to physical and actuator limitations, constrained control must be considered, accordingly, controller (4.52) is restricted to the set $U_{c,0} \subset U$, where $U_{c,0} = [u^-, u^+]$ is a design degree of freedom and must be chosen so that the closed-loop dynamics have a unique steady-state at the origin. The saturated control laws are

$$\boldsymbol{u} = \boldsymbol{\mu}_s(\boldsymbol{x}_1, \boldsymbol{x}_{2,n}, \boldsymbol{x}_{2,m}, d_2) := \mathrm{sat}_{\mathrm{u}^-}^{\mathrm{u}^+}[\boldsymbol{\mu}(\boldsymbol{x}_1, \boldsymbol{x}_{2,n}, \boldsymbol{x}_{2,m}, d_2)] \tag{4.54b}$$

where $\boldsymbol{\mu}$ is given in (4.52). The closed-loop robust stability is assured next.

4.4.3 *Closed-loop stability*

To ensure the stability of the closed-loop system and select the control limits, the effect of control saturation on: (i) the zero dynamics, (ii) the closed-loop system, and (iii) its steady-state multiplicity will be characterized to find stability conditions and a criterion to select the control limits so that uniqueness of the origin is attained to preclude additional undesired closed-loop steady-states (a possible phenomenon due to open-loop steady-state multiplicity and control saturation [35; 12]).

4.4.3.1 *Zero dynamics under saturated control*

Consider the constrained version of the zero dynamics controller (4.32):

$$\boldsymbol{u} = \boldsymbol{\mu}_{s,z}(\boldsymbol{x}_1, \boldsymbol{x}_{2,n}, d_2) := \operatorname{sat}_{\mathrm{u}^-}^{\mathrm{u}^+} \boldsymbol{\mu}_z(\boldsymbol{x}_1, \boldsymbol{x}_{2,n}, d_2)$$

where $\boldsymbol{\mu}_{s,z} : \mathcal{X}_z \subset X_z \to U_s \subset \mathcal{U}_z \subset \mathcal{U}$. The restricted zero dynamics results from the application of the above control to system (3.22) and is defined over the set

$$\mathcal{X}_z = \left\{ \boldsymbol{x}_1 \times \boldsymbol{x}_2 \in X \,|\, \boldsymbol{y} = \boldsymbol{0},\, \boldsymbol{\mu}_{z,s}(\boldsymbol{x}_1, \boldsymbol{x}_{2,n}) \in U_{c,0} \right\} \tag{4.55}$$

From a geometric perspective, the unconstrained zero dynamics, with control set U_z, has the origin as unique steady-state, then, all trajectories that begin in the set $X_z \subset X$ remain on it and exponentially converge to the origin. Contrary, for the constrained the zero dynamics, with $U_{c,0} \subset U_z$, the set X_z shrinks to $\mathcal{X}_z$, and there are three type of trajectories: (i) the ones born in $\mathcal{X}_z$ and that remain on it, (ii) the ones that born outside $\mathcal{X}_z$, and evolve in open-loop mode (with saturated control action) and after some transient enter the zero dynamics set and converge to the origin, and (iii) the ones that stay in an induced limit cycle due to saturation.

Accordingly, to rule out zero dynamics limit cycles, the control set $U_{c,0}$ must be chosen as close as possible to the zero dynamics control set U_z. This is stated next.

Lemma 4.1. *The open-loop system (3.22) is feedback equivalent to a passive system over the state-space $\mathcal{X}_z$ if and only if conditions of Proposition 4.4 are fulfilled, the closed-loop origin is unique and the control set $U_{c,0}$ is robustly included in its maximal one U_z, i.e., $U_{c,0} \subseteq U_z$.*

4.4.3.2 *Closed-loop stability*

The closed-loop dynamics are given by

$$\dot{\boldsymbol{x}}_1 = \boldsymbol{A}_1 \boldsymbol{x}_1 + B_{d,1} d_1 - \boldsymbol{\phi}(\boldsymbol{x}_1) - \boldsymbol{\varphi}_{n,m}(\boldsymbol{x}_1, \boldsymbol{x}_{2,n}, \boldsymbol{x}_{2,m}), \qquad \boldsymbol{x}_1(0) = \boldsymbol{x}_{1,0} \tag{4.56a}$$

$$\dot{\boldsymbol{x}}_{2,n} = \boldsymbol{A}_2^{n,n} \boldsymbol{x}_{2,n} + \boldsymbol{A}_2^{m,n} \boldsymbol{x}_{2,m} + \boldsymbol{B}_{d,2}^{n} d_2 + \boldsymbol{\psi}_n(\boldsymbol{x}_1, \boldsymbol{x}_{2,n}) + \boldsymbol{B}_{u,2}^{n} \boldsymbol{\mu}_s(\boldsymbol{x}_1, \boldsymbol{x}_{2,n}, \boldsymbol{x}_{2,m}, d_2), \quad \boldsymbol{x}_{2,n}(0) = \boldsymbol{x}_{2,n,0} \tag{4.56b}$$

$$\dot{\boldsymbol{x}}_{2,m} = \boldsymbol{A}_2^{m,m} \boldsymbol{x}_{2,m} + \boldsymbol{A}_2^{m,n} \boldsymbol{x}_{2,n} + \boldsymbol{B}_{d,2}^{m} d_2 + \boldsymbol{\psi}_m(\boldsymbol{x}_1, \boldsymbol{x}_{2,m}) + \boldsymbol{B}_{u,2}^{m} \boldsymbol{\mu}_s(\boldsymbol{x}_1, \boldsymbol{x}_{2,n}, \boldsymbol{x}_{2,m}, d_2), \quad \boldsymbol{x}_{2,m}(0) = \boldsymbol{x}_{2,m,0}. \tag{4.56c}$$

Assuming control limits that assure the origin is the unique steady-state, robust stability can be established by the robust stability of the zero dynamics and the Seibert's Reduction Principle [117].

When the control set $U_{c,0} = U_z$ is the maximal one, by the Seibert's Reduction Principle, the state trajectories converge to the zero dynamics set X_z in which the origin is the unique attractor, accordingly, due to the invariance of the state-space set X, all the trajectories converges to the origin. Closed-loop limit cycling is ruled out when the control set is the maximal one, meaning that the closed-loop reactor is robustly globally stable over X. This in turn implies that closed-loop robust stability can be attained by choosing the control set $U_{c,0} \subseteq \mathcal{U}_z$ as established in Lemma 4.1. Next, a practical criterion to select the control limits based on open-loop and closed-loop stability properties will be established.

4.4.3.3 *Closed-loop multiplicity and control limits selection criterion*

For the purpose at hand, consider the nominal closed-loop statics:

$$\mathbf{0} = \boldsymbol{A}_1 \boldsymbol{x}_1 - \boldsymbol{\phi}(\boldsymbol{x}_1) - \boldsymbol{\varphi}_{n,m}(\boldsymbol{x}_1, \boldsymbol{x}_{2,n}, \boldsymbol{x}_{2,m}), \tag{4.57a}$$

$$\mathbf{0} = \boldsymbol{A}_2^{n,n} \boldsymbol{x}_{2,n} + \boldsymbol{A}_2^{m,n} \boldsymbol{x}_{2,m} + \boldsymbol{\psi}_n(\boldsymbol{x}_1, \boldsymbol{x}_{2,n}) + \boldsymbol{B}_{u,2}^{n} \boldsymbol{u}, \tag{4.57b}$$

$$\mathbf{0} = \boldsymbol{A}_2^{m,m} \boldsymbol{x}_{2,m} + \boldsymbol{A}_2^{m,n} \boldsymbol{x}_{2,n} + \boldsymbol{\psi}_m(\boldsymbol{x}_1, \boldsymbol{x}_{2,m}) + \boldsymbol{B}_{u,2}^{m} \boldsymbol{u}, \tag{4.57c}$$

$$\bar{\boldsymbol{u}} = \boldsymbol{\mu}_s(\bar{\boldsymbol{x}}_1, \bar{\boldsymbol{x}}_{2,n}, \boldsymbol{x}_{2,m}). \tag{4.57d}$$

Note that, by construction, the static control law $\boldsymbol{\mu}_s$ is a restricted modification of the static equation (4.57c), accordingly, rewrite the control law $\boldsymbol{\mu}_s$ in explicit form:

$$\mathbf{0} = \boldsymbol{A}_2^{m,m} \boldsymbol{x}_{2,m} + \boldsymbol{A}_2^{m,n} \boldsymbol{x}_{2,n} + \boldsymbol{\psi}_m(\boldsymbol{x}_1, \boldsymbol{x}_{2,m}) + \boldsymbol{B}_u^{n} \boldsymbol{u} + \boldsymbol{K}_c \boldsymbol{x}_{2,m}, \quad u_i \in [u^-, u^+], \tag{4.58}$$

In the static equations (4.57), the triplet (4.57a)-(4.57b)-(4.57c) coincide with the open-loop statics (4.6), and the application of (4.11) leads to the IOBM hypersurface

$$\mathscr{O} = \{(\bar{\boldsymbol{u}}, \bar{\boldsymbol{y}}) \in U \times \mathcal{Y} \,|\, \bar{\boldsymbol{y}} = \mathfrak{f}_u(\boldsymbol{u})\}. \tag{4.59a}$$

The combination of (4.57a)-(4.57b)-(4.58), the closed-loop statics, by applying again the procedure in Section 4.2.1.2 yields the closed-loop control hypersurface

$$\mathscr{C} = \{(\bar{\boldsymbol{u}}, \bar{\boldsymbol{y}}) \in \mathcal{U}_{c,0} \times \mathcal{Y} \,|\, \bar{\boldsymbol{y}} = \mathfrak{f}_u^c(\boldsymbol{u})\}. \tag{4.59b}$$

The intersection of both curves

$$(\bar{\boldsymbol{u}}, \bar{\boldsymbol{y}}) = \mathscr{O} \cap \mathscr{C}, \quad \mathscr{O} \in U \times \mathcal{Y}, \mathscr{C} \in \mathcal{U}_{c,0} \times \mathcal{Y}, \tag{4.59c}$$

gives the input-output static pair while the rest of the steady-states can be computed from (4.11). According to Lemma 4.1, the closed-loop origin must be the unique steady-state, which is ensured if the unique intersection in (4.59c) is the origin, i. e.,

$$\mathscr{O} \cap \mathscr{C} = (\mathbf{0}_q, \mathbf{0}_q) \;\Rightarrow \mathbb{S}_c = \{\mathbf{0}_{2N_e}\}. \tag{4.59d}$$

This result is stated in the following lemma.

Lemma 4.2. *The closed-loop statics (4.57), related to the dynamics (4.56), has the origin as unique steady-state if and only if the unique point of intersection of the open and closed-loop bifurcation surfaces $\mathscr{O}$ and $\mathscr{C}$ is zero: if (4.59d) is satisfied.*

In the unconstrained version of static problem (5.39), the procedure described above leads to two hypersurfaces that intersects only at the origin. While in the constrained statics, the control limits may produce extra intersections leading to additional undesired closed-loop steady-states. To avoid that, the control limits must be selected to get a unique intersection at the origin. Since the open-loop IOBM is a rotated version of a bifurcation curve, the control bifurcation values can be identified to draw a control limits selection criterion as it was previously done in [112; 114; 113].

4.4.3.4 *Control limit selection criterion*

Here, a procedure to select the control limits, on the basis of the SISO case of controller (4.52), is drawn. The determined control limits can be inherited to each controller in the MIMO case. The procedure is based on bifurcation and continuation analyses and it can be performed with a suitable software package such as MATCONT [43].

Step 1 Use the open-loop static equations (4.57a)-(4.57b)-(4.57c) to get (4.11) and solve with continuation to draw the open-loop IOBM (4.59a).

Step 2 Identify the control values u_* and u^* where saddle-node bifurcation occurs.

Step 3 To ensure uniqueness of the closed-loop origin, select the control limits as

$$u^- < u_*, \quad u^+ > u^*, \tag{4.60}$$

Step 4 Use the closed-loop static equations (4.57a)-(4.57b)-(4.58) and repeat the procedure in Section 4.2.1.2 to draw the closed-loop IOBM (4.59b).

Step 5 Verify that with the selected control limits, zero is the unique intersection (4.59c).

Accordingly, the closed-loop dynamics (4.56) are robustly stable if the control limits are selected so that the set $U_{c,0}$ contains the bifurcation set $U^* = [u_*, u^*]$ of the open-loop IOBM, and by virtue ofLemma 4.1. This is stated next.

Proposition 4.5. *Closed-loop stability with saturated state feedback control.*
The closed-loop system (4.56) with saturated control (4.52), is robustly stable with the origin as unique steady-state if Lemma 4.1 and $U_{c,0}$ and $U^* \subset U_s \subseteq U_z(X_z)$ is met.

4.4.3.5 *Application to the case example*

Following the previous procedure, in Figure 4.5 shows the open-loop IOBM (with output at location $\varsigma_1 \approx 0.24$) of the model (4.1) with N_e. The identification of the bifurcation values, where the case study undergoes saddle-node bifurcation phenomenon, gives: $u_* = -0.38$, and $u^* = 0.28$. From Proposition 4.5, the control limits that assure the origin is the unique robustly stable steady-state are

$$u^- = -0.42 < u_* = -0.38 < \bar{u} = 0 < u^* = 0.28 < u^+ = 0.35. \tag{4.61}$$

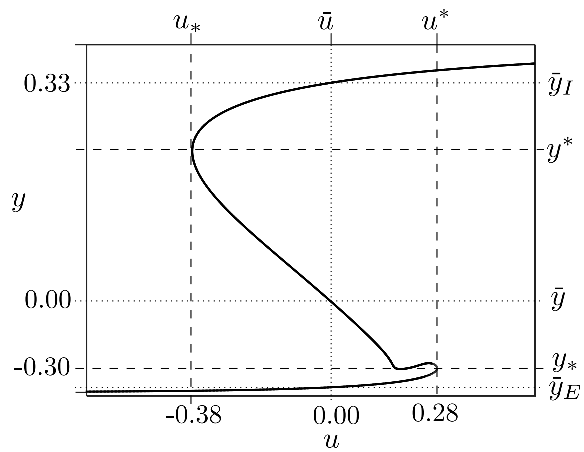

Figure 4.5: Open-loop IOBM (with output at location $s_y \approx 0.24$) of the open-loop N_e-stage model (4.1). The identified bifurcation set is $U^* = [u_*, u^*] = [-0.38, 0.28]$.

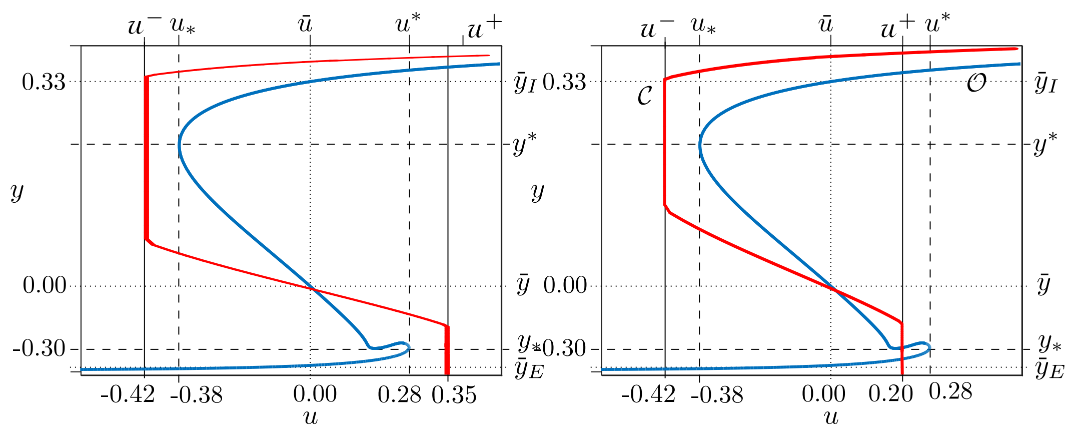

(a) Open-loop $\mathscr{O}$ and closed-loop $\mathscr{C}$ bifurcation curves. The control limits are appropriately selected as $(u^-, u^+) = (-0.42, 0.20)$ so that the origin is the unique steady-state.

(b) Open-loop $\mathscr{O}$ and closed-loop $\mathscr{C}$ bifurcation curves. The control limits are inappropriately selected as $(u^-, u^+) = (-0.42, 0.20)$ so that there is closed-loop steady-state multiplicity.

Figure 4.6: Illustration of the control limit selection criterion for the case example.

In Figure 4.6a, it is illustrated how with these control limits, the curve $\mathscr{C}$ and the open-loop IOBM $\mathscr{O}$ have zero as unique intersection.

In case the upper limit is not selected appropriately, for instance $u^+ = 0.20 < u^* = 0.28$, it can be seen, in Figure 4.6b, that the curves have three intersections: one at the zero and two additional ones that imply closed-loop steady-state multiplicity, an undesired condition. These results corroborate the effectiveness of the proposed criterion for the selection of control limits.

4.5 CONTROL-ESTIMATION SYSTEM

The proposed CES is made by the state feedback control (4.52) and an estimator which has two purposes: (i) output feedback control, and (ii) state monitoring. In this section, using the efficient early-lumping model (4.1)-(3.29d), such state estimator is constructed, on the basis of a closed-loop detectability property, and combined with (4.52) to obtain an advanced CES. Robust closed-loop stability is assured.

4.5.1 *Estimation model*

Recall the actual reactor dynamics (4.2b), use the partition form (4.4), and apply the state feedback control law (4.52) to get the actual closed-loop dynamics

$$\begin{aligned}
\dot{x}_1 &= f_1(x_1, x_2, d_1) + e_1^c(x_1, x_{2,n}, x_{2,m}, d_2, \pi, \tilde{p}), & x_1(0) &= x_{10}, && (4.62a)\\
\dot{x}_{2,n} &= f_{2,n}^c(x_1, x_{2,n}, x_{2,m}, d_2) + e_{2,n}^c(x_1, x_{2,n}, x_{2,m}, d_2, \pi, \tilde{p}), & x_{2,n}(0) &= x_{2n0}, && (4.62b)\\
\dot{x}_{2,m} &= f_{2,m}^c(x_1, x_{2,n}, x_{2,m}, d_2) + e_{2,m}^c(x_1, x_{2,n}, x_{2,m}, d_2, \pi, \tilde{p}), & x_{2,m}(0) &= x_{2m0}, && (4.62c)\\
\dot{\pi} &= \Pi^c(x_1, x_{2,n}, x_{2,m}, d; \pi, \nu), & \pi(0) &= \pi_0, && (4.62d)\\
y &= x_{2,m} + \tilde{h}_y(\pi), \quad z = C_{z,1}x_1 + \tilde{h}_z(\pi), & & && (4.62e)
\end{aligned}$$

where the closed-loop functions are defined in Section e.1. The functions $(e_1^c, e_{2,n}^c)$ (or $e_{2,m}^c$) manifest modeling errors in the unmeasured (or measured) state dynamics, and (4.62d) is the parasitic exosystem in closed-loop mode that satisfies (4.3). System (4.62) is robustly stable and has the origin as unique steady-state provided the separation of scales between fast and slow dynamics is largely enough [76].

To get an estimation model for observer design, neglect the parasitic dynamics and their coupling with the states of the reactor and the measured and controlled output, i. e.,

$$e_1^c(x_1, x_{2,n}, x_{2,m}, d_2, \pi, \tilde{p}) \approx \mathbf{0},\ e_{2,n}^c(x_1, x_{2,n}, x_{2,m}, d_2, \pi, \tilde{p}) \approx \mathbf{0},\ \tilde{h}_y(\pi) \approx 0,\ \tilde{h}_z(\pi) \approx 0,$$

retain the effect of model uncertainty on the output dynamics trough coupling function $e_{2,m}^c$, and define the exogenous input ι_y

$$\iota_y = e_{2,m}^c(x_1, x_{2,n}, x_{2,m}, d_2, \mathbf{0}, \tilde{p}). \qquad (4.63)$$

Thus, the closed-loop model for output-feedback design is

$$\begin{aligned}
\dot{x}_1 &= f_1(x_1, x_2, d_1), & x_1(0) &= x_{10},\\
\dot{x}_{2,n} &= f_{2,n}^c(x_1, x_{2,n}, x_{2,m}, d_2), & x_{2,n}(0) &= x_{2n0},\\
\dot{x}_{2,m} &= f_{2,m}^c(x_1, x_{2,n}, x_{2,m}, d_2) + \iota_y, & x_{2,m}(0) &= x_{2m0},\\
y &= x_{2,m}, \quad z = C_{z,1}x_1.
\end{aligned}$$

The enforcement of the convergent measured output signal $\boldsymbol{y}(t)$, solution to (4.51) on the preceding model yields the $n-q$-dimensional dynamic inverse

$$\begin{aligned}
\dot{\hat{\boldsymbol{x}}}_1 &= \boldsymbol{f}_1(\hat{\boldsymbol{x}}_1, \hat{\boldsymbol{x}}_{2,n}, \hat{\boldsymbol{x}}_{2,m}, d_1), & \boldsymbol{x}_1(0) &= \hat{\boldsymbol{x}}_{10}, && \text{(4.64a)}\\
\dot{\hat{\boldsymbol{x}}}_{2,n} &= \boldsymbol{f}^c_{2,n}(\hat{\boldsymbol{x}}_1, \hat{\boldsymbol{x}}_{2,n}, \hat{\boldsymbol{x}}_{2,m}, d_2), & \boldsymbol{x}_{2,n}(0) &= \hat{\boldsymbol{x}}_{2n0}, && \text{(4.64b)}\\
\hat{\boldsymbol{\iota}}_y &= \dot{\boldsymbol{y}} - \boldsymbol{e}^c_{2,m}(\hat{\boldsymbol{x}}_1, \hat{\boldsymbol{x}}_{2,n}, \boldsymbol{y}, d_2), & \boldsymbol{y}(0) &= \boldsymbol{y}_0, && \text{(4.64c)}\\
\hat{\boldsymbol{x}}_y &= \boldsymbol{y}, \quad \hat{z} = \boldsymbol{C}_{z,1}\hat{x}_1. &&&& \text{(4.64d)}
\end{aligned}$$

Which is robustly stable and coincides with the zero dynamics (4.35) when $\boldsymbol{y} = 0$. Since $\boldsymbol{y} \to 0$, the systems approaches exponentially to the stable zero dynamics.

The related estimation errors of model (4.64) are defined as

$$\tilde{\boldsymbol{x}}_1 = \hat{\boldsymbol{x}}_1 - \boldsymbol{x}_1, \quad \tilde{\boldsymbol{x}}_{2,n} = \hat{\boldsymbol{x}}_{2,n} - \boldsymbol{x}_{2,n},$$

and the related estimation error dynamics, driven by the convergent signal $\boldsymbol{y}(t)$, are:

$$\begin{aligned}
\dot{\tilde{\boldsymbol{x}}}_1 &= \tilde{\boldsymbol{f}}_1(\boldsymbol{x}_1, \boldsymbol{x}_{2,n}, \boldsymbol{y}, d_1; \tilde{\boldsymbol{x}}_1, \tilde{\boldsymbol{x}}_{2,n}), & \tilde{\boldsymbol{x}}_1(0) &= \tilde{\boldsymbol{x}}_{10}, && \text{(4.65a)}\\
\dot{\tilde{\boldsymbol{x}}}_{2,n} &= \tilde{\boldsymbol{f}}^c_{2,n}(\boldsymbol{x}_1, \boldsymbol{x}_{2,n}, \boldsymbol{y}, d_2; \tilde{\boldsymbol{x}}_1, \tilde{\boldsymbol{x}}_{2,n}), & \tilde{\boldsymbol{x}}_{2,n}(0) &= \tilde{\boldsymbol{x}}_{2n0}, && \text{(4.65b)}
\end{aligned}$$

where

$$\begin{aligned}
\tilde{\boldsymbol{f}}_1(\boldsymbol{x}_1, \boldsymbol{x}_{2,n}, \boldsymbol{y}, d_1; \tilde{\boldsymbol{x}}_1, \tilde{\boldsymbol{x}}_{2,m}) &= \boldsymbol{f}_1(\boldsymbol{x}_1 + \tilde{\boldsymbol{x}}_1, \boldsymbol{x}_{2,n} + \tilde{\boldsymbol{x}}_{2,n}, \boldsymbol{y}, d_1) - \boldsymbol{f}_1(\boldsymbol{x}_1, \boldsymbol{x}_{2,m}, \boldsymbol{y}, d_1),\\
\tilde{\boldsymbol{f}}^c_{2,n}(\boldsymbol{x}_1, \boldsymbol{x}_{2,n}, \boldsymbol{y}, d_1; \tilde{\boldsymbol{x}}_1, \tilde{\boldsymbol{x}}_{2,m}) &= \boldsymbol{f}^c_{2,n}(\boldsymbol{x}_1 + \tilde{\boldsymbol{x}}_1, \boldsymbol{x}_{2,n} + \tilde{\boldsymbol{x}}_{2,n}, \boldsymbol{y}, d_2) - \boldsymbol{f}^c_{2,n}(\boldsymbol{x}_1, \boldsymbol{x}_{2,m}, \boldsymbol{y}, d_2).
\end{aligned}$$

By the robust stability of the zero dynamics, the trajectories of the estimation model (4.64) converge to the real ones, with fixed convergence time λ_z, and due to the robust stability of the closed-loop system, the reactor trajectories converges to the origin:

$$(\hat{\boldsymbol{x}}_1, \hat{\boldsymbol{x}}_{2,n}, \hat{\boldsymbol{\iota}}_y) \xrightarrow{\lambda_z} (\boldsymbol{x}_1, \boldsymbol{x}_{2,n}, \boldsymbol{\iota}_y) \xrightarrow{\lambda_c} (\mathbf{0}, \mathbf{0}, \mathbf{0}).$$

Three important implications for estimation purposes can be established: (i) the inverse model (4.64) acts as a robustly convergent input-state estimator of the closed-loop system (4.56), with asymptotic error size proportional to the model errors $(\boldsymbol{e}^c_1, \boldsymbol{e}^c_{2,n})$, (ii) the closed-loop state motions $(\boldsymbol{x}_1, \boldsymbol{x}_{2,n})$ of system (4.64) are robustly detectable in the sense that the infinity (one per data perturbation) of indistinguishable perturbations $(\hat{\boldsymbol{x}}_1, \hat{\boldsymbol{x}}_{2,n}, \hat{\boldsymbol{\iota}}_y)$ robustly converge (with fixed rate λ_z and up to bounded offset) to the actual state-input signal $(\boldsymbol{x}_1, \boldsymbol{x}_{2,n}, \boldsymbol{\iota}_y)$ [96], and (iii) the state $(\tilde{\boldsymbol{x}}_1, \tilde{\boldsymbol{x}}_{2,n})$ of the estimation error dynamics (4.65) converge to zero. This is formally stated next.

Proposition 4.6. *The robust stability of the zero dynamics* (4.36) *related to the closed-loop system* (4.56)*, the state motions* $(\hat{\boldsymbol{x}}_1(t), \hat{\boldsymbol{x}}_{2,n}(t))$ *of the dynamical inverse* (4.64) *are robustly stable, meaning that these trajectories are detectable.*

This detectability property is exploited next to construct a CES for output feedback control and state estimation.

4.5.2 *Control-estimation system construction*

Here, a CES is constructed as the combination of a geometric estimator, drawn with the estimation model (4.64), and the state feedback control (4.52), the resulting system is enhanced with an output mismatch compensation term.

The estimation structure for the estimation model (4.64) is (see [52]):

$$\boldsymbol{o} = (\boldsymbol{\kappa}, (\boldsymbol{x}_{2,m} - \boldsymbol{x}_1, \boldsymbol{x}_{2,n})) : \ \boldsymbol{\kappa} = (\kappa_1, \ldots, \kappa_q), \ \kappa_i = 1, \quad \kappa_\iota = q.$$

for $i = 1, \ldots, q$. The $\boldsymbol{o}$-estimation structure has (i) q measured outputs of estimation order $\kappa_i = 1$, implying that the overall estimation order is $\kappa_\iota = q$, (ii) the measured temperatures $\boldsymbol{x}_{2,m}$ as innovated states, (iii) and the concentration and unmeasured temperature vectors pair $(\boldsymbol{x}_1^T, \boldsymbol{x}_{2,n}^T)^T$ as noninnovated states.

Following [52], the corresponding geometric estimator is

$$\dot{\hat{\boldsymbol{\iota}}}_y = \boldsymbol{K}_\iota(\boldsymbol{y} - \hat{\boldsymbol{y}}), \qquad \hat{\boldsymbol{\iota}}_y(0) = \hat{\boldsymbol{\iota}}_{y0}, \tag{4.66a}$$

$$\dot{\hat{\boldsymbol{x}}}_1 = \boldsymbol{f}_1(\hat{\boldsymbol{x}}_1, \hat{\boldsymbol{x}}_{2,n}, \hat{\boldsymbol{x}}_{2,m}, d_1), \qquad \boldsymbol{x}_1(0) = \hat{\boldsymbol{x}}_{10}, \tag{4.66b}$$

$$\dot{\hat{\boldsymbol{x}}}_{2,n} = \boldsymbol{f}_{2,n}^c(\hat{\boldsymbol{x}}_1, \hat{\boldsymbol{x}}_{2,n}, \hat{\boldsymbol{x}}_{2,m}, d_2), \qquad \boldsymbol{x}_{2,n}(0) = \hat{\boldsymbol{x}}_{2n0}, \tag{4.66c}$$

$$\dot{\hat{\boldsymbol{x}}}_{2,m} = \boldsymbol{f}_{2,m}^c(\hat{\boldsymbol{x}}_1, \hat{\boldsymbol{x}}_{2,n}, \hat{\boldsymbol{x}}_{2,m}, d_2) + \hat{\boldsymbol{\iota}}_y + \boldsymbol{K}_y(\boldsymbol{y} - \hat{\boldsymbol{y}}), \qquad \boldsymbol{x}_{2,m}(0) = \hat{\boldsymbol{x}}_{2m0}, \tag{4.66d}$$

$$\hat{\boldsymbol{y}} = \hat{\boldsymbol{x}}_{2,m}, \quad \hat{z} = \boldsymbol{C}_{z,1}\hat{\boldsymbol{x}}_1, \tag{4.66e}$$

where $\boldsymbol{\iota}_y$ is an integral action for uncertainty output mismatch compensation. The diagonal gain matrices $(\boldsymbol{K}_\iota, \boldsymbol{K}_y)$ are given as

$$\boldsymbol{K}_y = 2\text{diag}[\zeta_{\omega,1}\omega_1 \ \ldots \ \zeta_{\omega,q}\omega_q], \quad \boldsymbol{K}_\iota = \text{diag}(\omega_1^2 \ \ldots \ \omega_q^2)^T$$

and set with the pole placement scheme

$$(\boldsymbol{\zeta}_\omega, \boldsymbol{\omega}_y) : \quad \boldsymbol{\zeta}_\omega = [\zeta_{\omega,1} \ \ldots \ \zeta_{\omega,q}]^T, \quad \boldsymbol{\omega}_y = [\omega_1 \ \ldots \ \omega_q]^T,$$

set with the second order responses, one per output, of the characteristic polynomials

$$\lambda_{y,i}^2 + 2\zeta_{\omega,i}\omega_i\lambda_{y,i} + \omega_i^2 = 0, \quad i = 1, \ldots, q,$$

of the prescribed linear, noninteractive, pole assignable output error dynamics

$$\ddot{\tilde{y}}_i + 2\zeta_{\omega,i}\omega_i\dot{\tilde{y}}_i + \omega_i^2\tilde{y}_i = 0, \quad \tilde{y}_i = \hat{y}_i - y_i, \quad \hat{y}_i = \hat{x}_{2,m,i}, \quad i = 1, \ldots, q.$$

Typically, based on industrial application of geometric estimators with noisy measurements and parameter uncertainty [51; 52; 106], the frequencies are set from 5 to 50 times faster than the nominal output settling time, which in closed-loop is given by the i-th entry of the diagonal matrix $\boldsymbol{K}_1$, and the damping factor between 1.5-3, i. e.,

$$\omega_i = n_\omega k_i, \ n_\omega \in [5, 50], \ \zeta_i \in [1.5, 3].$$

The integral action of the geometric estimator (4.66) can be used to provide disturbance rejection capabilities to the state feedback controller (4.52). For this purpose, since the input $\boldsymbol{\iota}_y$ has bounded entries, the following bound can be established

$$\boldsymbol{\iota}_y^- \leq \boldsymbol{\iota}_y \approx \boldsymbol{e}_{2,m}^c(\boldsymbol{x}_1, \boldsymbol{x}_{2,n}, \boldsymbol{x}_{2,m}, d_2, \boldsymbol{\pi}, \tilde{\boldsymbol{p}}) \leq \boldsymbol{\iota}_y^+.$$

Set the corresponding control set enlargement

$$U_c = [u^-, u^+] \supseteq U_{c,0}, \quad u^- = u^- - \boldsymbol{\iota}_y^-/v, \quad u^+ = u^+ + \boldsymbol{\iota}_y^+/v \tag{4.67}$$

of the control set $U_{c,0}$, and enforce the output regulation dynamics (4.51) on model (4.1) with the control set U_c to obtain the saturated controller

$$\boldsymbol{u} = \boldsymbol{\mu}_{e,s}(\boldsymbol{x}_1, \boldsymbol{x}_{2,n}, \boldsymbol{x}_{2,m}, \boldsymbol{\iota}_y, d_2) \in U_c, \quad \boldsymbol{\mu}_{e,s}(\cdot) = \mathrm{sat}_{u^-}^{u^+}[\mu_{e,i}(\cdot)], \quad U_c = [u^-, u^+], \tag{4.68}$$

where ($\boldsymbol{\mu}$ is defined in (4.52))

$$\boldsymbol{\mu}_e(\boldsymbol{x}_1, \boldsymbol{x}_{2,n}, \boldsymbol{x}_{2,m}, \boldsymbol{\iota}_y, d_2) = \boldsymbol{\mu}_e(\boldsymbol{x}_1, \boldsymbol{x}_{2,n}, \boldsymbol{x}_{2,m}, d_2) - \boldsymbol{B}_u^{m-1}\boldsymbol{\iota}_y.$$

The combination of controller (4.68) with the estimator (4.66), yields the CES

$$\begin{aligned}
\dot{\hat{\boldsymbol{\iota}}}_y &= \boldsymbol{K}_\iota(\boldsymbol{y} - \hat{\boldsymbol{y}}), & \hat{\boldsymbol{\iota}}_y(0) &= \hat{\boldsymbol{\iota}}_{y0}, && \text{(4.69a)}\\
\dot{\hat{\boldsymbol{x}}}_1 &= \boldsymbol{f}_1(\hat{\boldsymbol{x}}_1, \hat{\boldsymbol{x}}_{2,n}, \hat{\boldsymbol{x}}_{2,m}, d_1), & \boldsymbol{x}_1(0) &= \hat{\boldsymbol{x}}_{10}, && \text{(4.69b)}\\
\dot{\hat{\boldsymbol{x}}}_{2,n} &= \boldsymbol{f}_{2,n}^c(\hat{\boldsymbol{x}}_1, \hat{\boldsymbol{x}}_{2,n}, \hat{\boldsymbol{x}}_{2,m}, d_2), & \boldsymbol{x}_{2,n}(0) &= \hat{\boldsymbol{x}}_{2n0}, && \text{(4.69c)}\\
\dot{\hat{\boldsymbol{x}}}_{2,m} &= \boldsymbol{f}_{2,m}^c(\hat{\boldsymbol{x}}_1, \hat{\boldsymbol{x}}_{2,n}, \hat{\boldsymbol{x}}_{2,m}, d_2) + \hat{\boldsymbol{\iota}}_y + \boldsymbol{K}_y(\boldsymbol{y} - \hat{\boldsymbol{y}}), & \boldsymbol{x}_{2,m}(0) &= \hat{\boldsymbol{x}}_{2m0}, && \text{(4.69d)}\\
\hat{\boldsymbol{y}} &= \hat{\boldsymbol{x}}_{2,m}, \quad \hat{z} = \boldsymbol{C}_{z,1}\hat{\boldsymbol{x}}_1 & & && \text{(4.69e)}\\
\hat{\boldsymbol{x}} &= [\boldsymbol{x}_1^T\, (\boldsymbol{C}_n^T\hat{\boldsymbol{x}}_{2,n} + \boldsymbol{C}_{y,2}^T\hat{\boldsymbol{x}}_{2,m})^T]^T, \quad \hat{\chi}_N = \boldsymbol{\mathcal{I}}(\hat{\boldsymbol{x}}), & & && \text{(4.69f)}\\
\boldsymbol{u} &= \boldsymbol{\mu}_{e,s}(\hat{\boldsymbol{x}}_1, \hat{\boldsymbol{x}}_{2,n}, \hat{\boldsymbol{x}}_{2,m}, \hat{\boldsymbol{\iota}}_y, d_2). & & && \text{(4.69g)}
\end{aligned}$$

The robust stability of the related closed-loop system is established next.

4.5.3 *Closed-loop stability*

The closed-loop stability with the controller (4.69) is established by analyzing the closed-loop dynamics as interconnections of robustly stable subsystems. First, conditions for stability of the interconnection of the fast (parasitic and innovated) and slow (unmeasured and closed-loop reactor state) subsystems are drawn. Then, conditions for the robust stability of the fast-slow interconnection are established.

The application of the control estimation system (4.69) to the actual open-loop dynamics (4.2) yields the following closed-loop system:

$$\begin{aligned}
\dot{\boldsymbol{\pi}} &= \boldsymbol{\Pi}_2^c(\boldsymbol{x}, \boldsymbol{d}; \boldsymbol{\pi}, \boldsymbol{\nu}, \tilde{\boldsymbol{x}}_{\iota e}, \tilde{\boldsymbol{x}}_n), & \boldsymbol{\pi}(0) &= \boldsymbol{\pi}_0, && \text{(4.70a)}\\
\dot{\tilde{\boldsymbol{x}}}_e &= \boldsymbol{A}_e\tilde{\boldsymbol{x}}_e + \tilde{\boldsymbol{f}}_e(\boldsymbol{x}; \boldsymbol{\pi}, \tilde{\boldsymbol{p}}, d_2, \tilde{\boldsymbol{x}}_e, \tilde{\boldsymbol{x}}_n), & \tilde{\boldsymbol{x}}_{\iota e} &= \tilde{\boldsymbol{x}}_{e0}, && \text{(4.70b)}\\
\dot{\tilde{\boldsymbol{x}}}_n &= \boldsymbol{f}_n(\tilde{\boldsymbol{x}}_{\iota e}, \tilde{\boldsymbol{x}}_n, \boldsymbol{d}) + \boldsymbol{\epsilon}_c^n(\boldsymbol{x}, \boldsymbol{d}; \boldsymbol{\pi}, \tilde{\boldsymbol{p}}, \tilde{\boldsymbol{x}}_e, \tilde{\boldsymbol{x}}_n, \boldsymbol{l}), & \tilde{\boldsymbol{x}}_n(0) &= \tilde{\boldsymbol{x}}_{n0}, && \text{(4.70c)}\\
\dot{\boldsymbol{x}} &= \boldsymbol{f}_c(\boldsymbol{x}, \boldsymbol{d}) + \boldsymbol{\epsilon}_c(\boldsymbol{x}, \boldsymbol{d}; \boldsymbol{\pi}, \tilde{\boldsymbol{p}}, \boldsymbol{d}, \tilde{\boldsymbol{x}}_e, \tilde{\boldsymbol{x}}_n, \boldsymbol{l}), & \boldsymbol{x}(0) &= \boldsymbol{x}_0, && \text{(4.70d)}
\end{aligned}$$

where

$$\tilde{\boldsymbol{x}}_e = \hat{\boldsymbol{x}}_e - \boldsymbol{x}_e, \quad \boldsymbol{x}_e = (\boldsymbol{x}_{2,m}, \boldsymbol{\iota}_y)^T, \quad \tilde{\boldsymbol{x}}_n = \hat{\boldsymbol{x}}_n - \boldsymbol{x}_n, \quad \boldsymbol{x}_n = (\boldsymbol{x}_1^T\, \boldsymbol{x}_{2,n}^T)^T. \tag{4.70e}$$

$\tilde{\boldsymbol{x}}_e$ is the fast estimation error, $\tilde{\boldsymbol{x}}_n$ is the slow estimation error, and $\boldsymbol{x}$ is the state of the plant in closed-loop. The involved functions are defined in Section e.2

Note that by construction the matrix $\boldsymbol{A}_e$ is Hurwitz and generates a matrix exponential that satisfies the following bound

$$\left\| \mathrm{e}^{\boldsymbol{A}_e t} \right\| \leq a_e \mathrm{e}^{-\lambda_e t}, \quad -\lambda_e = \max_{\lambda_j \in \sigma(\boldsymbol{A}_e)} \{\mathrm{Re}(\lambda_j)\}.$$

The closed-loop system (4.70) is made by four robustly stable subsystem, ordered from fast to slow dynamics: (i) the parasitic (4.70a), (ii) the fast (or slow) state estimation error dynamics (4.70b) (or (4.70c)), and (iii) the closed-loop dynamics (4.70d) with decaying rates $\lambda_\pi > 0$, $\lambda_e > 0$, $\lambda_z > 0$, $\lambda_c > 0$, respectively, and interconnected via the Lipschitz bounded disturbance maps $(\tilde{\boldsymbol{f}}_{\iota e}, \boldsymbol{\mathfrak{e}}_c^n, \boldsymbol{\mathfrak{e}}_c)$.

The following two lemmas ensure the stability of slow and fast subsystems.

Lemma 4.3. *Consider the fast dynamics interconnection (4.70a)-(4.70b), assume the other states as exogenous inputs, and that the matrix $\boldsymbol{A}_e$ is Hurwitz with dominant eigenvalue λ_e. Given that the parasitic dynamics is robustly stable with decaying rate λ_π and that the interconnection function $\tilde{\boldsymbol{f}}_e$ is Lipschitz bounded with respect to its arguments. Then, the fast subsystem is robustly stable if the matrix gain pair $(\boldsymbol{K}_y, \boldsymbol{K}_\iota)$ is set so that*

$$\nu_e = \lambda_e - a_e L_{x_e}^{\tilde{f}_e} > 0, \quad \nu_e \lambda_\pi > 0.$$

This ensures the stability of the fast dynamics if the matrix gain pair $(\boldsymbol{K}_y, \boldsymbol{K}_\iota)$ are selected so that the dominant eigenvalue of $\boldsymbol{A}_e$ dominates the destabilizing effect of the interconnection, measured by the Lipschitz constant $L_{x_e}^{\tilde{f}_e}$.

Lemma 4.4. *Consider the slow dynamics interconnection (4.70c)-(4.70d), assume the other states as exogenous inputs. Given that the nominal dynamics are exponentially stable with decaying parameters (a_z, λ_z) and (a_c, λ_c), and that the interconnection functions in $\boldsymbol{\mathfrak{e}}_n^c$-$\boldsymbol{e}_c$ are Lipschitz bounded with respect to its arguments, then the slow subsystem is robustly stable by construction because the following conditions are met:*

$$\nu_z = \lambda_z - a_n L_{x_n}^{\mathfrak{e}_c^n} > 0, \quad \nu_c = \lambda_c - a_c L_x^{\mathfrak{e}_c}, \quad \nu_z \nu_c > a_z a_x L_x^{\mathfrak{e}_c^n} L_{x_n}^{\mathfrak{e}_c}.$$

The next proposition gives conditions for the stability of the closed-loop system (4.70) by considering the interconnection of the fast and slow subsystems.

Proposition 4.7. *Robust stability of the closed-loop system (4.70). Proof in Section e.3. Assume that Lemma 4.3 and Lemma 4.4 are met. The closed-loop system (4.70) with the CES (4.69) is robustly stable if the estimator gains $(\boldsymbol{K}_y, \boldsymbol{K}_\iota)$ are chosen so that*

$$\lambda_e(\boldsymbol{K}_y, \boldsymbol{K}_\iota) - L_{x_e}^{\tilde{f}_e}(\boldsymbol{K}_y, \boldsymbol{K}_\iota) + \frac{a_f a_s \left\| \boldsymbol{B}_f(\boldsymbol{K}_y, \boldsymbol{K}_\iota) \right\| \left\| \boldsymbol{B}_s \right\|}{\lambda_s} > 0. \tag{4.71}$$

In the above expression, the stabilizing term $\lambda_{\iota e}$ depends linearly on the estimator gains $\boldsymbol{K}_y, \boldsymbol{K}_\iota$, while the second term, which resumes the self and interconnection destabilizing effects, grows at least quadratically on the estimator gains. Accordingly, the gains must be selected large enough to dominate destabilizing effects but no so far that the quadratic destabilizing effects dominates the linear stabilizing one.

Since $\boldsymbol{\iota}_y = \boldsymbol{e}^c_{2,m}$ reflects the combined effect of parameter error ($\tilde{\boldsymbol{p}}$) and parasitic dynamics, the quickly convergent estimate $\hat{\boldsymbol{\iota}}_y$ of $\boldsymbol{\iota}_y$ has feedforward-like disturbance rejection capability which enhance the performance of the controller.

From an advanced nonlinear control perspective, the CES (4.70) has: (i) systematic construction-tuning procedures, (ii) solvability in terms passivity and detetectability with constrained control, and (iii) assurance of robust closed-loop stability coupled with sensor location, control limits and control-estimator gains selection criteria. However, with respect its industrial PI control-based counterparts, the application of observer-based control should rise complexity and reliability concerns among practitioners, because the execution of the key stabilizing task requires the computation of a saturated output feedback control element driven by the on-line solution of $2N-1$ ODEs. The overcoming of this applicability obstacle is the subject of the next section.

4.6 REDESIGNED CONTROL-MONITORING SYSTEM

Here, the CES (4.69) is realized in a simplified and more robust form made by two components: (i) a saturated linear robust stabilizing Proportional-Integral control with Anti Windup scheme (PIAW), and (ii) a decoupled robust state estimator.

4.6.1 *Simplified model*

Along inseparability principle [122], PI control studies [13], and model free-based control [53] ideas employed in previous studies on polymerization [58] and biological [112; 114; 113] reactors as well as staged distillation columns [33; 34], the simplified realization of the CES (4.69) is based on a simplified model.

For this aim recall the actual open-loop model (4.4) in concentration-partitioned-temperature coordinate and rewrite it as follows

$$\begin{aligned}
\dot{\boldsymbol{x}}_1 &= \boldsymbol{f}_1(\boldsymbol{x}_1, \boldsymbol{x}_{2,n}, \boldsymbol{x}_{2,m}, \boldsymbol{d}_1) + \boldsymbol{e}_1(\boldsymbol{x}_1, \boldsymbol{x}_{2,n}, \boldsymbol{x}_{2,m}, \boldsymbol{u}, \boldsymbol{\pi}, \tilde{\boldsymbol{p}}), && \boldsymbol{x}_1(0) = \boldsymbol{x}_{10},\\
\dot{\boldsymbol{x}}_{2,n} &= \boldsymbol{f}_{2,n}(\boldsymbol{x}_1, \boldsymbol{x}_{2,n}, \boldsymbol{x}_{2,m}, \boldsymbol{d}_2) + \boldsymbol{B}^n_u\boldsymbol{u} + \boldsymbol{e}_{2,n}(\boldsymbol{x}_1, \boldsymbol{x}_{2,n}, \boldsymbol{x}_{2,m}, \boldsymbol{u}, \boldsymbol{\pi}, \tilde{\boldsymbol{p}}), && \boldsymbol{x}_{2,n}(0) = \boldsymbol{x}_{2n0},\\
\dot{\boldsymbol{x}}_{2,m} &= \boldsymbol{B}^m_{u,2}\boldsymbol{u} + \boldsymbol{\iota}, && \boldsymbol{x}_{2,m}(0) = \boldsymbol{x}_{2m0},\\
\dot{\boldsymbol{\pi}} &= \boldsymbol{\Pi}(\boldsymbol{x}_y, \boldsymbol{x}_z, \boldsymbol{d}, \boldsymbol{u}; \boldsymbol{\pi}, \boldsymbol{\nu}), && \boldsymbol{\pi}(0) = \boldsymbol{\pi}_0,\\
\boldsymbol{y} &= \boldsymbol{x}_{2,m} + \tilde{\boldsymbol{h}}_y(\boldsymbol{\pi}), \quad z = \boldsymbol{C}_{z,1}\boldsymbol{x}_1 + \tilde{\boldsymbol{h}}_z(\boldsymbol{\pi}),
\end{aligned}$$

where a new exogenous input is defined:

$$\boldsymbol{\iota} = \boldsymbol{e}_{2,m}(\boldsymbol{x}_1, \boldsymbol{x}_{2,n}, \boldsymbol{x}_{2,m}, \boldsymbol{u}, \boldsymbol{\pi}, \tilde{\boldsymbol{p}}) + \boldsymbol{f}_{2,m}(\boldsymbol{x}_1, \boldsymbol{x}_{2,n}, \boldsymbol{x}_{2,m}, \boldsymbol{d}_2), \tag{4.72}$$

which is the exogenous input (4.63) considered in the control-estimation system (4.69) plus the nominal dynamics of the measured state:

$$\boldsymbol{\iota}_y = \boldsymbol{e}_{2,m}(\boldsymbol{x}_1, \boldsymbol{x}_{2,n}, \boldsymbol{x}_{2,m}, \boldsymbol{u}, \boldsymbol{\pi}, \tilde{\boldsymbol{p}}) \Rightarrow \boldsymbol{\iota} = \boldsymbol{\iota}_y + \boldsymbol{f}_y(\boldsymbol{x}_y, \boldsymbol{x}_z, \boldsymbol{d}_m).$$

In the previous model, drop the parasitic dynamics $\boldsymbol{\pi}$ and the coupling error functions to get the passive-detectable model for output feedback-estimator design:

$$\begin{aligned} \dot{\boldsymbol{x}}_1 &= \boldsymbol{f}_1(\boldsymbol{x}_1, \boldsymbol{x}_{2,n}, \boldsymbol{x}_{2,m}, d_1), & \boldsymbol{x}_1(0) &= \boldsymbol{x}_{10}, && (4.73a)\\ \dot{\boldsymbol{x}}_{2,n} &= \boldsymbol{f}_{2,n}(\boldsymbol{x}_1, \boldsymbol{x}_{2,n}, \boldsymbol{x}_{2,m}, d_2) + \boldsymbol{B}_u^n \boldsymbol{u}, & \boldsymbol{x}_{2,n}(0) &= \boldsymbol{x}_{2n0}, && (4.73b)\\ \dot{\boldsymbol{x}}_{2,m} &= \boldsymbol{B}_u^m \boldsymbol{u} + \boldsymbol{\iota}, & \boldsymbol{x}_{2,m}(0) &= \boldsymbol{x}_{2m0}, && (4.73c)\\ \boldsymbol{y} &= \boldsymbol{x}_{2,m}, \quad z = \boldsymbol{C}_{z,1}\boldsymbol{x}_1, &&&& (4.73d) \end{aligned}$$

with input-measured output and exogenous input-measured output that have relative degree one for each pair of their entries, i. e.,

$$\mathrm{rd}(\boldsymbol{u}, \boldsymbol{y}) = \mathrm{rd}(\boldsymbol{\iota}, \boldsymbol{y}) = \begin{bmatrix} 1 & \dots & 1 \end{bmatrix}$$

meaning that: (i) the model (4.73) is passive with respect to the pair $(\boldsymbol{u}, \boldsymbol{y})$ with null zero dynamics, and (ii) the control-exogenous input pair $(\boldsymbol{u}, \boldsymbol{\iota})$ satisfy a matching condition that can be exploited for disturbance rejection [58; 113] based on the instantaneous observability property of the exogenous input: (4.73c) with $\boldsymbol{y} = \boldsymbol{x}_{2,m}$ has a unique solution for the unknown exogenous input $\boldsymbol{\iota}$

$$\boldsymbol{\iota} = \dot{\boldsymbol{y}} - \boldsymbol{B}_u^m \boldsymbol{u} \tag{4.74}$$

implying that $\boldsymbol{\iota}$ can be quickly (up to measurement noise) on-line reconstructed with a reduced order observer [58; 113] driven by the know signals $(\boldsymbol{u}, \boldsymbol{y})$.

For monitoring purposes, note that the model (4.73a)-(4.73b) driven by the stabilizing control law and a convergent input coincides with the estimation model (4.64) established in Section 4.5.1. Thus, model (4.73a)-(4.73b) can be used as the basis for the construction of an state estimator, or even used as an open-loop observer.

4.6.2 *Construction*

The enforcement of the output regulation dynamics (4.51) and control set U_c (4.57d):

$$\dot{\boldsymbol{y}} = -\boldsymbol{K}_c \boldsymbol{y}, \quad \boldsymbol{K}_c > 0, \quad U_c = [u^-, u^+] \tag{4.75}$$

on the reduced model (4.73), with $\boldsymbol{\iota}$ is known, yield the saturated linear controller

$$\boldsymbol{u} = \boldsymbol{\mu}_{r,s}(\boldsymbol{y}, \boldsymbol{\iota}), \quad \boldsymbol{\mu}_{s,r}(\cdot) = \mathrm{sat}_{u^-}^{u^+} \mu_{r,i}(\cdot), \quad i = 1, \dots, q, \tag{4.76a}$$

where

$$\boldsymbol{\mu}_r(\boldsymbol{y}, \boldsymbol{\iota}) = -\boldsymbol{B}_u^{m-1}(\boldsymbol{K}_c \boldsymbol{y} + \boldsymbol{\iota}). \tag{4.76b}$$

When there is no parasitic dynamics then $\boldsymbol{\iota} = \boldsymbol{\iota}_y(\boldsymbol{x}, d_2, \mathbf{0}, \mathbf{0}) + \boldsymbol{f}_{2,m}(\boldsymbol{x}_1, \boldsymbol{x}_{2,n}, \boldsymbol{x}_{2,m}, d_2)$, and controller (4.76) coincides with the state feedback controller $\boldsymbol{\mu}_{s,e}$ (4.68). Furthermore, when there is no parasitic dynamics nor disturbance input effects, the exogenous input $\boldsymbol{\iota}_y$ vanishes and $\boldsymbol{\iota} = \boldsymbol{f}_{2,m}(\boldsymbol{x}_1, \boldsymbol{x}_{2,n}, \boldsymbol{x}_{2,m}, d_2)$ and the controller (4.76) becomes the state feedback controller $\boldsymbol{\mu}$ in (4.52). This is:

$$(\boldsymbol{\pi}, \boldsymbol{v}) = (\mathbf{0}, \mathbf{0}) \Rightarrow \boldsymbol{\iota} = \boldsymbol{\iota}_y(\boldsymbol{x}, d_2, \mathbf{0}, \mathbf{0}) + \boldsymbol{f}_{2,m}(\boldsymbol{x}_1, \boldsymbol{x}_{2,n}, \boldsymbol{x}_{2,m}, d_2) \Rightarrow \boldsymbol{\mu}_{s,r} = \boldsymbol{\mu}_{s,e},$$
$$(\boldsymbol{\pi}, \boldsymbol{v}, \boldsymbol{d}) = (\mathbf{0}, \mathbf{0}, \mathbf{0}) \Rightarrow \boldsymbol{\iota} = \boldsymbol{f}_{2,m}(\boldsymbol{x}_1, \boldsymbol{x}_{2,n}, \boldsymbol{x}_{2,m}, d_2) \Rightarrow \boldsymbol{\mu}_{s,r} = \boldsymbol{\mu}_s.$$

This establishes and equivalence of the controller (4.76) with the state feedback controllers (4.52) and (4.58), which implies that the sensor location and control limits selection criteria of the previous controllers can be inherited to the present one.

From the instantaneously observability property (4.74), the unknown input $\boldsymbol{\iota}$ can be quickly on-line reconstructed with the linear observer [113]:

$$\dot{\boldsymbol{\Lambda}} = -\boldsymbol{K}_\omega \boldsymbol{\Lambda} - \boldsymbol{K}_\omega(\boldsymbol{K}_\omega \boldsymbol{y} + \boldsymbol{B}_u^m \boldsymbol{u}), \quad \boldsymbol{\Lambda}(0) = \boldsymbol{\Lambda}_0, \tag{4.77a}$$
$$\hat{\boldsymbol{\iota}} = \boldsymbol{\Lambda} + \boldsymbol{K}_\omega \boldsymbol{B}_u^m \boldsymbol{y}, \tag{4.77b}$$

with adjustable gain matrix $\boldsymbol{K}_\omega = \mathrm{diag}(\omega_1, \ldots, \omega_q)$, and estimation error dynamics

$$\dot{\tilde{\boldsymbol{\iota}}} = -\boldsymbol{K}_\omega \tilde{\iota}, \quad \tilde{\boldsymbol{\iota}} = \hat{\boldsymbol{\iota}} - \boldsymbol{\iota}, \quad \omega_i > \|\dot{\iota}_i / \iota_i\| \approx \lambda_x. \tag{4.77c}$$

The combination of the saturated controller (4.76), the input observer (4.77) and the open-loop estimation model (4.73a)-(4.73b) discussed in Section 4.6.1, yield the CES

$$\dot{\hat{\boldsymbol{x}}}_1 = \boldsymbol{f}_1(\hat{\boldsymbol{x}}_1, \hat{\boldsymbol{x}}_{2,n}, \boldsymbol{y}, d_1), \qquad \hat{\boldsymbol{x}}_1(0) = \hat{\boldsymbol{x}}_{10}, \tag{4.78a}$$
$$\dot{\hat{\boldsymbol{x}}}_{2,n} = \boldsymbol{f}_{2,n}(\hat{\boldsymbol{x}}_1, \hat{\boldsymbol{x}}_{2,n}, \boldsymbol{y}, d_2) + \boldsymbol{B}_u^n \boldsymbol{\mu}_s^o(\boldsymbol{y}, \boldsymbol{\xi}), \qquad \boldsymbol{x}_{2,n}(0) = \boldsymbol{x}_{2n0}, \tag{4.78b}$$
$$\hat{\boldsymbol{x}}_{2,m} = \boldsymbol{y}, \tag{4.78c}$$
$$\dot{\boldsymbol{\Lambda}} = -\boldsymbol{K}_\omega \boldsymbol{\Lambda} - \boldsymbol{K}_\omega(\boldsymbol{K}_\omega \boldsymbol{y} + \boldsymbol{B}_u^m \boldsymbol{\mu}_s^o(\boldsymbol{y}, \boldsymbol{\Lambda})), \qquad \boldsymbol{\Lambda}(0) = \boldsymbol{\Lambda}_0, \tag{4.78d}$$
$$\hat{z} = \boldsymbol{C}_{z,1} \hat{\boldsymbol{x}}_1, \quad \hat{\boldsymbol{x}} = (\hat{\boldsymbol{x}}_1^T, \boldsymbol{C}_n^T \hat{\boldsymbol{x}}_{2,n} + \boldsymbol{C}_{y,2}^T \boldsymbol{y})^T, \quad \hat{\boldsymbol{x}}_N = \boldsymbol{\mathcal{I}}(\hat{\boldsymbol{x}}), \tag{4.78e}$$
$$\boldsymbol{u} = \boldsymbol{\mu}_{o,s}(\boldsymbol{y}, \boldsymbol{\Lambda}), \tag{4.78f}$$

where

$$\boldsymbol{\mu}_{s,o}(\boldsymbol{y}, \boldsymbol{\xi}) = \mathrm{sat}_{u^-}^{u^+}[\mu_{o,i}(\boldsymbol{y}, \boldsymbol{\Lambda})], \quad \boldsymbol{\mu}_o(\boldsymbol{y}, \boldsymbol{\xi}) = -{\boldsymbol{B}_u^m}^{-1}((\boldsymbol{K}_c + \boldsymbol{K}_\omega)\boldsymbol{y} + \boldsymbol{\Lambda}). \tag{4.78g}$$

The structure $\mathfrak{S}_q$ of the CES is composed by $2N_e + 1$ ODEs: $2N_e$ for the estimation task, and q ODEs for the control task. It has a sensor location set, number of sensors and their locations, and suitable control limits, both determined with robust criteria. The set of gains is composed by matrices $\boldsymbol{K}_c$ and $\boldsymbol{K}_\omega$, two gains for each measured output:

$$\mathfrak{S}_q = (2N_e, \varsigma, U_c = [u^-, u^+]), \quad \boldsymbol{K}_\theta = (\boldsymbol{K}_c, \boldsymbol{K}_\omega). \tag{4.78h}$$

Differently from its detailed model-based counterpart (4.69), in the preceding CES the control stabilizing task is executed without needing the state estimate, and the output feedback controller does not depend on the detailed efficient model (4.73a)-(4.73b), but instead just on the knowledge of matrix $\boldsymbol{B}^m_{u,2}$, which depends on the heat transfer parameter v. This providing the CES (4.78) with a fastest and more robust performance compared with (4.69). Closed-loop stability conditions are drawn next.

4.6.3 *Closed-loop state stability and convergence*

Apply (4.78) to the actual open-loop dynamics (4.2b) to get the closed-loop system

$$\begin{aligned}
\dot{\boldsymbol{\pi}} &= \boldsymbol{\Pi}^3_c(\boldsymbol{x}, \boldsymbol{d}; \boldsymbol{\pi}, \boldsymbol{\nu}, \boldsymbol{d}, \tilde{\boldsymbol{\iota}}), & \boldsymbol{\pi}(0) &= \boldsymbol{\pi}_0, & (4.79a)\\
\dot{\tilde{\boldsymbol{\iota}}} &= -\boldsymbol{K}_\omega \tilde{\boldsymbol{\iota}} + \tilde{\boldsymbol{f}}_\iota(\boldsymbol{x}, \boldsymbol{d}; \boldsymbol{\pi}, \tilde{\boldsymbol{p}}, \tilde{\boldsymbol{\iota}}), & \tilde{\boldsymbol{\iota}}(0) &= \tilde{\boldsymbol{\iota}}_0, & (4.79b)\\
\dot{\tilde{\boldsymbol{x}}}_z &= \boldsymbol{f}_n(\boldsymbol{y}, \tilde{\boldsymbol{x}}_n, \boldsymbol{d}) + \boldsymbol{\mathfrak{e}}^o_n(\boldsymbol{x}, \boldsymbol{d}; \boldsymbol{\pi}, \tilde{\boldsymbol{p}}, \boldsymbol{d}, \tilde{\boldsymbol{\iota}}, \tilde{\boldsymbol{x}}_n, \boldsymbol{l}), & \tilde{\boldsymbol{x}}_n(0) &= \tilde{\boldsymbol{x}}_{n0}, & (4.79c)\\
\dot{\boldsymbol{x}} &= \boldsymbol{f}_c(\boldsymbol{x}, \boldsymbol{d}) + \boldsymbol{\mathfrak{e}}^o_c(\boldsymbol{x}, \boldsymbol{d}; \boldsymbol{\pi}, \tilde{\boldsymbol{p}}, \boldsymbol{d}, \tilde{\boldsymbol{\iota}}, \tilde{\boldsymbol{x}}_n, \boldsymbol{l}), & \boldsymbol{x}(0) &= \boldsymbol{x}_0, & (4.79d)
\end{aligned}$$

with parasitic state $\boldsymbol{\pi}$, states estimation error states $\tilde{\boldsymbol{\iota}} = \hat{\boldsymbol{\iota}} - \boldsymbol{\iota}$ and $\tilde{\boldsymbol{x}}_z = \hat{\boldsymbol{x}}_z - \boldsymbol{x}_z$, and closed-loop system state $\boldsymbol{x}$. The interconnecting Lipschitz bounded functions $\boldsymbol{\rho}^3_c$, $\tilde{\boldsymbol{f}}_\iota$, $\boldsymbol{e}^o_n$, and $\boldsymbol{e}^o_c$ are given in Section f.1.

System (4.79) is made of four individual robustly stable subsystems in fast to slow dynamics ordering: (i) the parasitic dynamics (4.79a), (ii) the input estimation error dynamics (4.79b), (iii) the unmeasured state error dynamics (4.79c), and (iv) the state dynamics (4.79d). Each individual subsystem is robustly stable: the parasitic dynamics by assumption, the exogenous input estimation error dynamics and the closed-loop state by construction, and the unmeasured state dynamics by the related detectability property. The decaying parameter of each subsystem are $\lambda_\pi, \omega_m, \lambda_z, \lambda_c > 0$.

The stability analysis is similar to the one performed in Section 4.5.3 and is performed first establishing the robust stability of the fast (4.79a)-(4.79b), and slow (4.79c)-(4.79d) interconnections. Then, the stability of the fast and slow subsystems is established. This result is summarized in the next.

Proposition 4.8. *Robust stability of the closed-loop system* (4.78). *Proof in Section f.2. Consider the closed-loop dynamics* (4.79). *Assume that the sensor location set and the control limits are selected according to conditions in Proposition 4.4 and Proposition 4.5. If the following condition is fulfilled*

$$l_o := \omega - L^f_\iota(\omega_\iota) - \frac{a_f a_s \left\|\mathscr{B}_f(\omega_\iota, \omega^2_\iota)\right\| \left\|\mathscr{B}_s\right\|}{\nu_c} > 0 \tag{4.80}$$

where $\mathscr{B}_f$, $\mathscr{B}_s$, and ν_c are defined in Section f.2, and ω_ι is the maximum entry of $\boldsymbol{K}_\omega$. Then, the closed-loop system is robustly stable in a nonlocal sense in X.

Condition (4.80) indicates that the stabilizing, linear-in-ω_ι, term dominates the potentially destabilizing term (that grows linearly and quadratically with ω_ι). The above result can be translated into a threshold condition for industrial-like tuning purposes. Denote by ω_ι^- and ω_ι^+ the two solutions of the equality case in (4.80), i.e.

$$l_o(\omega_\iota^-) = l_o(\omega_\iota^+) = 0, \quad 0 < \omega_\iota^- < \omega_\iota^+. \tag{4.81}$$

The gain ω_ι of $\boldsymbol{K}_\omega$ must be chosen above a lower threshold to ensure estimation error convergence, and below an upper threshold condition to avoid instability due to the excitation of the parasitic dynamics. This is stated next.

Corollary 4.1. *Consider the closed-loop dynamics (4.79). Assume that the sensor location set and the control limits are selected according to conditions in Proposition 4.4 and Proposition 4.5. The closed-loop system is robustly stable if the maximal estimator gain ω_ι is set sufficiently above (or below) its lower (or upper) limit ω_ι^- (or ω_ι^+):*

$$\omega^- < \omega < \omega^+ - . \tag{4.82}$$

In industrial practice, the upper bound ω^+ is called ultimate gain (where inadmissible oscillatory behavior by error-noise propagation starts with ω increase).

With the preceding CES (4.78): (i) the critical regulation-state stabilization task is performed with a considerably simpler, less model dependent and more reliable dynamic data processor than its detailed model-based realization (4.69) (where the regulating-stabilizing output feedback control component requires the detailed model-based on-line estimator), and (ii) the decoupled efficient model-based estimator can be used for setpoint adjustment and gain retuning in an optimizing control layer [90].

4.6.4 *Control component in PI form*

In industry most of the control loops are PIAW controllers. Accordingly, for implementation, the saturated linear dynamic output feedback control component (4.78d)-(4.78f) of the CES (4.78) is transformed into a saturated linear PIAW.

Recall the control component (4.78d)-(4.78f) of the CES (4.78) and rewrite it as

$$\dot{\boldsymbol{\Lambda}} = -\boldsymbol{K}_\omega \boldsymbol{\Lambda} - \boldsymbol{K}_\omega^2 \boldsymbol{y} - \boldsymbol{K}_\omega \boldsymbol{B}_u^m \boldsymbol{\mu}_o(\boldsymbol{y}, \boldsymbol{\xi}) - \boldsymbol{K}_\omega \boldsymbol{B}_u^m (\boldsymbol{\mu}_{o,s}(\boldsymbol{y}, \boldsymbol{\Lambda}) - \boldsymbol{\mu}_o(\boldsymbol{y}, \boldsymbol{\Lambda})), \quad \boldsymbol{\Lambda}(0) = \boldsymbol{\Lambda}_0,$$
$$\boldsymbol{u} = \boldsymbol{\mu}_{o,s}(\boldsymbol{y}, \boldsymbol{\Lambda}),$$

substitute $\boldsymbol{\mu}_o$, given in (4.78g), in the second term of the right hand-side of the first equation to get

$$\dot{\boldsymbol{\Lambda}} = \boldsymbol{K}_\omega \boldsymbol{K} \boldsymbol{y} - \boldsymbol{K}_\omega \boldsymbol{B}_u^m (\boldsymbol{\mu}_{o,s}(\boldsymbol{y}, \boldsymbol{\Lambda}) - \boldsymbol{\mu}_o(\boldsymbol{y}, \boldsymbol{\Lambda})), \qquad \boldsymbol{\Lambda}(0) = \boldsymbol{\Lambda}_0,$$
$$\boldsymbol{u} = \boldsymbol{\mu}_{o,s}(\boldsymbol{y}, \boldsymbol{\xi}).$$

Integrate with $\boldsymbol{\Lambda}_0 = \mathbf{0}$, substitute the resulting $\boldsymbol{\Lambda}$ in $\boldsymbol{\mu}_{o,s}(\boldsymbol{y}, \boldsymbol{\xi})$, and rearrange to obtain the saturated linear PIAW of back-calculation type

$$\boldsymbol{u} = \boldsymbol{\mu}_{pi,s}(\boldsymbol{y}) = \mathrm{sat}_{u^-}^{u^+}[\mu_{pi,i}(y_i, \Lambda_i)], \tag{4.83a}$$

where the control maps are given as

$$\mu_{pi,s}(\boldsymbol{y}) = -k_{p,i}\left(\boldsymbol{y} + t_{I,i}^{-1}\int_0^t \boldsymbol{y}\mathrm{d}t\right) + t_{a,i}^{-1}\int_0^t (\mu_{pi,s}(\boldsymbol{y}) - \mu_s(\boldsymbol{y}))\mathrm{d}t, \tag{4.83b}$$

with gains

$$\boldsymbol{K}_p = (\boldsymbol{B}_u^m)^{-1}(\boldsymbol{K} + \boldsymbol{K}_\omega) = \frac{1}{v}\mathrm{diag}(k_1 + \omega_1, \ldots, k_q + \omega_q) = \mathrm{diag}(k_{p,1}, \ldots, k_{p,q}), \tag{4.83c}$$

$$\boldsymbol{T}_I^{-1} = \boldsymbol{K}^{-1} + \boldsymbol{K}_\omega^{-1} = \mathrm{diag}(k_1^{-1} + \omega_1^{-1}, \ldots, k_q^{-1} + \omega_q^{-1}) = \mathrm{diag}(t_{I,1}, \ldots, t_{I,q}), \tag{4.83d}$$

$$\boldsymbol{T}_a = \boldsymbol{K}_\omega^{-1} = \mathrm{diag}(\omega_1^{-1}, \ldots, \omega_q^{-1}) = \mathrm{diag}(t_{a,1}, \ldots, t_{a,q}). \tag{4.83e}$$

$\boldsymbol{K}_p$ (or $\boldsymbol{T}_I$) is the proportional gain (or integral time) matrix and $\boldsymbol{T}_a$ is the integral time of its AW component. All matrices are diagonal and contain the gains of the corresponding PIAW controller. The MIMO controller (4.83) is actually a set of decentralized PIAW controllers, each one operating independently of the others.

The replacement of (4.78d)-(4.78f) by (4.83) in (4.78) yields the industrial-type realization of the simplified model-based CES (4.78) as a saturated robust stabilizing PIAW, and a decoupled efficient model-based robustly convergent state estimator:

$$\dot{\hat{\boldsymbol{x}}}_1 = \boldsymbol{f}_1(\hat{\boldsymbol{x}}_1, \hat{\boldsymbol{x}}_{2,n}, \hat{\boldsymbol{x}}_{2,m}, d_1), \qquad \hat{\boldsymbol{x}}_1(0) = \hat{\boldsymbol{x}}_{10}, \tag{4.84a}$$

$$\dot{\hat{\boldsymbol{x}}}_{2,n} = \boldsymbol{f}_{2,n}(\hat{\boldsymbol{x}}_1, \hat{\boldsymbol{x}}_{2,n}, \boldsymbol{y}, d_2) + \boldsymbol{B}_u^n \boldsymbol{\mu}_{pi,s}(\boldsymbol{y}), \qquad \boldsymbol{x}_{2,n}(0) = \boldsymbol{x}_{2n0}, \tag{4.84b}$$

$$\hat{\boldsymbol{x}}_{2,m} = \boldsymbol{y}, \tag{4.84c}$$

$$\hat{z} = \boldsymbol{C}_{z,1}\hat{\boldsymbol{x}}_1, \quad \hat{\boldsymbol{x}} = (\hat{\boldsymbol{x}}_1^T, \boldsymbol{C}_n^T \hat{\boldsymbol{x}}_{2,n} + \boldsymbol{C}_{y,2}^T \boldsymbol{y})^T, \quad \hat{\boldsymbol{x}}_N = \boldsymbol{\mathcal{I}}(\hat{\boldsymbol{x}}), \tag{4.84d}$$

$$\boldsymbol{u} = \boldsymbol{\mu}_{pi,s}(\boldsymbol{y}), \tag{4.84e}$$

with two components in cascade interconnection: (i) the temperature PIAW (4.84e), and (ii) a pointwise-like robustly convergent state estimator (4.84a)-(4.84d), similar to the early-lumping implementation of the pointwise observer introduced in [111].

From an advanced control perspective, the PI control with AW scheme-Pointwise Observer (PIAW-PWO) system (4.84): (i) is a simplified-robustified realization of the estimator-based saturated stabilizing control (4.69), and (ii) has a comprehensive design with solvability in terms of passivity and detectability, as well as criteria to choose the model order, sensor location, and control limits and gains. Two fundamental conclusions are: (i) the critical joint temperature regulation-state stabilization task must be executed with the saturated linear PIAW instead of the nonlinear output feedback controller of the control-estimation system (4.69), and (ii) the estimation task can be performed independently of the control one with an estimator that can be used to perform setpoint adjustment in an optimizing control layer.

From and industrial control perspective, the theoretical developments associated to the proposed MIMO PIAW-PWO CES design (4.84) explain with formal advanced control arguments the effective functioning of the industrial saturated PI with back-calculation AW for exothermic tubular reactors [89; 121; 100; 14; 42]. Furthermore, the proposed CES (4.84) is an upgrade of the saturated PI temperature control employed in industrial reactors, with the upgrade consisting in an all-embracing design with: (i) criteria to choose the sensor location, control limits, and kind of AW protector for the saturated PI control, and (ii) the model order and control gain of a decoupled state estimator that should be used for monitoring and setpoint adjustment purposes. These considerations and conclusions are along current industrial control trends [90].

4.6.5 *Implementation and tuning*

Here, implementation guidelines and a tuning procedure are developed for the proposed MIMO PIAW-PWO CES (4.84).

Rewrite model (4.4) in original coordinate to obtain the lumped

$$\dot{\chi}_1 = \boldsymbol{A}_1\chi_1 + \boldsymbol{B}_{d,1}\chi_{1,e} - \boldsymbol{r}(\chi_1,\chi_2), \qquad \chi_1(0) = \chi_{10}, \tag{4.85a}$$

$$\dot{\chi}_2 = \boldsymbol{A}_2\chi_2 + \boldsymbol{B}_{d,2}\chi_{2,e} + \boldsymbol{r}(\chi_1,\chi_2) + \boldsymbol{B}_{u,2}\boldsymbol{\tau}_c, \qquad \chi_2(0) = \chi_{20}, \tag{4.85b}$$

$$\boldsymbol{\tau}_m = \boldsymbol{C}_{y,2}\boldsymbol{x}_2, \quad c_o = \boldsymbol{C}_{z,1}\chi_1, \tag{4.85c}$$

where (χ_1,χ_2) are the concentration and temperature states. Using the previous model in partitioned coordinate (4.4), the proposed CES (4.84) is implemented as

$$\dot{\hat{\chi}}_1 = \boldsymbol{A}_1\hat{\chi}_1 + \boldsymbol{B}_{d,1}\bar{\chi}_{1,e} - \boldsymbol{r}(\hat{\chi}_1,\hat{\chi}_2), \qquad \hat{\chi}_1(0) = \hat{\chi}_{10}, \tag{4.86a}$$

$$\dot{\hat{\chi}}_{2,n} = \boldsymbol{A}_2^{n,n}\hat{\chi}_{2,n} + \boldsymbol{A}_2^{n,m}\hat{\chi}_{2,m} + \boldsymbol{B}_{d,2}^{n}\chi_{2,e} + \boldsymbol{r}_n(\hat{\chi}_1,\hat{\chi}_{2,n}) + \boldsymbol{B}_{u,2}^{n}\boldsymbol{\tau}_c, \; \hat{\chi}_{2,n}(0) = \hat{\chi}_{2,n0}, \tag{4.86b}$$

$$\hat{\chi}_{2,m} = \boldsymbol{\tau}_m, \tag{4.86c}$$

$$\hat{c}_o = \boldsymbol{C}_{z,1}\hat{\chi}_1, \quad \hat{\chi}_2 = \boldsymbol{C}_n^T\hat{\chi}_{2,n} + \boldsymbol{C}_{y,2}^T\hat{\chi}_{2,m}, \quad \hat{\chi}_N = \boldsymbol{\mathcal{I}}(\hat{\chi}), \tag{4.86d}$$

$$\boldsymbol{\tau}_c = \boldsymbol{\mu}_{pi,s}(\boldsymbol{\tau}_m) = \left[\mathrm{sat}_{\tau_c^-}^{\tau_c^+}\mu_{pi,1}(\tau_{m,1}) \quad \ldots \quad \mathrm{sat}_{\tau_c^-}^{\tau_c^+}\mu_{pi,q}(\tau_{m,q})\right]^T, \tag{4.86e}$$

where the control inputs are

$$\begin{aligned}\mu_{i,pi}(\tau_{m,i}) = \bar{\tau}_{c,i} - k_{p,i}\left((\tau_{m,i} - \bar{\tau}_{m,i}) - t_i^{-1}\int_0^t(\tau_{m,i} - \bar{\tau}_{m,i})\mathrm{d}t\right) + \\ + t_a^{-1}\int_0^t\left(\mathrm{sat}_{\tau_c^-}^{\tau_c^+}\;\mu_{pi,i}(\tau_{m,i}) - \mu_{pi,i}(\tau_{m,i})\right)\mathrm{d}t, \qquad i = 1,\ldots,q,\end{aligned} \tag{4.86f}$$

with control limits and gains

$$\tau_c^- = u^- - \bar{\tau}_c,\ \tau_c^+ = u^+ - \bar{\tau}_c,\ k_{p,i} = \frac{k_i + \omega_i}{v},\ t_i = k_i^{-1} + \omega_i^{-1},\ t_a = \omega_i^{-1}. \quad (4.86g)$$

The above CES has the following structure $\mathfrak{S}_q$ and gains $\boldsymbol{K}_\theta$ that must be selected appropriately to ensure good closed-loop performance:

$$\mathfrak{S}_q = (2N_e, q, \boldsymbol{\varsigma}, (\tau_c^-, \tau_c^+)), \quad \boldsymbol{K}_\theta = (\boldsymbol{K}_c, \boldsymbol{K}_\omega), \quad (4.87)$$

where $n_\theta 2N_e$ is the dimension of the CES: $2N_e - q$ is the dimension of the estimator and the controller has q integral actions, N_e is the efficient discretization order Section 3.2, q is the number of actuator-sensor pairs. The sensor location set $\boldsymbol{\varsigma}$ is determined in Section 4.3.3, and the control limits (τ_c^-, τ_c^+) are determined in Section 4.4.3.4. The gain matrices $(\boldsymbol{K}, \boldsymbol{K}_\omega)$ contains parameters from which the proportional gain, integral time, and AW time matrices of the decentralized PIAW controllers are computed.

The theoretical developments of the previous sections are summarized next in a structure-gain tuning procedure. The first step, of structure tuning, include the determination of: (i) the efficient discretization order N_e, (ii) the sensor set $\boldsymbol{\varsigma}$, and (iii) the control limit pair (τ_c^-, τ_c^+). The second step, for gain tuning and structure calibration, is set in the light of simulation-based conventional-like tuning guidelines for robust functioning meaning with realistic initial condition, input step and fluctuating disturbance, parameter uncertainty, and reference setpoint change).

Step I: Off-line structural tuning:

I.1 Use the efficient modeling approach of Section 3.2 to draw the efficient discretization order N_e of the lumped model (3.19). This low dimensional model should be used for the remaining off-line structure and on-line gain tuning and structure calibration.

I.2 On the basis of the zero dynamics multiplicity analysis and maximal control set $U_{c,0} = U_z$, of Section 4.3.3.2, determine the admissible sensor set $\mathcal{S}_m$ for $q = 1$, and then choose the sensor locations with the best compromise between speed, robustness, and control effort, according the sensor location criterion (4.48).

I.3 Use the control limit criterion of Section 4.4.3.4 to choose (u^-, u^+) above and below the bifurcation values (u_*, u^*) of the IOBM $\mathscr{O}$: $u^- < u^*$, $u^+ > u^*$.

I.4 Set the closed-loop system with the proposed CES (4.86) in robust testing mode with appropriate: (i) parameter errors and measurement noise, load input, and setpoint changes, (ii) initial state and estimate errors, (iii) fluctuating modeling errors generated by a suitable parasitic dynamics model (4.79a) (typically, 50 times faster than the reactor natural dynamics i. e., $\lambda_\pi \approx 50\lambda_x$), and (iv) perform the corresponding control set $U_{c,0}$-to-U_c enlargement (4.67), and compute the control limits (τ_c^-, τ_c^+) as $\tau_c^- = u^- + \bar{\tau}_c$, $\tau_c^+ = u^+ + \bar{\tau}_c$.

Step II: On-line gain tuning and structural-gain fine adjustment:

II.1 Set the control (or estimator) gain, conservatively, n_k times (or n_ω) faster than the natural (or closed-loop) dynamics λ_x (or λ_c)

$$(\boldsymbol{K}, \boldsymbol{K}_\omega) \approx (n_k, n_\omega)\lambda_x \boldsymbol{I}, \quad n_k \in [1, 3], \quad n_\omega \in [15, 30].$$

II.2 For the i-th output, $i = 1, \ldots, q$, gradually increase the i-th control $\boldsymbol{k}_{c,i}$ or estimator ω_i gain, with the other gains fixed, up to its ultimate value $k^+_{c,i}$ or ω^+_i (where excessive oscillatory behavior occurs) and back off to

$$k_{i,c} \approx k^+_{c,i}/n_b, \quad \omega_i \approx \omega^+_i/n_b, \quad n_b \in [2, 3].$$

II.3 Perform fine calibration: adjust the model order $n_e = 2N_e$, the sensor location set ς, the control limit pair (τ_c^-, τ_c^+), and the gain pair $(\boldsymbol{K}, \boldsymbol{K}\omega)$ to improve behavior.

II.4 The number q of actuator-sensor pairs can be incremented up to 2 or 3 to explore if there is some behavior improvement.

4.7 CONTROL-ESTIMATION SYSTEM FUNCTIONING

In this section, the on-line functioning of the proposed CES (4.86) is illustrated and tested with numerical simulation for the case example presented in Section 2.5.

CES functioning of nominal and robust type will be assessed. Nominal (or robust) functioning means in the absence (or presence) of modeling error, for verification of theoretical developments (or implementation-tuning and behavior comparison).

The application of the off-line Step I (Section 4.7.2) to the tubular reactor case study of Section 2.5, was performed in Section 3.2.3 for the model order, in Section 4.3.3.3 for the sensor location for $q = 1, 2, 3$, and in Section 4.4.3.5 for the control limits (u^-, u^+) with suitable enlargement (4.67), in the light of the size of the exogenous inputs in Table 2.1. Accordingly, the initial (before calibration) CES structures for $q = 1, 2, 3$ are:

$$\begin{aligned}
\mathfrak{S}_{1,0} &= \{40, 1, \varsigma_1 \approx 0.24, (1.1, 1.9)\}, \\
\mathfrak{S}_{2,0} &= \{40, 2, \{\varsigma_1 \approx 0.24\, \varsigma_2 \approx 0.95\}, (1.1, 1.9)\}, \\
\mathfrak{S}_{3,0} &= \{40, 3, \{\varsigma_1 \approx 0.24\, \varsigma_2 \approx 0.65, \varsigma_3 \approx 0.95\}, (1.1, 1.9)\}.
\end{aligned}$$

The design of the proposed CES suggest the initial gain values (before on-line tuning)

$$\boldsymbol{K}_0 \approx 1.2\lambda_x \boldsymbol{I}_q, \quad \boldsymbol{K}_{\omega,0} = 20\boldsymbol{K}_0.$$

The results on the conclusive structural and gain tuning resulting is done on-line with Step II of Section 4.7.2. As it is done in the implementation of PDE model-based control studies [42; 36; 22], the reactor dynamics model (4.85) will be simulated with a standard FD-based numerical PDE solver with $N_{pde} = 200$ internal nodes, meaning that the reactor model is composed by of 400 ODEs.

4.7.1 *Robust testing scheme*

The tubular reactor is simulated with model (4.85) and $N_{pde} = 200$. The initial concentration (or temperature) vector χ_1 (or χ_2) is set with 10 % (or -5 %) deviation with respect to nominal value $\bar{\chi}_1$ (or $\bar{\chi}_2$):

$$\chi_{1,0} = 1.1\bar{\chi}_1, \quad \chi_{2,0} = 0.95\bar{\chi}_2.$$

The fluctuating error $\boldsymbol{e}$ of the actual closed-loop dynamics (4.2) was generated with the linear (2nd-order oscillator) parasitic dynamics driven by low-amplitude and high-frequency (close to resonant one) sinusoidal inputs w_j, $j = 1, 2$:

$$\begin{aligned}
\dot{\pi}_{1,j} &= \pi_{2,j}, & \pi_{1,j}(0) &= 0,\\
\dot{\pi}_{2,j} &= -\lambda^2_{\pi,j}\pi_{j,1} + w_j(t), & \pi_{2,j}(0) &= 0,\\
\boldsymbol{e}_j &= \boldsymbol{b}_\pi \pi_{j,2}, & &\\
w_1(t) &= 0.01\sin(50t + 12.57), \quad w_2(t) = 0.02\sin(25t + .35). & &
\end{aligned}$$

where $\lambda_{\pi,j} \approx 50\nu_j$, $j = 1, 2$, with ν_j are determined in Section 4.2.3, and $\boldsymbol{b}_\pi = [1 \ldots 1]^T$.

In the testing scheme the tubular reactor is operated over the dimensionless time interval [0,30]. The closed-loop system (4.85)-(4.86) is subjected to the following flow feed temperature $\chi_{2,e}$ load input disturbance, feed (w_e) and output $(\boldsymbol{w}_m)$ temperature measurement sinusoidal noises, and setpoint change $(\Delta\bar{\boldsymbol{\tau}}_m)$:

$$t \in [0, 30] : \ \chi_2 = \chi_{2,e} + w_2, \ \chi_{1,e} = \bar{\chi}_{1,e}, \quad \boldsymbol{\tau}_m = \boldsymbol{\chi}_{2,m} + \boldsymbol{w}_m, \ \bar{\boldsymbol{\tau}}_m = \bar{\boldsymbol{\chi}}_{2,m} + \Delta\bar{\boldsymbol{\tau}}_m,$$

where $w_j(t) = 0.02\sin(2.9t + \pi/18)$, $\quad j = 2, m$. In addition: (i) over the time subinterval $[5, 25)$ the feed temperature $\chi_{2,e}$ undergoes step changes sequences (H: Heaviside's function)

$$t \in [4, 25) : \chi_{2,e}(t) = \bar{\chi}_{2,e} + 0.02[H(t,5) - H(t,10)] - 0.05[H(t,15) + H(t,20)],$$

and (ii) over the interval $[26, 30]$ a control setpoint change was applied

$$t \in [25, 30] : \quad \Delta\bar{\boldsymbol{\tau}}_m = 0.2\bar{\boldsymbol{\tau}}_m H(t-25), \quad \chi_{2,e} = \bar{\chi}_{2,e}.$$

The CES (4.86a)-(4.86d) is build with the deviated transport-kinetics parameters

$$(\hat{P}e_m, \hat{P}e_h) = (0.91Pe_m, 1.11Pe_h), \quad \hat{v} = 0.95v, \quad (\hat{a}_r, \hat{b}_r) = (1.035a_r, 1.03b_r),$$

and initial unmeasured state estimate:

$$(\hat{\boldsymbol{\chi}}_1, \hat{\boldsymbol{\chi}}_{2,n}) = (\bar{\boldsymbol{\chi}}_1, \bar{\boldsymbol{\chi}}_{2,n}).$$

4.7.2 *Gain tuning and structure calibration*

The application of Steps II.1 to II.3 of the gain-structure procedure of Section 4.6.5 yields the CE gains $(\boldsymbol{K}, \boldsymbol{K}_\omega)$:

$$\boldsymbol{K}_c = 1\boldsymbol{I}_{q\times q}, \quad \boldsymbol{K}_\omega = 25\boldsymbol{I}_{q\times q}. \tag{4.88}$$

The corresponding standard PIAW gain triplets are

$$(k_{p,i}, t_{I,i}, t_{a,i}) = (27.37, 0.96, 0.04), \quad i = 1, \ldots, q$$

with AW integral times $t_{a,i}$: (i) about twenty time smaller than the integral ones $t_{I,i}$, and (ii) equal or thirty times smaller than the obtained with standard tuning [21; 132].

The advanced control-estimation system (4.69) is used for comparison purposes in the case $q = 1$ with the initial state estimates

$$\chi_{2,m} = y_0, \quad (\hat{\chi}_1, \hat{\chi}_{2,n}) = (\bar{\chi}_1, \bar{\chi}_{2,n}), \quad \hat{\iota}_{y0} = \mathbf{0}$$

and the triplet gain

$$(\boldsymbol{K}, \boldsymbol{K}_\omega, \zeta_\omega) = (1, 225, 1.5),$$

drawn from the application of the tuning procedure (Steps II.1 to II.3) of Section 4.6.5. While the control gain K is the one the proposed CES with PIAW control, the observer gain K_ω is ten times faster. This is so because $K_\omega = 225$ was needed to attain similar disturbance rejection capability by overcoming, at the cost of some noise propagation, the dependency of the state feedback control on the slowly convergent unmeasured state. This agrees with the comparative robust stability assessments of Proposition 4.7 and Proposition 4.8 of the advanced and proposed CESs, respectively.

4.7.3 *SISO case*

The closed-loop functioning comparison, under nominal and robust testing conditions, of the proposed SISO PIAW-PWO (4.86), against its advanced Output Feedback control with Geometric Observer (OF-GO) CES counterpart (4.69), and the State Feedback controller (SF) (4.52), is performed next with two objectives: (i) corroborate theoretical results on sensor sensor location, control limits, and attainable behavior under nominal conditions, and (ii) to show how, as predicted in the theoretical developments, PIAW-PWO produce the best performance under robust conditions.

4.7.3.1 *Nominal functioning*

The nominal functioning is performed with the gains and structure obtained with the robust testing scheme. While the step changes in the inlet temperature and the

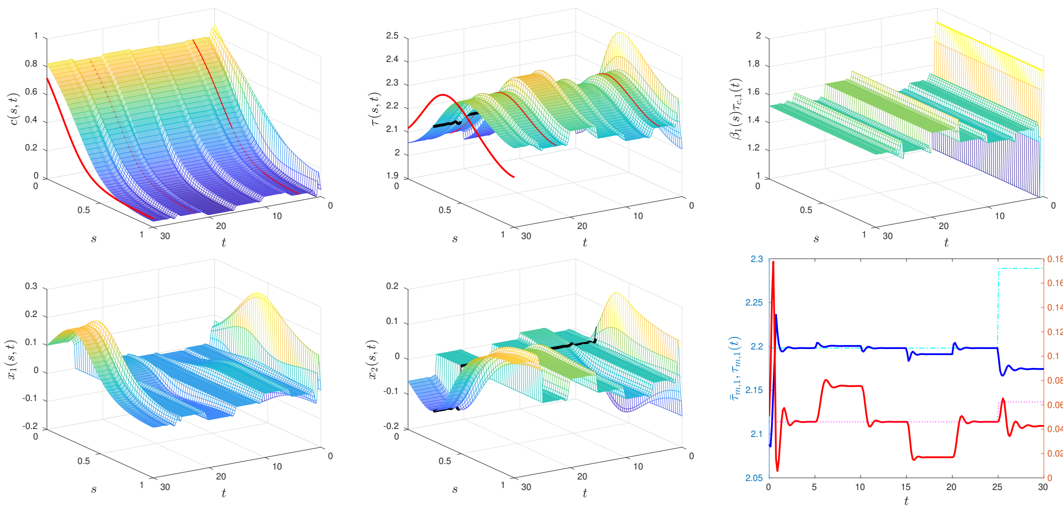

Figure 4.7: Nominal closed-loop functioning with SF. Top left: concentration profile $c(s,t)$. Top center: temperature profile $\tau(s,t)$. Top right: control effort $\beta_1(s)\tau_{c,1}(t)$. Bottom left: deviated concentration profile $x_1(s,t)$. Bottom center: deviated temperature profile $x_2(s,t)$. Bottom right: measured $\tau_{m,1}$ (continuous blue) and regulated $c_o(t)$ (continuous red) outputs and their setpoints (dashed-dotted cyan or dotted magenta, respectively).

output setpoint are present, the fluctuating disturbances, the parasitic dynamics and the sinusoidal noise-like signals are not at play. For state feedback control, the output setpoint change is accompanied with the related value of the control input that corresponds with the new steady-state. The other controllers, since have integral actions do not need this actualized data.

In Figure 4.7, Figure 4.8a and Figure 4.9a, the nominal closed-loop control functioning with the SF (4.52), the advanced OF-GO CES (4.69), and the PIAW-PWO CES (4.86), respectively, are shown. The closed-loop estimation functioning of the estimators of the proposed control-estimation system (4.86) and the geometric one in (4.69) are shown in Figure 4.8b and Figure 4.9, respectively. The norms of the distributed state and estimation error and control input profiles are presented in Figure 4.10a.

Regarding control functioning, on one hand, with respect to regulation task, in terms of settling time, disturbance rejection, control saturation and effort, the SF yields the best behavior, closely followed by the PIAW-PWO and the OF-GO CESs; on the other hand, for the setpoint change tracking, while the PIAW-PWO and OF-GO perform adequately with accurate regulation to the new target steady-state, the SF, which do not have integral action, lacks behind with large asymptotic deviation.

Specifically, (i) for $t \in [0,5)$ (where only response to initial condition is at play) the PIAW-PWO and OF-GO CESs yield larger overshoots and control effort (due to estimator error dynamics), (ii) for $t \in [5,25)$ (where step disturbances occur) the OF-GO produce slightly more oscillatory response, and (iii) for $t \in [25,30]$ (where control setpoint

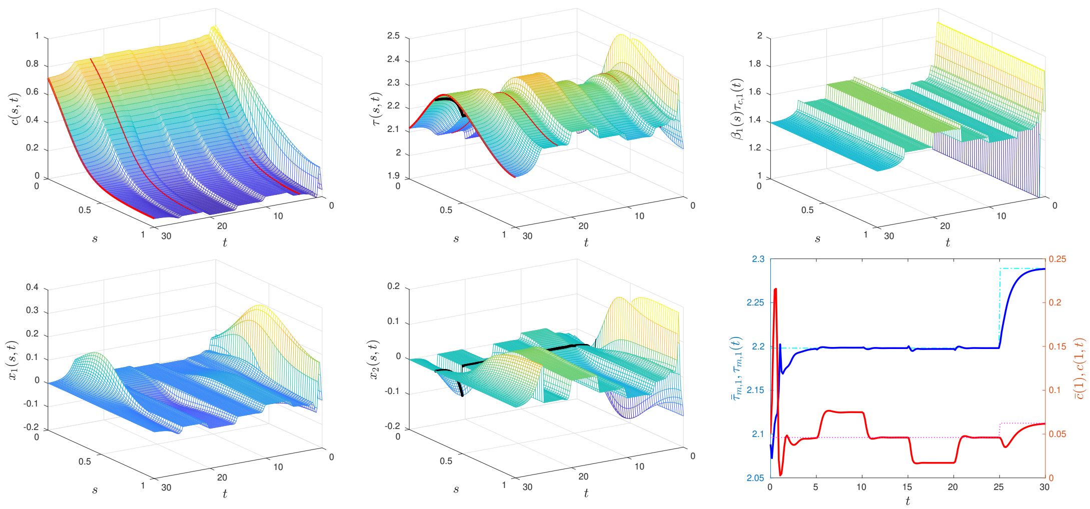

(a) Control functioning. Top left: concentration profile $c(s,t)$. Top center: temperature profile $\tau(s,t)$. Top right: control effort $\beta_1(s)\tau_{c,1}(t)$. Bottom left: deviated concentration profile $x_1(s,t)$. Bottom center: deviated temperature profile $x_2(s,t)$. Bottom right: measured $\tau_{m,1}$ (continuous blue) and regulated $c_o(t)$ (continuous red) outputs and their setpoints (dashed-dotted cyan or dotted magenta, respectively).

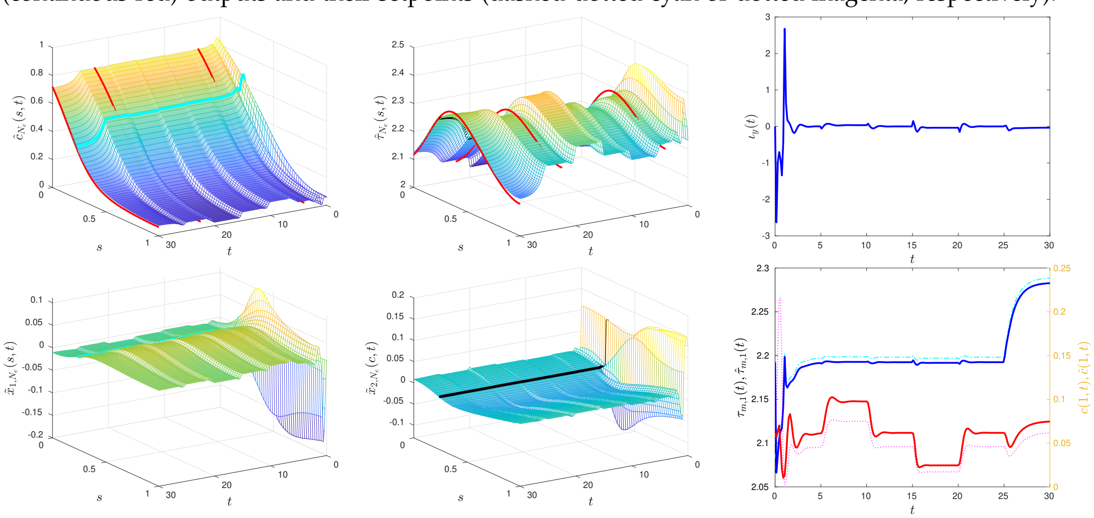

(b) Estimator functioning. Top left: estimated concentration profile $\hat{c}(s,t)$. Top center: estimated temperature profile $\hat{\tau}(s,t)$. Top right: estimated exogenous input $\iota(t)$. Bottom left: concentration estimation error profile $\tilde{c}_1(s,t)$. Bottom center: temperature estimation error profile $\tilde{\tau}_2(s,t)$. Bottom right: real measured $(\tau_{m,1}(t))$ (dashed-dotted cyan) an regulated $c_o(t)$ (dotted magenta) outputs and their estimates $(\hat{\tau}_{m,1}(t), \hat{c}_o(t))$ (continuous blue and red, respectively).

Figure 4.8: Nominal closed-loop CE functioning with the advanced OF-GO CES.

change happens) the PIAW-PWO and OF-GO CESs produce adequate responses while the SF cannot reach the new operating conditions.

Regarding estimation functioning, in terms of settling time and offset, the estimators of the proposed PIAW-PWO and OF-GO CESs perform almost equally well, both present

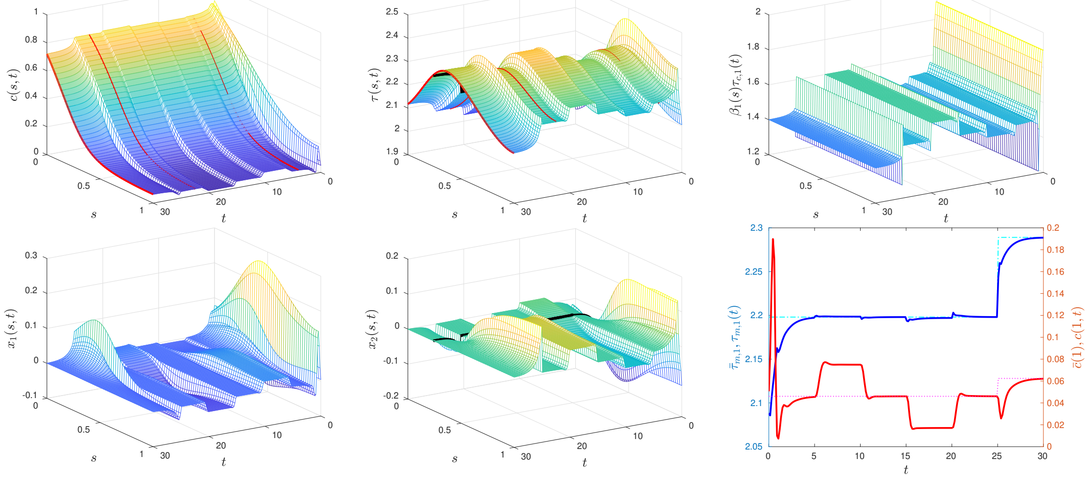

(a) Control functioning. Top left: concentration profile $c(s,t)$. Top center: temperature profile $\tau(s,t)$. Top right: control effort $\beta_1(s)\tau_{c,1}(t)$. Bottom left: deviated concentration profile $x_1(s,t)$. Bottom center: deviated temperature profile $x_2(s,t)$. Bottom right: measured $\tau_{m,1}$ (continuous blue) and regulated $c_o(t)$ (continuous red) outputs and their setpoints (dashed-dotted cyan or dotted magenta, respectively).

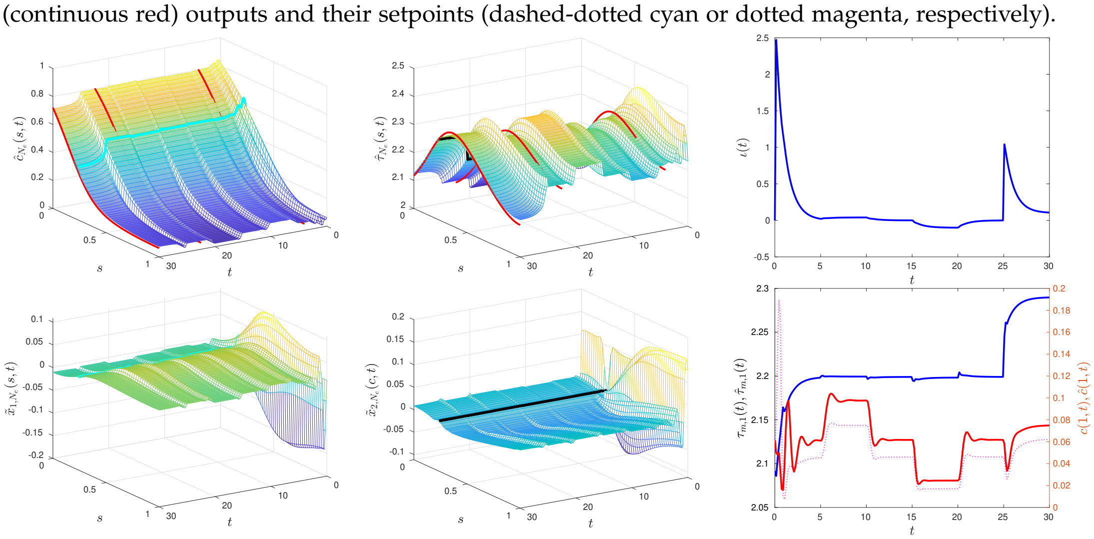

(b) Estimator functioning. Top left: estimated concentration profile $\hat{c}(s,t)$. Top center: estimated temperature profile $\hat{\tau}(s,t)$. Top right: estimated exogenous input $\iota(t)$. Bottom left: estimation error of the concentration profile $\tilde{c}_1(s,t)$. Bottom center: estimation error of the temperature profile $\tilde{\tau}_2(s,t)$. Bottom right: real measured $\tau_{m,1}(t)$ (continuous blue) and regulated $c_o(t)$ (dotted magenta) and their estimates $(\hat{\tau}_{m,1}(t), \hat{c}_o(t))$ (continuous blue and red, respectively).

Figure 4.9: Nominal closed-loop CE functioning with the PIAW-PWO CES.

some expected and allowed persistent estimation error due to the number of ODEs used for the estimators: 41 for the geometric observer and 40 for the pointwise-like one, which are the 10 % of the 400 used to simulate the tubular reactor dynamics.

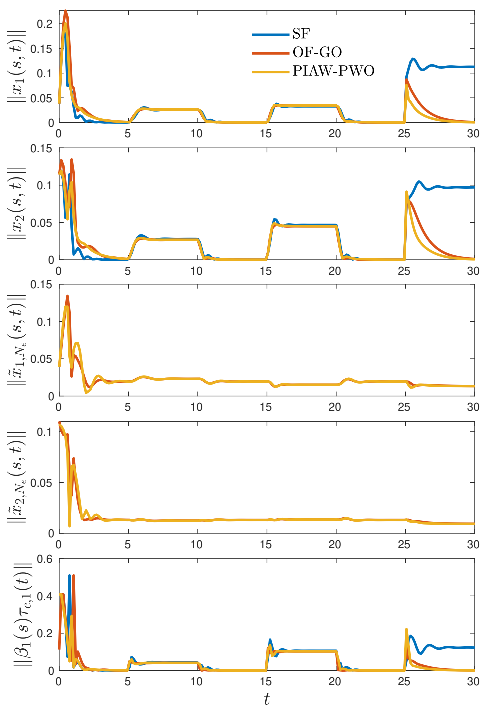

(a) Nominal case.

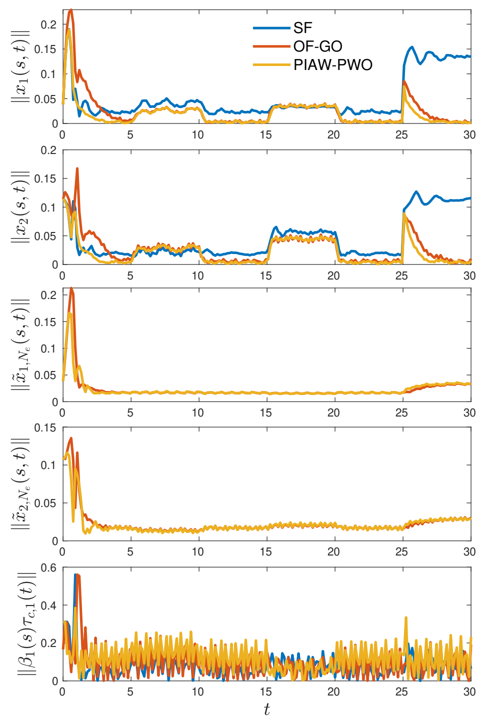

(b) Robust case.

Figure 4.10: Norms of distributed states in deviation, estimation errors and control input.

As expected, in the regulation task the SF (driven, and benefited, by the exact state and inputs) has the best overall behavior, with smaller transients and less control effort, closely followed by the PIAW-PWO and OF-GO CESs, the latter two recover the closed-loop behavior obtained with the first one after the corresponding transients (up to observer convergence). In the setpoint change scenario the behavior of the SF degrades while the PIAW-PWO and OF-GO CESs perform adequately.

To test the sensor location and control limit necessary conditions for robust closed-loop stability of Proposition 4.5 and Proposition 4.4, on purpose those conditions are violated. First, the control limit pair condition is met, and the sensor location condition is violated by placing the temperature measurement at the following location

$$\varsigma_1 = 0.57, \quad \tau_{m,1} = \chi_{2,11},$$

after the hotspot, with bistable zero dynamics. The corresponding norms of the distributed profiles in closed-loop behavior are presented in Figure 4.11a, showing that, as expected, the reactor, with the three CES, do not reach the prescribed steady-state profile pair, and instead it reaches an undesired ignition stable steady-state. The estimation task is fulfilled showing the efficiency of the estimators in this unfavorable scenario and confirming their use for monitoring purposes.

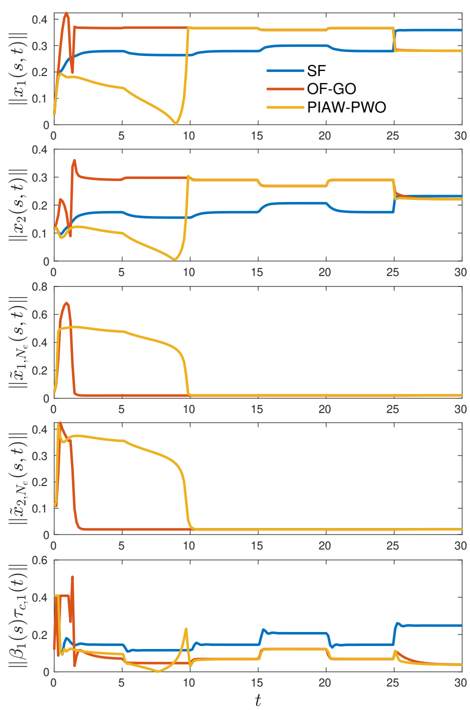

(a) Nominal case where the sensor location condition is not met.

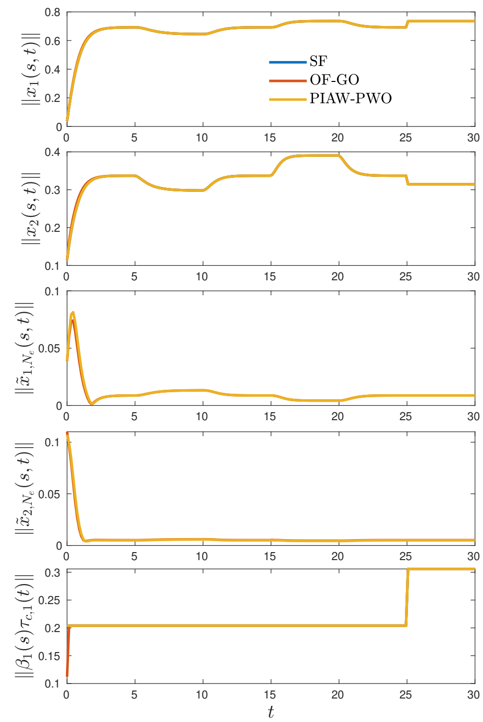

(b) Nominal case with upper control limit not selected appropriately.

Figure 4.11: Norms of distributed states in deviation, estimation errors and control input for violated conditions in the sensor location and control limits criteria.

Then, the sensor location condition is met with $\varsigma_1 \approx 0.24$, and the upper control limit condition violated with

$$\tau_c^+ = 0.2 < u^* = 0.28. \tag{4.89}$$

The corresponding norms of the distributed profiles in closed-loop behavior are presented in Figure 4.11b, showing that, as predicted, with the three CES the concentration-temperature profile pair reaches an undesired extinction steady-state, induced by control saturation. The estimators, again, function adequately.

4.7.3.2 *Robust functioning*

In Figure 4.12, Figure 4.13a and Figure 4.14a, the robust closed-loop control functioning with the SF (4.52), the advanced OF-GO (4.69), and the proposed PIAW-PWO (4.86) CESs, respectively, are shown. The robust closed-loop estimation functioning of the estimators of the OF-GO and the PIAW-PWO CES are shown in Figure 4.13b and Figure 4.14b, respectively. The norms of the distributed state and estimation error and control input profiles are presented in Figure 4.10b.

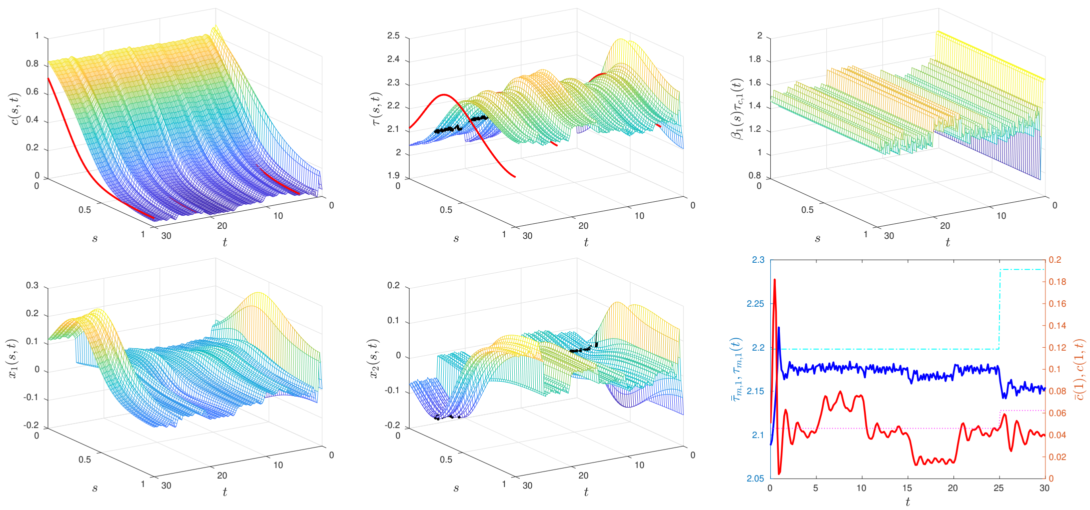

Figure 4.12: Robust closed-loop functioning with SF.Top left: concentration profile $c(s,t)$. Top center: temperature profile $\tau(s,t)$. Top right: control effort $\beta_1(s)\tau_{c,1}(t)$. Bottom left: deviated concentration profile $x_1(s,t)$. Bottom center: deviated temperature profile $x_2(s,t)$. Bottom right: measured $\tau_{m,1}$ (continuous blue) and regulated $c_o(t)$ (continuous red) outputs and their setpoints (dashed-dotted cyan or dotted magenta, respectively).

Accordingly, with respect to the regulation task and in terms of settling time, disturbance rejection, control saturation and effort, and setpoint regulation: the PIAW-PWO outperforms its OF-GO and SF counterparts. Regarding the estimation task, in terms of convergence settling time and offset, the estimator of the proposed PIAW-PWO performs slightly better than the one of the OF-GO. Thus, in agreement with theoretical developments, the proposed PIAW-PWO CES outperforms the detailed observer-based OF-GO CES, and the SF, substantially degraded due to its dependency on the parameters and in spite of using the current state of the tubular reactor.

Specifically, for $t \in [0,5)$ (with response to initial condition deviation), with respect to the PIAW-PWO: (i) the OF-GO has larger settling times with oscillatory response and large control action, and (ii) the SF has comparatively larger overshoot as well as asymptotic offset, accompanied by wasteful control action. For $t \in [5,25)$ (with persistent periodic and step disturbances as well as setpoint change) the OF-GO regulate almost equally well the temperature output as well as the outlet concentration and the state profiles with larger transients. For $t \in [25,30]$ (with setpoint change) the SF produces large asymptotic offsets on the measured temperature and effluent concentration, with wasteful control action.

Following the previous results, it is confirmed that the proposed PIAW-PWO CES (4.86) is the one with the best closed-loop performance in both tasks: control and estimation. What is left is to assess is there is some benefit of considering the MIMO cases in comparison with the SISO one. This is evaluated next.

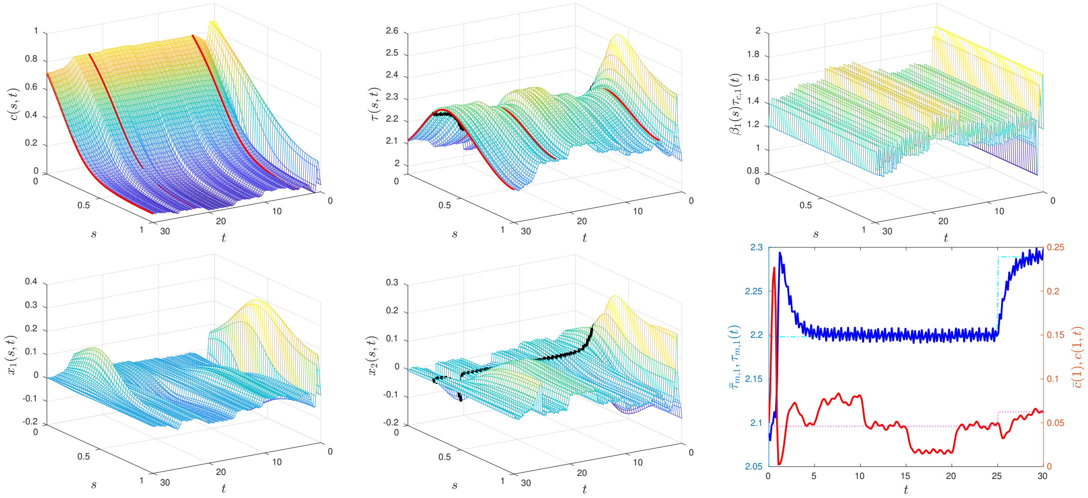

(a) Control functioning. Top left: concentration profile $c(s,t)$. Top center: temperature profile $\tau(s,t)$. Top right: control effort $\beta_1(s)\tau_{c,1}(t)$. Bottom left: deviated concentration profile $x_1(s,t)$. Bottom center: deviated temperature profile $x_2(s,t)$. Bottom right: measured $\tau_{m,1}$ (continuous blue) and regulated $c_o(t)$ (continuous red) outputs and their setpoints (dashed-dotted cyan or dotted magenta, respectively).

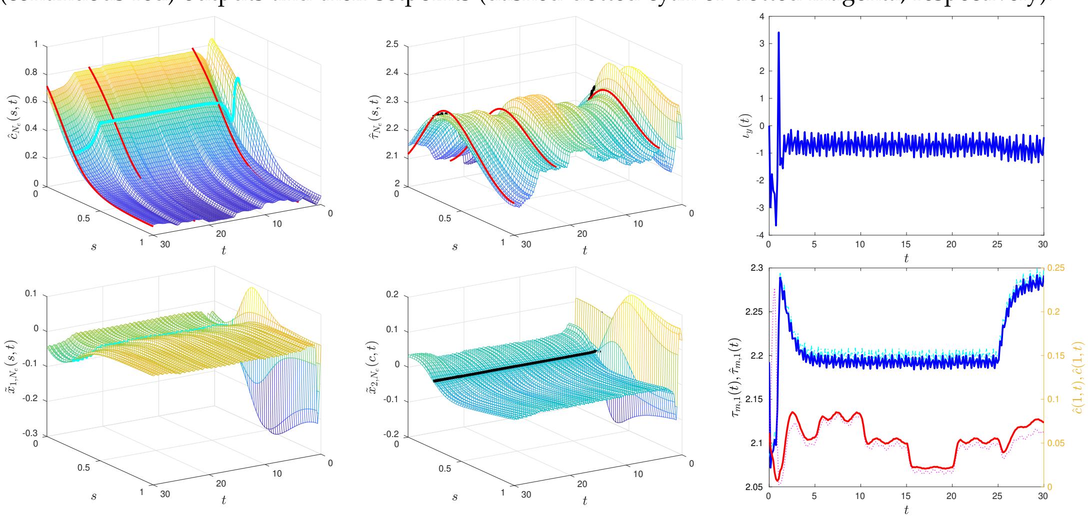

(b) Estimator functioning. Top left: estimated concentration profile $\hat{c}(s,t)$. Top center: estimated temperature profile $\hat{\tau}(s,t)$. Top right: estimated exogenous input $\iota(t)$. Bottom left: concentration estimation error profile $\tilde{c}_1(s,t)$. Bottom center: temperature estimation error profile $\tilde{\tau}_2(s,t)$. Bottom right: real measured $(\tau_{m,1}(t))$ (dashed-dotted cyan) an regulated $c_o(t)$ (dotted magenta) outputs and their estimates $(\hat{\tau}_{m,1}(t), \hat{c}_o(t))$ (continuous blue and red, respectively).

Figure 4.13: Robust closed-loop CE functioning with the SISO-OF-GO CES.

4.7.4 *MIMO case*

The SISO and MIMO for $q = 2, 3$, versions of the proposed PIAW-PWO CES (4.86) are set with the structures and parameters obtained in Section 4.7.2. The closed-loop CE

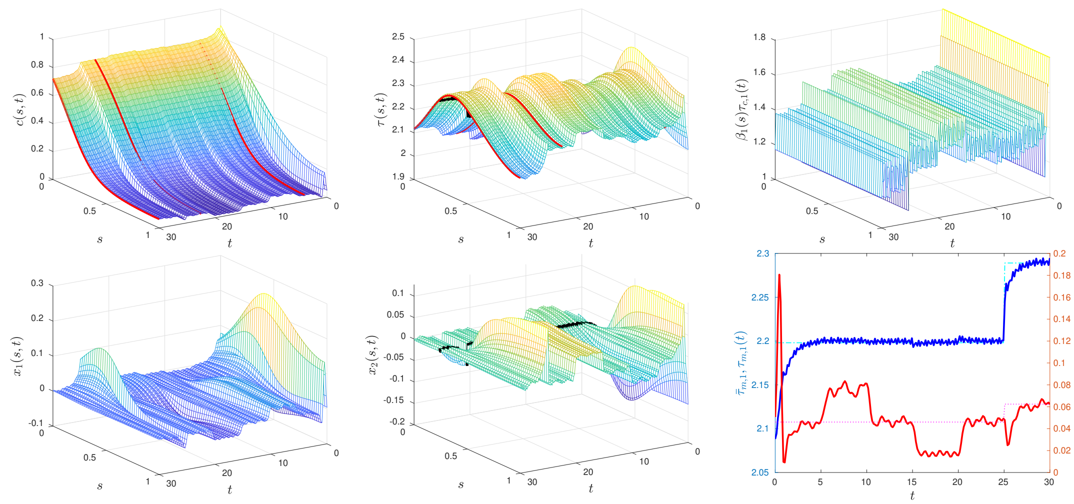

(a) Control functioning. Top left: concentration profile $c(s,t)$. Top center: temperature profile $\tau(s,t)$. Top right: control effort $\beta_1(s)\tau_{c,1}(t)$. Bottom left: deviated concentration profile $x_1(s,t)$. Bottom center: deviated temperature profile $x_2(s,t)$. Bottom right: measured $\tau_{m,1}$ (continuous blue) and regulated $c_o(t)$ (continuous red) outputs and their setpoints (dashed-dotted cyan or dotted magenta, respectively).

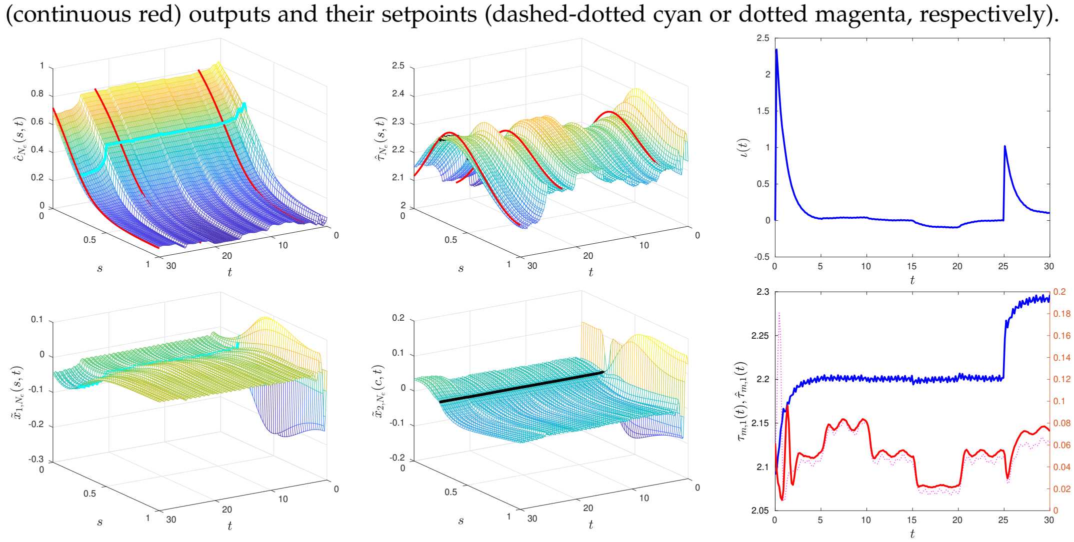

(b) Estimator functioning. Top left: estimated concentration profile $\hat{c}(s,t)$. Top center: estimated temperature profile $\hat{\tau}(s,t)$. Top right: estimated exogenous input $\iota(t)$. Bottom left: estimation error of the concentration profile $\tilde{c}_1(s,t)$. Bottom center: estimation error of the temperature profile $\tilde{\tau}_2(s,t)$. Bottom right: real measured $\tau_{m,1}(t)$ (continuous blue) and regulated $c_o(t)$ (dotted magenta) and their estimates $(\hat{\tau}_{m,1}(t), \hat{c}_o(t))$ (continuous blue and red, respectively).

Figure 4.14: Robust closed-loop CE functioning SISO-PIAW-PWO CES.

performances under robust testing conditions are presented in Figure 4.14, Figure 4.15, and Figure 4.16, for the SISO and 2-MIMO and 3-MIMO cases, respectively.

From the simulation results, it can be seen that the proposed PIAW-PWO CES benefits from the use of a MIMO sensor-actuator configuration: the CES dispose of more information and produce more robust closed-loop behavior in both control and estimation tasks. Specifically, for $t \in [5, 25)$ (when inlet temperature step disturbances arise), regarding control functioning, PIAW-PWO produce precise and coordinated control actions that have the effect of ensuring the accurate rejection of the disturbances in the steady-state profiles. Regarding estimation, it is appreciated that the PIAW-PWO improve their performance since the estimation error at steady-state, in the presence of exogenous disturbances, decreases as q increases, this in despite of the use a low dimensional estimation model. Note that this is produced, with an overall control action that has a similar norm as in the two MIMO and the SISO cases.

Thus, it is concluded that the proposed PIAW-PWO CES (4.86), clearly benefits with the use of more sensors and actuators and the 3-MIMO configuration produces the best closed-loop performance, in terms of measured disturbance rejection capabilities with adequate control effort.

4.7.5 *Concluding remarks on control-estimation functioning*

The preceding assessment of CES functioning results corroborate and illustrate the theoretical developments of Chapter 4, under realistic industrial-like testing conditions: (i) the proposed PIAW-PWO CES (4.86) outperformed its estimator-based saturated OF-GO (4.69) counterpart, and (ii) the theoretical-based claim that the proposed CES is a simplified-robustified application-oriented realization of its and advanced counterpart has been confirmed with on-line functioning assessment.

It was corroborated: (i) the effectiveness of the proposed passivity-based sensor location and bifurcation-based control limits selection criteria (Proposition 4.4 and Proposition 4.5, respectively), and (ii) that the proposed two-gain PIAW tuning is simpler and more efficient than the conventional three-gain one [21; 132]. With respect to industrial reactor control, the proposed PIAW-PWO CES design: (i) is simpler, more systematic and has robust functioning conditions in terms of sensor location, control limits and CE gains, (ii) has passivity-based sensor location criterion that corresponds to the industrial one (at the slope inflection before the hotspot) for exothermic tubular reactors [68; 100; 108], (iii) has simple control limit selection criterion, and (iv) a two-gain parameterization that enables a simpler and more efficient tuning than the conventional one.

Finally, it was also concluded that the decentralized MIMO versions of the proposed PIAW-PWO CES enhance their performance on both CE tasks.

4.8 Summary of the early lumping approach

The joint problem of robustly stabilizing, through saturated output feedback control, and estimating the state of a (possibly open-loop unstable) spatially distributed continuous exothermic tubular reactor was solved by constructing a CES within an

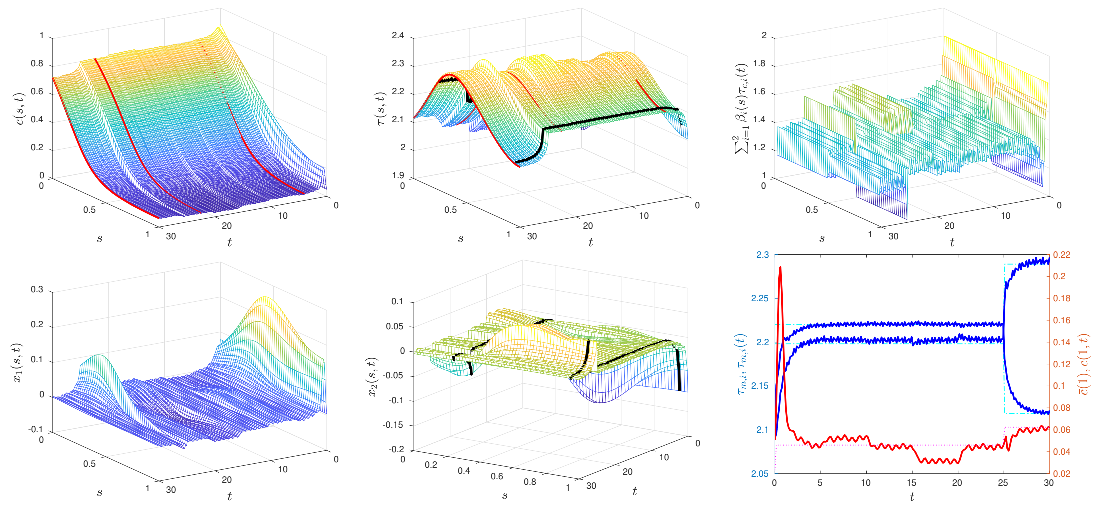

(a) Control functioning. Top left: concentration profile $c(s,t)$. Top center: temperature profile $\tau(s,t)$. Top right: control effort $\sum_{i=1}^{2} \beta_i(s)\tau_{c,i}(t)$. Bottom left: deviated concentration profile $x_1(s,t)$. Bottom center: deviated temperature profile $x_2(s,t)$. Bottom right: measured $\tau_{m,i}$, $i = 1,2$ (continuous blue) and regulated $c_o(t)$ (continuous red) outputs and their setpoints (dashed-doted cyan or dotes magenta, respectively).

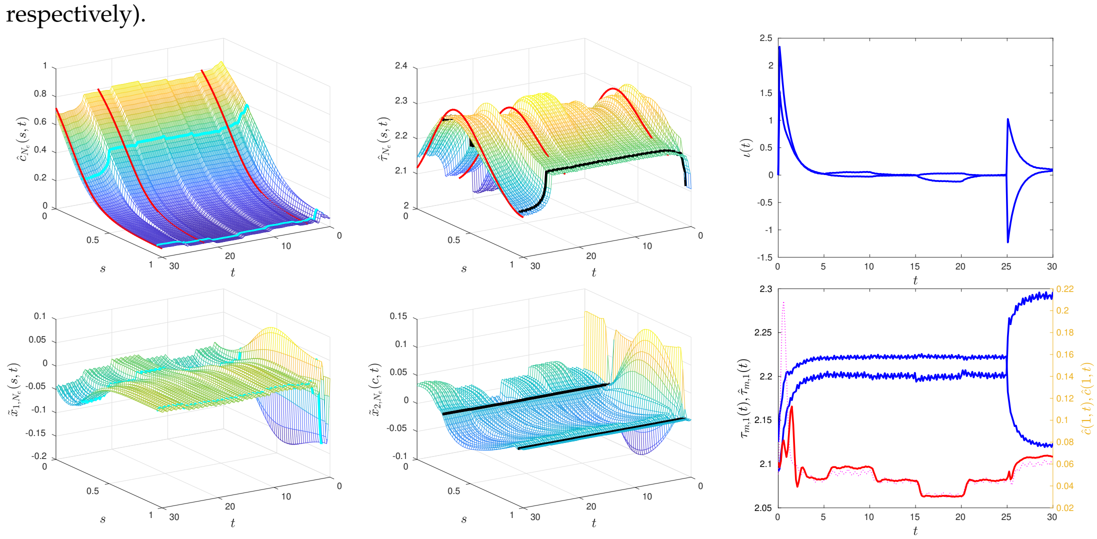

(b) Estimator functioning. Top left: estimated concentration profile $\hat{c}(s,t)$. Top center: estimated temperature profile $\hat{\tau}(s,t)$. Top right: estimated exogenous input $\iota(t)$. Bottom left: estimation error of the concentration profile $\tilde{c}_1(s,t)$. Bottom center: estimation error of the temperature profile $\tilde{\tau}_2(s,t)$. Bottom right: real measured $\tau_{m,i}(t)$, $i = 1,2$ (continuous blue) and regulated $c_o(t)$ (dotted magenta) and their estimates $(\hat{\tau}_{m,i}(t), \hat{c}_o(t))$ (continuous blue and red, respectively).

Figure 4.15: Nominal closed-loop CE functioning with the 2-MIMO-PIAW-PWO CES.

early lumping-based constructive approach. The solution consists in: (i) a set of decentralized saturated linear temperature PIAW decoupled from a pointwise-like state estimator, and (ii) assurance of robust functioning accompanied by a systematic

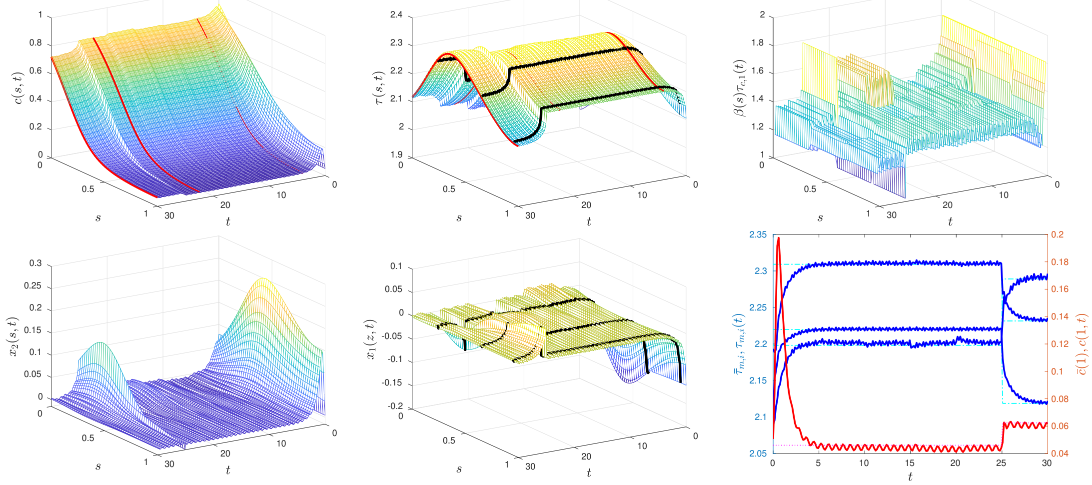

(a) Control functioning. Top left: concentration profile $c(s,t)$. Top center: temperature profile $\tau(s,t)$. Top right: control effort $\sum_{i=1}^{3}\beta_i(s)\tau_{c,i}(t)$. Bottom left: deviated concentration profile $x_1(s,t)$. Bottom center: deviated temperature profile $x_2(s,t)$. Bottom right: measured $\tau_{m,i}$, $i=1,2,3$ (continuous blue) and regulated $c_o(t)$ (continuous red) outputs and their setpoints (dashed-dotted cyan or dotted magenta, respectively).

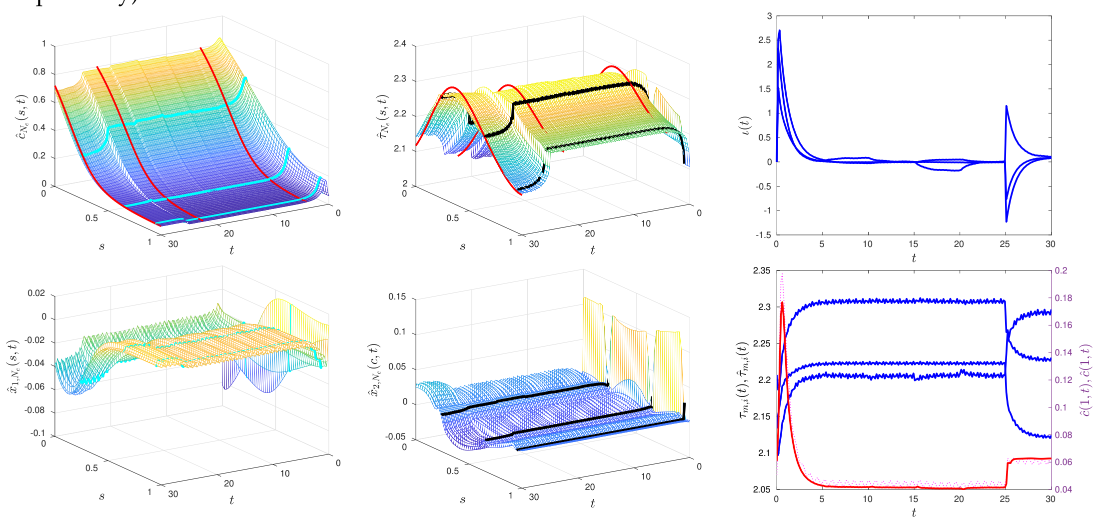

(b) Estimator functioning. Top left: estimated concentration profile $\hat{c}(s,t)$. Top center: estimated temperature profile $\hat{\tau}(s,t)$. Top right: estimated exogenous input $\iota(t)$. Bottom left: estimation error of the concentration profile $\tilde{c}_1(s,t)$. Bottom center: estimation error of the temperature profile $\tilde{\tau}_2(s,t)$. Bottom right: real measured $\tau_{m,i}(t)$, $i=1,2,3$ (continuous blue) and regulated $c_o(t)$ (dotted magenta) and their estimates $(\hat{\tau}_{m,i}(t),\hat{c}_o(t))$ (continuous blue and red, respectively).

Figure 4.16: Robust closed-loop CE functioning with the 3-MIMO-PIAW-PWO CES.

procedure to choose and tune sensor-actuator configuration, control limits and control-estimator gains. In terms of a compromise between simplicity, robustness, control effort and on-line computational load the proposed cCES design outperforms its

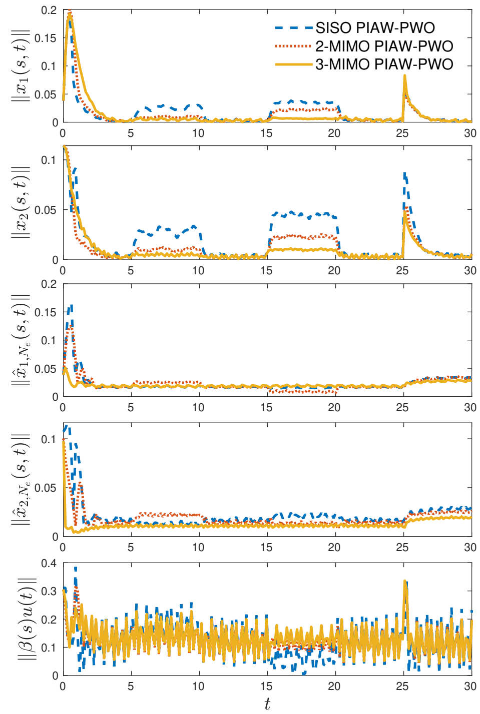

Figure 4.17: Norms of distributed states in deviation, estimation errors and control input for decentralized SISO, 2-MIMO, and 3-MIMO PIAW-PWO CESs.

advanced counterpart. The robust functioning of the proposed CES was illustrated and tested with a representative case example through numerical simulation.

Methodologically speaking, the proposed design: (i) is based on a series of (PDE and ODE) models along off and on-line development steps, (ii) is underlain by feedback passivity and closed-loop detectability properties, (iii) connects industrial saturated PIAW with passive control, and (iv) has reduced on-line computational load, attained with efficient modeling approach for tubular reactors.

The methodology consisted in the use of an efficiently lumped ODE model that is used fro model-based design of a saturated state feedback controller and a robust estimator, drawn from sensor dependent passivity and closed-loop detectability properties. The combination of these algorithms leads to an advanced CES which assurance of robust stability, and criteria for the selection of sensor locations and control limits. For reliable functioning and implementation purposes, using model redesign, the advanced CES was realized as a set of decoupled PIAW and a decoupled pointwise-like estimator.

The efficiency of the proposed CES was corroborated with an extensive simulation study leading to conclude that the decentralized MIMO version has better closed-loop performance in comparison with the SISO case.

Part III

LATE LUMPING APPROACH

This part of the present study regards the solution of the control-estimation problem at hand within a late lumping approach. The control-monitoring design methodology is traversed by a constructive spirit. The unstable steady-state of the tubular reactor is stabilized by an output linearizing controller, its stabilizing capabilities are characterized in terms of the number of sensors and their locations. Then, an additional control term, drawn with inventory control ideas and feedback passivation by output selection, is added to the control design to improve closed-loop performance. A pointwise innovation observer is introduced for output feedback control and estimation purposes. Exponential stability of the related closed-loop dynamics are established by using small gain arguments in terms of the sensor locations and gains. The implementation of the control-estimation system is done with the employment of the efficient modeling approach to get an efficient late lumping implementable algorithm. The effectiveness of the approach is illustrated with closed-loop simulations on the case study.

5 CONTROL-ESTIMATION SYSTEM DESIGN WITH LATE LUMPING APPROACH

In this chapter, within the late lumping approach, a Control-Estimation System (CES) will be designed by combining feedback passivity, industrial inventory control ideas, and nonlinear estimation theory. All this within an application-oriented framework and exploiting the natural stabilizing mechanisms of the tubular reactor dynamics.

The CES is composed by a state feedback controller and a distributed observer. The state feedback controller is a partial linearizing control that keeps the open-loop stabilizing linear terms on the output dynamics. The closed-loop system with this controller is passivated be choosing a virtual output that produce an inventory-like control component. Finally, for implementation and monitoring purposes, a pointwise observer is added to the design. The observer has as unique degree of freedom the number of temperature measurements and their locations. The Single Input-Single Output (SISO) and the Multiple Input Multiple Output (MIMO) cases are considered. The closed-loop stability is ensured and the efficient modeling approach recalled (see Section 3.2) for the late lumping implementation of the proposed CES.

5.1 LATE LUMPING CONTROL-ESTIMATION PROBLEM SETTING

The control problem treated in this chapter, consist in designing, on the basis of the tubular reactor distributed Partial Differential Equation (PDE) model (2.7), a distributed CES, to perform the stabilization task of the concentration-temperature profile pair on an open-loop unstable steady-state of the tubular reactor, and to estimate the related state of the system. The distributed CES must assure closed-loop stability on the PDE model (2.7) in a suitable norm and have an efficient implementation.

Specifically, the distributed CES has the form

$$\dot{\boldsymbol{\theta}} = \boldsymbol{\mathcal{G}}(\boldsymbol{\theta}, \boldsymbol{\tau}_m, \chi_e, \boldsymbol{p}, \mathfrak{S}, \boldsymbol{K}_\theta), \qquad \boldsymbol{\theta}(0) = \boldsymbol{\theta}_0, \tag{5.1a}$$

$$\hat{\chi} = \boldsymbol{\mathcal{E}}(\boldsymbol{\theta}, \mathfrak{S}), \tag{5.1b}$$

$$\boldsymbol{\tau}_c = \boldsymbol{\mu}(\boldsymbol{\theta}, \boldsymbol{\tau}_m, \chi_e, \boldsymbol{p}, \boldsymbol{K}_\theta, \mathfrak{S}), \tag{5.1c}$$

where $\boldsymbol{\theta}$ is the infinite dimensional internal state, $\boldsymbol{\mathcal{G}}$ and $\boldsymbol{\mathcal{E}}$ are the infinite dimensional functions that determines the internal dynamics of the controller and the estimated state, and $\boldsymbol{\mu}$ is the finite dimensional control output map that determines the jacket temperatures. The CES structure $\mathfrak{S}_q$ (the number of sensor/actuators and their lo-

cations, design degrees of freedom, and the control set) and gains $\boldsymbol{K}_\theta$ are given as

$$\mathfrak{S}_q = (n_\infty, q, \varsigma, \subset \mathbb{R}), \quad \boldsymbol{K}_\theta = (\boldsymbol{K}_c, \boldsymbol{K}_e), \tag{5.1d}$$

where $\boldsymbol{K}_e$ (or $\boldsymbol{K}_c$) contains controller (or estimator) gains, $n_\infty = \infty$ indicates the infinite dimension of the control-estimation system, q is the number of coolant jacket sections and sensors, ς is the sensor set (2.5b), and $\mathscr{T}_c \subset \mathbb{R}$, indicate that the control action is unconstrained. The consideration of constrained control action may be explored. Again, as in the early lumping case and according to [67], only the cases for $q = 1, 2, 3$ will be considered. The late lumping approximation, obtained with the application of efficient modeling approach of Section 3.2, to the CES (5.1a) yields to a finite dimensional system of the form (2.11).

Throughout this chapter, the notion of stability that will be used is similar to the one of robust stability employed in Chapter 4, but using the concept exponential stability in the L^2 norm. This property of stability can be used to establish similar results on Input-to-State Stability (ISS) as the ones employed in Chapter 4.

The remaining of this chapter is structured as follows. First, the PDE model (2.7) is described in a Hilbert product space in which its open-loop dynamics are characterized. Secondly, a state feedback controller with three components, two stabilizing ones and a third one for performance enhancement is constructed. Finally, this controller is coupled with a pointwise observer for implementation purposes. The efficient modeling approach is used to get a late lumping approximation of the controller for on-line functioning which is assessed in a simulation study.

5.2 OPEN-LOOP DYNAMICS

Here, the tubular reactor PDE dynamic model (2.7) is redefined as an abstract system in the product space of two Hilbert spaces, one for each distributed state. An integrating factor is used to get a system with selfadjoint operators, and the related operators and functions are described in the corresponding Hilbert space. Then, using this abstract model and within a physical perspective, the interplay between stabilizing and destabilizing mechanisms of the reactor model are discussed on the basis of: (i) the characterization of the spectra of the heat and mass transport operators, and (ii) the dynamic interaction between stabilization by heat transport and destabilization by heat generation due to chemical reaction.

For the purpose at hand, recall the tubular reactor model (2.7). From standard modeling assumptions [129], bounded feed temperature, concentration, and coolant temperature exogenous inputs

$$\tau_e^- \leq \tau_e(t) \leq \tau_e^+, \quad 0 \leq c_e(t) \leq 1, \quad 0 < \tau_c^- \leq \tau_{c,i}(t) \leq \tau_c^+,$$

produce a bounded temperature–concentration state profile $[c(s,t)\, \tau(s,t)]^T$, over the spatial $s \in [0, 1]$ and temporal $t \in \mathbb{R}_+$ domains.

Introduce the deviated weighted state, control, and outputs coordinate change

$$x_1 = \omega_m(s)(c(s,t) - \bar{c}(s)), \quad x_2 = \omega_h(s)(\tau(s,t) - \bar{\tau}(s)),$$

$$\boldsymbol{u} = \begin{bmatrix} \tau_{c,1} - \bar{\tau}_c \\ \vdots \\ \tau_{c,q} - \bar{\tau}_c \end{bmatrix}, \quad \boldsymbol{y} = \text{I}_h(s) \begin{bmatrix} \tau_{m,1}(t) - \bar{\tau}_{m,1} \\ \vdots \\ \tau_{m,q}(t) - \bar{\tau}_{m,q} \end{bmatrix}, \quad z = \omega_m(s)(c_z - \bar{c}_z),$$

where the weighting functions

$$\omega_m(s) = \mathrm{e}^{-\frac{Pe_m}{2}s}, \quad \omega_h(s) = \mathrm{e}^{-\frac{Pe_h}{2}s},$$

are integrating factors that produce selfadjoint spatial operators. The corresponding inverses are

$$\omega_m^{-1}(s) = \mathrm{e}^{\frac{Pe_m}{2}s}, \quad \omega_h^{-1}(s) = \mathrm{e}^{\frac{Pe_h}{2}s}.$$

The application of the above coordinate change to the PDE reactor model (2.7) yields to the abstract system

$$\dot{x}_1 = \mathcal{A}_1 x_1 - \rho_1(x_1, x_2), \qquad x_1(0) = x_{10}, \tag{5.2a}$$

$$\dot{x}_2 = \mathcal{A}_2 x_2 + \rho_2(x_1, x_2) + \boldsymbol{\mathcal{B}}_u \boldsymbol{u}, \qquad x_2(0) = x_{20}, \tag{5.2b}$$

$$\boldsymbol{y} = \boldsymbol{\mathcal{C}}_y x_2, \quad z = \mathcal{C}_z x_1, \tag{5.2c}$$

where $x_j(s,t): (0,1) \times \mathbb{R}_+ \to \mathcal{H}_j$ are the states, each one evolving in the Hilbert space $\mathcal{H}_j$. The initial conditions $x_{j0}(s) \in H_j^2(0,1)$, $j = 1,2$, are defined in the Sobolev spaces $H_j^2(0,1)$ of functions with second derivative in $L^2(0,1)$, $\boldsymbol{u}$ is the vector of control inputs, $\boldsymbol{y}$ is the vector of measured outputs, and z is the controlled output. $\mathcal{A}_1$ (or $\mathcal{A}_2$), with domain $\mathcal{D}(\mathcal{A}_j) \subset \mathcal{H} \to \mathcal{H}$, $j = 1,2$, is the selfadjoint heat (or mass) Riesz spectral operator [38], $\boldsymbol{\mathcal{B}}_u$ is the input operator, $\boldsymbol{\mathcal{C}}_y$ and $\mathcal{C}_z$ are the measured and controlled output operators, and ρ is a weighted version of the reaction rate function. All the definitions are given below

$$\mathcal{A}_1 x_1 = \frac{1}{Pe_m}\partial_s^2 x_1 - \frac{Pe_m}{4}x_1, \quad \mathcal{D}(\mathcal{A}_1) = \left\{x_1 \in \mathcal{H}^2 \mid \mathcal{A}_1 x_1 \in \mathcal{H}, \ \mathscr{B}_1 x_1 = \mathbf{0}\right\},$$

$$\mathcal{A}_2 x_2 = \frac{1}{Pe_h}\partial_s^2 x_2 - \left(\frac{Pe_h}{4} + v\right)x_2, \quad \mathcal{D}(\mathcal{A}_2) = \left\{x_2 \in \mathcal{H} \mid \mathcal{A}_2 x_2 \in \mathcal{H}, \ (\mathscr{B}_2 x_2) = \mathbf{0}\right\},$$

$$\mathscr{B}_j x_j = \begin{bmatrix} \frac{1}{Pe_a}\partial_s x_j(0,t) - \frac{1}{2}x_j(0,t) \\ \frac{1}{Pe_a}\partial_s x_j(1,t) + \frac{1}{2}x_j(1,t), \end{bmatrix}, \quad j = 1,2, \quad a = m,h,$$

$$\boldsymbol{\mathcal{B}}_u \boldsymbol{u} = v\omega_h \boldsymbol{\beta}\boldsymbol{u} = v\omega_h \sum_{i=1}^{q} \beta_i u_i, \quad \boldsymbol{\beta} = \begin{bmatrix} \beta_1(s) & \dots & \beta_q(s) \end{bmatrix},$$

$$\boldsymbol{\mathcal{C}}_y x_2 = \begin{bmatrix} \left\langle \delta(s - \varsigma_1), \omega_h^{-1} x_2 \right\rangle \\ \vdots \\ \left\langle \delta(s - \varsigma_q), \omega_h^{-1} x_2 \right\rangle \end{bmatrix}, \quad \mathcal{C}_z x_1 = \left\langle \delta(s-1), \omega_m^{-1} x_1 \right\rangle,$$

$$\rho_1(x_1, x_2) = \omega_m \left(r(\omega_m^{-1} x_1 + \bar{c}, \omega_h^{-1} x_2 + \bar{\tau}) - r(\bar{c}, \bar{\tau}) \right),$$
$$\rho_2(x_1, x_2) = \omega_h \left(r(\omega_m^{-1} x_1 + \bar{c}, \omega_h^{-1} x_2 + \bar{\tau}) - r(\bar{c}, \bar{\tau}) \right).$$

The state $\boldsymbol{x} = [x_1\ x_2]^T$ evolves in the product space

$$\mathcal{X} = \{[x_1\ x_2]^T \in \mathcal{H}^2 \mid [x_1(s),\ x_2(s)]^T \in [x_1^-, x_1^+] \times [x_2^-, x_2^+]\ \forall\, s \in [0, 1]\}$$

where

$$x_1^- = -\max_{s\in[0,1]} \bar{c}(s), \quad x_1^+ = 1 - \max_{s\in[0,1]} \bar{c}(s), \quad x_2^- = \tau^- - \max_{s\in[0,1]} \bar{\tau}(s), \quad x_2^+ = \tau^+ - \max_{s\in[0,1]} \bar{\tau}(s).$$

where $\tau^- = \min\{\tau_e^-, \tau_c^-\}$, $\tau^+ = \tau_a + \max\{\tau_e^+, \tau_c^+\}$, and τ_a is the adiabatic temperature rise. $\mathcal{H} = L^2(0, 1)$ is the product Hilbert space of real-valued square integrable vector functions with inner product $\langle(\cdot)_1, (\cdot)_2\rangle$ and induced norm $\|(\cdot)\|$

$$\langle x_1, x_2\rangle = \int_0^1 x_1 x_2 \mathrm{d}s, \quad \|x\| = \sqrt{\langle x, x\rangle}, \quad x, x_1, x_2 \in \mathcal{H}.$$

$\mathcal{H}^2$ is the related product space with inner product and induced norm defined as

$$\langle \boldsymbol{x}_1, \boldsymbol{x}_2\rangle_{\mathcal{X}} = \int_0^1 \boldsymbol{x}_1^T \boldsymbol{x}_2 \mathrm{d}s, \quad \|\boldsymbol{x}\|_{\mathcal{X}} = \sqrt{\|x_1\|^2 + \|x_2\|^2}, \ \boldsymbol{x} = [x_1\ x_2]^T \in \mathcal{X}.$$

From the Lipschitz boundedness of the function $r(c, \tau)$ in model (2.7), the following assumptions on the functions $\rho_1(x_1, x_2)$ and $\rho_2(x_1, x_2)$ can be established.

Assumption 5.1. *For any admissible state $[x_1(s,t), x_2(s,t)]^T \in \mathcal{X}$, the reaction rate functions $\rho_j(x_2, x_2) \in \mathcal{H}$, $j = 1, 2$, are Lipschitz bounded, i.e.,*

$$\left\|\rho_j(x_1, x_2)\right\| \leq L_{x_1}^{\rho_j} \|x_1\| + L_{x_2}^{\rho_j} \|x_2\|, \quad L_{x_l}^{\rho_j} = \max_{x_l \in [x_l^-, x_l^+]} \left|\partial_{x_l} \rho_j\right|, \quad j, l = 1, 2, \tag{5.3}$$

where $L_{x_l}^{\rho_j}$ are the Lipschitz constants, and vanishes only at the origin $\rho_j(0, 0) = 0$.

Assumption 5.2. *The reaction rate function $r(c, \tau)$ is strictly monotonically increasing in the concentration state c, i.e., $\partial_c r(\tau, c) > 0$.*

5.2.1 *Stability analysis of the open-loop dynamics*

As it was done in Section 4.2.2 of Chapter 4, the concentration (or temperature) dynamics can be studied as a Lur'e system: a linear component in term (or positive) feedback with a nonlinearity. This enables to analyze the stability of each individual state by first characterizing the properties of the linear part and then its interconnection in negative (or positive) feedback with the nonlinear reaction rate function.

For the purpose at hand, recall system (2.7) with $\boldsymbol{u} = \mathbf{0}_q$

$$\dot{x}_1 = \mathcal{A}_1 x_1 - \rho_1(x_1, x_2), \qquad x_1(0) = x_{10}, \tag{5.4a}$$

$$\dot{x}_2 = \mathcal{A}_2 x_2 + \rho_2(x_1, x_2), \qquad x_2(0) = x_{20}. \tag{5.4b}$$

The concentration (or temperature) dynamics are composed by the stabilizing linear mass (or heat) transport operator $\mathcal{A}_1$ (or $\mathcal{A}_2$) in negative (or positive) feedback with the nonlinearity ρ_1 (or ρ_2), which reflects the stabilizing (or destabilizing) capability of the sync (or source) effect of the consumption of reactant (or heat generation) by the chemical reaction. The nonlinearity ρ_1 (or ρ_2) interconnects the concentration (or temperature) with temperature (or concentration) states dynamics.

The spectrum of the operators $\mathcal{A}_j$, $j = 1, 2$, denoted as $\sigma(\mathcal{A}_j)$ has real eigenvalues, for which the algebraic and geometric multiplicities are the same, $\lambda_{j,n} \in \sigma(\mathcal{A}_j) \subset \mathbb{R}$, $n \in \mathbb{N}$ given by

$$\lambda_{1,n} = -\frac{\omega_n^2}{Pe_m} - \frac{Pe_m}{4}, \qquad \lambda_{2,n} = -\frac{\omega_n^2}{Pe_h} - \frac{Pe_h}{4} - v, \tag{5.5a}$$

where the eigenfrequencies $\omega_{j,n} \neq 0$ are the solutions to the transcendental equations

$$\tan(\omega_{1,n}) = \frac{Pe_m \omega_{1,n}}{\omega_{1,n}^2 - \left(\frac{Pe_m}{2}\right)^2}, \qquad \tan(\omega_{2,n}) = \frac{Pe_h \omega_{2,n}}{\omega_{2,n}^2 - \left(\frac{Pe_h}{2}\right)^2}.$$

The eigenvalues of both operators have the following ordering property

$$0 > \lambda_{j,1} \geq \lambda_{j,2} \geq \cdots, \quad \lim_{n\to\infty} \lambda_{j,n} = -\infty, \quad j = 1, 2. \tag{5.5b}$$

The associated eigenfunctions, which form a Riesz basis of the state space $\mathcal{X}$, are

$$\phi_{1,n} = B_{1,n}\left[\sin(\omega_{1,n}s) + \frac{2\omega_{1,n}}{Pe_m}\cos(\omega_{1,n}s)\right], \quad \langle \phi_{1,n}, \phi_{1,m}\rangle = \delta_{n,m}, \tag{5.5c}$$

$$\phi_{2,n} = B_{2,n}\left[\sin(\omega_{2,n}s) + \frac{2\omega_{2,n}}{Pe_h}\cos(\omega_{2,n}s)\right], \quad \langle \phi_{2,n}, \phi_{2,m}\rangle = \delta_{n,m}, \tag{5.5d}$$

where $B_{j,n}$ are normalization constants, $\delta_{n,m}$ is the Kronecker delta, and $n, m \in \mathbb{N}$.

As a consequence of the previous result, the operators $\mathcal{A}_j$ are infinitesimal generators of C_0-semigroups of contractions $S_j(t) = e^{\mathcal{A}_j t}$ that satisfy the spectrum determined growth assumption [38], i.e.,

$$\left\|S_j(t)\right\|_{\mathfrak{O}} \leq e^{-\lambda_j^* t}, \; j = 1, 2, \quad -\lambda_j^* = \sup_{\lambda_i \in \sigma(\mathcal{A}_j)} \lambda_i, \tag{5.5e}$$

with growth bound $-\lambda_j^*$, where $\left\|S_j\right\|_{\mathfrak{O}} = \sup_{\|x\|=1} \left\|S_j x\right\|$ is the operator norm of S_j.

Accordingly, the concentration (or temperature) state of the system (5.4) with $\rho_1 = 0$ (or $\rho_2 = 0$), has the origin as exponentially stable steady-state due to the stabilizing properties of the mass (or heat) transport operator. What follows is to analyze the effect of the negative (or positive) interconnection, of the reaction rate function ρ_1 (or ρ_2) with the mass (ore heat) transport operator $\mathcal{A}_1$ (or $\mathcal{A}_2$), and the effect of the concentration and temperature interconnection through the reaction rate functions.

5.2.1.1 *Concentration dynamics*

The reaction rate function $\rho(x_1, x_2) \in \mathcal{H}$ can be rewritten as

$$\rho_1(x_1, x_2) = \varrho_1(x_1) + \varrho_{12}(x_1, x_2), \tag{5.6a}$$

where

$$\varrho(x_1) = \rho_1(x_1, 0), \quad \varrho_{12}(x_1, x_2) = \rho_1(x_1, x_2) - \rho_1(x_1, 0). \tag{5.6b}$$

By virtue of Assumption 5.1, the function ϱ satisfies the sector condition

$$\langle \varrho_1 - \mathfrak{a} x_1, \varrho_1 - \mathfrak{b} x_1 \rangle \leq 0,$$

which es equivalent to

$$\mathfrak{c} \langle x_1, \varrho_1 \rangle + \mathfrak{d} \langle \varrho_1, \varrho \rangle \leq \langle x_1, \varrho_1 \rangle, \quad \mathfrak{c} = \frac{\mathfrak{a}\mathfrak{b}}{\mathfrak{a} + \mathfrak{b}}, \quad \mathfrak{d} = \frac{1}{\mathfrak{a} + \mathfrak{b}}, \tag{5.7}$$

and the function $\varrho_{12}(x_1, x_2)$ is Lipschitz bounded with respect to x_2, uniformly in x_1:

$$\|\varrho_{12}(x_1, x_2)\| \leq L_{x_2}^{\varrho_{12}} \|x_2\|, \forall x_1. \tag{5.8}$$

Using the above stated properties, and following a similar procedure as in Section 4.2.2.1, the stability of the concentration dynamics is established next considering the temperature profile as exogenous input and using the direct Lyapunov method.

Consider the Lyapunov functional

$$V_1 = \langle x_1, x_1 \rangle, \tag{5.9}$$

compute its time derivative along the concentration trajectories of the distributed temperature dynamics and use (5.6) and (5.7) to obtain

$$\begin{aligned}
\dot{V}_1 &= \langle \dot{x}_1, x_1 \rangle + \langle x_1, \dot{x}_1 \rangle, \\
&= \langle \mathcal{A}_1 x_1 - \rho_1(x_1, x_2), x_1 \rangle + \langle x_1, \mathcal{A}_1 x_1 - \rho_1(x_1, x_2) \rangle, \\
&= \langle \mathcal{A}_1 x_1, x_1 \rangle + \langle x_1, \mathcal{A}_1 x_1 \rangle - 2 \langle \rho_1(x_1, x_2), x_1 \rangle, \\
&= \langle \mathcal{A}_1 x_1, x_1 \rangle + \langle x_1, \mathcal{A}_1 x_1 \rangle - 2 \langle \varrho_1(x_1), x_1 \rangle - 2 \langle \varrho_{12}(x_1, x_2), x_1 \rangle, \\
&\leq \langle \mathcal{A}_1 x_1, x_1 \rangle + \langle x_1, \mathcal{A}_1 x_1 \rangle - 2\mathfrak{c} \langle x_1, x_1 \rangle - 2\mathfrak{d} \langle \varrho(x_1), \varrho(x_1) \rangle - 2 \langle \varrho_{12}(x_1, x_2), x_1 \rangle,
\end{aligned}$$

using the fact that

$$\langle \mathcal{A}_1 x_1, x_1 \rangle + \langle x_1, \mathcal{A}_1 x_1 \rangle \leq -2\lambda_1^* \|x_1\|^2, \tag{5.10}$$

considering that $\langle \varrho_1, \varrho_1 \rangle = \|\varrho_1\|^2 > 0$ and using (5.8), it follows

$$\begin{aligned}
\dot{V}_1 &\leq -2\lambda_1^* \|x_1\|^2 - 2\mathfrak{c} \langle x_1, x_1 \rangle - 2 \langle \varrho_{12}(x_1, x_2), x_1 \rangle, \\
&\leq -2\lambda_1^* \|x_1\|^2 - 2\mathfrak{c} \langle x_1, x_1 \rangle + 2 \|\varrho_{12}(x_1, x_2)\| \|x_1\|, \\
&\leq -2(\lambda_1^* + \mathfrak{c}) \|x_1\|^2 + 2L_{x_2}^{\varrho_{12}} \|x_1\| \|x_2\|, \\
&= -2(\lambda_1^* + \mathfrak{c}) V_1 + 2L_{x_2}^{\varrho_{12}} \|x_2\| V_1^{\frac{1}{2}}.
\end{aligned}$$

Using the comparison lemma [76], the estimate

$$\|x_1(t)\| \leq \|x_{10}\| \, \mathrm{e}^{-\nu_1 t} + L_{x_2}^{\varrho_{12}} \int_0^t \mathrm{e}^{-\nu_1(t-\mathrm{t})} \, \|x_2(\mathrm{t})\| \, \mathrm{dt}, \quad \nu_1 = |\lambda_1^*| + >0, \tag{5.11}$$

is obtained for the concentration state. For bounded input $\|x_2(t)\| \leq \varepsilon_2(t) \leq \varepsilon_2^+$ and bounded initial condition $\|x_{10}\| \leq \delta_{10}$, the state is bounded as

$$\|x_1(t)\| \leq \delta_{10}\mathrm{e}^{-\nu_1 t} + \frac{L_{x_2}^{\varrho_{12}}}{\nu_1}\varepsilon_2^+ \leq \delta_{10} + \frac{L_{x_2}^{\varrho_{12}}}{\nu_1}. \tag{5.12}$$

Thus, the above estimate, shows that the zero solution is exponentially stable when there is no interconnection with the temperature dynamics, and that the system is robustly stable with respect to small enough temperature profile trajectories. For tubular reactors with open-loop multiplicity, the estimate (5.11) holds locally.

Note the the stabilizing effect of reactant conversion by reaction as well as the mass transport contribute to the convergence to zero of the concentration state as measured by the two components of ν_1.

5.2.1.2 *Temperature dynamics*

Consider the temperature dynamics (5.4b), compute its solution to obtain

$$x_2(t) = x_{20}\mathrm{e}^{\mathcal{A}_2 t} + \int_0^t \mathrm{e}^{\mathcal{A}_2(t-\mathrm{t})}\rho_2(x_1, x_2)\mathrm{dt},$$

take norms on both sides of the above expression and use the triangle inequality and the Lipschitz boundedness of ρ to obtain the estimate

$$\|x_2(t)\| \leq \|x_{20}\| \, \mathrm{e}^{-\nu_2 t} + L_{x_1}^{\rho_2} \int_0^t \|x_1(\mathrm{t})\| \, \mathrm{dt}, \quad \nu_2 = |\lambda_2^*| - L_{x_2}^{\rho} \tag{5.13}$$

For bounded input $\|x_1(t)\| \leq \varepsilon_1(t) \leq \varepsilon_1^+$ and bounded initial conditions $\|x_{20}\| \leq \delta_{20}$, the state is bounded as

$$\|x_2(t)\| \leq \delta_{20}\mathrm{e}^{-\nu_2 t} + \frac{L_{x_2}^{\rho_2}}{\nu_1}\varepsilon_2^+ \leq \delta_{20} + \frac{L_{x_1}^{\rho_2}}{\nu_2}. \tag{5.14}$$

This above stability conditions is satisfied if

$$\nu_2 = |\lambda_2{}^*| - L_{x_2}^{\rho_2} > 0, \tag{5.15}$$

is fulfilled. Is this is so, (5.14) ensures the local exponential stability of the zero profile when the concentration dynamics are not present or decay to zero, and local robust stability when the concentration remains bounded. If the origin is unique, then the result is valid in the nonlocal sense.

In this case, while the transport operator has an stabilizing effect on the temperature dynamics, quantified by $-\lambda_2^*$, the heat generation by reaction has a destabilizing one measured by the Lipschitz constant $L_{x_2}^{\rho_2}$.

5.2.1.3 *Interconnected dynamics*

Recall model (5.4), in the previous two subsections, it has been shown that each individual state dynamics, are robustly stable, considering the other state as exogenous input, in the L^2-norm. The stability of the interconnected system can be assessed with a small gain argument, as in Proposition 3.1, but using the L^2-norm and the corresponding product space norm $\|\cdot\|_{\mathcal{X}}$. Accordingly, the next result follows.

Proposition 5.1. *Open-loop stability of the distributed dynamics*
Consider the tubular reactor abstract model (5.4), assume that (5.11) and (5.13) are satisfied with $\nu_1, \nu_2 > 0$. If the following condition is met

$$\nu_2 - \frac{L_{x_1}^{\rho_2} L_{x_2}^{\varrho_{12}}}{\nu_1} > 0, \tag{5.16}$$

then, the zero solution $[x_1 \ x_2]^T = \mathbf{0}$ of (5.4) is locally exponentially stable and satisfy

$$\|\boldsymbol{x}(t)\|_{\mathcal{X}} \leq \|\boldsymbol{x}_0\|_{\mathcal{X}} \, \mathrm{e}^{-\lambda^* t}, \quad -\lambda^* = \max_{\lambda \in \sigma(\boldsymbol{A}_x)} \lambda_j, \, j = 1, 2, \quad \boldsymbol{A}_x = \begin{bmatrix} -\nu_1 & L_{x_2}^{\varrho_{12}} \\ L_{x_1}^{\rho_2} & -\nu_2 \end{bmatrix}. \tag{5.17}$$

If the origin is unique, then the result is valid in the nonlocal sense.

Proof. Starting with (5.11) and (5.14), apply Proposition 3.1 to obtain that the zero solution of the system (5.4) is exponentially stable if condition (5.16) is met. □

A physical interpretation of the previous stability result is as follows: the PDE model (5.2) is made by two transport–reaction subsystems: each one with a linear transport operator ($\mathcal{A}_j$, $j = 1, 2$) and a mass (or heat) sink (or source) nonlinear term (ρ_1 or ρ_2) that interconnects both subsystems and have: (i) a positive-feedback destabilizing effect for the temperature dynamics, and (ii) a negative feedback stabilizing mechanism for the concentration dynamics. From a control perspective, the control aim is to enhance the heat transport stabilizing mechanism: (i) directly on the temperature dynamics (5.2a), and (ii) indirectly – trough the temperature profile – on the concentration dynamics (5.2b). In other words, the source of open-loop instability resides in the impossibility of dominating, through heat transport-exchange stabilization, the destabilizing contribution due to heat generation by reaction.

Following the previous discussion, the control task is to choose the sensor-actuator structure and adjust the heat exchange rate so that the positive-feedback due to heat generation by reaction is dominated with an admissible compromise between regulation speed, robustness and control effort.

5.2.1.4 *Stability analysis of the case example*

To assess if $\nu_1, \nu_2 > 0$, assumption of required in Proposition 5.1, the maximum eigenvalues of (5.5), for the parameters of the case study (see Table 2.1 in Section 2.5) the following values are obtained

$$|\lambda_1{}^*| \approx 1.94, \quad |\lambda_2{}^*| \approx 2.94.$$

The computation of c and the Lipschitz constants in (5.16) cannot be performed analytically, following a similar approach as the one used in Section 4.2.3, the following values for the lumped and weighted approximations of the reaction rate functions ρ_1 and ρ_2 were found

$$c \approx 0.45, \quad L_{x_2}^{\rho_2} \approx 2.54, \quad L_{x_2}^{\rho_2} \approx 8.12, \quad L_{x_1}^{\varrho_{12}} \approx 5.46. \tag{5.18}$$

Accordingly, the concentration dynamics are stable since

$$\nu_1 = |\lambda_1{}^*| + c \approx 1.94 + 0.45 \approx 2.39 > 0, \tag{5.19}$$

for the temperature dynamics the condition $\nu_2 > 0$ is not fulfilled

$$\nu_2 = |\lambda_1{}^*| - L_{x_2}^{\rho_2} \approx 2.94 - 8.12 \not> 0, \tag{5.20}$$

which does not imply the instability of the origin, because $\nu_2 > 0$ in (5.13) is only a condition of sufficiency, the instability can be corroborated by evaluating the eigenvalues of linear operator of the distributed linearized model obtained from (5.4).

5.3 STATE FEEDBACK CONTROL

As first step for the CES design, in this section a state feedback controller is build. Following a constructive approach, a controller with two components is designed: the first component, with two terms, is a feedback linearaizing control that deals with the stabilization task, the second components is an inventory-like one, obtained through feedback passivity, for performance enhancement.

The output measurements of the tubular reactor model (5.2) are given in terms of the output operator $\mathcal{C}_y$ which use has Dirac delta distributions as characteristic functions (see (2.5a)) of the point temperature measurements $\boldsymbol{y}$. Nevertheless, it is well-known that for technical purposes is useful to use an approximation of the delta functions so that the related output operator is bounded in an induced norm [38]. Accordingly, introduce the synthetic averaged pointlike output

$$\boldsymbol{y} = \boldsymbol{\mathcal{C}}_y x_2 := \begin{bmatrix} \left\langle \gamma_1, w_h^{-1} x_2 \right\rangle \\ \vdots \\ \left\langle \gamma_q, w_h^{-1} x_2 \right\rangle \end{bmatrix}, \quad \gamma_i(s) = \begin{cases} \frac{1}{2\epsilon} & \text{if } s \in [\varsigma_i - \epsilon, \varsigma_i + \epsilon] \\ 0 & \text{else,} \end{cases} \tag{5.21}$$

where $\gamma_i(s)$, $i = 1, \ldots, q$, is the i-th characteristic function, ς_i are the sensor locations of the sensor set $\boldsymbol{\varsigma}$ and 2ϵ is the length of the spatial domain in which the temperature is averaged.

The proposed state feedback controller is decentralized, this is, each jacket temperature depends only on the measurement of the corresponding section. The control has the form

$$\boldsymbol{u} = \boldsymbol{\mu}_l(x_1, x_2) + \boldsymbol{\mu}_p(x_1, x_2). \tag{5.22}$$

with output linearizing component $\boldsymbol{\mu}_l$, driven by temperature point-like measurements, to ensure closed-loop robust stability through favorable modification of the interplay between stabilizing transport and destabilizing reaction mechanisms, and component $\boldsymbol{\mu}_p$, driven by the temperature profile deviation on each jacket section, to improve transient versus control effort behavior by compensating in inventory control-like manner [119] the heat excess in the corresponding jacket section.

5.3.1 *State feedback stabilizing controller*

In the following developments, the state feedback stabilizing control component $\boldsymbol{\mu}_l$ of (5.22) is built. For this purpose, the following lemma ensures the existence of a well defined characteristic index equal to one for each sensor-actuator pair. This result is a consequence of the heat exchange wall diathermicity ($v > 0$). The notion of characteristic index is the extension of the concept of relative degree for SISO and MIMO finite dimensional systems [36].

Lemma 5.1. *The reactor model (5.2) has characteristic index equal to one with respect to the input–output pairs $(\boldsymbol{u}, \boldsymbol{y})$, because the heat exchange number $v > 0$ is positive.*

Proof. Take the time derivative of the synthetic output (5.21) to get

$$\begin{aligned}\dot{\boldsymbol{y}} &= \boldsymbol{\mathcal{C}}_y \dot{x}_2 \\ &= \boldsymbol{\mathcal{C}}_y \mathcal{A}_2 x_2 + \boldsymbol{\mathcal{G}}_y \rho_2(x_1, x_2) + \boldsymbol{\mathcal{C}}_y \boldsymbol{\mathcal{B}}_u \boldsymbol{u}.\end{aligned}$$

Accordingly, the characteristic index of the each entry pair of the input–output pair $(\boldsymbol{u}, \boldsymbol{y})$ is one if the term $\boldsymbol{\mathcal{C}}_y \boldsymbol{\mathcal{B}}_u \boldsymbol{u}$ is well-defined. Considering the specific structure of the input $\boldsymbol{\mathcal{B}}_u$ and the synthetic output $\boldsymbol{\mathcal{C}}_y$ operators it follows that

$$\begin{aligned}\boldsymbol{\mathcal{G}}_y, \boldsymbol{\mathcal{B}}_u \boldsymbol{u} &= \begin{bmatrix} \left\langle \gamma_1, w_h^{-1} \mathcal{B}_u \boldsymbol{u} \right\rangle, \\ \vdots \\ \left\langle \gamma_q, w_h^{-1} \mathcal{B}_u \boldsymbol{u} \right\rangle, \end{bmatrix} = \begin{bmatrix} \left\langle \gamma_1, w_h^{-1} v w_h \boldsymbol{\beta} \boldsymbol{u} \right\rangle, \\ \vdots \\ \left\langle \gamma_q, w_h^{-1} v w_h \boldsymbol{\beta} \boldsymbol{u} \right\rangle, \end{bmatrix} = v \begin{bmatrix} \left\langle \gamma_1, \sum_{i=1}^q \beta_i u_i \right\rangle, \\ \vdots \\ \left\langle \gamma_q, \sum_{i=1}^q \beta_i u_i \right\rangle, \end{bmatrix}, \\ &= \frac{v}{2\epsilon} \begin{bmatrix} \int_0^1 \gamma_1 \sum_{i=1}^q \beta_i u_i \mathrm{d}s, \\ \vdots \\ \int_0^1 \gamma_q \sum_{i=1}^q u_1 \mathrm{d}s, \end{bmatrix} = \frac{v}{2\epsilon} \begin{bmatrix} \int_{\zeta_1 - \epsilon}^{\zeta_1 + \epsilon} u_1 \mathrm{d}s, \\ \vdots \\ \int_{\zeta_q - \epsilon}^{\zeta_q + \epsilon} u_q \mathrm{d}s, \end{bmatrix},\end{aligned}$$

the last expression in the previous developments is well-defined given that $v, \epsilon > 0$ and for all $i = 1, \ldots, q$, γ_i is contained in the support of β_i, i.e., $[\varsigma_i - \epsilon, \varsigma_i + \epsilon] \subset \mathscr{R}_i$. $\square$

Accordingly, for the considered tubular reactor class and the particular sensor-actuator configuration, the fact that the characteristic index one conditions is always met manifests a connection with joint process–control design [116]: in the collocated sensor and actuator configuration, the characteristic index is always well-defined, while in the case of noncollocated configurations the characteristic index may be infinite [36]. In the present particular noncollocated sensor–actuator configuration the characteristic index is well defined (as stated in Lemma 5.1).

Consider the decentralized linearizing MIMO state feedback controller

$$\boldsymbol{u}_l = \boldsymbol{\mu}_l(\boldsymbol{y}, x_1, x_2), \tag{5.23a}$$

where

$$\boldsymbol{\mu}_l(\boldsymbol{y}, x_1, x_2) = -\boldsymbol{B}_m{}^{-1}\left(\boldsymbol{K}_y \boldsymbol{y} + \boldsymbol{\mathcal{C}}_y \rho_2(x_1, x_2)\right), \tag{5.23b}$$

$$\boldsymbol{B}_m{}^{-1} = (\boldsymbol{\mathcal{C}}_y \boldsymbol{\mathcal{B}}_{u,2})^{-1} = \frac{1}{v}\boldsymbol{I}_{q\times q}, \quad \boldsymbol{K}_y = \boldsymbol{K}_y^T > 0. \tag{5.23c}$$

The controller gain matrix $\boldsymbol{K}_y$ is diagonal, one entry for each jacket temperature controller, with gains $k_{y,i}$, $i = 1, \ldots, q$. The two components of the above controller, that ensure closed-loop stability with output regulation, are: (i) a nonlinear feedback, driven by pointlike information of the reaction rate function, to compensate its destabilizing effect on the temperature dynamics by performing partial linarization, and (ii) a linear proportional feedback, driven by the pointlike temperature output $\boldsymbol{y}$, to improve stabilization by heat transport phenomena.

Note that, on one hand, controller (5.23) is the distributed version of the early lumping controller (4.54): an output linearizing state feedback law that cancels out the destabilizing effect of the projection of the nonlinear term ρ_2 on the output dynamics while kept the stabilizing effect of the projected transport operator on the output dynamics. On the other hand, the distributed version of the controller (4.52) is

$$\boldsymbol{u}_l = \boldsymbol{\mu}_{l,2}(\boldsymbol{y}, x_1, x_2), \tag{5.24a}$$

where

$$\boldsymbol{\mu}_l(\boldsymbol{y}, x_1, x_2) = -\boldsymbol{B}_m{}^{-1}\left(\boldsymbol{K}_c \boldsymbol{y} + \boldsymbol{\mathcal{C}}_y \mathcal{A}_2 x_2 + \boldsymbol{\mathcal{C}}_y \rho(x_1, x_2)\right), \tag{5.24b}$$

$$\boldsymbol{B}_m{}^{-1} = (\boldsymbol{\mathcal{C}}_y \boldsymbol{\mathcal{B}}_u)^{-1} = \frac{1}{v}\boldsymbol{I}_{q\times q}, \quad \boldsymbol{K}_c = \boldsymbol{K}_c^T > 0, \tag{5.24c}$$

where $\boldsymbol{K}_y$ is a diagonal matrix with diagonal elements $k_{y,i}$, $i = 1, \ldots, q$. The properties of this control law, within a late lumping perspective will be explored in Chapter 6.

The application of the MIMO state feedback control (5.23) to the reactor model (5.2) yields the closed-loop dynamics

$$\dot{x}_1 = \mathcal{A}_1 x_1 - \varrho_1(x_1) - \varrho_{12}(x_1, x_2), \qquad x_1(0) = x_{10}, \tag{5.25a}$$
$$\dot{x}_2 = \mathcal{A}_2^c x_2 + \Delta\rho_2(x_1, x_2), \qquad x_2(0) = x_{20}. \tag{5.25b}$$

where $\mathcal{A}_2^c$ (with domain) is the heat transport closed-loop operator defined as

$$\mathcal{A}_2^c x_2 = \mathcal{A}_2 x_2 - \boldsymbol{\mathcal{B}}_u \boldsymbol{B}_m{}^{-1} \boldsymbol{K}_y \boldsymbol{\mathcal{C}}_y x_2, \quad \mathcal{D}(\mathcal{A}_2^c) = \mathcal{D}(\mathcal{A}_2). \tag{5.25c}$$

The function $\Delta\rho_2$ is the closed-loop reaction rate, that depends on the considered configuration of sensor and actuators (number of actuator-sensor pairs and the sensor locations which manifests through the input and output operators) and is Lipschitz bounded with respect to its arguments:

$$\Delta\rho(x_1, x_2) = \rho_2(x_1, x_2) - \boldsymbol{\mathcal{B}}_y \boldsymbol{B}_m{}^{-1} \boldsymbol{\mathcal{C}}_y \rho_2(x_1, x_2), \tag{5.25d}$$
$$\|\Delta\rho(x_1, x_2)\| \leq L_{x_1}^{\Delta\rho}(\varsigma)\|x_1\| + L_{x_2}^{\Delta\rho}(\varsigma)\|x_2\|. \tag{5.25e}$$

Each component of the decentralized controller (5.23) is driven by pointlike information at each sensor location ς_i, and acts on the i-th jacket domain $\mathscr{R}_i$ (2.4). Thus, each controller have the following effects on the temperature dynamics at each subdomain $\mathscr{R}_i$: (i) the stabilizing capability of the heat transport operator is enhanced by the linear injections $-\boldsymbol{\mathcal{B}}_y \boldsymbol{B}_m{}^{-1} \boldsymbol{K}_y \boldsymbol{\mathcal{C}}_y$ that favorably modifies the spectra of the heat transport operator $\mathcal{A}_2$, and (ii) the destabilizing effect of heat generation by reaction (measured by the sensor dependent Lipschitz constants $L_{x_j}^{\Delta\rho_2}(\varsigma)$, $L_{x_j}^{\Delta\varrho_{12}}(\varsigma)$ (5.25e)) is attenuated by the injection term $-\boldsymbol{\mathcal{B}}_y \boldsymbol{B}_m{}^{-1} \boldsymbol{\mathcal{C}}_y \rho_2$.

The effectiveness of the heat removal exchange mechanism associated with the MIMO state feedback controller (5.23) depends on the choice of the sensor location set ς: (i) the linear injection must maximize its effect on the the spectrum of the open-loop operator, and (ii) the compensation of destabilization by heat generation requires sensor locations at sensitive regions – where the axial slope temperature change is maximum [101].

The fact that the Lur'e structure of the temperature dynamics (5.2a) is preserved in the open to closed-loop passage, motivates the subsequent closed-loop stability analysis: first (in 5.2) conditions for the favorable modification of the spectrum of the closed-loop heat transport operator $\mathcal{A}_2^c$ are identified, and then (in 5.2) conditions for the domination of enhanced heat transport-based stabilization over reaction-based destabilization are presented.

Lemma 5.2. *Set* $\mathfrak{b}_{i,1} = \langle \omega_h \beta_i, \phi_{2,1} \rangle$ *and* $\mathfrak{c}_{i,1} = \left\langle \gamma_i, \omega_h^{-1} \phi_{2,1} \right\rangle$, *where* $\phi_{2,1}$ *is the first eigenfunction of the selfadjoint transport operator* $\mathcal{A}_2$ (5.5c)*. If the sensor location set* ς *and the* *controller gain $\boldsymbol{K}_y$ are selected so that the stabilizability–detectability (5.26a) and diagonal dominance (5.26b) conditions hold true:*

$$\sum_{i=1}^{q} \mathfrak{b}_{i,1}\mathfrak{c}_{i,1} > 0, \tag{5.26a}$$

$$l_y := \frac{\left(\sum_{i=1}^{q} k_{y,i} \left\|\omega_h \beta_i\right\|^2 \sum_{i=1}^{q} k_{y,i} \left\|\omega_h^{-1}\gamma_i\right\|^2\right)^{\frac{1}{2}}}{\left|\lambda_{2,1} - \sum_{i=1}^{q} k_{y,i}\mathfrak{b}_{i,2}\mathfrak{c}_{i,2}\right|} < 1. \tag{5.26b}$$

Then the eigenvalues $\lambda^{\mathfrak{c}}_{2,n}$, $n \in \mathbb{N}$ of the operator $\mathcal{A}^{\mathfrak{c}}_2$ are bounded as

$$\lambda^{\mathfrak{c}}_{2,n} \leq \lambda^{\mathfrak{c}*}_{2} = \lambda_{2,1} - \left(\sum_{i=1}^{q} k_{y,i}\mathfrak{b}_{i,2}\mathfrak{c}_{i,2} - \left(\sum_{i=1}^{q} k_{y,i} \left\|\omega_h \beta_i\right\|^2 \sum_{i=1}^{q} k_{y,i} \left\|\omega_h^{-1}\gamma_i\right\|^2\right)^{\frac{1}{2}}\right). \tag{5.26c}$$

Thus, the closed-loop operator $\mathcal{A}^{\mathfrak{c}}_2$ generates a C_0-semigroup of contractions, with growth bound $-\lambda^{\mathfrak{c}*}_{2}(\boldsymbol{K}_y, \varsigma)$, that satisfies

$$\|S^{\mathfrak{c}}_2(t)\|_{\mathfrak{D}} \leq e^{-\lambda^{\mathfrak{c}*}_{2} t}. \tag{5.26d}$$

The proof of the above Lemma is given in Appendix g. This result, indicates the output injection in (5.23) affects the whole spectrum of the open-loop operator $\mathcal{A}_2$, in contrast with modal control, where if a certain stabilizability-detectability condition is met, an output feedback control that affects only a finite number of slow modes can be constructed [38; 1]. The left shifting of the entire spectrum requires that for all $n, m \in \mathbb{N}$ it holds that $\mathfrak{b}_{i,n}\mathfrak{c}_{i,m} > 0$ for $i = 1, \ldots, q$. This condition is only valid in the collocated case where $\mathfrak{b}_{i,n} = \mathfrak{c}_{i,m}$ for $n, m \in \mathbb{N}$.

Accordingly, Lemma 5.2 gives sufficient conditions to assure the left shifting of the maximum eigenvalue of the closed-loop transport operator $\mathcal{A}^{\mathfrak{c}}_2$ (ensured by (5.26a)). For the remaining spectra, it is assured, by the diagonal dominance condition (5.26b) that restricts the gains $k_{y,i}$, that the eigenvalues, shifted to the left or to the right, remain inside bounded regions. Thus, the ordering (5.5b) of the eigenvalues (5.5) is preserved and enables the estimation of the eigenvalues within prescribed bounds by using modal analysis for infinite dimensional matrices [6] (see Appendix g).

Once the stability of the linear component of the closed-loop heat balance (5.25b) has been established, it remains to assure the the closed-loop stability of the dynamic heat balance (5.25b) and its interconnection with the mass balance. This is done exploiting the Lur'e system property of the heat balance and the bounding condition for the mass balance established in (5.11).

Proposition 5.2. *Stability of the closed-loop system (5.25)*
Consider the closed-loop system (5.25) with the MIMO state feedback control (5.23) with

diagonal gain matrix $\boldsymbol{K}_y$ and sensor location set $\boldsymbol{\varsigma}$ has the origin as unique steady-state. Furthermore, the concentration state satisfy (5.11), and let the conditions of 5.2 be met. If the matrix $\boldsymbol{K}_y$, and the sensor location set $\boldsymbol{\varsigma}$ are chosen so that $\nu_c(k_1, \boldsymbol{\varsigma})$ in (5.26d) and $L_{x_2}^{\Delta\rho}(\boldsymbol{\varsigma})$ in (5.25e) meet the inequality

$$l_c := |\lambda_2^{c*}(\boldsymbol{K}_y, \boldsymbol{\varsigma})| - L_{x_2}^{\Delta\rho}(\boldsymbol{\varsigma}) - \frac{L_{x_1}^{\Delta\rho}(\boldsymbol{\varsigma}) L_{x_2}^{\varrho_{12}}}{\nu_1} > 0 \tag{5.27}$$

with Lipschitz constant $L_{x_2}^{\varrho_{12}}$ (5.8). Then, there exists $M_c \geq 1$, and $-\lambda_c$ so that

$$\|\boldsymbol{x}(t)\|_{\mathcal{X}} \leq M_c \|\boldsymbol{x}_0\|_{\mathcal{X}} \mathrm{e}^{-\lambda_c t}. \tag{5.28}$$

Accordingly, the origin of (5.25) is exponentially stable in a nonlocal sense.

Proof. The formal solution of the closed-loop temperature dynamics (5.25) is

$$x_2(t) = S_2^c(t) x_{20} + \int_0^t S_2^c(t - \mathfrak{t}) \Delta\rho(x_1, x_2) \mathrm{d}\mathfrak{t}.$$

From the application of norms on both sides, substitution of (5.26d), use of the triangle inequality, enforcement of (5.25e), and employment of inequality (5.11) it follows that

$$\begin{aligned}
\|x_1\| &\leq \|x_{10}\| \, \mathrm{e}^{-(\nu_1+\gamma_1)t} + L_{x_2}^{\varrho_{12}} \int_0^t \mathrm{e}^{-(\nu_1+\gamma_1)(t-\mathfrak{t})} \, \|x_2\| \, \mathrm{d}\mathfrak{t}, \\
\|x_2\| &\leq a_2 \|x_{20}\| \mathrm{e}^{-\nu_c t} + a_2 \int_0^t \mathrm{e}^{-\nu_c(t-\mathfrak{t})} (L_{x_1}^{\Delta\rho_2} \|x_1\| + L_{x_2}^{\Delta\rho} \|x_2\|) \mathrm{d}\mathfrak{t}.
\end{aligned}$$

Apply Proposition 3.1 to obtain that if condition (5.27) is met, then the estimate

$$\|\boldsymbol{x}\|_{\mathcal{X}} \leq a_c \, \|\boldsymbol{x}_0\|_{\mathcal{X}} \, \mathrm{e}^{-\lambda_c t}, \tag{5.29}$$

where $a_c = a_2 \geq 1$ and

$$-\lambda_c = \sup_{\lambda_j \in \sigma(\boldsymbol{A}_c)} \lambda_j, \quad \boldsymbol{A}_c = \begin{bmatrix} -\nu_1 & L_{x_2}^{\varrho_{12}} \\ L_{x_1}^{\Delta\rho} & -\nu_{2,c} \end{bmatrix}, \quad \nu_{2,c} = |\lambda_2^{c*}(\boldsymbol{K}_y, \boldsymbol{\varsigma})| - L_{x_2}^{\Delta\rho}(\boldsymbol{\varsigma}). \tag{5.30}$$

holds true. □

The stability measure l_c is composed by: (i) $\nu_c(\boldsymbol{k}_{y,i}, \boldsymbol{\varsigma})$ which reflects enhanced stability by the artificial heat dissipation induced by the control law (5.23), and increases linearly with the entries of the gain matrix $\boldsymbol{K}_y$ according to (5.26c)–(5.26d), (ii) $L_{x_2}^{\Delta\rho}$ which reflects selfdestabilization of the dynamic heat balance due to the positive feedback of heat generation by reaction, and (iii) $\frac{L_{x_1}^{\Delta\rho}(\boldsymbol{\varsigma}) L_{x_2}^{\varrho_{12}}}{\nu_1}$ which measures the destabilizing potential of the interconnected dynamic mass and heat balances

5.3.2 *Inventory control component*

Following inventory control ideas [119], the state feedback control component $\boldsymbol{\mu}_p$ (5.22) is constructed to improve the behavior of the closed-loop system with the decentralized MIMO state feedback control (5.23) driven by pointlike measurements.

For this aim, set the inventory control component

$$\boldsymbol{u}_p = \boldsymbol{B}_m{}^{-1}\boldsymbol{\mu}_p(x_2), \quad \boldsymbol{B}_m{}^{-1} = \frac{1}{v}\boldsymbol{I}_{q\times q}, \tag{5.31}$$

Thus, the closed-loop dynamics with the controller (5.22) with (5.23) and (5.31) are

$$\dot{x}_1 = \mathcal{A}_1 x_1 - \varrho_1(x_1) - \varrho_{12}(x_1, x_2), \qquad x_1(0) = x_{10}, \tag{5.32a}$$

$$\dot{x}_2 = \mathcal{A}_2^c x_2 + \Delta\rho_2(x_1, x_2) + \boldsymbol{\mathcal{B}}_u \boldsymbol{u}_p, \qquad x_2(0) = x_{20}. \tag{5.32b}$$

Consider the control (5.33) with the control map

$$\boldsymbol{\mu}_p(x_2) = -\boldsymbol{K}_{\mathfrak{z}}\boldsymbol{\mathcal{C}}_{\mathfrak{z}}x_2, \quad \boldsymbol{\mathcal{C}}_{\mathfrak{z}} = \boldsymbol{\mathcal{B}}_u^*, \quad \boldsymbol{K}_{\mathfrak{z}} = \boldsymbol{K}_{\mathfrak{z}}^T > 0, \tag{5.33a}$$

where $\boldsymbol{K}_{\mathfrak{z}}$ is a diagonal gain matrix and $\boldsymbol{\mathcal{B}}_2^*$, the adjoint of the input operator $\boldsymbol{\mathcal{B}}_2$, is

$$\boldsymbol{\mathcal{B}}_2^* x_2 = v \begin{bmatrix} \langle \omega_h \beta_1, x_2 \rangle \\ \vdots \\ \langle \omega_h \beta_q, x_2 \rangle \end{bmatrix}. \tag{5.33b}$$

Note that the above control law considers averaged section-wise temperatures and works as an inventory component that compensates the excess or shortage of sensible heat on the corresponding section of the heat balance.

It can be shown, with a standard passivity argument, that the closed-loop system (5.32) is passive with a quadratic storage function and the input-output pair conformed by $\boldsymbol{u}_p$ and a new synthetic output $\mathfrak{z}$ given as

$$\mathfrak{z} = \boldsymbol{\mathcal{C}}_{\mathfrak{z}} x_2. \tag{5.34}$$

This result is established next.

Proposition 5.3. *Let the conditions of Proposition 5.2 be met. Then, the closed-loop system (5.32) with the two-component (point (5.23) plus section-wise (5.33) driven) control is: (i) passive with the storage function*

$$V(\boldsymbol{x}) = \frac{1}{2}\|\boldsymbol{x}\|_{\mathcal{X}}^2, \tag{5.35}$$

with respect to the input–output pair $(\boldsymbol{u}_p, \mathfrak{z})$, and (ii) there are constants $a_p \geq 1$, and $\lambda_p > 0$ so that for all $\boldsymbol{x}_0 \in \mathcal{X}$

$$\|\boldsymbol{x}\|_{\mathcal{X}} \leq a_p \|\boldsymbol{x}_0\|_{\mathcal{X}} \, \mathrm{e}^{-\lambda_p t}. \tag{5.36}$$

Proof. Note that the storage function $V(\boldsymbol{x})$ is equivalent to

$$\begin{aligned} V(\boldsymbol{x}) &= \frac{1}{2}\|x_1\|^2 + \frac{1}{2}\|x_2\|^2, \\ &= \frac{1}{2}\langle x_1, x_1\rangle + \frac{1}{2}\langle x_2, x_2\rangle. \end{aligned}$$

The time derivation followed by substitution of the closed-loop dynamics (5.32) yields

$$\begin{aligned} \dot{V}(\boldsymbol{x}) \leq \frac{1}{2}(\langle x_1, \mathcal{A}_1 x_1\rangle + \langle \mathcal{A}_1 x_1, x_1\rangle + \langle x_2, \mathcal{A}_2^c x_2\rangle + \langle \mathcal{A}_2^c x_2, x_2\rangle) - \\ - \langle x_1, \varrho(x_1)\rangle + \langle x_1, \varrho_{12}(x_1, x_2)\rangle + \langle x_2, \Delta\rho_2(x_1, x_2)\rangle + \langle x_2, \boldsymbol{\mathcal{B}}_u \boldsymbol{u}_p\rangle, \end{aligned}$$

using (5.10) for $\mathcal{A}_1$ and $\mathcal{A}_2^c$ it follows

$$\begin{aligned} \dot{V}(\boldsymbol{x}) \leq \lambda_1^* \|x_1\|^2 - \lambda_2^{c*}\|x_2\|^2 - \langle x_1, \varrho(x_1)\rangle + \langle x_1, \varrho_{12}(x_1, x_2)\rangle + \langle x_2, \Delta\rho_2(x_1, x_2)\rangle + \\ + \langle x_2, \boldsymbol{\mathcal{B}}_u \boldsymbol{u}_p\rangle, \end{aligned}$$

Proceeding as in Section 5.2.1.1 and using (5.25e) yields to

$$\dot{V}(\boldsymbol{x}) \leq -\nu_1 \|x_1\|^2 - \nu_{2,c}\|x_2\|^2 + (L_{x_1}^{\rho_2} + L_{x_2}^{\varrho})\|x_1\|\,\|x_2\| + \langle x_2, \boldsymbol{\mathcal{B}}_u \boldsymbol{u}_p\rangle,$$

or equivalently

$$\dot{V}(\boldsymbol{x}) \leq -\nu_p \|\boldsymbol{x}\|_{\mathcal{X}}^2 + \langle x_2, \boldsymbol{\mathcal{B}}_u \boldsymbol{u}_p\rangle, \quad \nu_p = \max\{\nu_1, \nu_{2,c}|\} - (L_{x_1}^{\rho_2} + L_{x_2}^{\varrho}) > 0,$$

which by construction is positive, $(\nu_1, \nu_{2,c})$ are defined in (5.11) and (5.30), respectively.

Rewriting the last expression for the time derivative of the storage function with the control map (5.33) yields to

$$\begin{aligned} \dot{V}(\boldsymbol{x}) &\leq -\nu_p \|\boldsymbol{x}\|_{\mathcal{X}}^2 + \left\langle x_2, \boldsymbol{\mathcal{B}}_u \boldsymbol{B}_m{}^{-1}\boldsymbol{\mu}_p(x_2)\right\rangle, \\ &\leq -\nu_p \|\boldsymbol{x}\|_{\mathcal{X}}^2 + \boldsymbol{B}_m{}^{-1}\left\langle x_2, \boldsymbol{\mathcal{B}}_u \boldsymbol{\mu}_p(x_2)\right\rangle. \end{aligned}$$

Substituting $\boldsymbol{B}_m{}^{-1}$ and employing the adjoint representation of $\boldsymbol{\mathcal{B}}_u$ gives

$$\dot{V}(\boldsymbol{x}) \leq -\nu_p \|\boldsymbol{x}\|_{\mathcal{X}}^2 + \frac{1}{v}\left\langle \boldsymbol{\mu}_p^T(x_2), \boldsymbol{\mathcal{B}}_u^* x_2\right\rangle.$$

The substitution of the synthetic output $\mathfrak{z} = \boldsymbol{\mathcal{B}}_u{}^* x_2$ yields

$$\dot{V}(\boldsymbol{x}) \leq -\nu_p \|\boldsymbol{x}\|_{\mathcal{X}}^2 + \frac{1}{v}\left\langle \boldsymbol{\mu}_p(x_2)^T, \mathfrak{z}\right\rangle, \tag{5.37}$$

ensuring the strict passivity of system (5.32) for the input–output pair $(\boldsymbol{u}_p, \mathfrak{z})$, with dissipation rate ν_p, supply rate $\frac{1}{v}\left\langle \boldsymbol{\mu}_p^T, \mathfrak{z}\right\rangle$, and storage function (5.35) [38].

Considering $\boldsymbol{\mu}_p = -\boldsymbol{K}_{\mathfrak{z}}\mathfrak{z}$ the exponential stability follows from the dissipation inequality

$$\begin{aligned}
\dot{V}(\boldsymbol{x}) &\leq -\nu_p \|\boldsymbol{x}\|^2_{\mathcal{X}} - \frac{1}{v}\left\langle \mathfrak{z}^T \boldsymbol{K}_{\mathfrak{z}}, \mathfrak{z} \right\rangle, \\
&\leq -\nu_p \|\boldsymbol{x}\|^2_{\mathcal{X}} - \frac{\boldsymbol{K}_{\mathfrak{z}}}{v}\left\|\boldsymbol{\mathcal{B}}^*_{u,2} x_2\right\|^2, \\
&\leq -\nu_p \|\boldsymbol{x}\|^2_{\mathcal{X}} - \frac{\boldsymbol{K}_{\mathfrak{z}}}{v}\left\|\boldsymbol{\mathcal{B}}^*_{u,2}\right\|^2 \|x_2\|^2, \\
&\leq -\nu_p \|\boldsymbol{x}\|^2_{\mathcal{X}} - \frac{\boldsymbol{K}_{\mathfrak{z}}}{v}\left\|\boldsymbol{\mathcal{B}}^*_{u,2}\right\|^2 \|\boldsymbol{x}\|^2_{\mathcal{X}}, \\
&\leq -\nu_p \|\boldsymbol{x}\|^2_{\mathcal{X}},
\end{aligned}$$

and application of the comparison lemma [76]. □

According to the proof of Proposition 5.3, the inventory control component (5.33) improves the exponential convergence rate with respect to the control (5.23).

The combination of (5.33) and (5.23) yields the proposed MIMO state feedback Linear-Inventory-like control (LIOF) (5.22) in the form

$$\boldsymbol{u} = \boldsymbol{\mu}_{lp}(x_1, x_2), \tag{5.38a}$$

where

$$\boldsymbol{\mu}_{lp}(x_1, x_2) = -\boldsymbol{B}_m{}^{-1}\left(\boldsymbol{K}_y \boldsymbol{\mathcal{C}}_y x_2 + \boldsymbol{\mathcal{C}}_y \rho(x_1, x_2) \boldsymbol{K}_{\mathfrak{z}} \boldsymbol{\mathcal{C}}_{\mathfrak{z}} x_2\right), \tag{5.38b}$$

$$\boldsymbol{B}_m{}^{-1} = \frac{1}{v}\boldsymbol{I}_{q\times q}, \quad \boldsymbol{K}_y = \boldsymbol{K}_y^T > 0, \quad \boldsymbol{K}_{\mathfrak{z}} = \boldsymbol{K}_{\mathfrak{z}}^T > 0. \tag{5.38c}$$

Proposition 5.2 and Proposition 5.3 ensure the closed-loop stability with the proposed controller (5.23) assuming that the sensor locations set ς has been chosen adequately. Nevertheless, these existence-type results does not give guidelines for the selection of the number of sensors and their locations and the corresponding number of jacket sections. Accordingly, in what follows, along constructive ideas, a procedure to determine the sensor location set ς and the gain matrices $\boldsymbol{K}_y$, $\boldsymbol{K}_{\mathfrak{z}}$, is drawn.

5.3.3 *Sensor location and gain selection criteria*

Proceeding in a similar manner as in Section 4.3.3, two conditions must be assessed to construct the sensor location criterion associated to controller (5.38), a static one and a dynamic one: (i) in the single sensor case, the sensor location must ensures the uniqueness of the closed-loop origin solution, and (ii) with a single or multiple sensors the stability measure l_c is maximized. These conditions are characterized next and then a simple procedure for the determination of the sensor location set is proposed.

5.3.3.1 *Closed-loop steady-state multiplicity*

Consider the closed-loop statics associated to (5.32) with controller (5.38) for the SISO case $q = 1$:

$$0 = \mathcal{A}_1 x_1 - \rho(x_1, x_2), \tag{5.39a}$$

$$0 = \mathcal{A}_2 x_2 + \Delta\rho(x_1, x_2), \tag{5.39b}$$

$$y = 0, \quad \mathfrak{y} = 0, \quad z_c = 0. \tag{5.39c}$$

It is needed to ensure that no undesired steady-states are present in the closed-loop statics: the zero solution of (5.39) must be unique.

The statics (5.39) are a constrained boundary value problem that must satisfy the additional condition $y = 0$. The solution may be drawn by splitting the heat balance in two pieces by using the null output restriction as an additional boundary condition: the right one for the first piece and the left one for the second piece.

According to the previous discussion, since the unique degree of freedom is the sensor location $\varsigma_1 \in (0,1)$, it must me swept in its domain to find out the location that ensure the uniqueness of the zero solution. This can be done with a bifurcation analysis constructed with the related late lumping model obtained with the application of the efficient modeling approach (see Section 3.2) to the static system (5.39).

The above procedure, that parallels the zero dynamics multiplicity analysis performed in the early lumping approach (see Section 4.3.3.1), can be elaborated within an efficient late lumping procedure by using an auxiliary bifurcation analysis and with the use of a continuation software package such as MATCONT [43]:

Step 0: Perform and a late lumping procedure by employing FD or a finite element approximation and use N_{pde} (or instead use the algorithm presented in Section 3.2 to obtain N_e) to obtain a large (or efficiently) lumped version of the static problem (5.39) and rewrite it in partitioned coordinates (4.4).

Step 1: Set $k = 1$ and $\varsigma_{m_1} = s_k$.

Step 2: Use the actual partitioned closed-loop dynamics to construct the Input-Output Bifurcation Map (IOBM) (4.11) for $q = 1$.

Step 3: Collect the steady-states related to the nominal case $\bar{u} = 0$.

Step 4: Plot the first steady-state value $\bar{x}_{2,1} \in X_{2,1} \subset X$ of the temperature sequence $\bar{x}_2$ versus the sensor location ς_1 in the plane $\mathcal{S} \times X_{2,1}$.

Step 5: Set $k = k + 1$ and proceed again from Step 2, if $k = \frac{N}{\Delta s}$ the procedure stops.

From the previous algorithm, the suitable sensor location region $\mathcal{S}_m$, a subset of the spatial domain $\mathcal{S} = (0,1)$, in which the the closed-loop zero solution uniqueness can be identified. Accordingly, this region is characterized as

$$\mathcal{S}_m = \{\varsigma_1 \in \mathcal{S} \mid (x_1, x_2) = (0,0) \text{ Is the unique steady-state}\}. \tag{5.40}$$

As long as this sensor location is fixes, in the MIMO cases the uniqueness of the zero solution for the corresponding closed-loop statics will not change. This, the restriction $\varsigma_1 \in \mathcal{S}_m$ can be inherited to the MIMO scenarios ($q = 2, 3$). The exact location of ς_1 together with the locations of the remaining sensors must be established so that the dynamic condition $l_c > 0$ given in (5.27) is maximized.

5.3.3.2 *Sensor locations determination and gain selection*

Having characterized the region in which the single sensor case ensure the uniqueness of the closed-loop zero solution, next the sensor locations can be identified as the locations that maximize the stability measure l_c given in (5.27). An elegant option would be to maximize l_c by setting a mixed-integer optimization problem. Instead, in what follows, a constructive procedure to choose the control gain-sensor set pair $(\boldsymbol{K}_y, \boldsymbol{\varsigma})$, and as a byproduct the number of jacket sections, is introduced.

The stability measure $l_c > 0$ must be characterized for each possible sensor location set $\boldsymbol{\varsigma}$ restricted with $\varsigma_1 \in \mathcal{S}_m$ of the single sensor case, in which the closed-loop origin of (5.39) is unique, so that the maximum value for l_c (5.27) is obtained. Accordingly, define the hypersurface $\Gamma_{c,0}(\boldsymbol{K}_y = \boldsymbol{0}_{q\times q}, \boldsymbol{\varsigma})$ as the geometric loci spanned by l_c with null gain and all possible combinations of sensor locations $\boldsymbol{\varsigma}$ with the restriction (5.40) of the SISO case as well as (5.26a) in Lemma 5.2:

$$\Gamma_{c,0}(\boldsymbol{\varsigma}) = l_{c,0}(\boldsymbol{K}_y = \boldsymbol{0}_{q\times q}, \boldsymbol{\varsigma}), \quad s.t. \quad \left\{ \varsigma_{siso} \in \mathcal{S}_m, \quad l_y = \sum_{i=1}^{q} \mathfrak{b}_{i,1}\mathfrak{c}_{1,i} \neq 0 \right\}, \tag{5.41a}$$

and denote as $\Gamma^+_{c,0}(\boldsymbol{\varsigma})$ the maximum value of the hypersurface $\Lambda_{c,0}(\boldsymbol{\varsigma})$, i. e.,

$$\Gamma^+_{c,0}(\boldsymbol{\varsigma}) = \max \Gamma^+_{c,0}(\boldsymbol{\varsigma}). \tag{5.41b}$$

Thus, the sensor location set is defined as

$$\boldsymbol{\varsigma} = \left\{ \varsigma_i \in \mathscr{R}_i \subset \mathcal{S} \,|\, \Gamma_{c,0}(\boldsymbol{\varsigma}) = \Gamma^+_c(\boldsymbol{\varsigma}) \right\}. \tag{5.41c}$$

Finally, define $\Gamma_c(\boldsymbol{\varsigma})$ as

$$\Gamma_c(\boldsymbol{K}_y, \boldsymbol{\varsigma}) = \Gamma_{c,0}(\boldsymbol{K}_y, \boldsymbol{\varsigma}), \quad s.t. \quad l_y < 1 \tag{5.42}$$

and select the initial gain matrix $\boldsymbol{K}_y$, before fine tuning, that ensure the last condition in the above expression, the gain-restricting condition $l_y < 1$ is given in (5.26c)

Within a geometric perspective, for the SISO case, $q = 1$, $\Lambda_c(\varsigma)$ is a curve, while for $q = 2, 3$ $\Lambda_c(\varsigma)$ is a surface and a hypersurface, respectively. Nevertheless, since in the MIMO cases the sensor $\varsigma_1 \in \mathcal{S}_m$ must be fixed, the geometric loci can be replaced for a curve, for $q = 2$, and a surface, for $q = 3$. The application of the proposed sensor location criterion the case study of Section 2.5 is performed next.

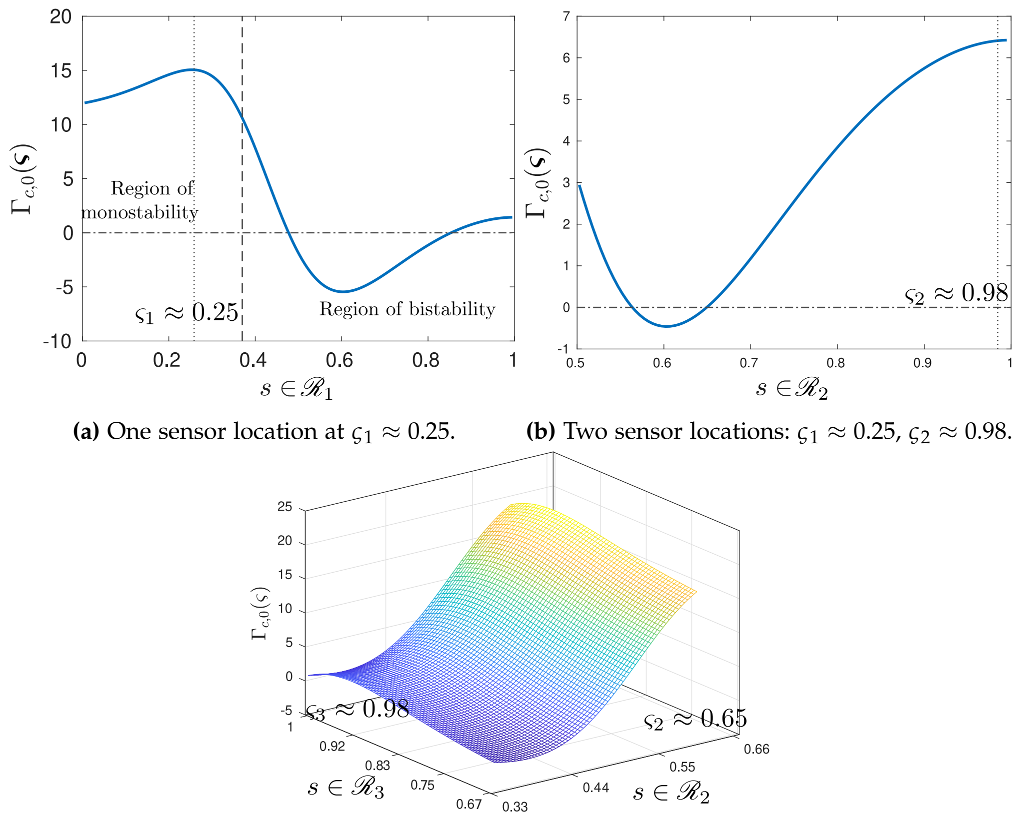

(a) One sensor location at $\varsigma_1 \approx 0.25$.

(b) Two sensor locations: $\varsigma_1 \approx 0.25$, $\varsigma_2 \approx 0.98$.

(c) Three sensor locations: $\varsigma_1 \approx 0.25$, $\varsigma_2 \approx 0.65$, $\varsigma_3 \approx 0.98$.

Figure 5.1: Sensor location criterion: evaluation of the surface $\Gamma_{c,0}(\varsigma)$ (5.41)

5.3.3.3 *Application to the case example*

The execution of the procedure in Section 5.3.3.2, produces Figure 5.1 which shows the surfaces $\Gamma_{c,0}(\varsigma)$ given in (5.41) for $q = 1, 2, 3$. Thus, the sensors, for each case, must be placed according to: (i) for the single-sensor case, the sensor location region that ensures robust stability is $(0, 0.5)$, and the sensor is placed at $\varsigma_1 \approx 0.25$, where $\Gamma_{c,0}(\varsigma)$ (5.41) is maximum, (ii) for the two-sensor case, with $\varsigma_1 \approx 0.25$ fixed, the best region for the second sensor is are $\varsigma_2 \in [0.9, 1]$, thus $\varsigma_2 \approx 0.98$ is chosen, finally (iii) in the three-sensor case, with $\varsigma_1 \approx 0.25$ fixed, the best regions are $\{\varsigma_2 \in [0.6, 0.67], \varsigma_3 \in [0.9, 1]\}$, consequently, the positions $\varsigma_2 \approx 0.65$ and $\varsigma_3 \approx 0.98$ are selected.

It must be pointed out that the preceding sensor location, in the single-sensor case $q = 1$, coincides with the industrial criteria [25; 100; 108]: at the convexity–concavity inflection point before the hotspot of the steady-state temperature profile (where heat transport diffusion vanishes and stabilization by convective heat transport is not sufficient to compensate the heat generation by reaction. Similar sensor location results have been drawn with different theoretical tools (see [100; 108]). The two-sensor (or three-sensor) location result of the proposed criterion is also in agreement with industrial configurations: one sensor before and one after the hotspot.

5.4 CONTROL-ESTIMATION SYSTEM

In this section, a CES is constructed by combining the state feedback controller (5.23) and a pointwise innovation based observer introduced in [111]. The closed-loop stability is assured and tuning and implementation guidelines are given

5.4.1 *Point-wise observer*

The pointwise observer constructed in [111] is considered because it has a simple structure since the unique parameter to be tunes is the sensor location set for which there is an *a priori* selection given in Section 5.3.3. The observer is briefly described and the main idea behind its functioning and convergence conditions are given.

Consider the following observer

$$\dot{\hat{x}}_1 = \mathcal{A}_1 \hat{x}_1 - \rho_1(\hat{x}_1, \hat{x}_2), \qquad \hat{x}_2(0) = \hat{x}_{10}, \tag{5.43a}$$

$$\dot{\hat{x}}_2 = \mathcal{A}_2 \hat{x}_2 + \rho_2(\hat{x}_1, \hat{x}_2) + \boldsymbol{\mathcal{B}}_u \boldsymbol{u}, \qquad \hat{x}_2(0) = \hat{x}_{20}, \tag{5.43b}$$

$$\boldsymbol{\mathcal{C}}_{y,2} \hat{x}_2 = \boldsymbol{y}, \tag{5.43c}$$

$$\hat{z}_c = \mathcal{C}_z \hat{x}_1, \tag{5.43d}$$

composed by a copy of the tubular reactor model (5.43a)-(5.43b) and a pointwise innovation scheme (5.43c) which directly injects the measured output information on the dynamic model of the observer, or in other words, the real state of the tubular reactor model at locations ς_i is imposed as the estimated temperature at the measurement points ς_i $i = 1, \ldots, q$. These output injections enforce the exponential convergence of the distributed estimation error dynamics to zero. Note that observer (5.43) is the distributed version of the pointwise-like observer (4.84a)-(4.84d), obtained by decoupling the CE components of (4.73a) through model redesign (see Section 4.6).

As it is done in [111], to facilitate the stability proof, the pointwise observer (5.43) is written in enthalpy-temperature coordinate (up to a linear transformation and assuming that the mas and heat Peclet numbers are equals, i. e.$Pe_m = Pe_h = P_e$):

$$\dot{\hat{x}}_h = \mathcal{A}_1 \hat{x}_h - v \hat{x}_2 + \boldsymbol{\mathcal{B}}_u \boldsymbol{u}, \qquad \hat{x}_h(0) = \hat{x}_{h0}, \tag{5.44a}$$

$$\dot{\hat{x}}_2 = \mathcal{A}_2 \hat{x}_2 + \rho(\hat{x}_1, \hat{x}_2) + \boldsymbol{\mathcal{B}}_u \boldsymbol{u}, \qquad \hat{x}_2(0) = \hat{x}_{20}, \tag{5.44b}$$

$$\boldsymbol{\mathcal{C}}_{y,2} \hat{x}_2 = \boldsymbol{y}, \tag{5.44c}$$

$$\hat{x}_1 = \hat{x}_h - \hat{x}_2, \quad \hat{z}_c = \mathcal{C}_z \hat{x}_1, \tag{5.44d}$$

where $x_h = x_1 + x_2$ is the enthalpy, and the pointwise observer (5.47b)–(5.47c) is driven by the point injections of the measured temperatures $\boldsymbol{y}$ at locations $\boldsymbol{\varsigma}$.

Following [111, Theorem 1], the q sensor locations on model (5.44) divide the temperature estimation error dynamics in $q+1$ intervals

$$\mathcal{J}_0 = [0, \varsigma_1), \quad \mathcal{J}_i = [\varsigma_{i-1}, \varsigma_i), \;\; i = 1, \dots, q, \quad \mathcal{J}_{q+1} = [\varsigma_{q-1}, 1].$$

On each interval, the heat transport operator $\mathcal{A}_2$ and the related reaction rate function in error estimation coordinate

$$\rho_h(\tilde{x}_h, \tilde{x}_2) = \rho_2(\hat{x}_2 - \hat{x}_h, \hat{x}_2) - \rho_2(\hat{x}_2 - \hat{x}_h, x_2), \tag{5.45}$$

manifest their effects by the section-wise operators $\mathcal{A}_2^i$ and reaction rates $\rho_{h,i}(\tilde{x}_h, \tilde{x}_2)$.

Exploiting the Lur'e structure of the dynamics on each interval, the exponential convergence of the estimation error dynamics can be drawn in terms of the eigenvalues of the transport operators (sensor locations dependent), the Lipschitz constants of the function (5.45), and the system parameters. This is summarized next (see [111]).

Theorem 5.1 ([111]). *Consider the tubular reactor (5.2) with sensor set $\boldsymbol{\varsigma}$. Let $L^{\rho_h}_{x_{2,i}}$, $L^{\rho_h}_{x_{h,i}}$, $i = 0 \dots, q+1$ denote the Lipschitz constant of the function (5.45). The estimation errors $\tilde{x}_2 = \hat{x}_2 - x_2$, and $\tilde{x}_h = \hat{x}_h - x_h$ vanish exponentially if: (i) the local temperature dissipation inequalities are met (with $\omega_{2,1}$, $\omega_{2,q+1}$ being the smallest solutions for $\omega_{2,n}$ in (5.5c)):*

$$\begin{aligned}
\varpi_1 &= \frac{\omega_{2,1}^2}{Pe\varsigma_1} + \frac{Pe}{4} + \eta - L^{\rho_h}_{x_{2,1}} > 0, \\
\varpi_i &= \frac{\pi^2}{Pe(\varsigma_i - \varsigma_{i-1})} + \frac{Pe}{4} + v - L^{\rho_h}_{x_{2,i}} > 0, \quad \forall i = 1, \dots, q, \\
\varpi_{q+1} &= \frac{\omega_{2,q+1}^2}{Pe(1-\varsigma_q)} + \frac{Pe}{4} + v - L^{\rho_h}_{x_{2,q}} > 0,
\end{aligned}$$

and (ii) the following global dissipation condition holds

$$|\lambda_1{}^*| \le v \sum_{i=1}^{q+1} \frac{L^{\rho_h}_{x_{h,i}}}{\varpi_i}, \tag{5.46}$$

with $\lambda_1{}^*$ the growth bound of the C_0-semigroup of contractions generated by $\mathcal{A}_1$.

5.4.2 *Control-estimation system and closed-loop stability*

The implementation of the proposed MIMO state feedback control (5.38) with the pointwise observer (5.43) yields the Linear-Inventory-like control-Pointwise Observer (LIOF-PWO) CES:

$$\begin{aligned}
\dot{\hat{x}}_1 &= \mathcal{A}_1 \hat{x}_1 - \rho_1(\hat{x}_1, \hat{x}_2), & \hat{x}_2(0) &= \hat{x}_{10}, & \text{(5.47a)}\\
\dot{\hat{x}}_2 &= \mathcal{A}_2 \hat{x}_2 + \rho_2(\hat{x}_1, \hat{x}_2) + \boldsymbol{\mathcal{B}}_u \boldsymbol{u}, & \hat{x}_2(0) &= \hat{x}_{20}, & \text{(5.47b)}\\
\boldsymbol{\mathcal{C}}_2 \hat{x}_2 &= \boldsymbol{y}, & & & \text{(5.47c)}\\
\hat{z}_c &= \mathcal{C}_z \hat{x}_1, & & & \text{(5.47d)}\\
\boldsymbol{u} &= \boldsymbol{\mu}_{lp}(\hat{x}_1, \hat{x}_2). & & & \text{(5.47e)}
\end{aligned}$$

where

$$\boldsymbol{\mu}_{lp}(\hat{x}_1, \hat{x}_2) = -\boldsymbol{B}_m{}^{-1}\left(\boldsymbol{K}_y\boldsymbol{\mathcal{C}}_y\hat{x}_2 + \boldsymbol{\mathcal{C}}_y\rho_2(\hat{x}_1, \hat{x}_2) + \boldsymbol{K}_{\mathfrak{z}}\boldsymbol{\mathcal{C}}_{\mathfrak{z}}\hat{x}_2\right). \tag{5.47f}$$

The corresponding closed-loop system, considering the enthalpy-temperature coordinate for the pointwise observer, is given as

$$\begin{aligned}
\dot{\tilde{x}}_h &= \mathcal{A}_1\tilde{x}_h - v\tilde{x}_2, & \tilde{x}_h(0) &= \tilde{x}_{h0}, && (5.48a)\\
\dot{\tilde{x}}_2 &= \mathcal{A}_2\tilde{x}_2 + \rho_h(\tilde{x}_h, \tilde{x}_2), & \tilde{x}_2(0) &= \tilde{x}_{20}, && (5.48b)\\
\boldsymbol{\mathcal{C}}_{y,2}\tilde{x}_2 &= \mathbf{0}_q, & & && (5.48c)\\
\dot{x}_1 &= \mathcal{A}_1 x_1 - \varrho(x_1) - \varrho_{12}(x_1, x_2), & x_1(0) &= x_{10}, && (5.48d)\\
\dot{x}_2 &= \mathcal{A}_2^c x_2 + \Delta\rho(x_1, x_2) + \boldsymbol{\mathcal{E}}x_2 + \boldsymbol{\mathcal{B}}_u, \boldsymbol{\mu}_e(\tilde{x}_1, \tilde{x}_2), & x_2(0) &= x_{20}. && (5.48e)
\end{aligned}$$

where ρ_h, defined in (5.45), is Lipschitz bounded in the estimated states uniformly in the actual ones, with constants $L_{\tilde{x}_j}^{\rho_2}$, $j = h, 2$, and

$$\boldsymbol{\mu}_e(\tilde{x}_1, \tilde{x}_2) = \boldsymbol{\mu}_{lp}(x_1 + \tilde{x}_1, x_2 + \tilde{x}_2) - \boldsymbol{\mu}_{lp}(x_1, x_2), \qquad \boldsymbol{\mathcal{E}}x_2 = \boldsymbol{\mathcal{B}}_u\boldsymbol{B}_m{}^{-1}\boldsymbol{K}_{\mathfrak{z}}\boldsymbol{\mathcal{B}}_u^* x_2.$$

Sufficient conditions for the stability of the zero solution $(\tilde{\boldsymbol{x}}^T, \boldsymbol{x}^T) = (\mathbf{0}_2, \mathbf{0}_2)^T$, $\tilde{\boldsymbol{x}} = [\tilde{x}_h\ \tilde{x}_2]^T$, $\boldsymbol{x} = [x_1\ x_2]^T$, of the preceding closed-loop system (5.48) are given next.

Proposition 5.4. *Closed-loop stability of system* (5.48)
Consider the closed-loop system (5.48) *with the* MIMO CES (5.47) *and let* $\boldsymbol{K}_y, \boldsymbol{K}_{\mathfrak{z}}, \varsigma$ *be chosen so that the conditions of* 5.2, 5.3 *(closed-loop stability with* MIMO *state feedback control* (5.38)*) and* 5.1 *(pointwise observer convergence) are met. Then, the steady-state* $(\tilde{\boldsymbol{x}}, \boldsymbol{x}) = (\mathbf{0}, \mathbf{0})$ *of the closed-loop system* (5.48) *is exponentially stable.*

Proof. Proposition 5.1 ensures the existence of constants $a_e \geq 1$ and $\nu_e > 0$ so that the estimation error dynamics (5.48a)-(5.48b)-(5.48c) are exponentially bounded as

$$\|\tilde{\boldsymbol{x}}(t)\|_{\mathcal{X}} \leq a_e \|\tilde{\boldsymbol{x}}_0\|_{\mathcal{X}}\, \mathrm{e}^{-\lambda_e t}.$$

By construction, from Proposition 5.2 and Proposition 5.3, subsystem (5.48d)–(5.48e) without interconnection is exponentially stable and satisfy (5.36). Consequently, the solution of (5.48d)–(5.48e) is bounded as

$$\|\boldsymbol{x}(t)\|_{\mathcal{X}} \leq \|\boldsymbol{x}_0\|_{\mathcal{X}}\, \mathrm{e}^{-\lambda_c t} + \|\boldsymbol{\mathcal{B}}_u\|\left(L_{\tilde{x}_h}^{\mu_e} + L_{\tilde{x}_2}^{\mu_e}\right)\int_0^t \mathrm{e}^{-\lambda_c(t-\mathrm{t})}\, \|\tilde{\boldsymbol{x}}\|_{\mathcal{X}}\, \mathrm{dt}.$$

Note that the above estimates compose a cascaded system, thus, from the application of Proposition 3.1, it can be concluded that, if $\lambda_e, \lambda_c > 0$, or equivalently the conditions stated in Proposition 5.4 are met, each state of the cascaded interconnected system converges to the zero solution exponentially with decaying rate $-\lambda_{xe}$ given by

$$-\lambda_{xe} = \max_{\lambda_j \in \sigma(A_{xe})}\{\mathrm{Re}\lambda_j\}, \quad \boldsymbol{A}_{xe} = \begin{bmatrix} -\lambda_c & 0 \\ \|\boldsymbol{\mathcal{B}}_u\|\left(L_{\tilde{x}_h}^{\mu_e} + L_{\tilde{x}_2}^{\mu_e}\right) & -\lambda_e. \end{bmatrix}$$

□

The preceding results establish nonlocal exponential stability in the domain of interest $\mathcal{X}$. In the presence of additive disturbances and parameter uncertainty, Proposition 5.4 ensures roust stability in the sense of Input-to-State Stability (ISS) for parabolic systems (see [80; 75]) of the nonlinear closed-loop system (5.48). This establishes a compromise between stabilizing capabilities and selection of suitable gains such that the LIOF-PWO CES ensures good performance.

5.5 EFFICIENT LATE-LUMPING IMPLEMENTATION AND TUNING

Here, as final application-oriented step, the efficient modeling approach of Section 3.2 is applied to obtain an efficient late lumping implementation of the proposed LIOF-PWO CES. Note that differently from what is done in Section 4.6, the implementation of the proposed CES in done with the use of the advanced observer (4.86a)-(4.86d) coupled with the control law (5.23) since it is not possible to realize the tubular reactor model (4.13) as a simplified model with am instantaneously observable load input.

The proposed MIMO LIOF-PWO CES (5.47) in explicit original coordinates (2.9) is

$$
\begin{aligned}
\partial_t \hat{\chi}_1 &= \frac{1}{Pe_m}\partial_s^2 \hat{\chi}_1 - \partial_s \hat{\chi}_1 - r(\hat{\chi}_1, \hat{\chi}_2) \\
\partial_t \hat{\chi}_2 &= \frac{1}{Pe_h}\partial_s^2 \hat{\chi}_2 - \partial_s \hat{\chi}_2 - \upsilon \hat{\chi}_2 + r(\hat{\chi}_1, \hat{\chi}_2) - \upsilon \boldsymbol{\beta} \boldsymbol{\tau}_c \\
\frac{1}{Pe_m}\partial_s \hat{\chi}_1(0,t) &= \hat{\chi}_1(0,t) - \chi_{1,e}(t), \qquad \partial_s \hat{\chi}_1(1,t) = 0 \\
\frac{1}{Pe_h}\partial_s \hat{\chi}_2(0,t) &= \hat{\chi}_2(0,t) - \chi_{2,e}(t), \qquad \partial_s \hat{\chi}_2(1,t) = 0 \\
\hat{\chi}_1(s,0) &= \hat{\chi}_{10}(s) \\
\hat{\chi}_2(s,0) &= \hat{\chi}_{20}(s), \\
\hat{\chi}_2(\varsigma_i, t) &= \tau_{m,i}(t), \quad i = 1, \ldots, q, \\
\hat{\chi}_z &= \hat{\chi}_1(1,t), \\
\boldsymbol{\tau}_c &= \boldsymbol{\mu}_m(\hat{\chi}_1, \hat{\chi}_2),
\end{aligned}
$$

where the entries of the control map $\boldsymbol{\mu}_m$ are

$$
\begin{aligned}
\mu_i(\hat{\chi}_1, \hat{\chi}_2) = \bar{\tau}_c - \frac{1}{\upsilon}\Bigg(\frac{1}{2\epsilon}\int_{\varsigma_i - \epsilon}^{\varsigma_i + \epsilon} \big(k_{y,i}(\hat{\chi}_2 - \bar{\chi}_2) + (r(\hat{\chi}_1, \hat{\chi}_1) - r(\bar{\chi}_1, \bar{\chi}_1))\big)\, \mathrm{d}s + \\
+ k_{\mathfrak{z},i} \int_{\frac{(i-1)}{q}}^{\frac{i}{q}} \mathrm{e}^{-Pe_h s}\, (\hat{\chi}_2 - \bar{\chi}_2)\, \mathrm{d}s \Bigg), \quad i = 1, \ldots, q. \qquad (5.49)
\end{aligned}
$$

Recalling the FD-based spatially discretized version of model (2.7) with efficient discretization order (3.31), to construct the efficient late lumping version of the above controller (see Section 3.2.1). The application of the measured-unmeasured partition (4.4) (see Section 4.2.1) yields the implementable LIOF-PWO CES :

$$\dot{\hat{\chi}}_1 = \boldsymbol{A}_1\hat{\chi}_1 + \boldsymbol{B}_{d,1}\bar{\chi}_{1,e} - \boldsymbol{r}(\hat{\chi}_1, \hat{\chi}_2), \qquad \hat{\chi}_1(0) = \hat{\chi}_{10}, \tag{5.50a}$$

$$\dot{\hat{\chi}}_{2,n} = \boldsymbol{A}_2^{n,n}\hat{\chi}_{2,n} + \boldsymbol{A}_2^{n,m}\hat{\chi}_{2,m} + \boldsymbol{B}_{d,2}^{n}\chi_{2,e} + \boldsymbol{r}_n(\hat{\chi}_1, \hat{\chi}_{2,n}) + \boldsymbol{B}_{u,2}^{n}\boldsymbol{\tau}_c, \; \hat{\chi}_{2,n}(0) = \hat{\chi}_{2,n0}, \tag{5.50b}$$

$$\hat{\chi}_{2,m} = \boldsymbol{\tau}_m, \tag{5.50c}$$

$$\hat{c}_o = \boldsymbol{C}_1\hat{\chi}_1, \quad \hat{\chi}_2 = \boldsymbol{C}_n^T\hat{\chi}_{2,n} + \boldsymbol{C}_{y,2}^T\hat{\chi}_{2,m}, \quad \hat{\chi}_N = \boldsymbol{\mathcal{I}}(\hat{\chi}), \tag{5.50d}$$

$$\boldsymbol{\tau}_c = \boldsymbol{\mu}_m(\hat{\chi}_1, \hat{\chi}_2), \tag{5.50e}$$

where the state of the finite dimensional observer are given by the sequences $\hat{\chi}_i = [\hat{\chi}_{j,1} \ \ldots \ \hat{\chi}_{j,N_e}]^T$, $j = 1, 2$. The entries of the control map $\boldsymbol{\mu}_m$, with the parameter ϵ chosen small enough, are

$$\mu_i(\hat{\chi}_1, \hat{\chi}_2) = \bar{\tau}_c - \frac{1}{v}\left(\frac{1}{2\epsilon}\left(k_{y,i}(\tau_{m,i} - \bar{\tau}_{m,i}) + (r_{m,i}(\hat{\chi}_{1,m_i}, \tau_{m,i}) - r_{m,i}(\bar{\chi}_{1,m_i}, \bar{\tau}_{m,i}))\right) + \right.$$
$$\left. + k_{\mathfrak{z},i}\frac{1}{N_e}\sum_{k=\frac{(i-1)N_e}{q}}^{\frac{iN_e}{q}} \mathrm{e}^{-Pe_h s_k}\left(\hat{\chi}_{2,k} - \bar{\chi}_{2,k}\right)\right). \tag{5.50f}$$

The spatial integrals in controller (5.49) have been approximated with the Gaussian quadrature rule, but other approximations might be used, i. e., the trapezoidal rule.

The MIMO LIOF-PWO CES implementation (5.50) has the following structure $\mathfrak{S}_q$ and gains $\boldsymbol{K}_\theta$, that must be chosen to ensure good closed-loop performance:

$$\varsigma = \{2N_e - q, q, \boldsymbol{\varsigma}, U\}, \quad \boldsymbol{K}_\theta = \boldsymbol{K}_c = (\boldsymbol{K}_y, \boldsymbol{K}_{\mathfrak{z}}), \tag{5.51}$$

where the dimension of the CES is $n_\theta = N_e$, where N_e is the efficient discretization order, determined in Section 3.2, $2N_e - q$ is the dimension of the pointwise observer, q is the number of actuator-sensor pairs, each one paired with a controller. The sensor location set $\boldsymbol{\varsigma}$ includes the number of sensors q and their locations, determined in Section 5.3.3. The control is unconstrained and the gains matrices $(\boldsymbol{K}_{y,0}, \boldsymbol{K}_{\mathfrak{z},0})$ must be chosen with to the procedure given in Section 5.3.3.2.

The theoretical developments of the previous sections are summarized next in a structure-gain tuning procedure. The first step, of off-line structural tuning, include the determination of the: (i) efficient model order $n_e = 2N_e$, (ii) the sensor set $\boldsymbol{\varsigma}$, and (iii) *a priori* (before implementation) gain values $(\boldsymbol{K}_y, \boldsymbol{K}_{\mathfrak{z}})$. The second step, for on-line gain tuning and structure calibration, is set in the light of simulation-based conventional-like tuning guidelines for robust functioning: with realistic initial condition, input step and fluctuating disturbance, and parameter and actuation-measurement errors).

Step I: Off-line structural tuning:

I.1 Use the efficient modeling approach of Section 3.2 to draw the late efficient discretization order N_e use the model order $n_e = 2N_e$ for the remaining off-line structural and on-line gain tuning and structure calibration.

I.2 Use the bifurcation-based procedure of Section 5.3.3.2 to characterize the closed-loop multiplicity of (5.39), to determine the admissible sensor set $\mathcal{S}_m$ for $q = 1$

$$\mathcal{S}_m = \{\varsigma_1 \in \mathcal{S} \,|\, (x_1, x_2) = (0, 0) \text{ is the unique steady-state}\}, \tag{5.52}$$

and choose the location which maximize the stability measure l_c according to and the sensor location criterion (5.41).

I.3 From the procedure inSection 5.3.3.2, choose the initial gain matrix $\boldsymbol{K}_{y,0}$, before fine tuning, that ensures the fulfillment of conditions in Lemma 5.2.

I.4 Set the closed-loop system with the proposed control-estimation system (5.50) in the robust testing mode with appropriate: (i) parameter errors and measurement noise, as well as load input and setpoint changes, (ii) initial state and estimate errors, (iv) measurement noise.

Step II: On-line gain tuning and structural-gain fine adjustment:

II.1 Set the control gain matrix $\boldsymbol{K}_y$ as in step I.3 and $\boldsymbol{K}_{\mathfrak{z}}$ five times faster than the natural output response of the system. Repeat the procedure for each output.

II.2 Perform fine calibration: adjust the stage number N_e, sensor locations ς, and the control gain matrices to improve behavior.

II.3 The number q of actuator-sensor pairs can be incremented up to 2 or 3 to explore if there is some behavior improvement.

For the case study of Section 2.5, the execution of step I.1 of the above procedure was done in Section 3.2: the efficient model order for on-line implementation of the MIMO LIOF-PWO CES (5.50) is $n_e = 2N_e = 40$.

5.6 CONTROL-ESTIMATION SYSTEM FUNCTIONING

In this section, the proposedthe MIMO LIOF-PWO CES design is: (i) illustrated and tested with the case study described in Section 2.5 with open-loop multiplicity and closed-loop operation about an unstable steady-state, and (ii) compared with a recent adaptive control design that has been applied to multi-jacket reactors [26; 27; 28]. Closed-loop behavior under nominal testing (without measurement noise, disturbances and model parameter errors) is employed to corroborate theoretical results and assess attainable control functioning. Closed-loop behavior under robust testing (with measurement noise, disturbances and model parameter errors) is employed to assess control functioning under realistic industrial conditions.

The application of the off-line Step I of the tuning procedure given in Section 5.5 to the case study (see Section 2.5), was performed in Section 3.2.3 for the model order, and in Section 5.3.3 for the sensor location in the three cases $q = 1, 2, 3$. Accordingly, the initial (before fine adjustment) control structures for $q = 1, 2, 3$ are:

$$\varsigma_{1,0} = \{40, 1, \varsigma_1 \approx 0.24, U\}, \tag{5.53a}$$
$$\varsigma_{2,0} = \{40, 2, \{\varsigma_1 \approx 0.24\, \varsigma_2 \approx 0.95\}, U\}, \tag{5.53b}$$
$$\varsigma_{3,0} = \{40, 3, \{\varsigma_1 \approx 0.24\, \varsigma_2 \approx 0.65, \varsigma_3 \approx 0.95\}, U\}, \tag{5.53c}$$

where the sensor locations have been fitted to the closets discretization grid points. The procedure in Section 5.5 suggests the gains

$$\boldsymbol{K}_{c,0} = (K_{y,0}, K_{\mathfrak{z},0}) = (0.7, 15), \tag{5.53d}$$
$$\boldsymbol{K}_{c,0} = (\boldsymbol{K}_{y,0}, \boldsymbol{K}_{\mathfrak{z},0}), \quad K_{y,0} = \begin{bmatrix} 0.2 & 0 \\ 0 & 0.5 \end{bmatrix}, \quad K_{\mathfrak{z},0} = \begin{bmatrix} 1 & 0 \\ 0 & 5 \end{bmatrix}, \tag{5.53e}$$
$$\boldsymbol{K}_{q,0} = (\boldsymbol{K}_{y,0}, \boldsymbol{K}_{\mathfrak{z},0}, \quad K_{y,0} = \begin{bmatrix} 0.2 & 0 & 0 \\ 0 & 0.5 & 0 \\ 0 & 0 & 0.5 \end{bmatrix}, \quad K_{\mathfrak{z},0}) = \begin{bmatrix} 0.2 & 0 & 0 \\ 0 & 5 & 0 \\ 0 & 0 & 5 \end{bmatrix}. \tag{5.53f}$$

The results on the conclusive structural and gain tuning resulting on the on-line Step II is the subject of the subsequent developments.

5.6.1 *Robust testing scheme*

The tubular reactor is simulated with (4.85) with $N_{pde} = 200$ internal nodes, meaning that the reactor model (4.1) consists of 400 ODEs. The testing scheme for the robust functioning assessment of the proposed MIMO LIOF-PWO CES (5.50) with order $n_\theta = 2N_e - q = 37$ is set as follow.

The initial concentration (or temperature) vector χ_1 (or χ_2) is set with 10 % (or -5 %) deviation with respect to nominal value $\bar{\chi}_1$ (or $\bar{\chi}_2$):

$$\chi_{1,0} = 1.1\bar{\chi}_1, \quad \chi_{2,0} = 0.95\bar{\chi}_2.$$

The fluctuating error $\boldsymbol{e}$ of the actual closed-loop dynamics (4.2) was generated with the linear (2nd-order oscillator) parasitic dynamics driven by low-amplitude and high-frequency (close to resonant one) sinusoidal inputs w_j, $j = 1, 2$:

$$\begin{aligned} \dot{\pi}_{1,j} &= \pi_{2,j}, & \pi_{1,j}(0) &= 0, \\ \dot{\pi}_{2,j} &= -\lambda_{\pi,j}^2 \pi_{j,1} + w_j(t), & \pi_{2,j}(0) &= 0, \\ \boldsymbol{e}_j &= \boldsymbol{b}_\pi \pi_{j,2}, & & \\ w_1(t) &= 0.01 \sin(50t + 12.57), \quad w_2(t) = 0.02 \sin(25t + .35). & & \end{aligned}$$

where $\lambda_{\pi,j} \approx 50\nu_j$, $j = 1,2$, with ν_j are determined in Section 4.2.3, and $\boldsymbol{b}_\pi = [1 \ldots 1]^T$.

In the testing scheme the tubular reactor is operated over the dimensionless time interval [0,25]. The closed-loop system (4.85)-(4.86) is subjected to the following flow feed temperature $\chi_{2,e}$ load input disturbance, feed (w_e) and output $(\boldsymbol{w}_m)$ temperature measurement sinusoidal noises

$$t \in [0,30] : \ \chi_2 = \chi_{2,e} + w_2, \ \chi_{1,e} = \bar{\chi}_{1,e}, \quad \boldsymbol{\tau}_m = \boldsymbol{\chi}_{2,m} + \boldsymbol{w}_m,$$

where $w_j(t) = 0.00\sin(2.9t + \pi/18)$, $j = 2, m$. In addition, over the time subinterval $[5, 25)$ the feed temperature $\chi_{2,e}$ suffers step changes sequences (H: Heaviside's function)

$$t \in [4,25) : \chi_{2,e}(t) = \bar{\chi}_{2,e} + 0.02[H(t,5) - H(t,10)] - 0.05[H(t,15) + H(t,20)]$$

The CES (4.86a)-(4.86d) is build with the deviated transport-kinetics parameters

$$(\hat{P}e_m, \hat{P}e_h) = (0.91Pe_m, 1.11Pe_h), \quad \hat{v} = 0.95v, \quad (\hat{a}_r, \hat{b}_r) = (1.035a_r, 1.03b_r),$$

and initial unmeasured state estimate:

$$(\hat{\chi}_1, \hat{\boldsymbol{\chi}}_{2,n}) = (\bar{\chi}_1, \bar{\boldsymbol{\chi}}_{2,n}).$$

5.6.2 *Gain tuning and structure calibration*

The application of Steps II of the gain-structure procedure of Section 5.5 yields the adjusted structures

$$\varsigma_{1,0} = \{40, 1, \varsigma_1 \approx 0.24, U\}, \tag{5.54a}$$
$$\varsigma_{2,0} = \{40, 2, \{\varsigma_1 \approx 0.24\, \varsigma_2 \approx 0.95\}, U\}, \tag{5.54b}$$
$$\varsigma_{3,0} = \{40, 3, \{\varsigma_1 \approx 0.24\, \varsigma_2 \approx 0.65, \varsigma_3 \approx 0.95\}, U\}, \tag{5.54c}$$

and the final gain tuning

$$\boldsymbol{K}_{q,0} = (K_{y,0}, K_{\mathfrak{z},0}) = (0.7, 15), \tag{5.54d}$$

$$\boldsymbol{K}_{q,0} = (\boldsymbol{K}_{y,0}, \boldsymbol{K}_{\mathfrak{z},0}), \quad K_{y,0} = \begin{bmatrix} 0.2 & 0 \\ 0 & 0.5 \end{bmatrix}, \quad K_{\mathfrak{z},0} = \begin{bmatrix} 0.2 & 0 \\ 0 & 15 \end{bmatrix}, \tag{5.54e}$$

$$\boldsymbol{K}_{q,0} = (\boldsymbol{K}_{y,0}, \boldsymbol{K}_{\mathfrak{z},0}, \quad K_{y,0} = \begin{bmatrix} 0.2 & 0 & 0 \\ 0 & 0.5 & 0 \\ 0 & 0 & 0.5 \end{bmatrix}, \quad K_{\mathfrak{z},0} = \begin{bmatrix} 0.2 & 0 & 0 \\ 0 & 15 & 0 \\ 0 & 0 & 15 \end{bmatrix}. \tag{5.54f}$$

In all cases, the initial sensor locations produce nice performance and are kept as the initial setting (5.53d).

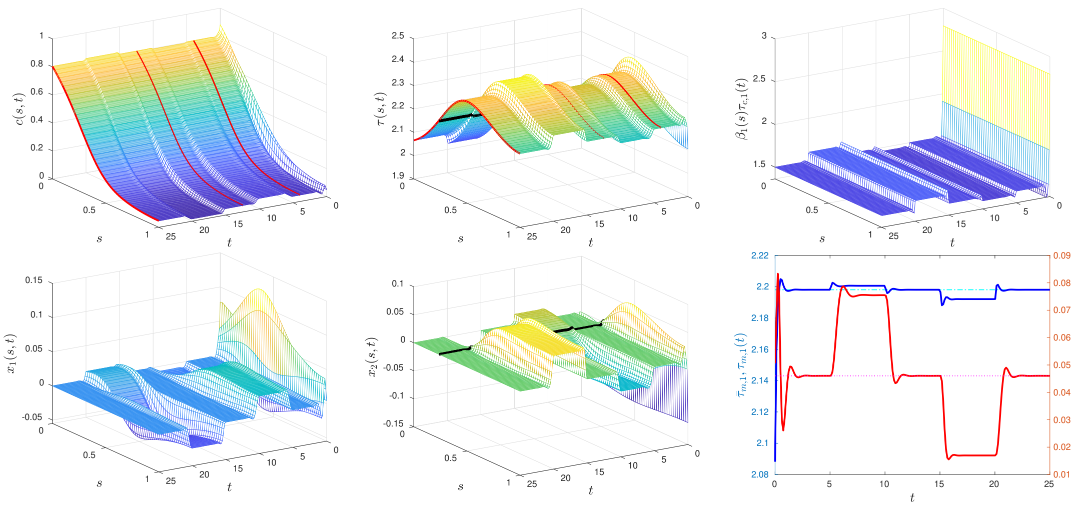

Figure 5.2: Nominal closed-loop functioning with SF. Top left: concentration profile $c(s,t)$. Top center: temperature profile $\tau(s,t)$. Top right: control effort $\beta_1(s)\tau_{c,1}(t)$. Bottom left: deviated concentration profile $x_1(s,t)$. Bottom center: deviated temperature profile $x_2(s,t)$. Bottom right: measured $\tau_{m,1}$ (continuous blue) and regulated $c_o(t)$ (continuous red) outputs and their setpoints (dashed-dotted cyan or dotted magenta, respectively).

5.6.3 *SISO case*

The closed-loop functioning comparison, under nominal and robust testing conditions, of the SISO version of the proposed LIOF-PWO CES (5.50), against its detailed model-based state State Feedback controller (SF) counterpart (5.23), is performed next with two objectives: (i) corroborate theoretical results on sensor location and attainable closed-loop functioning (under nominal conditions), and (ii) to show how the controllers perform under realistic unfavorable operating conditions.

5.6.3.1 *Nominal functioning*

The nominal functioning is performed with the gains and structure obtained with the robust testing scheme. Step changes in the inlet temperature, the fluctuating disturbances, and parasitic dynamics are not at play.

In Figure 5.2 and Figure 5.3a, the nominal closed-loop control functioning with the SF (5.23) and the LIOF-PWO CES (5.50) are shown. The corresponding estimation functioning is shown in Figure 5.3b. The norms of the distributed state and estimation error and control input profiles are presented in Figure 5.4a.

Regarding control functioning, on one hand, with respect to regulation task, in terms of settling time, disturbance rejection, and control effort, the SF yields the best behavior, closely followed by the LIOF-PWO CES.

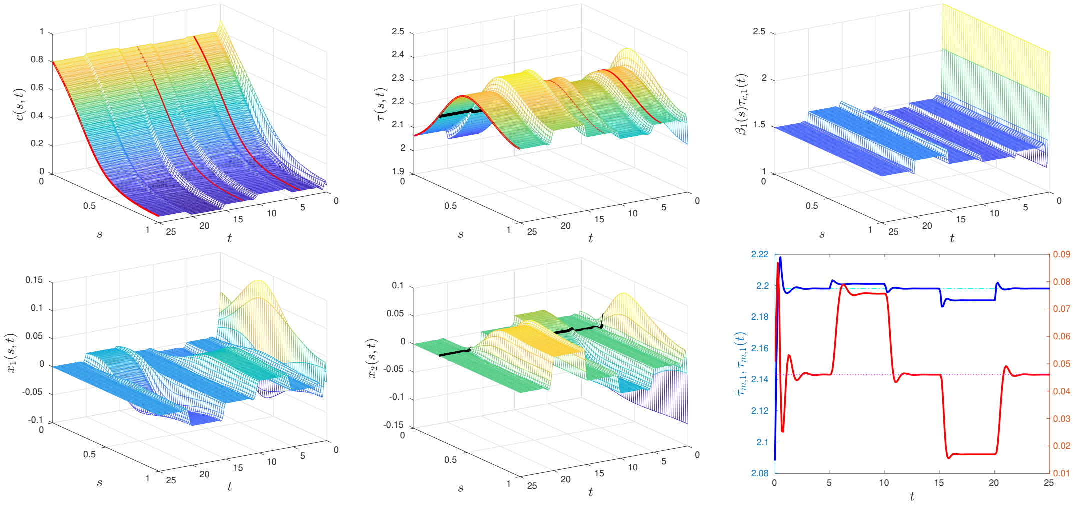

(a) Control functioning. Top left: concentration profile $c(s,t)$. Top center: temperature profile $\tau(s,t)$. Top right: control effort $\beta_1(s)\tau_{c,1}(t)$. Bottom left: deviated concentration profile $x_1(s,t)$. Bottom center: deviated temperature profile $x_2(s,t)$. Bottom right: measured $\tau_{m,1}$ (continuous blue) and regulated $c_o(t)$ (continuous red) outputs and their setpoints (dashed-dotted cyan or dotted magenta, respectively).

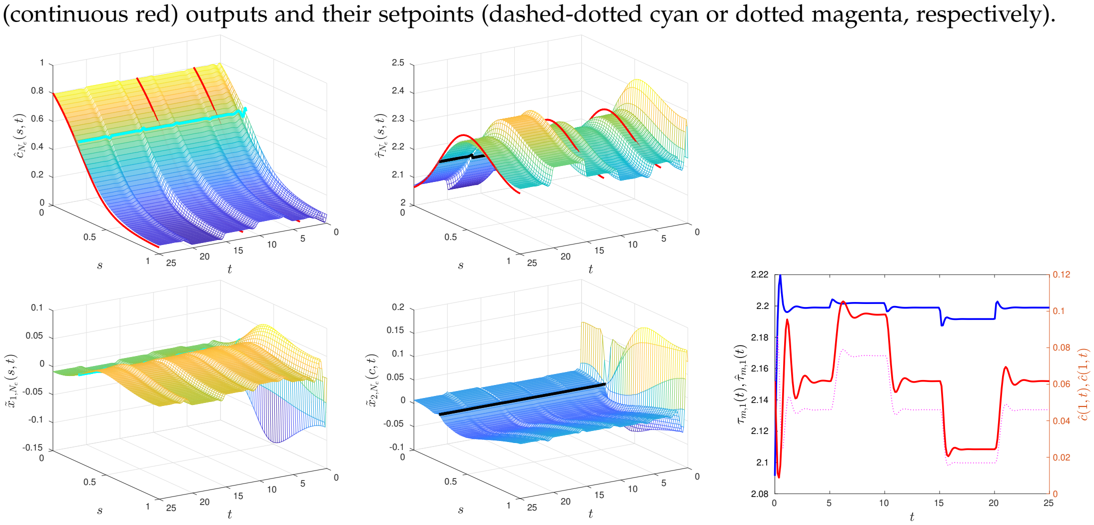

(b) Estimator functioning. Top left: estimated concentration profile $\hat{c}(s,t)$. Top center: estimated temperature profile $\hat{\tau}(s,t)$. Bottom left: concentration estimation error profile $\tilde{c}_1(s,t)$. Bottom center: temperature estimation error profile $\tilde{\tau}_2(s,t)$. Bottom right: real measured $\tau_{m,1}(t)$ (continuous blue) and regulated $c_o(t)$ (dotted magenta) and their estimates $(\hat{\tau}_{m,1}(t), \hat{c}_o(t))$ (continuous blue and red, respectively).

Figure 5.3: Nominal closed-loop control functioning with the SISO LIOF-PWO CES.

Specifically, the LIOF-PWO: (i) for $t \in [0,5)$ (response to initial condition) yields larger overshoots and control effort (due to estimator error dynamics), and (ii) for $t \in [5,25)$ (where step disturbances occur) produce slightly more oscillatory response.

With respect to estimation functioning, in terms of convergence settling time and offset, the estimator of the proposed LIOF-PWO performs well and present some

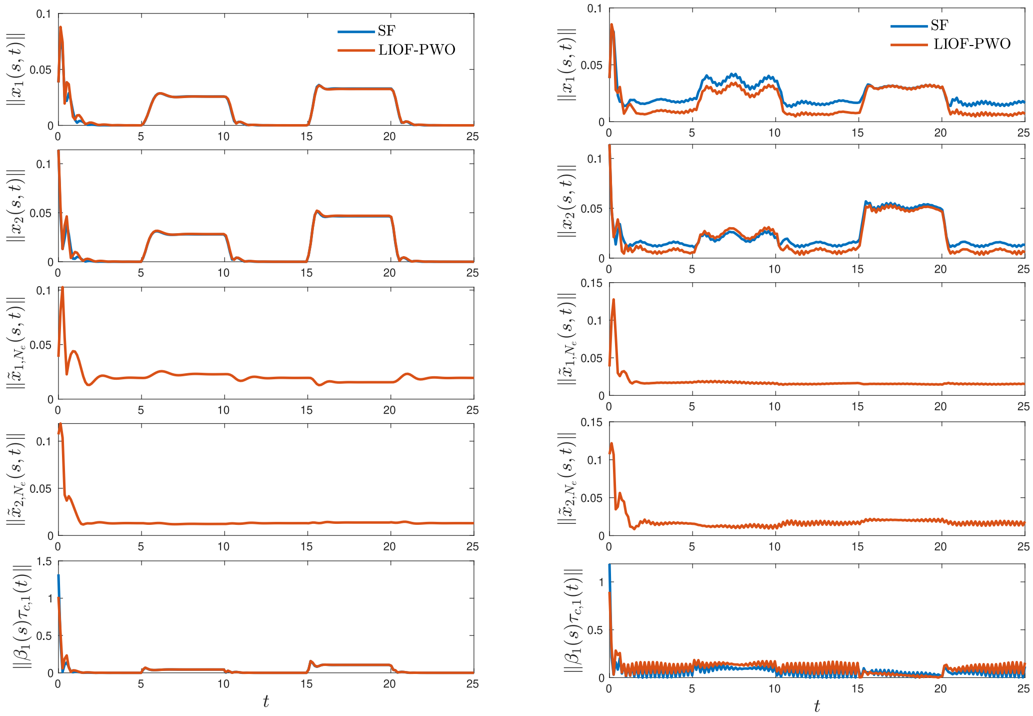

(a) Nominal case.

(b) Robust case.

Figure 5.4: Norms of distributed states in deviation, estimation errors and control input.

expected and allowed persistent estimation error due to parameter uncertainty and modeling errors.

As expected, in the nominal setting, the SF, benefited from full state knowledge, presents the best behavior and corroborates the efficiency of the proposed control law. The LIOF-PWO produce acceptable performance driven by a pointwise observer.

To test the sensor location condition needed for the adequate closed-loop functioning, given in Section 5.3.3.2, on purpose the sensor location condition (5.40) is violated,i. e.., the sensor is placed at the following location

$$\varsigma_1 = 0.57, \quad \tau_{m,1} = \chi_{2,11},$$

after the hotspot, where $\Gamma_{k,0}(\varsigma) < 0$. The corresponding norms of the distributed profiles in closed-loop behavior are presented in Figure 5.5, showing that, as expected, the reactor, with all the controllers, does not reach the prescribed steady-state profile pair, and instead it reaches an undesired ignition stable steady-state. The estimation task is fulfilled showing the efficiency of the estimator in this unfavorable scenario and confirming their use for monitoring purposes.

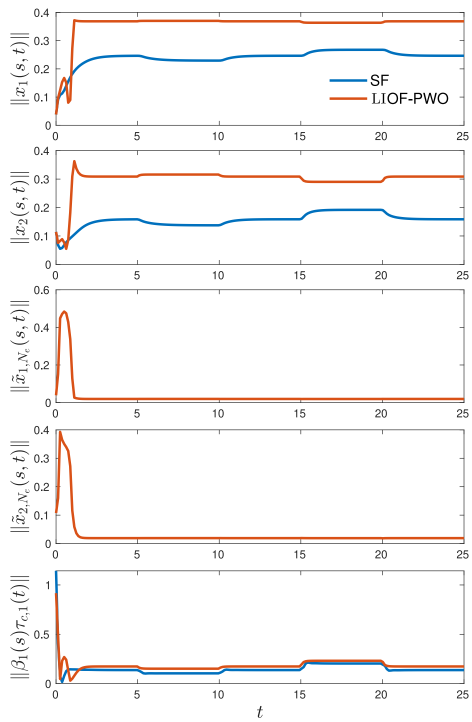

Figure 5.5: Nominal case where the sensor location condition is not met: norms of distributed states in deviation, estimation errors and control input.

5.6.3.2 *Robust functioning*

In Figure 5.6 and Figure 5.7a, the robust closed-loop control functioning with the SF (5.23) and the advanced SISO LIOF-PWO CES (5.50), respectively, are shown. The robust closed-loop estimation functioning of the estimator of the proposed CES (5.50) is shown in Figure 4.13b. The norms of the distributed state and estimation error and control input profiles are presented in Figure 5.4b.

From these simulation results, with respect to the regulation task and in terms of settling time, disturbance rejection, and control effort: the LIOF-PWO CES outperforms its SF counterpart. Regarding the estimation task, in terms of convergence settling time and offset, the estimator of the proposed CES efficiently executes the estimation task. Thus, in agreement with theoretical developments, the proposed CES outperforms the SF which is substantially degraded due to its dependency on exact knowledge of parameters and in spite of knowing the real state of the tubular reactor.

Specifically, for $t \in [0, 5)$ (with response to initial condition deviation): (i) the CES produces slower measured-regulated outputs and state settling times with small oscillations and adequate control action, and (ii) the SF has comparatively larger output and state overshoot as well as asymptotic offset, with wasteful control action. For $t \in [5, 25)$ (with persistent periodic and step disturbances as well as setpoint

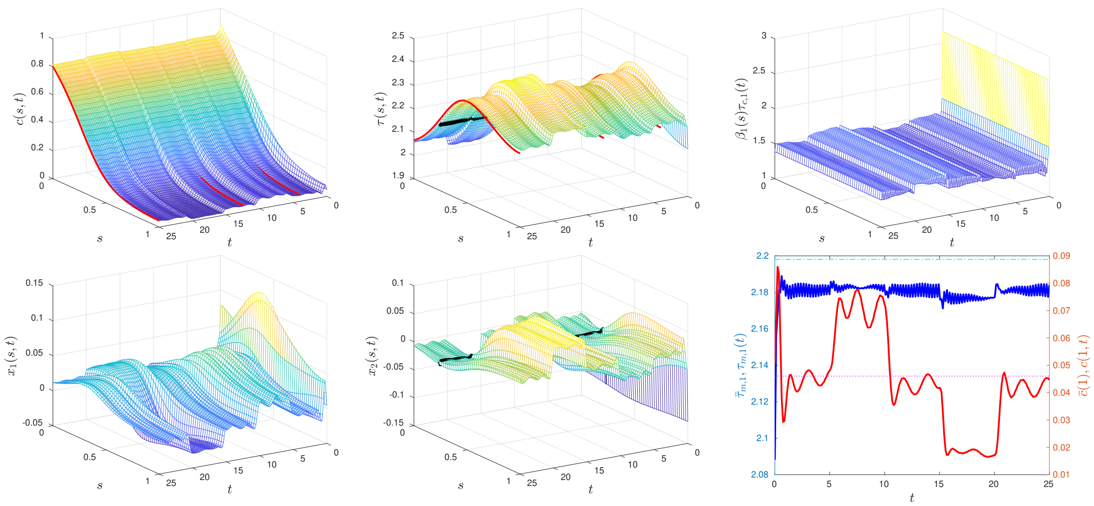

Figure 5.6: Robust closed-loop functioning with SF. Top left: concentration profile $c(s,t)$. Top center: temperature profile $\tau(s,t)$. Top right: control effort $\beta_1(s)\tau_{c,1}(t)$. Bottom left: deviated concentration profile $x_1(s,t)$. Bottom center: deviated temperature profile $x_2(s,t)$. Bottom right: measured $\tau_{m,1}$ (continuous blue) and regulated $c_o(t)$ (continuous red) outputs and their setpoints (dashed-dotted cyan or dotted magenta, respectively).

change) the CES presents enhanced attenuation of the inlet temperature disturbances on the measured and regulated output as well as on the distributed profiles.

Following the previous results, it is confirmed that the proposed LIOF-PWO CES (5.50) is the one with the best closed-loop performance in both control and estimation tasks. What is left is to assess is there is some benefit of considering the MIMO cases in comparison with the SISO one. This is evaluated next in robust testing conditions.

5.6.4 *MIMO case*

The SISO and MIMO, for $q = 2, 3$, versions of the proposed LIOF-PWO CES (5.50) are set with the structures and parameters given in (5.54). The closed-loop CE functioning under robust testing conditions are presented in Figure 5.7, Figure 5.8, and Figure 5.9, for the SISO, 2-MIMO, and 3-MIMO cases, respectively.

From the simulation results, it can be seen that the MIMO cases benefits from the use of additional information of the system and produce more robust closed-loop behavior in both control and estimation tasks. Specifically, for $t \in [5, 25)$ (when inlet temperature step disturbances arise), regarding control functioning, the decentralized controllers produce precise control actions that coordinate and attenuate the effect of the disturbances in the steady-state profiles. Regarding estimation, it is appreciated that the pointwise-like observers improve their performance since the estimation error, in the presence of exogenous disturbances, decreases as the number of sensors increase. Thus, this rejection capability is enhanced as the number of actuator-sensor

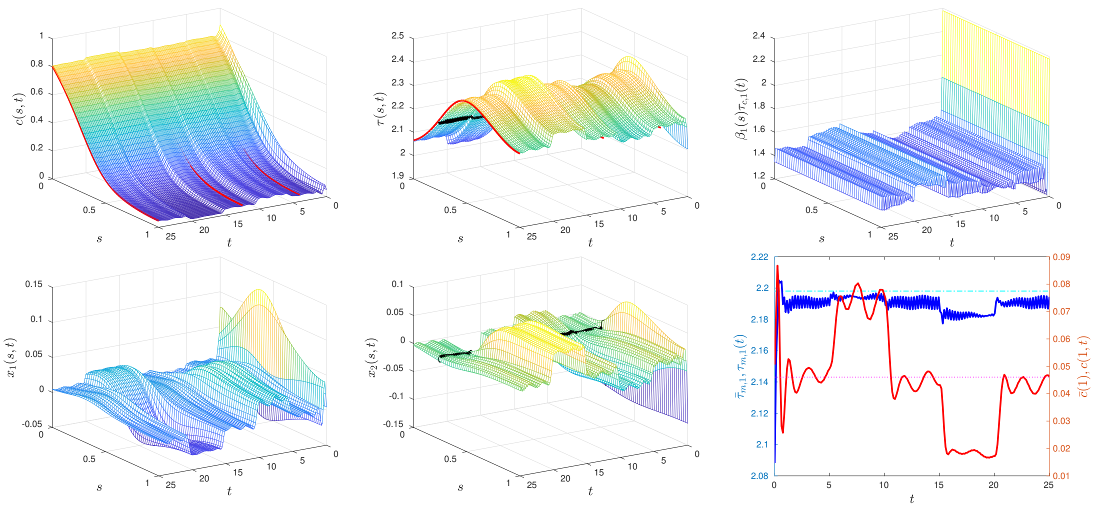

(a) Control functioning. Top left: concentration profile $c(s,t)$. Top center: temperature profile $\tau(s,t)$. Top right: control effort $\beta_1(s)\tau_{c,1}(t)$. Bottom left: deviated concentration profile $x_1(s,t)$. Bottom center: deviated temperature profile $x_2(s,t)$. Bottom right: measured $\tau_{m,1}$ (continuous blue) and regulated $c_o(t)$ (continuous red) outputs and their setpoints (dashed-dotted cyan or dotted magenta, respectively).

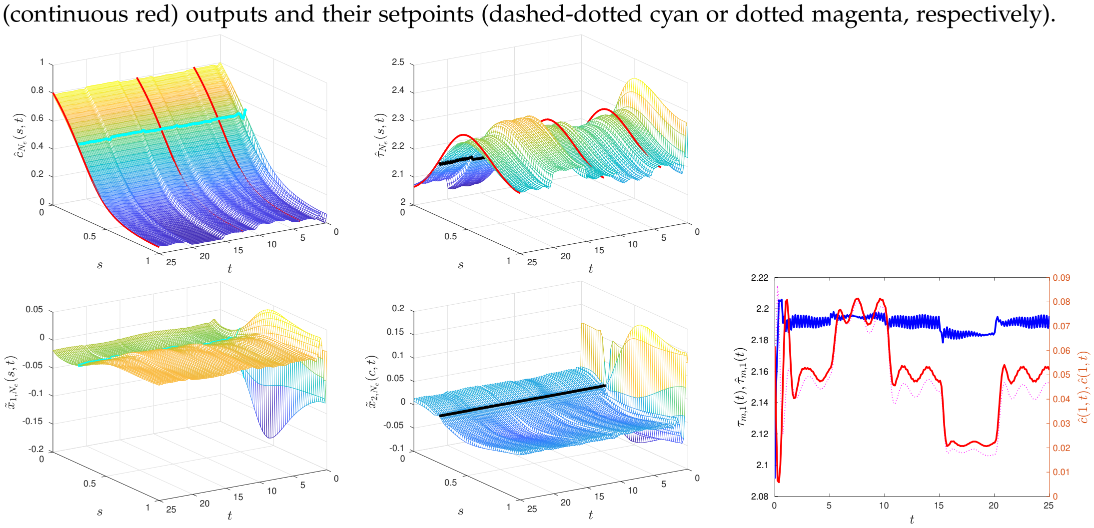

(b) Estimator functioning. Top left: estimated concentration profile $\hat{c}(s,t)$. Top center: estimated temperature profile $\hat{\tau}(s,t)$. Bottom left: concentration estimation error profile $\tilde{c}_1(s,t)$. Bottom center: temperature estimation error profile $\tilde{\tau}_2(s,t)$. Bottom right: real measured $\tau_{m,1}(t)$ (continuous blue) and regulated $c_o(t)$ (dotted magenta) and their estimates $(\hat{\tau}_{m,1}(t), \hat{c}_o(t))$ (continuous blue and red, respectively).

Figure 5.7: Nominal closed-loop control functioning with the SISO LIOF-PWO CES.

pair increase. No that this is produced, with an overall control action that has a similar norm as in the two MIMO cases and SISO one.

Thus, it is concluded that the proposed LIOF-PWO CES (5.50), clearly benefits with the MIMO with $q = 3$ as the one that produces the best performance. Further enhancement can be achieved if the efficient model order $n_e = 2N_e$ is increased up to $n_e = 160$.

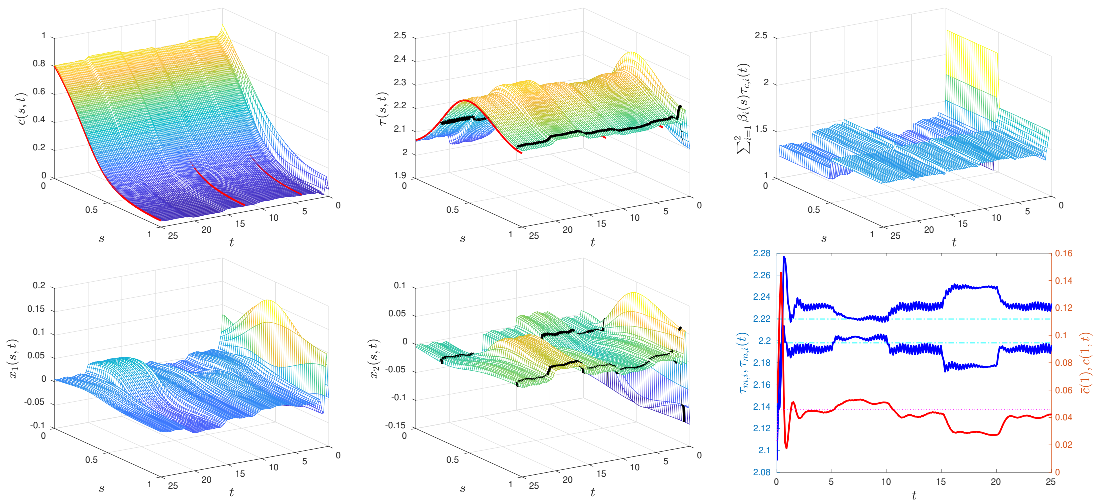

(a) Control functioning. Top left: concentration profile $c(s,t)$. Top center: temperature profile $\tau(s,t)$. Top right: control effort $\sum_{i=1}^{2} \beta_i(s)\tau_{c,i}(t)$. Bottom left: deviated concentration profile $x_1(s,t)$. Bottom center: deviated temperature profile $x_2(s,t)$. Bottom right: measured $\tau_{m,i}(t)$, $i = 1,2$ (blue continuous) and regulated $c_o(t)$ (red continuous) outputs and their setpoints (dashed-dotted cyan and dotted magenta, respectively).

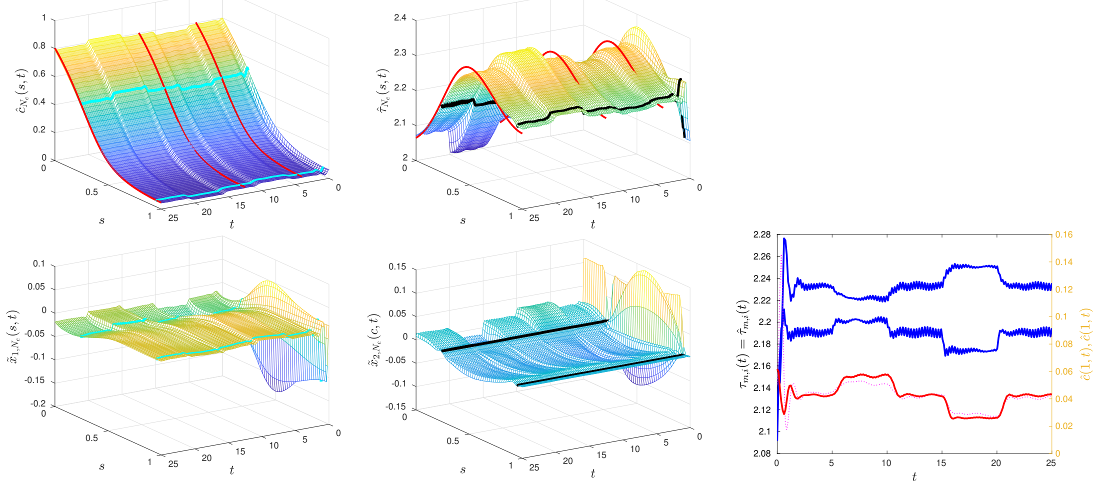

(b) Estimator functioning. Top left: estimated concentration profile $\hat{c}(s,t)$. Top center: estimated temperature profile $\hat{\tau}(s,t)$. Bottom left: estimation error of the concentration profile $\tilde{c}_1(s,t)$. Bottom center: estimation error of the temperature profile $\tilde{\tau}_2(s,t)$. Bottom right: real measured $\tau_{m,i}(t)$, $i = 1,2$ (continuous blue) and regulated $c_o(t)$ (dotted magenta) and their estimates $(\hat{\tau}_{m,i}(t), \hat{c}_o(t))$ (continuous blue and red, respectively).

Figure 5.8: Robust closed-loop control functioning with the 2-MIMO-LIOF-PWO CES.

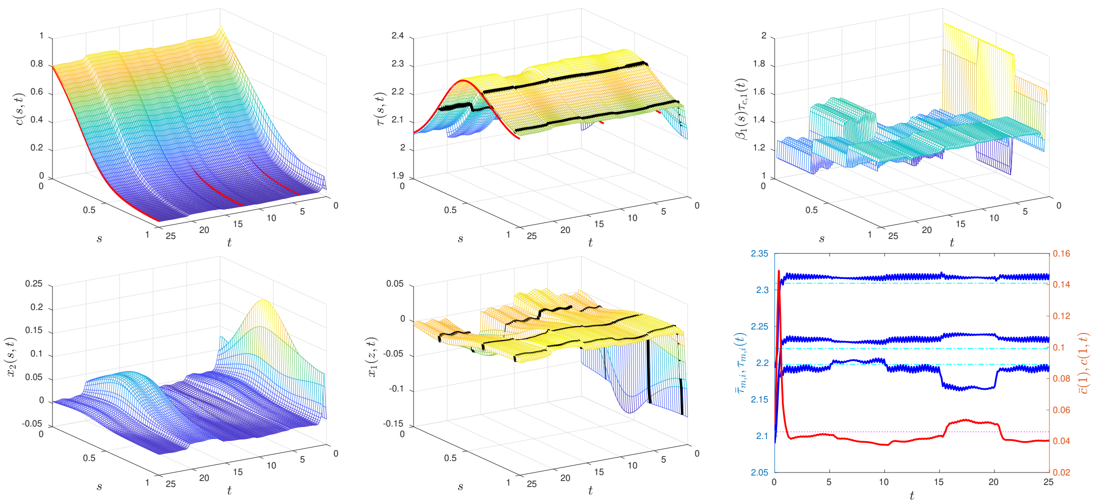

(a) Control functioning. Top left: concentration profile $c(s,t)$. Top center: temperature profile $\tau(s,t)$. Top right: control effort $\sum_{i=1}^{3} \beta_i(s)\tau_{c,i}(t)$. Bottom left: deviated concentration profile $x_1(s,t)$. Bottom center: deviated temperature profile $x_2(s,t)$. Bottom right: measured $\tau_{m,i}(t)$, $i = 1,2,3$ (blue continuous) and regulated $c_o(t)$ (red continuous) outputs and their setpoints (dashed-dotted cyan and dotted magenta, respectively).

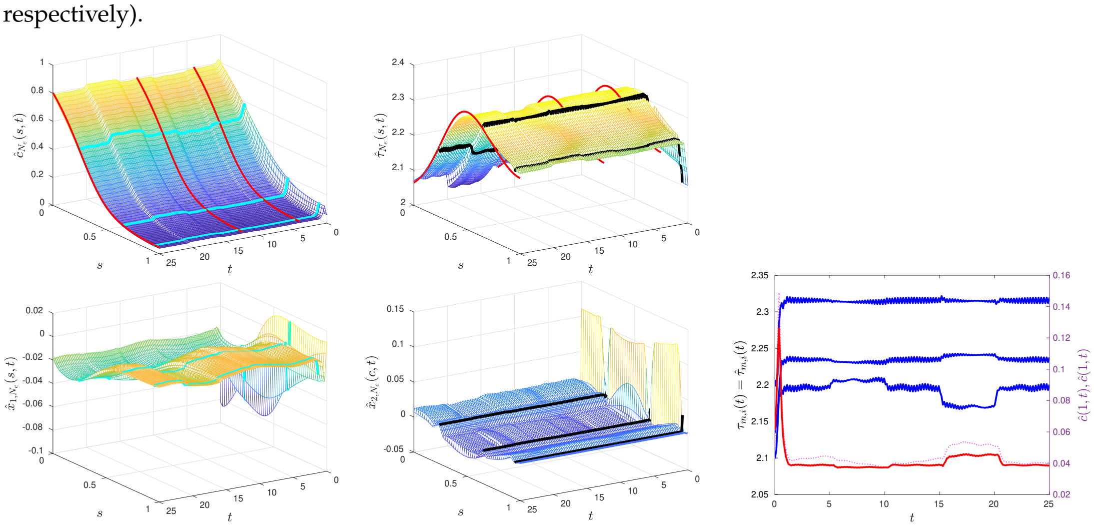

(b) Estimator functioning. Top left: estimated concentration profile $\hat{c}(s,t)$. Top center: estimated temperature profile $\hat{\tau}(s,t)$. Bottom left: estimation error of the concentration profile $\tilde{c}_1(s,t)$. Bottom center: estimation error of the temperature profile $\tilde{\tau}_2(s,t)$. Bottom right: real measured $\tau_{m,i}(t)$, $i = 1,2,3$ (continuous blue) and regulated $c_o(t)$ (dotted magenta) and their estimates $(\hat{\tau}_{m,i}(t), \hat{c}_o(t))$ (continuous blue and red, respectively).

Figure 5.9: Robust closed-loop control functioning with the 3-MIMO-LIOF-PWO CES.

5.7 SUMMARY OF THE LATE LUMPING APPROACH

A MIMO CES, build as an observer-based output feedback controller with linearizing and inventory-like control components has been drawn for a multi-jacket exothermic

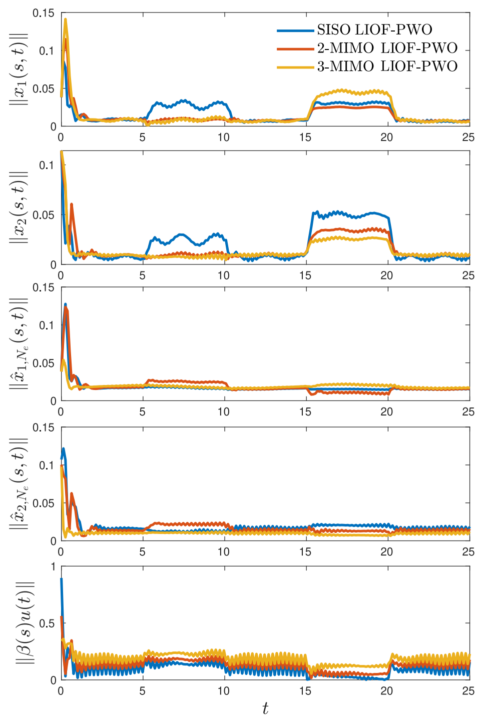

Figure 5.10: Norms of distributed states in deviation, estimation errors and control input for decentralized SISO, 2-MIMO, and 3-MIMO LIOF-PWO CESs.

tubular (possibly open-loop unstable) reactor. The problem has been solved within a constructive framework, by fruitfully combining concepts from chemical reactor engineering, PDE control systems theory, and efficient late lumping. The methodological solution is a pointwise observer-based state feedback stabilizing controller with: (i) the multi-jacket structure as design degree of freedom, (ii) closed-loop stability condition in terms of control gain and MIMO structure, (iii) gain-structure tuning guidelines, and (iv) an efficient late lumping on-line implementation.

The control component of the CES has three components: (i) the first two, that ensure closed-loop stability, are a pointwise driven linearizing controller that compensates nonlinear destabilization by reaction and retains stabilizing effects of heat transport, and (ii) the third one, which underlain by passivity improves functioning versus control effort, resembles a calorimetric industrial control. The proposed approach: (i) systematizes and improves existing designs for single or multi-jacket reactors, and (ii) includes, as key application-oriented ingredient, formal closed-loop stability proofs and efficient late lumping. The design was applied to stabilize the open-loop unstable steady-state of the reactor example of Section 2.5 through numerical simulation.

Part IV

FROM EARLY TO LATE LUMPING AND VICE VERSA

This is an exploratory chapter in which the proposed control-estimation systems, either designed within a early or late lumping approach, are put in perspective between them. This is done by, first, performing a simulation-based comparative study, including comparisons with an additional control-estimation scheme composed by an existing adaptive controller (which produce distributed control action) and a pointwise observer. Then, the extension of the early and late lumping design strategies to their opposites, late or early, is explored in an informal manner. At last, the benefits and advantageous characteristics of the control component of each control-estimation systems are combined to produce an algorithm that have nice characteristics of both approaches.

6 GOING FROM EARLY TO LATE LUMPING AND VICE VERSA

As solutions to the control-estimation problem for a distributed tubular reactor, established in Section 2.3, two different decentralized Multiple Input Multiple Output (MIMO) Control-Estimation System (CES) have been designed: (i) the PI control with AW scheme-Pointwise Observer (PIAW-PWO), and (ii) an the Linear-Inventory-like control-Pointwise Observer (LIOF-PWO). The first system constructed within a early lumping approach and the latter one within a late lumping approach and both employing an efficient lumped model for implantation.

In this chapter, the advantages of each design are highlighted by performing a simulation study where the proposed 3-MIMO CESs with constrained control action are compared with a MIMO CES build as the combination of an existing adaptive constrained controller and the pointwise observer proposed in [111]. Then, the construction of each control-estimation system starting in the opposite lumping approach is explored, i. e., a try to mimic each methodology starting in the opposite, late or early lumping, is studied without establishing formal proofs. Furthermore, alternative methodologies to perform this methodological extension are delineated. At the end of the chapter, both proposed CESs are combined to obtain a new scheme that have the benefits from both approaches, its performance is shown through simulations.

6.1 COMPARISONS WITH ADAPTIVE CONTROL-ESTIMATION SYSTEM

The closed-loop performance of the two proposed 3-MIMO CESs, the early (4.86) and the late (5.50) lumped ones, with constrained control are compared with a 3-MIMO adaptive output feedback controller with constrained distributed control, composed by an adaptive proportional controller [28] and the pointwise observer (5.43).

While the PIAW-PWO is implemented as in (4.86), the control map of the LIOF-PWO is saturated to account for limited control action, i. e., (5.50e) is replaced by

$$\boldsymbol{\tau}_c = \boldsymbol{\mu}_{m,s}(\hat{\chi}_1, \hat{\chi}_2), \quad \boldsymbol{\mu}_{m,s} = \begin{bmatrix} \mathrm{sat}_{\tau_c^-}^{\tau_c^+} \mu_{m,1}(\hat{\chi}_1, \hat{\chi}_2) \\ \vdots \\ \mathrm{sat}_{\tau_c^-}^{\tau_c^+} \mu_{m,q}(\hat{\chi}_1, \hat{\chi}_2) \end{bmatrix},$$

where each entry $\mu_{m,i}$, $i = 1, \ldots, q$ is given in (5.50f). The control limits obtained for the PIAW-PWO (4.86) are inherited to the LIOF-PWO (5.50). No formal proof is given to show that with this control limits avoidance of undesired closed-loop steady-states due to saturation is ensured. Both control-estimation systems are implemented with the efficient model order $n_e = 2N_e = 40$.

The adaptive CES used for comparison purposes is composed by the saturated adaptive controller proposed in [28], a distributed linear proportional state feedback proportional, with nonlinear adaptive gain, driven by an estimate of the distributed temperature obtained from the pointwise observer (5.43) with point temperature measurements. It is worth noting that this adaptive CES requires a jacket with section that can produce distributed control actions, differently from the ones employed in the both proposed CESs that operates with a jacket that produce constant constant control action along space. This may give some advantages to the adaptive scheme.

The Adaptive Output Feedback controller-Pointwise Observer (AOF-PWO) CES is explicit original coordinate (2.9) is given as

$$\partial_t \hat{\chi}_1 = \frac{1}{Pe_m} \partial_{ss} \hat{\chi}_1 - \partial_s \hat{\chi}_1 - r(\hat{\chi}_1, \hat{\chi}_2) \tag{6.1a}$$

$$\partial_t \hat{\chi}_2 = \frac{1}{Pe_h} \partial_{ss} \hat{\chi}_2 - \partial_s \hat{\chi}_2 - \upsilon \hat{\chi}_2 + r(\hat{\chi}_1, \hat{\chi}_2) - \upsilon \boldsymbol{\beta} \boldsymbol{\tau}_c \tag{6.1b}$$

$$\frac{1}{Pe_m} \partial_s \hat{\chi}_1(0,t) = \hat{\chi}_1(0,t) - \chi_{1,e}(t), \qquad \partial_s \hat{\chi}_1(1,t) = 0 \tag{6.1c}$$

$$\frac{1}{Pe_h} \partial_s \hat{\chi}_2(0,t) = \hat{\chi}_2(0,t) - \chi_{2,e}(t), \qquad \partial_s \hat{\chi}_2(1,t) = 0 \tag{6.1d}$$

$$\hat{\chi}_1(s,0) = \hat{\chi}_{10}(s) \tag{6.1e}$$

$$\hat{\chi}_2(s,0) = \hat{\chi}_{20}(s), \tag{6.1f}$$

$$\hat{\chi}_2(\varsigma_i, t) = \tau_{i,q}(t), \quad i = 1, \dots, q, \tag{6.1g}$$

$$\hat{\chi}_z = \hat{\chi}_1(1,t), \tag{6.1h}$$

$$\boldsymbol{\tau}_c = \boldsymbol{\mu}_{a,s}(\hat{\chi}_2), \tag{6.1i}$$

where $\boldsymbol{\mu}_{a,s} = [\mathrm{sat}_{\tau_c^-}^{\tau_c^+} \mu_{a,1} \ \dots \ \mathrm{sat}_{\tau_c^-}^{\tau_c^+} \mu_{a,q}]^T$ and

$$\mu_{a,i}(\hat{\chi}_2) = \bar{\tau}_c - \hbar(t)\vartheta_i(s)(\hat{\chi}_2 - \bar{\chi}_2), \quad \vartheta_i(s) = \begin{cases} 1 & \text{if } s \in \Omega_i \subset \mathscr{R}_i \\ 0 & \text{else} \end{cases}, \tag{6.1j}$$

$$\dot{\hbar}(t) = K_a \begin{cases} \left(\left\| \sum_{i=1}^2 \vartheta_i (\hat{\chi}_2 - \bar{\chi}_2) \right\| - g \right)^{\ell} & \text{if } \left\| \sum_{i=1}^2 \vartheta_i (\hat{\chi}_2 - \bar{\chi}_2) \right\| > g \\ 0 & \text{if } \left\| \sum_{i=1}^2 \vartheta_i (\hat{\chi}_2 - \bar{\chi}_2) \right\| \leq g \end{cases}. \tag{6.1k}$$

where ϑ_i are the actuator characteristic functions, i. e., the spatial domains Ω_i contained in the total domain $\mathscr{R}_i$ of the i-th jacket section, $\hbar$ is an adaptive gain with initial condition $\hbar(0) = \hbar_0$, and g and ℓ are tuning parameters.

Using Finite Differences (FD) approximation and the efficient modeling approach (see Chapter 3), the efficient late lumping implementation of the above controller is

$$\dot{\hat{\chi}}_1 = \boldsymbol{A}_1\hat{\chi}_1 + \boldsymbol{B}_{d,1}\bar{\chi}_{1,e} - \boldsymbol{r}(\hat{\chi}_1, \hat{\chi}_2), \qquad \hat{\chi}_1(0) = \hat{\chi}_{10}, \tag{6.2a}$$

$$\dot{\hat{\chi}}_{2,n} = \boldsymbol{A}_2^{n,n}\hat{\chi}_{2,n} + \boldsymbol{A}_2^{n,m}\hat{\chi}_{2,m} + \boldsymbol{B}_{d,2}^{n}\chi_{2,e} + \boldsymbol{r}_n(\hat{\chi}_1, \hat{\chi}_{2,n}) + \boldsymbol{B}_{u,2}^{n}\boldsymbol{\tau}_c, \ \hat{\chi}_{2,n}(0) = \hat{\chi}_{2,n0}, \tag{6.2b}$$

$$\hat{\chi}_{2,m} = \boldsymbol{\tau}_m, \tag{6.2c}$$

$$\hat{c}_z = \boldsymbol{C}_1\hat{\chi}_1, \quad \hat{\chi}_2 = \boldsymbol{C}_n^T\hat{\chi}_{2,n} + \boldsymbol{C}_{y,2}^T\hat{\chi}_{2,m}, \quad \hat{\chi}_N = \mathcal{I}(\hat{\chi}), \tag{6.2d}$$

$$\boldsymbol{\tau}_c = \boldsymbol{\mu}_{a,s}(\hat{\chi}_1, \hat{\chi}_2) \tag{6.2e}$$

where the state of the finite dimensional observer are given by the sequences $\hat{\chi}_i = [\hat{\chi}_{j,1} \ \dots \ \hat{\chi}_{j,N_e}]^T$, $j = 1, 2$. The entries of the control map $\boldsymbol{\mu}_a$ are

$$\mu_{a,i}(\hat{\chi}_2) = \bar{\tau}_c - \hbar(t)\Theta_i(s_k)(\hat{\chi}_2 - \chi_2), \quad \Theta_i(s_k) = \begin{cases} 1 & \text{if } s_k \in o_i \subset \mathcal{R}_i \\ 0 & \text{else} \end{cases}, \tag{6.2f}$$

$$\dot{\hbar}(t) = K_a \begin{cases} \left(\left\|\sum_{i=1}^{2} \vartheta_i(\hat{\chi}_2 - \bar{\chi}_2)\right\| - g\right)^{\ell} & \text{if } \left\|\sum_{i=1}^{2} \vartheta_i(\hat{\chi}_2 - \bar{\chi}_2)\right\| > g \\ 0 & \text{if } \left\|\sum_{i=1}^{2} \vartheta_i(\hat{\chi}_2 - \bar{\chi}_2)\right\| \leq g \end{cases}. \tag{6.2g}$$

where Θ_i is the discrete spatial actuator characteristic function, o_i the related discrete domain of influence of each actuator, and lumped observer use $N_e = 20$ (37 ODEs).

The AOF-PWO is set with the following actuation domains

$$\Omega_1 = [0.05, 0.3], \quad \Omega_2 = [0.36, 0.6], \quad \Omega_3 = [0.68, 0.9],$$

an the same sensor locations as the proposed PIAW-PWO and LIOF-PWO: $\{\varsigma_1 \approx 0.24, \varsigma_2 \approx 0.62, \varsigma_3 \approx 0.95\}$. The AOF-PWO, PIAW-PWO and LIOF-PWO CESs are tuned and tested with the same robust testing conditions established in Section 5.6.1. The tuning of the AOF-PWO yields the following control parameters and limits

$$K_a = 2, \quad g = 1, \quad \ell = 10, \quad \hbar_0 = 5, \quad \tau_c^- = 0.5, \quad \tau_c^+ = 2.2.$$

Note that the control set, delimited by the above control limits, is wider than the control limits (4.88) used in the two proposed CES. The proposed CES are simulated with the tuning in Section 4.7.2 and Section 5.6.2.

In this comparative study, there are two control objectives: (i) regulation from deviated initial profiles to the target steady-states, and (ii) disturbance rejection for step changes in the inlet temperature. The closed-loop functioning of the three CESs, under robust testing conditions, is presented in Figure 6.1, Figure 6.2 and Figure 6.3, for the PIAW-PWO, LIOF-PWO, and AOF-PWO, respectively. The norms of the distributed controlled and estimated profiles, and the control action are shown in Figure 6.4.

Regarding regulation, it is appreciated that while the LIOF-PWO and AOF-PWO produce faster responses with aggressive control profiles that reach both saturation

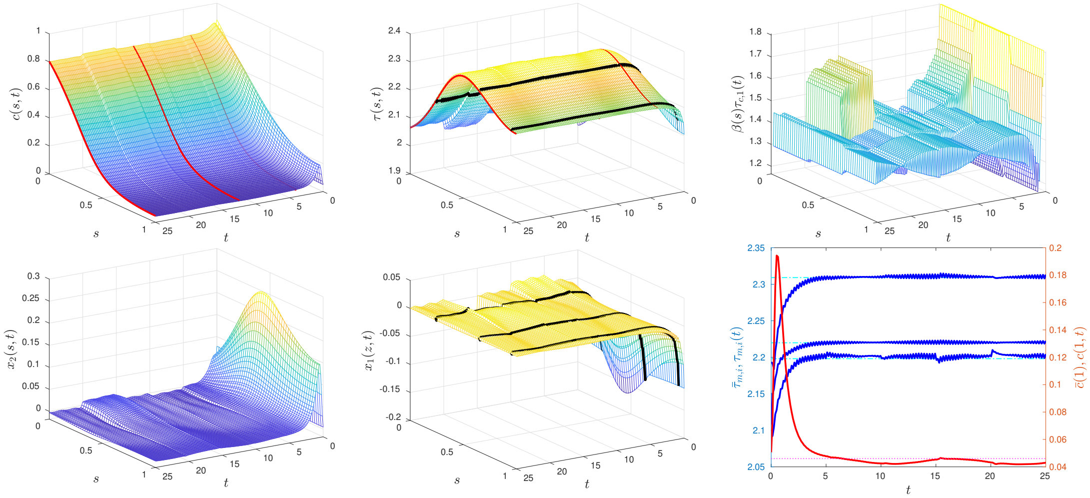

(a) Control functioning. Top left: concentration profile $c(s,t)$. Top center: temperature profile $\tau(s,t)$. Top right: control effort $\sum_{i=1}^{3} \beta_i(s)\tau_{c,i}(t)$. Bottom left: deviated concentration profile $x_1(s,t)$. Bottom center: deviated temperature profile $x_2(s,t)$. Bottom right: measured $\tau_{m,i}$, $i = 1,2,3$ (continuous blue) and regulated $c_o(t)$ (continuous red) outputs and their setpoints (dashed-dotted cyan or dotted magenta, respectively).

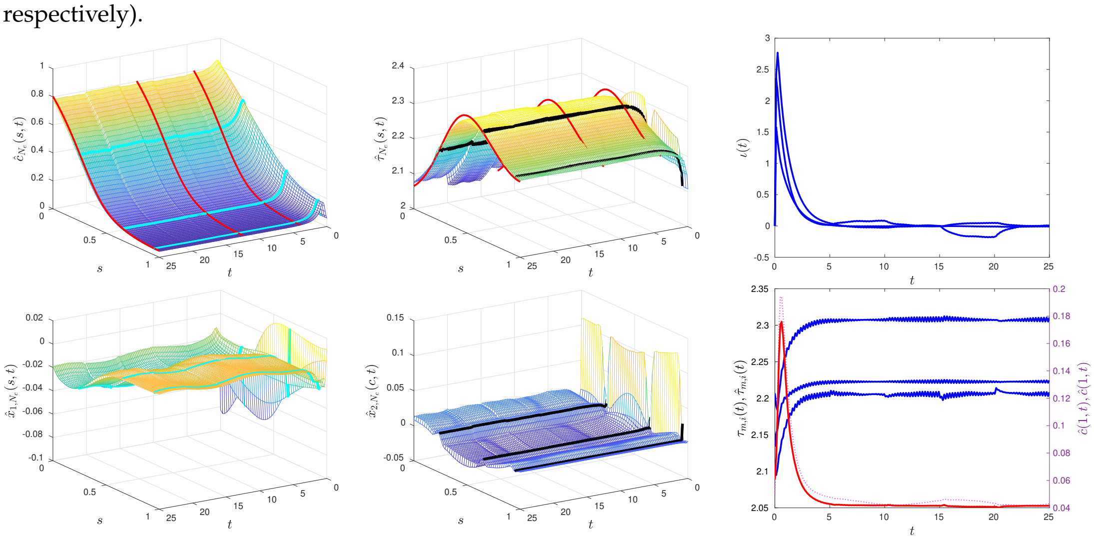

(b) Estimator functioning. Top left: estimated concentration profile $\hat{c}(s,t)$. Top center: estimated temperature profile $\hat{\tau}(s,t)$. Top right: estimated exogenous input $\iota(t)$. Bottom left: estimation error of the concentration profile $\tilde{c}_1(s,t)$. Bottom center: estimation error of the temperature profile $\tilde{\tau}_2(s,t)$. Bottom right: real measured $\tau_{m,i}(t)$, $i = 1,2,3$ (continuous blue) and regulated $c_o(t)$ (dotted magenta) and their estimates $(\hat{\tau}_{m,i}(t), \hat{c}_o(t))$ (continuous blue and red, respectively).

Figure 6.1: Robust closed-loop control functioning with the 3-MIMO PIAW-PWO CES.

limits in the transient behavior, the PIAW-PWO controller produce a smoother and slower control profile that only reaches its upper control limit. In the disturbance rejection task, it can be seen that the three CESs perform well, but the PIAW-PWO

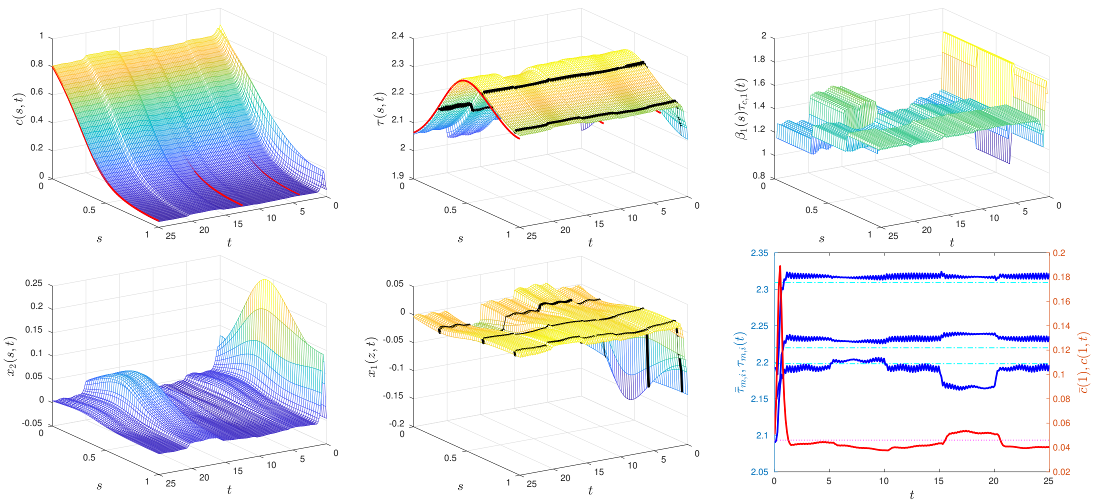

(a) Control functioning. Top left: concentration profile $c(s,t)$. Top center: temperature profile $\tau(s,t)$. Top right: control effort $\sum_{i=1}^{3} \beta_i(s)\tau_{c,i}(t)$. Bottom left: deviated concentration profile $x_1(s,t)$. Bottom center: deviated temperature profile $x_2(s,t)$. Bottom right: measured $\tau_{m,i}(t)$, $i = 1,2,3$ (blue continuous) and regulated $c_o(t)$ (red continuous) outputs and their setpoints (dashed-dotted cyan and dotted magenta, respectively).

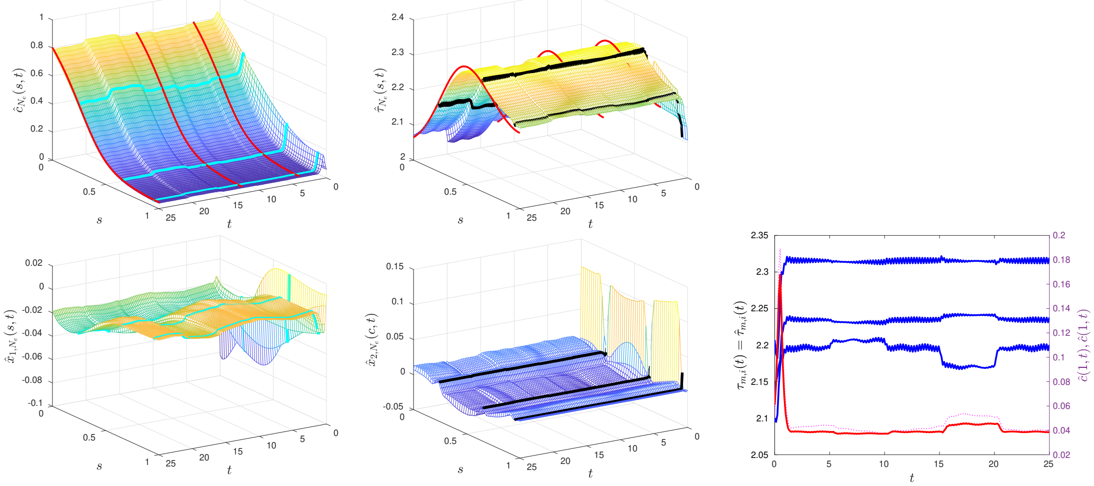

(b) Estimator functioning. Top left: estimated concentration profile $\hat{c}(s,t)$. Top center: estimated temperature profile $\hat{\tau}(s,t)$. Bottom left: estimation error of the concentration profile $\tilde{c}_1(s,t)$. Bottom center: estimation error of the temperature profile $\tilde{\tau}_2(s,t)$. Bottom right: real measured $\tau_{m,i}(t)$, $i = 1,2,3$ (continuous blue) and regulated $c_o(t)$ (dotted magenta) and their estimates $(\hat{\tau}_{m,i}(t), \hat{c}_o(t))$ (continuous blue and red, respectively).

Figure 6.2: Robust closed-loop control functioning with the 3-MIMO LIOF-PWO CES

has the best disturbance rejection capability with a more aggressive control effort that keeps the entire concentration and temperature profiles almost insensible to step disturbances in the inlet concentrations in despite of the presence of noise

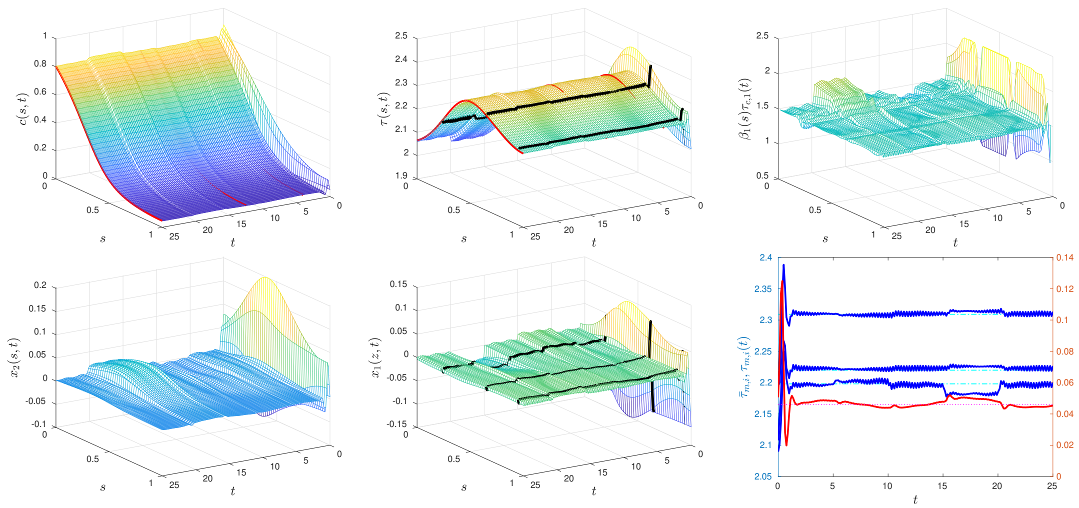

(a) Control functioning. Top left: concentration profile $c(s,t)$. Top center: temperature profile $\tau(s,t)$. Top right: control effort $\sum_{i=1}^{3} \vartheta_i(s)\tau_{c,i}(t)$. Bottom left: deviated concentration profile $x_1(s,t)$. Bottom center: deviated temperature profile $x_2(s,t)$. Bottom right: measured $\tau_{m,i}(t)$, $i = 1,2,3$ (blue continuous) and regulated $c_o(t)$ (red continuous) outputs and their setpoints (dashed-dotted cyan and dotted magenta, respectively).

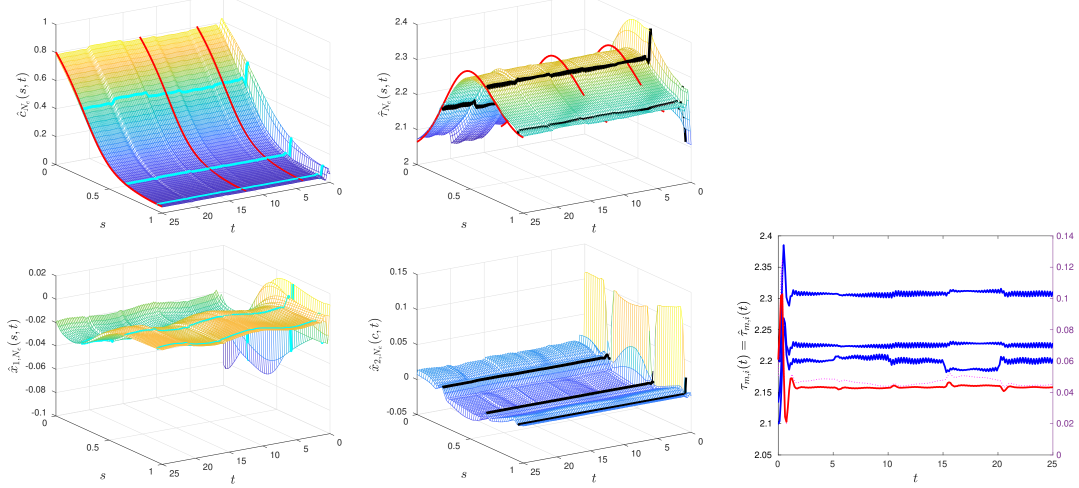

(b) Estimator functioning. Top left: estimated concentration profile $\hat{c}(s,t)$. Top center: estimated temperature profile $\hat{\tau}(s,t)$. Bottom left: estimation error of the concentration profile $\tilde{c}_1(s,t)$. Bottom center: estimation error of the temperature profile $\tilde{\tau}_2(s,t)$. Bottom right: real measured $\tau_{m,i}(t)$, $i = 1,2,3$ (continuous blue) and regulated $c_o(t)$ (dotted magenta) and their estimates $(\hat{\tau}_{m,i}(t), \hat{c}_o(t))$ (continuous blue and red, respectively).

Figure 6.3: Robust closed-loop control functioning with the 3-MIMO AOF-PWO CES

and parameter errors; followed by the AOF-PWO and LIOF-PWO CESs. The estimation performance is almost the same for the three CESs.

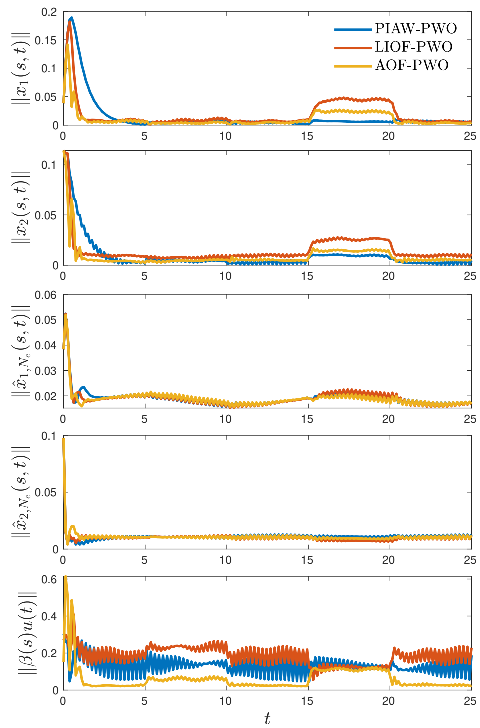

Figure 6.4: Norms of distributed states in deviation, estimation errors and control input for the closed-loop system with the 3-MIMO: PIAW-PWO, LIOF-PWO and AOF-PWO CESs.

Note that the AOF-PWO requires a larger control set to achieve the regulation task, in comparison with the PIAW-PWO and the LIOF-PWO which handle better control constraints. Furthermore, the AOF-PWO CES produce distributed control that have an enhanced stabilizing effect on the temperature dynamics. Also, both PIAW-PWO and LIOF-PWO CESs have an adapting mechanism (the integral action or the adaptive gain) that provide each controller with a better way to confront disturbances, this explains that the LIOF-PWO present some problems in the disturbance rejection task.

In an overall balance, the PIAW-PWO CES has the best performance: adequate regulation from initial profiles, almost perfect disturbance rejection, and good handling of control constraints. All this with a simple industrial control structure: a set of decentralized PI controllers with a decoupled pointwise-like observer for monitoring.

6.2 LATE LUMPING PIAW-PWO CONTROL-ESTIMATION SYSTEM

Here, two issues related to the PIAW-PWO CES (4.86) are explored: (i) how it looks like going from its FD representation to the infinite one, i. e., in the limit when the discretization order goes to infinity and the spatial differences becomes derivatives, and (ii) its design with a similar methodology but within a late lumping approach.

Regarding the first issue, from numerical methods [85], it is known that the solution of a PDE solved by FD approximations, converges to the actual solution of the PDE in the L^2-norm as the discretization mesh becomes infinitesimal. It will be explored, without rigorous mathematical proofs, how this extends to the solution of the CE problem drawn in Chapter 4: the spatial differences in the early lumping model (3.19), in the limit, converges to continuous spatial derivatives.

For the second issue, the methodological ingredients used in the early lumping approach of Chapter 4 (passivity, closed-loop detectability and realization theory) will be used to draw the PIAW-PWO CES (4.86), within a late lumping approach.

6.2.1 *PIAW-PWO control-estimation system from lumped to distributed*

Recall the FD based implementation PIAW-PWO (4.86) over the finite dimensional spatial mesh (3.16), where the distributed state profiles are approximated by the sequences $\chi_{j,k}$, $j = 1, 2$, $k = 1, \ldots, N$ given in (3.17a). The first and second spatial derivatives are approximated with FD as in (3.17b). In the limit, when $N \to \infty$ and $\Delta s \to 0$, the discretization mesh becomes the spatial domain $(0, 1)$, this is

$$N \to \infty \;\Rightarrow\; \Delta_s \to 0 \;\Rightarrow\; \mathcal{S} = \left[\frac{1}{\Delta s}, \frac{N}{\Delta s}\right] \to (0,1), \quad \chi_{k,j}(t) = \chi_j(s_j, t) \to \chi_j(s,t).$$

Following the same reasoning, it follows that

$$\begin{aligned} N \to \infty \;\Rightarrow\; \Delta_s \to 0 \;\Rightarrow\; & \frac{\chi_{j,k}(t) - \chi_{j,k-1}(t)}{\Delta s} \to \partial_s \chi_j(s,t), \\ & \frac{\chi_{j,k+1}(t) - 2\chi_{j,k}(t) + \chi_{j,k-1}(t)}{\Delta s^2} \to \partial_s^2 \chi_j(s,t). \end{aligned}$$

Thus, when $N \to \infty$, the lumped model (3.22) becomes the PDE one (2.7). Consequently, the distributed version of the CES (4.86) becomes

$$\partial_t \hat{\chi}_1 = \frac{1}{Pe_m} \partial_{ss} \hat{\chi}_1 - \partial_s \hat{\chi}_1 - r(\hat{\chi}_1, \hat{\chi}_2) \tag{6.3a}$$

$$\partial_t \hat{\chi}_2 = \frac{1}{Pe_h} \partial_{ss} \hat{\chi}_2 - \partial_s \hat{\chi}_2 - v\hat{\chi}_2 + r(\hat{\chi}_1, \hat{\chi}_2) - v\boldsymbol{\beta}\boldsymbol{\tau}_c \tag{6.3b}$$

$$\frac{1}{Pe_m} \partial_s \hat{\chi}_1(0,t) = \hat{\chi}_1(0,t) - \chi_{1,e}(t), \qquad \partial_s \hat{\chi}_1(1,t) = 0 \tag{6.3c}$$

$$\frac{1}{Pe_h} \partial_s \hat{\chi}_2(0,t) = \hat{\chi}_2(0,t) - \chi_{2,e}(t), \qquad \partial_s \hat{\chi}_2(1,t) = 0 \tag{6.3d}$$

$$\hat{\chi}_1(s,0) = \hat{\chi}_{10}(s) \tag{6.3e}$$

$$\hat{\chi}_2(s,0) = \hat{\chi}_{20}(s), \tag{6.3f}$$

$$\hat{\chi}_2(\varsigma_i, t) = \tau_{m,i}(t), \quad i = 1 \ldots, q, \tag{6.3g}$$

$$\hat{\chi}_z = \hat{\chi}_1(1,t), \tag{6.3h}$$

$$\boldsymbol{\tau}_c = \boldsymbol{\mu}_{s,pi}(\boldsymbol{\tau}_m), \tag{6.3i}$$

where the entries of the control map (6.3i) are given in (4.86f).

The above distributed PIAW-PWO CES is composed by a set of decentralized PIAWs that use the measurements of the distributed tubular model, and the distributed pointwise observer (5.43). In what follows, it will be explored if the methodology employed in Chapter 4 translated into a late lumping approach, yields a similar CES as (6.3) and a similar implementation as the one in (4.86).

6.2.2 *PIAW-PWO control-estimation system in distributed form: a late lumping approach*

The tree methodological steps of the early lumping approach in Chapter 4 were: (i) set a passive state feedback control based on a minimum phase property, (ii) build an observer-based output feedback control driven by a closed-loop detectability property, and (iii) the PIAW-PWO implementation enabled by model redesign. The extension to a late lumping setting of these methodological steps is explored next.

For the purpose at hand, on the basis of the PDE model (5.2), the requirements for the construction of a passive state feedback controller are: (i) that the characteristic index is a vector with one entries, and (ii) the related zero dynamics is exponentially stable. The first requirement was established in Lemma 5.1, and it is always satisfied for the tubular reactor class since the heat exchange between the jacket and the reactor is enabled by design. The stability of the zero dynamics is briefly analyzed next.

6.2.2.1 *Distributed partitioned dynamics*

The partition of the state into unmeasured-measured temperature shown to be useful in Chapter 4, a similar partition in the distributed model (5.2) is given next.

Recall that for technical purposes the output operators $\mathcal{C}_y$, defined with Dirac delta functions, is replaced with its approximation $\mathcal{C}_y$. Accordingly, the measurement locations ς_i, $i = 1, \dots, q$ split the reactor into $q + q + 1$ consecutive intervals: the $q + 1$ intervals $\mathcal{I}_{n,j}$ where the temperature is not measured, and the q intervals $\mathcal{I}_{m,i}$ where the averaged temperature is measured,:

$$\mathcal{I}_{n,1} = [0, \varsigma_1 - \epsilon], \dots, \mathcal{I}_{n,j} = (\varsigma_{j-1} + \epsilon, \varsigma_j + \epsilon], \mathcal{I}_{n,q+1} = (\varsigma_q + \epsilon, 1], \tag{6.4a}$$

$$\mathcal{I}_{m,i} = [\varsigma_i - \epsilon, \varsigma_i + \epsilon], \quad j = 1, \dots, q, \quad i = 1, \dots, q. \tag{6.4b}$$

Each interval has the following characteristic function

$$\Omega_{n,j}(s) = \begin{cases} 1, & s \in \mathcal{I}_{n,j} \\ 0, & \text{else} \end{cases}, \quad \Omega_{m,i}(s) = \begin{cases} 1, & s \in \mathcal{I}_{m,i} \\ 0, & \text{else} \end{cases}, \tag{6.4c}$$

for $j = 1, \dots, q + 1$ and $i = 1, \dots, q$. Imposing an inhomogenous Dirichlet type boundary condition at each measurement location, the dynamics of the tubular reactor can be split into $q + 1$ unmeasured temperatures $x_{2,n,j}(s, t)$ for $s \in \mathcal{I}_{n,j}$, $j = 1 \dots, q + 1$, and q measured ones $x_{2,n,j}(s,t)$ for $s \in \mathcal{I}_{m,i}$, $i = 1\dots,q$. Accordingly, the actual temperature state at a given location $s \in [0,1]$ can be determined by means of the characteristic functions (6.4):

$$x_2 = \boldsymbol{\Omega}_n \boldsymbol{x}_{2,n} + \boldsymbol{\Omega}_m \boldsymbol{x}_{2,m} = \sum_{j=1}^{q+1} \Omega_{n,j} x_{2,j} + \sum_{i=1}^{q} \Omega_{m,i} x_{2,i}$$

where $\boldsymbol{\Omega}_n = [\Omega_{n,1} \dots \Omega_{n,q+1}]$, $\boldsymbol{\Omega}_m = [\Omega_{m,1} \dots \Omega_{m,q}]$, and

$$\boldsymbol{x}_{2,n} = \begin{bmatrix} x_{2,n,1} & \dots & x_{2,n,q+1} \end{bmatrix}^T, \quad \boldsymbol{x}_{2,n} = \begin{bmatrix} x_{2,m,1} & \dots & x_{2,m,q} \end{bmatrix}^T.$$

where $\boldsymbol{x}_{2,n}$ is the unmeasured temperature profile state, and the measured one is $\boldsymbol{x}_{2,m}$.

With this representation, the tubular reactor model can be written as

$$\dot{x}_1 = \mathcal{A}_1 x_1 - \rho_1(x_1, x_2), \qquad x_1(0) = x_{10}, \tag{6.5a}$$
$$\dot{\boldsymbol{x}}_{2,n} = \boldsymbol{\mathcal{A}}_{2,n} \boldsymbol{x}_{2,n} + \boldsymbol{\rho}_{2,n}(x_1, \boldsymbol{x}_{2,n}) + \boldsymbol{\mathcal{B}}_u^n \boldsymbol{u}, \qquad \boldsymbol{x}_{2,n}(0) = \boldsymbol{x}_{2,n0}, \tag{6.5b}$$
$$\dot{\boldsymbol{x}}_{2,m} = \boldsymbol{\mathcal{A}}_{2,m} \boldsymbol{x}_{2,m} + \boldsymbol{\rho}_{2,m}(x_1, \boldsymbol{x}_{2,m}) + \boldsymbol{\mathcal{B}}_u^m \boldsymbol{u}, \qquad \boldsymbol{x}_{2,m}(0) = \boldsymbol{x}_{2,m0}, \tag{6.5c}$$
$$x_2 = \boldsymbol{\Omega}_n \boldsymbol{x}_{2,n} + \boldsymbol{\Omega}_m \boldsymbol{x}_{2,m}, \tag{6.5d}$$
$$\boldsymbol{y} = \boldsymbol{\mathcal{C}}_y^m \boldsymbol{x}_{2,m}, \quad \boldsymbol{y} = \boldsymbol{\mathcal{C}}_y^m \boldsymbol{x}_{2,m}, \quad z = \mathcal{C}_z x_1, \tag{6.5e}$$

where the operators $\boldsymbol{\mathcal{A}}_{2,n}$, $\boldsymbol{\mathcal{A}}_{2,m}$, $\boldsymbol{\mathcal{B}}_u^n$, $\boldsymbol{\mathcal{B}}_u^m$, $\boldsymbol{\mathcal{C}}_y^m$ and $\boldsymbol{\mathcal{C}}_y^m$ are defined as follows:

$$\boldsymbol{\mathcal{A}}_{2,n} \boldsymbol{x}_{2,n} = \begin{bmatrix} \mathcal{A}_{n,1} x_{2,n,1} & & \\ & \ddots & \\ & & \mathcal{A}_{n,q+1} x_{2,n,q+1} \end{bmatrix}, \ \boldsymbol{\mathcal{A}}_{2,m} \boldsymbol{x}_{2,m} = \begin{bmatrix} \mathcal{A}_{m,1} x_{2,m,1} & & \\ & \ddots & \\ & & \mathcal{A}_{m,q} x_{2,m,q} \end{bmatrix}$$

where each unmeasured or measured temperature operator is given as

$$\mathcal{A}_{n,j} x_{2,n,j} = \partial_s^2 x_{2,n,j} - \left(\frac{Pe_h}{4} + v \right) x_{2,n,j}, \quad \mathcal{D}_{n,j}(\mathcal{A}_{2,j}) = \{ f \in H^2 \,|\, \mathscr{B}_{m,j} x_{2,n,j} = \mathbf{0} \},$$
$$\mathcal{A}_{m,i} x_{2,m,i} = \partial_s^2 x_{2,m,i} - \left(\frac{Pe_h}{4} + v \right) x_{2,m,i}, \quad \mathcal{D}_{m,i}(\mathcal{A}_{2,i}) = \{ f \in H^2 \,|\, \mathscr{B}_{n,i} x_{2,m,i} = \mathbf{0} \},$$

for $j = 1, \dots, q+1$ and $i = 1, \dots, q$. The domains $\mathcal{D}_{n,j}$ of the unmeasured temperature intervals are given in terms the following boundary conditions:

$$\mathscr{B}_{n,1} x_{2,n,1} = \begin{bmatrix} \frac{1}{Pe_h} \partial_s x_{2,n,1}(0,t) - \frac{1}{2} x_{2,n,1}(0,t) \\ x_{2,n,1}(\varsigma_1 - \epsilon, t) - x_{2,m,1}(\varsigma_1 - \epsilon, t) \end{bmatrix},$$
$$\mathscr{B}_{n,j} x_{2,n,j} = \begin{bmatrix} x_{2,n,j}(\varsigma_{j-1} + \epsilon, t) - x_{2,m,i}(\varsigma_i + \epsilon, t) \\ x_{2,n,j}(\varsigma_j - \epsilon, t) - x_{2,m,i}(\varsigma_{i+1} - \epsilon, t) \end{bmatrix}, \quad j = 2 \dots q,$$
$$\mathscr{B}_{n,q+1} x_{2,n,q+1} = \begin{bmatrix} x_{2,n,q}(\varsigma_q + \epsilon, t) - x_{2,m,q}(\varsigma_q + \epsilon, t), \\ \frac{1}{Pe_h} \partial_s x_{2,n,q+1}(1,t) + \frac{1}{2} x_{2,n,q+1}(1,t) \end{bmatrix}.$$

The domains $\mathcal{D}_{m,i}$ of the measured temperature intervals are given in terms the following boundary conditions:

$$\mathscr{B}_{m,i}x_{2,m,i} = \begin{bmatrix} x_{2,n,1}(\varsigma_i - \epsilon, t), \\ x_{2,n,1}(\varsigma_i + \epsilon, t) \end{bmatrix}, \quad i = 1, \dots, q.$$

Note that the above boundary conditions are the measured temperatures at the extremes of the intervals $\mathcal{I}_m$ (6.4b). The input operators for the unmeasured temperature are defined as

$$\boldsymbol{\mathcal{B}}_u^n \boldsymbol{u} = \begin{bmatrix} v\Omega_{n,1}\omega_h \boldsymbol{\beta u} \\ \vdots \\ v\Omega_{n,j}\omega_h \boldsymbol{\beta u} \\ \vdots \\ v\Omega_{n,q+1}\omega_h \boldsymbol{\beta u} \end{bmatrix} = \begin{bmatrix} v\Omega_{n,1}\omega_h \sum_{i=1}^q \beta_i u_i \\ \vdots \\ v\Omega_{n,j}\omega_h \sum_{i=1}^q \beta_i u_i \\ \vdots \\ v\Omega_{n,q+}\omega_h \sum_{i=1}^q \beta_i u_i \end{bmatrix} = v \begin{bmatrix} \omega_h \Omega_{n,1}\beta_1 u_1 \\ \vdots \\ \omega_h \sum_{i=j-1}^{j} \Omega_{n,1}\beta_i u_i \\ \vdots \\ \omega_h \Omega_{q+1,1}\beta_q u_q \end{bmatrix}.$$

While the input operators for the measured temperature are

$$\boldsymbol{\mathcal{B}}_u^m \boldsymbol{u} = \begin{bmatrix} v\Omega_{m,1}\omega_h \boldsymbol{\beta u} \\ \vdots \\ v\Omega_{m,q}\omega_h \boldsymbol{\beta u} \end{bmatrix} = \begin{bmatrix} v\Omega_{m,1}\omega_h \sum_{i=1}^q \beta_i u_i \\ \vdots \\ v\Omega_{m,q}\omega_h \sum_{i=1}^q \beta_i u_i \end{bmatrix} = v \begin{bmatrix} v\omega_h \Omega_{m,1}\beta_1 u_1 \\ \vdots \\ v\omega_h \Omega_{m,q}\beta_q u_q \end{bmatrix}.$$

The output operators are

$$\boldsymbol{\mathcal{C}}_y^m \boldsymbol{x}_{2,m} = \begin{bmatrix} \left\langle \gamma_1(s), \omega_h^{-1} x_{2,m,1} \right\rangle \\ \vdots \\ \left\langle \gamma_1(s), \omega_h^{-1} x_{2,m,q} \right\rangle \end{bmatrix}, \qquad \boldsymbol{\mathcal{C}}_y^m \boldsymbol{x}_{2,m} = \begin{bmatrix} \left\langle \delta(s - \varsigma_1), \omega_h^{-1} x_{2,m,1} \right\rangle \\ \vdots \\ \left\langle \delta(s - \varsigma_q), \omega_h^{-1} x_{2,m,q} \right\rangle \end{bmatrix}.$$

Finally, the nonlinear reaction rate functions are

$$\boldsymbol{\rho}_{2,n} = \begin{bmatrix} \rho_2(x_1, x_{2,n,1}) \\ \vdots \\ \rho_2(x_1, x_{2,n,q+1}) \end{bmatrix}, \quad \boldsymbol{\rho}_{2,m} = \begin{bmatrix} \rho_2(x_1, x_{2,m,1}) \\ \vdots \\ \rho_2(x_1, x_{2,m,q}) \end{bmatrix}.$$

Note that in the above model, when $\epsilon \to 0$, the point-like output $\boldsymbol{y}$ becomes the point measurement $\boldsymbol{y}$, and the measured state dynamics becomes pointwise also.

6.2.2.2 *Distributed zero dynamics*

The first time-derivative of the point or point-like output is given by

$$\begin{aligned} \dot{\boldsymbol{y}} &= \boldsymbol{\mathcal{C}}_y \dot{\boldsymbol{x}}_{2,m}, \\ &= \boldsymbol{\mathcal{C}}_y \left(\boldsymbol{\mathcal{A}}_{2,m}\boldsymbol{x}_{2,m} + \boldsymbol{\rho}_{2,m}(x_1, \boldsymbol{x}_{2,m}) + \boldsymbol{\mathcal{B}}_u^m \boldsymbol{u} \right), \\ &= \boldsymbol{\mathcal{C}}_y \boldsymbol{\mathcal{A}}_{2,m}\boldsymbol{x}_{2,m} + \boldsymbol{\mathcal{C}}_y \boldsymbol{\rho}_{2,m}(x_1, \boldsymbol{x}_{2,m}) + \boldsymbol{\mathcal{C}}_y \boldsymbol{\mathcal{B}}_u^m \boldsymbol{u}. \end{aligned}$$

As a consequence of Lemma 5.1, it is known that

$$\boldsymbol{\mathcal{C}}_y \boldsymbol{\mathcal{B}}_u^m := \boldsymbol{B}_m = v \boldsymbol{I}_{q \times q},$$

and thus, a control law that impose the zero dynamics condition $\boldsymbol{y} = \mathbf{0}$ is given by

$$\boldsymbol{u} = \boldsymbol{\mu}_{z,2}(x_1), \tag{6.6a}$$

where

$$\boldsymbol{\mu}_{z,2}(x_1, \mathbf{0}), \quad \boldsymbol{\mu}_{z,2}(x_1, \boldsymbol{x}_{2,m}) = -\boldsymbol{B}_m{}^{-1} \left(\boldsymbol{\mathcal{C}}_y \boldsymbol{\mathcal{A}}_{2,m} \boldsymbol{x}_{2,m} + \boldsymbol{\mathcal{C}}_y \boldsymbol{\rho}_{2,m}(x_1, \boldsymbol{x}_{2,m}) \right). \tag{6.6b}$$

The application of the above controller to (6.5) yields the zero dynamics

$$\begin{aligned}
\dot{x}_1 &= \mathcal{A}_1 x_1 - \rho_1(x_1, x_2), & x_1(0) &= x_{10}, \qquad (6.7a)\\
\dot{\boldsymbol{x}}_{2,n} &= \boldsymbol{\mathcal{A}}_{2,n}^z \boldsymbol{x}_{2,n} + \boldsymbol{\rho}_{2,z}(x_1, \boldsymbol{x}_{2,n}), & \boldsymbol{x}_{2,n}(0) &= \boldsymbol{x}_{2,n0}, \qquad (6.7b)\\
\boldsymbol{x}_2 &= \boldsymbol{\Omega}_n \boldsymbol{x}_{2,n} + \boldsymbol{\Omega}_m \mathbf{0}, & & \qquad (6.7c)\\
\boldsymbol{y} &= \mathbf{0}, \quad \boldsymbol{y} = \mathbf{0}, \quad z = \mathcal{C}_z x_1, & & \qquad (6.7d)
\end{aligned}$$

where the zero dynamics operator $\boldsymbol{\mathcal{A}}_{2,z}$ is given by

$$\boldsymbol{\mathcal{A}}_{2,n} \boldsymbol{x}_{2,n} = \begin{bmatrix} \mathcal{A}_{n,1}^z x_{2,n,1} & & \\ & \ddots & \\ & & \mathcal{A}_{n,q+1}^z x_{2,n,q+1} \end{bmatrix}, \tag{6.7e}$$

with entries defined as

$$\mathcal{A}_{n,j}^z x_{2,n,j} = \partial_s^2 x_{2,n,j} - \left(\frac{Pe_h}{4} + v \right) x_{2,n,j}, \quad \mathcal{D}_{z,j}(\mathcal{A}_{n,j}^z) = \{ f \in H^2 \,|\, \mathscr{B}_{n,j}^z x_{2,j} = \mathbf{0} \}, \tag{6.7f}$$

for $j = 1, \dots, q+1$. The domains $\mathcal{D}_{z,j}$ of the unmeasured temperature intervals are given in terms the following boundary conditions:

$$\mathscr{B}_{n,1}^z x_{2,n,1} = \begin{bmatrix} \frac{1}{Pe_h} \partial_s x_{2,n,1}(0,t) - \frac{1}{2} x_{2,n,1}(0,t) \\ x_{2,n,1}(\varsigma_1 - \epsilon, t) \end{bmatrix}, \tag{6.8}$$

$$\mathscr{B}_{n,j}^z x_{2,n,j} = \begin{bmatrix} x_{2,n,j}(\varsigma_{j-1} + \epsilon, t), \\ x_{2,n,j}(\varsigma_j - \epsilon, t) \end{bmatrix}, \quad j = 2 \dots q, \tag{6.9}$$

$$\mathscr{B}_{n,q+1}^z x_{2,n,q+1} = \begin{bmatrix} x_{2,n,q+1}(\varsigma_q + \epsilon, t), \\ \frac{1}{Pe_h} \partial_s x_{2,n,q+1}(1,t) + \frac{1}{2} x_{2,n,q+1}(1,t) \end{bmatrix}. \tag{6.10}$$

The zero dynamics nonlinearity is $\boldsymbol{\rho}_{2,z}$ is

$$\boldsymbol{\rho}_{2,z}(x_1, \boldsymbol{x}_{2,n}) = \boldsymbol{\rho}_{2,n}(x_1, \boldsymbol{x}_{2,n}) - \boldsymbol{\mathcal{B}}^{n}_{2,u}\frac{1}{v}\boldsymbol{I}_{q\times q}\boldsymbol{\mathcal{C}}_y\boldsymbol{\rho}_{2,m}(x_1, \mathbf{0}),$$

$$= \begin{bmatrix} \rho_2(x_1, x_{2,n,1}) \\ \vdots \\ \rho_2(x_1, x_{2,n,j}) \\ \vdots \\ \rho_2(x_1, x_{2,n,q+1}) \end{bmatrix} - \frac{1}{v}\begin{bmatrix} \omega_h\Omega_{n,1}\beta_1\left\langle \gamma_1, \omega_h^{-1}\rho_{2,m,1}(x_1,0)\right\rangle \\ \vdots \\ \omega_h\sum_{i=j-1}^{j}\Omega_{n,j}\beta_i\left\langle \gamma_i, \omega_h^{-1}\rho_{2,m,i}(x_1,0)\right\rangle \\ \vdots \\ \omega_h\Omega_{n,q+1}\beta_q\left\langle \gamma_q, \omega_h^{-1}\rho_{2,m,q}(x_1,0)\right\rangle \end{bmatrix}.$$

This modified nonlinearity may have a smaller Lipschitz constant with respect to x_1, and this may enhance the stability of the zero dynamics, as it will be seen later.

For control design purposes, it is required that the zero dynamics (6.7) has the origin as unique exponentially stable steady-state. The related statics are

$$0 = \mathcal{A}_1 x_1 - \varrho(x_1) - \varrho_{12}(x_1, x_2), \tag{6.11a}$$

$$\mathbf{0} = \boldsymbol{\mathcal{A}}^{z}_{2,n}\boldsymbol{x}_{2,n} + \boldsymbol{\rho}_{2,z}(x_1, \boldsymbol{x}_{2,n}), \tag{6.11b}$$

$$\boldsymbol{x}_2 = \boldsymbol{\Omega}_n\boldsymbol{x}_{2,n} + \boldsymbol{\Omega}_m\mathbf{0}, \tag{6.11c}$$

$$\boldsymbol{y} = \mathbf{0}, \quad \boldsymbol{y} = \mathbf{0}, \quad 0 = \mathcal{C}_z x_1. \tag{6.11d}$$

The above static equations is a boundary value problem that depends on the sensor location set ς. A similar procedure as in Section 4.3.3 can be used: the case of a unique sensor location may be considered to find out which is the set in which the zero dynamics statics has the origin as unique steady-state. From Section 4.3.3.2 and Section 5.3.3.2, the recommended location for the first sensor is $\varsigma_1 \approx 0.24$.

To characterize the exponential stability, the Lur'e structure of the zero dynamics is exploited: first stability of the linear part is studied, then the interconnection between linear and nonlinear components are studied and finally the interconnection of mass and heat balances is analyzed to find conditions for exponential stability.

Lemma 6.1. *Characterization of the zero dynamics operators $\mathcal{A}^{z}_{n,j}$. Proof in Section h.1 Consider the distributed zero dynamics (6.7), if $\epsilon \to 0$, then $\boldsymbol{\mathcal{C}}_y \to \boldsymbol{\mathcal{C}}_y$ and $\boldsymbol{y} = \boldsymbol{y}$. Furthermore, the boundary conditions (6.8) shift to the sensor locations ς_i, i. e.,*

$$\mathscr{B}^{z}_{n,1}x_{2,n,1} = \begin{bmatrix} \frac{1}{Pe_h}\partial_s x_{2,n,1}(0,t) - \frac{1}{2}x_{2,n,1}(0,t) \\ x_{2,n,1}(\varsigma_1, t) \end{bmatrix}, \tag{6.12a}$$

$$\mathscr{B}^{z}_{n,j}x_{2,n,j} = \begin{bmatrix} x_{2,n,j}(\varsigma_{j-1}, t), \\ x_{2,n,j}(\varsigma_j, t) \end{bmatrix}, \quad j = 2\ldots q, \tag{6.12b}$$

$$\mathscr{B}^{z}_{n,q+1}x_{2,n,q+1} = \begin{bmatrix} x_{2,n,q+1}(\varsigma_q, t), \\ \frac{1}{Pe_h}\partial_s x_{2,n,q+1}(1,t) + \frac{1}{2}x_{2,n,q+1}(1,t) \end{bmatrix}. \tag{6.12c}$$

Thus, the zero dynamics operators $A^z_{n,j}$ in (6.7e) have the following eigenvalues and eigenfunctions

$$\phi_{2,1,n}(s) = B_{2,1,n}\left(\frac{2\omega_{2,1,1n}}{Pe_h\varsigma_1}\cos\left(\omega_{2,1,n}\frac{s}{\varsigma_1}\right) + \sin\left(\omega_{2,1,n}\frac{s}{\varsigma_1}\right)\right), \tag{6.13a}$$

$$\phi_{2,j,l}(s) = B_{2,j,n}\sin\left(\omega_{2,j,n}\frac{s-\varsigma_{j-1}}{\varsigma_j-\varsigma_{j-1}}\right), \quad j=2,\ldots,q, \tag{6.13b}$$

$$\phi_{2,q+1,n}(s) = B_{2,q+1,n}\sin\left(\omega_{2,j+1,n}\frac{s-\varsigma_q}{1-\varsigma_q}\right), \tag{6.13c}$$

for $n \in \mathbb{N}$ with normalization constants $B_{2,j,n}$ and eigenfrequencies $\omega_{2,j,n}$ given as the solution of the implicit algebraic equations

$$\tan(\omega_{2,1,n}) = -\frac{2\omega_{2,1,n}}{Pe_h\varsigma_1}, \quad \omega_{2,1,l} \neq 0, \quad s \in [0, \varsigma_1], \tag{6.13d}$$

$$\tan(\omega_{2,j,n}) = j\pi, \quad j = 2,\ldots,q, \quad s \in [\sigma_{j-1} - \varsigma_j], \tag{6.13e}$$

$$\tan(\omega_{2,q+1,n}) = -\frac{2\omega_{2,q+1,n}}{Pe_h(1-\varsigma_q)}, \quad \omega_{2,1,n} \neq 0, \quad s \in [\varsigma_q, 1], \tag{6.13f}$$

for $n \in \mathcal{N}$. The associated eigenvalues are given by

$$\lambda_{2,j,n} = -\frac{Pe_h}{4} - v - \frac{\omega^2_{2,j,n}}{(\varsigma_i - \varsigma_{i-1})^2}, \quad j = 1\ldots,q+1, \quad n \in \mathbb{N}. \tag{6.13g}$$

As a consequence of the above lemma, since the operators $\mathcal{A}^z_{2,n}$ are infinitesimal generators of C_0-semigroups of contractions S_j, $j = 1,\ldots,q+1$, and given that the determined growth assumption [38] holds, the following expression is satisfied for each temperature component

$$\left\|S_j(t)\right\|_{\mathfrak{D}} \leq \mathrm{e}^{-\lambda^*_{2,j}t}, \quad -\lambda^*_{2,j} = \sup_{\lambda_{2,j,n}\in\sigma(\mathcal{A}^z_{n,j})}\{\lambda_{2,j,n}\}, \quad j = 1,\ldots,q+1, \quad n \in \mathbb{N}. \tag{6.14}$$

Furthermore, note that the spectrum of the operators $\mathcal{A}^z_{2,n}$ can be shifted to the left in the complex plane by selecting an adequate number of sensors and their locations. This having the effect of accelerating the convergence to zero of the above defined C_0-semigroups.

Using the previous fact, together with the entry wise Lipschitz constants related to the bounding condition

$$\left\|\rho_{2,z,j}\right\| \leq L^{\rho_{2,z,j}}_{x_1}\left\|x_1\right\| + L^{\rho_{2,z,j}}_{x_{2,n,j}}\left\|x_{2,n,j}\right\|, \quad j = 1,\ldots q+1 \tag{6.15}$$

and the consideration of the concentration bound (5.11), the exponential stability of the zero dynamics can be assured. This is established in the following proposition.

Proposition 6.1. *Exponential stability of the zero dynamics* (6.6). *Proof in Section h.2 Consider the distributed zero dynamics* (6.7), *assume that the sensor location set* ς *has been chosen so that the origin is the unique steady-state. Furthermore, assume Lemma 6.1 is satisfied together with the spectrum determined growth assumption for the operators* $\mathcal{A}^z_{2,n}$, *and the Lipschitz bounding conditions in* (6.15). *Thus, if the following conditions are met*

$$\nu_{2,1} = \frac{Pe_h}{4} + v + \frac{\omega_{2,1,1}}{\varsigma_1} - L^{\rho_{2,z,1}}_{x_{2,n,1}} > 0, \tag{6.16a}$$

$$\nu_{2,j} = \frac{Pe_h}{4} + v + \frac{\pi^2}{(\varsigma_i - \varsigma_{i-1})} - L^{\rho_{2,z,j}}_{x_{2,n,j}} > 0, \quad j = 2, \ldots, q, \tag{6.16b}$$

$$\nu_{2,q+1} = \frac{Pe_h}{4} + v + \frac{\omega_{2,q+1,1}}{1 - \varsigma_q} - L^{\rho_{2,z,q+1}}_{x_{2,n,q+1}} > 0, \tag{6.16c}$$

$$l_{z,1} := |\lambda_1{}^*| + c - \sum_{j=1}^{q+1} \frac{L^{\rho_{2,z,j}}_{x_1} L^{\rho_{2,z,j}}_{x_{2,n,j}}}{\nu_{2,j}} > 0. \tag{6.16d}$$

then the zero dynamics origin is exponentially stable.

An alternative way to study the zero dynamics stability in original coordinates, which is only stated and not developed, is to characterize the stabilizing properties of the zero dynamics operator employing modal analysis as it is done in [Fra+19]. For this aim, consider the first time derivative of the synthetic output

$$\begin{aligned}
\dot{\boldsymbol{y}} &= \boldsymbol{\mathcal{C}}_y \dot{x}_2, \\
&= \boldsymbol{\mathcal{C}}_y \left(\mathcal{A}_2 x_2 + \rho_2(x_1, x_2) + \boldsymbol{\mathcal{B}}_u \boldsymbol{u}\right), \\
&= \boldsymbol{\mathcal{C}}_y \mathcal{A}_2 x_2 + \boldsymbol{\mathcal{C}}_y \rho_2(x_1, x_2) + \boldsymbol{\mathcal{C}}_y \boldsymbol{\mathcal{B}}_u \boldsymbol{u},
\end{aligned}$$

knowing that $\boldsymbol{\mathcal{C}}_y \boldsymbol{\mathcal{B}}_u = v \boldsymbol{I}_{q\times q}$, the zero dynamics is imposed by the control law

$$\boldsymbol{u} = -\frac{1}{v}\left(\boldsymbol{\mathcal{C}}_y \mathcal{A}_2 x_2 + \boldsymbol{\mathcal{C}}_y \rho_2(x_1, x_2)\right). \tag{6.17a}$$

The application of the above controller yields the zero dynamics in original coordinate

$$\dot{x}_1 = \mathcal{A}_1 x_1 - \varrho_1(x_1) - \mathfrak{r}(x_1, x_2), \qquad x_1(0) = x_{10}, \tag{6.18a}$$

$$\dot{x}_2 = \mathcal{A}^z_2 x_2 + \rho_{2,z}(x_1, x_2), \qquad x_2(0) = x_{20}, \tag{6.18b}$$

$$0 = \boldsymbol{\mathcal{C}}_y x_2, \tag{6.18c}$$

where

$$\mathcal{A}^z_2 x_2 = \mathcal{A}_2 x_2 - \boldsymbol{\mathcal{B}}_u \frac{1}{v} \boldsymbol{I}_{q\times q} \boldsymbol{\mathcal{C}}_y \mathcal{A}_2 x_2, \quad \mathcal{D}(\mathcal{A}_{2,z}) = \mathcal{D}(\mathcal{A}_2), \tag{6.18d}$$

is the zero dynamics operator in original coordinate. The zero dynamics nonlinearity is defined as

$$\rho_{2,z}(x_1, x_2) = \rho_2(x_1, x_2) - \boldsymbol{\mathcal{B}}_u \frac{1}{v} \boldsymbol{I}_{q\times q} \boldsymbol{\mathcal{C}}_y \rho_2(x_1, x_2). \tag{6.18e}$$

As before, it is required that the zero dynamics has the origin as unique steady-state, this can be assessed as by performing a sensor location-based bifurcation analysis for the SISO case (as in Section 4.3.3.2). The exponential stability of the origin can be established by performing a combination of Lyapunov and modal analyses as it was done in Section 5.3.

6.2.2.3 *Advanced control-estimation system*

Once the stability of the zero dynamics is ensured, a saturated passive state feedback controller, that is the distributed version of (4.52), is given as

$$\boldsymbol{u} = \boldsymbol{\mu}_{p,s}(x_1, \boldsymbol{x}_{2,n}, \boldsymbol{y}), \tag{6.19a}$$

where

$$\boldsymbol{\mu}_p(x_1, x_2, \boldsymbol{y}) = -\boldsymbol{B}_m{}^{-1}\left(\boldsymbol{K}_m\boldsymbol{y} + \boldsymbol{\mathcal{C}}_y\mathcal{A}_2x_2 + \boldsymbol{\mathcal{C}}_y\rho_2(x_1, x_2)\right), \quad \boldsymbol{K}_c = \boldsymbol{K}_c^T > 0. \tag{6.19b}$$

where $\boldsymbol{K}_c$ is a diagonal gain matrix.

The saturation limits may be chosen to equals the ones of the (4.86) developed in Chapter 4. The closed-loop exponential stability may be established by using the Seibert's reduction principle [117]. The rationale is as follows: when the closed-loop dynamics are in normal operation mode, the state feedback controller (6.19) force the output converge to zero, thus, the system dynamics approach exponentially to the zero dynamics. There, the origin is the unique attractor and by Seibert's reduction principle the exponential stability of the origin follows. When the controller is saturated, if the control limits are appropriately chosen, the state will present some transient behavior to eventually enter the region of no saturation and settle down at the origin.

The direct combination of the state feedback controller (6.19) with a pointwise observer gives the distributed version of the CES (4.69):

$$\dot{\hat{x}}_1 = \mathcal{A}_1\hat{x}_1 - \rho_1(\hat{x}_1, \hat{x}_2), \qquad \hat{x}_2(0) = \hat{x}_{10}, \tag{6.20a}$$

$$\dot{\hat{x}}_2 = \mathcal{A}_2\hat{x}_2 + \rho_2(\hat{x}_1, \hat{x}_2) + \boldsymbol{\mathcal{B}}_u\boldsymbol{u}, \qquad \hat{x}_2(0) = \hat{x}_{20}, \tag{6.20b}$$

$$\boldsymbol{\mathcal{C}}_y\hat{x}_2 = \boldsymbol{y}, \tag{6.20c}$$

$$\hat{\boldsymbol{y}} = \boldsymbol{\mathcal{C}}_y\hat{x}_2, \quad \hat{z}_c = \mathcal{C}_z\hat{x}_1, \tag{6.20d}$$

$$\boldsymbol{u} = \boldsymbol{\mu}_{p,s}(\hat{x}_1, \hat{x}_2, \boldsymbol{y}). \tag{6.20e}$$

The closed-loop stability can be established following a similar procedure as in Section 5.4.2, i. e., the closed-loop dynamics are a cascaded interconnection. Thus, the direct application of Proposition 3.1 establish conditions for exponential stability.

The direct application of FD to controller (6.19) (or (6.20)) leads to its discrete version (4.52) (or (4.69) without innovated dynamics). This fact suggests the equivalence between the early and late lumping version controllers. Consequently, the realization of (6.19) (or (6.20)) as a PIAW (with decouples observer) can be done in the lumped version. However, in what follows the realization, the PIAW-PWO equivalence is explored next in the late lumping setting.

6.2.2.4 *Realization as PIAW-PWO control-estimation system*

Recall the open-loop distributed dynamics in partitioned form with pointwise output

$$
\begin{aligned}
\dot{x}_1 &= \mathcal{A}_1 x_1 - \rho_1(x_1, x_2), & x_1(0) &= x_{10},\\
\dot{\boldsymbol{x}}_{2,n} &= \boldsymbol{\mathcal{A}}_{2,n}\boldsymbol{x}_{2,n} + \boldsymbol{\rho}_{2,n}(x_1, \boldsymbol{x}_{2,n}) + \boldsymbol{\mathcal{B}}^n_{u,2}\boldsymbol{u}, & \boldsymbol{x}_{2,n}(0) &= \boldsymbol{x}_{2,n0},\\
\dot{\boldsymbol{x}}_{2,m} &= \boldsymbol{\mathcal{A}}_{2,m}\boldsymbol{x}_{2,m} + \boldsymbol{\rho}_{2,m}(x_1, \boldsymbol{x}_{2,m}) + \boldsymbol{\mathcal{B}}^m_{u,2}\boldsymbol{u}, & \boldsymbol{x}_{2,m}(0) &= \boldsymbol{x}_{2,m0},\\
\boldsymbol{x}_2 &= \boldsymbol{\Omega}_n \boldsymbol{x}_{2,n} + \boldsymbol{\Omega}_m \boldsymbol{x}_{2,m},\\
\boldsymbol{y} &= \boldsymbol{\mathcal{C}}_y \boldsymbol{x}_{2,m}, \quad z = \mathcal{C}_z x_1.
\end{aligned}
$$

As it was done in Section 4.6.1, an exogenous load input is defined as

$$
\boldsymbol{\iota} = \boldsymbol{\mathcal{A}}_{2,m}\boldsymbol{x}_{2,m} + \boldsymbol{\rho}_{2,m}(x_1, \boldsymbol{x}_{2,m}). \tag{6.21}
$$

Note that in the pointwise output representation, the measured output and the measured state are the same, i. e., $\boldsymbol{y} = \boldsymbol{x}_{2,m}$. Putting all this consideration together, the model for CE redesign is then the reactor dynamics are

$$
\begin{aligned}
\dot{x}_1 &= \mathcal{A}_1 x_1 - \rho_1(x_1, x_2), & x_1(0) &= x_{10},\\
\dot{\boldsymbol{x}}_{2,n} &= \boldsymbol{\mathcal{A}}_{2,n}\boldsymbol{x}_{2,n} + \boldsymbol{\rho}_{2,n}(x_1, \boldsymbol{x}_{2,n}) + \boldsymbol{\mathcal{B}}^n_{u}\boldsymbol{u}, & \boldsymbol{x}_{2,n}(0) &= \boldsymbol{x}_{2,n0},\\
\dot{\boldsymbol{x}}_{2,m} &= \boldsymbol{\iota} + \boldsymbol{\mathcal{B}}^m_{u}\boldsymbol{u}, & \boldsymbol{x}_{2,m}(0) &= \boldsymbol{x}_{2,m0},\\
\boldsymbol{x}_2 &= \boldsymbol{\Omega}_n \boldsymbol{x}_{2,n} + \boldsymbol{\Omega}_m \boldsymbol{x}_{2,m},\\
\boldsymbol{y} &= \boldsymbol{x}_{2,m}, \quad z = \mathcal{C}_z x_1,
\end{aligned}
$$

The above model is composed by the decoupled concentration, and unmeasured-measured temperature components. An instantaneous observability property can be established since the measured temperature dynamics can be used to solve for the load exogenous input in terms of measured variables:

$$
\boldsymbol{\iota} = \dot{\boldsymbol{y}} - \boldsymbol{\mathcal{B}}^m_u \boldsymbol{u},
$$

thus a simple observer may be used to reconstruct this load input signal. On the other hand, the concentration and unmeasured temperature dynamics coincide with the model used for the employment of a pointwise observer.

Furthermore, the simplified measured dynamics has characteristic index vector with one entries only and it has no zero dynamics. Following the same procedure as in Section 4.6, the following CES can be constructed, in partitioned coordinate,

$$
\begin{aligned}
\dot{\hat{x}}_1 &= \mathcal{A}_1 \hat{x}_1 - \rho_1(\hat{x}_1, \hat{x}_2), & \hat{x}_2(0) &= \hat{x}_{10},\\
\dot{\hat{\boldsymbol{x}}}_{2,n} &= \boldsymbol{\mathcal{A}}_{2,n}\hat{\boldsymbol{x}}_{2,n} + \boldsymbol{\rho}_{2,n}(\hat{x}_1, \hat{\boldsymbol{x}}_{2,n}) + \boldsymbol{\mathcal{B}}^n_{u}\boldsymbol{u}, & \hat{\boldsymbol{x}}_{2,n}(0) &= \hat{\boldsymbol{x}}_{2,n0},\\
\boldsymbol{\mathcal{C}}_{y,2}\hat{x}_2 &= \boldsymbol{y},\\
\dot{\boldsymbol{\Lambda}} &= -\boldsymbol{K}_\omega \boldsymbol{\Lambda} - \boldsymbol{K}_\omega(\boldsymbol{K}_\omega \boldsymbol{y} + \boldsymbol{\mathcal{B}}^m_u \boldsymbol{\mu}_{s,s}(\boldsymbol{y}, \boldsymbol{\Lambda})), & \boldsymbol{\Lambda}(0) &= \boldsymbol{\Lambda}_0,\\
\hat{z}_c &= \mathcal{C}_z \hat{x}_1,\\
\boldsymbol{u} &= \boldsymbol{\mu}_{s,s}(\boldsymbol{y}, \boldsymbol{\Lambda}).
\end{aligned}
$$

where $\boldsymbol{K}_\omega = \boldsymbol{K}_\omega^T$ is a diagonal estimator gain matrix, and

$$\boldsymbol{\mu}_{s,s}(\boldsymbol{y}, \boldsymbol{\Lambda}) = \boldsymbol{\mathcal{B}}_u^{m^{-1}}((\boldsymbol{K}_c + \boldsymbol{K}_\omega)\boldsymbol{y} + \boldsymbol{\Lambda}).$$

Rewriting the above controller in original coordinates, with the control component in PI from, as is is done in Section 4.6.4, the above CES takes the form of (6.3). Finally, after the application of the late lumping scheme of Section 5.5 the CES is obtained (4.86). This fact suggest, in an informal manner, that there is a one-to-one correspondence in designing the proposed PIAW-PWO CES within the early or late lumping approach. In other words, the controller can be constructed from an early or late lumping approach and the resulting algorithm (4.86) (ready for implementation) is exactly the same.

6.3 EARLY LUMPING LIOF-PWO CONTROL-ESTIMATION SYSTEM

Here, again in an informal manner, is explored how the CES (5.50) can be constructed within an early lumping approach and following a similar methodological procedure as the late lumping-based approach of Chapter 5.

6.3.1 *LIOF-PWO control-estimation system from distributed to lumped*

In Section 5.3, the control component of the LIOF-PWO was designed as a distributed state feedback controller with two components: a linearizing one, for stabilization purposes, and a inventory-like for performance enhancement purposes. The linearizing term of this controller was first considered in Section 4.4.2, given in (4.54) as an alternative to (4.52) since it is less dependent on the model and it retains the stabilizing effects of the projection of the heat transport operator on the output dynamics. Here, on the basis of (4.54), a early lumping version of (5.24a) is constructed and then its late lumping implementation leads to (5.50).

6.3.1.1 *Linearizing stabilizing control component*

Recall the unconstrained version of controller (4.54):

$$\boldsymbol{u} = \boldsymbol{\mu}_2(\boldsymbol{x}_1, \boldsymbol{x}_{2,n}, \boldsymbol{x}_{2,m}, d_2),$$

where

$$\boldsymbol{\mu}_2(\boldsymbol{x}_1, \boldsymbol{x}_{2,n}, \boldsymbol{x}_{2,m}, d_2) = -\boldsymbol{B}_{u,2}^{m^{-1}}\left(\boldsymbol{B}_{d,2}^m d_2 + \boldsymbol{\psi}_m(\boldsymbol{x}_1, \boldsymbol{x}_{2,m}) + \boldsymbol{K}_c \boldsymbol{y}\right), \quad \boldsymbol{K}_c = \boldsymbol{K}_c^T > 0.$$

The corresponding closed-loop dynamics are given as

$$\dot{\boldsymbol{x}}_1 = \boldsymbol{A}_1 \boldsymbol{x}_1 + B_{d,1} d_1 - \boldsymbol{\varphi}_1(\boldsymbol{x}_1) - \boldsymbol{\varphi}_{n,m}(\boldsymbol{x}_1, \boldsymbol{x}_{2,n}, \boldsymbol{x}_{2,m}), \qquad \boldsymbol{x}_1(0) = \boldsymbol{x}_{1,0} \tag{6.22a}$$

$$\dot{\boldsymbol{x}}_{2,n} = \boldsymbol{A}_2^{n,n} \boldsymbol{x}_{2,n} + \boldsymbol{A}_{2,c}^{n,m} \boldsymbol{x}_{2,m} + \boldsymbol{B}_{d,2}^n d_2 + \boldsymbol{\psi}_{n,c}(\boldsymbol{x}_1, \boldsymbol{x}_{2,n}), \qquad \boldsymbol{x}_{2,n}(0) = \boldsymbol{x}_{2,n,0} \tag{6.22b}$$

$$\dot{\boldsymbol{x}}_{2,m} = \boldsymbol{A}_{2,c}^{m,m} \boldsymbol{x}_{2,m} + \boldsymbol{A}_2^{m,n} \boldsymbol{x}_{2,n} + \boldsymbol{B}_{d,2}^m d_2 + \boldsymbol{\psi}_{m,c}(\boldsymbol{x}_1, \boldsymbol{x}_{2,m}), \qquad \boldsymbol{x}_{2,m}(0) = \boldsymbol{x}_{2,m,0}, \tag{6.22c}$$

where

$$\boldsymbol{A}_{2,c}^{n,m} = \boldsymbol{A}_2^{m,n} - \boldsymbol{B}_{u,2}^{n}\boldsymbol{B}_{u,2}^{m}{}^{-1}\boldsymbol{K}_c, \quad \boldsymbol{A}_{2,c}^{m,m} = \boldsymbol{A}_2^{m,m} - \boldsymbol{B}_{u,2}^{n}\boldsymbol{B}_{u,2}^{m}{}^{-1}\boldsymbol{K}_c,$$
$$\boldsymbol{\psi}_{n,c}(\boldsymbol{x}_1, \boldsymbol{x}_{2,n}, \boldsymbol{x}_{2,m}) = \boldsymbol{\psi}_n(\boldsymbol{x}_1, \boldsymbol{x}_{2,n}, \boldsymbol{x}_{2,m}) - \boldsymbol{B}_{u,2}^{n}\boldsymbol{B}_{u,2}^{m}{}^{-1}\boldsymbol{\psi}_n(\boldsymbol{x}_1, \boldsymbol{x}_{2,m}),$$
$$\boldsymbol{\psi}_{m,c}(\boldsymbol{x}_1, \boldsymbol{x}_{2,m}) = \boldsymbol{\psi}_m(\boldsymbol{x}_1, \boldsymbol{x}_{2,m}) - \boldsymbol{B}_{u,2}^{n}\boldsymbol{B}_{u,2}^{m}{}^{-1}\boldsymbol{\psi}_m(\boldsymbol{x}_1, \boldsymbol{x}_{2,m}).$$

Thus, the matrix $\boldsymbol{K}_c$ must be chosen so that the matrix $\boldsymbol{A}_{2,c}^{m,m}$ is Hurwitz. Furthermore, it is expected that the nonlinear term $\boldsymbol{\psi}_{m,c}$ has smaller Lipschitz constants with respect to its open-loop counterpart. The stability of the above closed-loop system can be established with the recursive application of Proposition 3.1. Accordingly, the next result follows.

Proposition 6.2. *Closed-loop stability of the system* (6.22).
Consider the closed-loop dynamics (6.22). *Assume that the sensor locations have been selected so that the origin is the unique closed-loop steady-state. Furthermore, assume that there exist two positive definite matrices* $\boldsymbol{P}_{2,n}$ *and* $\boldsymbol{P}_{2,m}$ *that satisfy the Lyapunov inequalities*

$$\boldsymbol{A}_2^{n,n\,T}\boldsymbol{P}_{2,n} + \boldsymbol{P}_{2,n}\boldsymbol{A}_2^{n,n} + 2\zeta_n < 0, \quad \boldsymbol{A}_2^{m,m\,T}\boldsymbol{P}_{2,m} + \boldsymbol{P}_{2,m}\boldsymbol{A}_2^{m,m} + 2\zeta_m < 0.$$

If the gain matrix $\boldsymbol{K}_2$ *is selected so that* $\boldsymbol{A}_{2,c}^{m,m}$ *is Hurwitz, then the system is robustly stable if the following condition holds*

$$\nu_m - \frac{a_{2,n}a_{2,m}\,\|\boldsymbol{A}_2^{m,n}\|\left(\left\|\boldsymbol{A}_{2,c}^{n,m}\right\| + L_{x_{2,m}}^{\psi_{n,c}}\right)}{\nu_n} > 0, \tag{6.23a}$$
$$\lambda_{2,c}^{*} - \frac{a_1 a_2\,\|\boldsymbol{B}_2\|\,L_{x_2}^{\psi_{n,m}}}{\nu_1} > 0, \tag{6.23b}$$

where

$$\nu_m = \zeta_m - L_{x_{2,n}}^{\psi_{m,c}}, \quad \nu_n = \zeta_n - L_{x_{2,m}}^{\psi_{m,c}}, \quad \lambda_{2,c} = \max_{\lambda_j\in\sigma(\boldsymbol{A}_{2,c})} \Re\lambda_j,$$

$$\boldsymbol{A}_{2,c} = \begin{bmatrix} -\nu_n & a_{2,m}\left(\left\|\boldsymbol{A}_{2,c}^{n,m}\right\| + L_{x_{2,m}}^{\psi_{n,c}}\right) \\ a_{2,n}\left\|\boldsymbol{A}_{2,n}^{m,n}\right\| & -\nu_n \end{bmatrix}, \quad \boldsymbol{B}_2 = \begin{bmatrix} L_{x_1}^{\psi_{n,c}} \\ L_{x_1}^{\psi_{m,c}} \end{bmatrix},$$

and a_2, $a_{2,n}$, $a_{2,m}$ *are positive constants.*

Next, the inventory-like control component is constructed in the early lumping setting.

6.3.1.2 *Passivity of the closed-loop dynamics*

In attempt to parallel the methodology employed in Section 5.3.2, consider the closed-loop system (6.22) with the control law

$$\boldsymbol{u} = \boldsymbol{\mu}_l(\boldsymbol{x}_1, \boldsymbol{x}_{2,m}) + \boldsymbol{\mu}_p(\boldsymbol{x}_{2,m}),$$

and the exogenous input vector at zero. Use the Lyapunov function

$$V(\boldsymbol{x}_1, \boldsymbol{x}_{2,n}, \boldsymbol{x}_{2,m}) = \frac{1}{2}\boldsymbol{x}_1^T \boldsymbol{P}_1 \boldsymbol{x}_1 + \frac{1}{2}\boldsymbol{x}_{2,n}^T \boldsymbol{P}_{2,n} \boldsymbol{x}_{2,n} + \boldsymbol{x}_{2,m}^T \boldsymbol{P}_{2,m} \boldsymbol{x}_{2,m},$$

where $\boldsymbol{P}_1 = \boldsymbol{P}_1^T > 0$, $\boldsymbol{P}_{2,n} = \boldsymbol{P}_{2,n}^T > 0$, and $\boldsymbol{P}_{2,m} = \boldsymbol{P}_{2,m}^T > 0$. Taking the time derivative of the proposed candidate Lyapunov function along the trajectories of the closed-loop dynamics (6.22). Employing inequalities as in (3.8c) and the definition of $\boldsymbol{B}_{u,2}^n$ and $\boldsymbol{B}_{u,2}^m$, and after algebraic manipulations it can be shown that the next expression hold

$$\dot{V} \leq -\nu^* \|\boldsymbol{x}\|^2 + \boldsymbol{u}_p^T \boldsymbol{B}_{u,2}^T \boldsymbol{P}_2 \boldsymbol{x}_2,$$

where $-\nu^*$ is a function of Lipschitz constants and eigenvalues of matrices $\boldsymbol{P}_1, \boldsymbol{P}_{2,n}$, and $\boldsymbol{P}_{2,m}$, the state is defined as $\boldsymbol{x} = [\boldsymbol{x}_1 \ \boldsymbol{x}_2]^T$ with $\boldsymbol{x}_2 = \boldsymbol{C}_n^T \boldsymbol{x}_{2,n} + \boldsymbol{C}_m^T \boldsymbol{x}_{2,m}$, and matrix $\boldsymbol{P}_2 = \boldsymbol{P}_2^T > 0$ is a positive definite matrix, according to the following expressions:

$$\begin{aligned}
\nu^* &= \max\{\nu_1, \nu_{2,n}, \nu_{2,m}\} - L_{x_{2,n}}^{\psi_{n,c}} - L_{x_{2,m}}^{\psi_{m,c}} - \frac{\lambda_{P_1}{}^*}{\lambda_{P_1 *}} \left(\frac{L_{x_{2,n}}^{\psi_{n,m}}}{\lambda_{P_{2,n}*}} + \frac{L_{x_{2,m}}^{\psi_{n,m}}}{\lambda_{P_{2,n}*}} \right) - \\
&\quad - \frac{\lambda_{P_{2,n}}{}^*}{\lambda_{P_{2,n}*}} \left(\frac{L_{x_1}^{\psi_{n,c}}}{\lambda_{P_1 *}} + \frac{L_{x_{2,m}}^{\psi_{n,m}}}{\lambda_{P_{2,m}*}} \right) - \frac{\lambda_{P_{2,m}}{}^*}{\lambda_{P_{2,m}*}} \left(\frac{L_{x_1}^{\psi_{m,c}}}{\lambda_{P_1 *}} + \frac{L_{x_{2,n}}^{\psi_{m,c}}}{\lambda_{P_{2,n}*}} \right), \\
\boldsymbol{P}_2 &= \begin{bmatrix} \boldsymbol{C}_n^T \boldsymbol{P}_{2,n} \boldsymbol{C}_n & \boldsymbol{0}_{N-q \times q} \\ \boldsymbol{0}_{q \times N-q} & \boldsymbol{C}_{y,2}^T \boldsymbol{P}_{2,m} \boldsymbol{C}_{y,2} \end{bmatrix}.
\end{aligned}$$

Defining the new output

$$\boldsymbol{y} = \boldsymbol{B}_{2,u}^T \boldsymbol{P}_2 \boldsymbol{x}_2,$$

then the closed-loop dynamics are strictly state passive with respect to the input-output pair $(\boldsymbol{\mu}_p, \boldsymbol{y})$. Accordingly, the output feedback of a passive function can be used to accelerate the output convergence. For instance,

$$\boldsymbol{\mu}_p = -\boldsymbol{K}_p \boldsymbol{y}, \quad \boldsymbol{K}_p = \boldsymbol{K}_p^T > 0,$$

yields to

$$\dot{V} \leq -\nu^* \|\boldsymbol{x}\|^2 - \boldsymbol{y}^T \boldsymbol{K}_p \boldsymbol{y},$$

which indicates that the closed-loop system is exponentially stable.

In connection with its late lumping counterpart, the above control law is constructed by considering a new output for passivity, and the matrix $\boldsymbol{P}_2$ must be chosen solving a Kalman-Yakubovich-Popov equation [76]. Its equivalence in the late lumping setting is the integrating factor ω_h used to make the heat transport operator selfadjoint.

6.3.1.3 *Control estimation system and its implementation*

For implementation, the combination with a pointwise-like observer yields the early lumped-based LIOF-PWO CES given as

$$\dot{\hat{\boldsymbol{x}}}_1 = \boldsymbol{f}_1(\hat{\boldsymbol{x}}_1, \hat{\boldsymbol{x}}_{2,n}, \hat{\boldsymbol{x}}_{2,m}, d_1), \qquad \hat{\boldsymbol{x}}_1(0) = \hat{\boldsymbol{x}}_{10}, \tag{6.24}$$

$$\dot{\hat{\boldsymbol{x}}}_{2,n} = \boldsymbol{f}_{2,n}(\hat{\boldsymbol{x}}_1, \hat{\boldsymbol{x}}_{2,n}, \boldsymbol{y}, d_2) + \boldsymbol{B}_u^n \boldsymbol{\mu}_s^{PI}(\boldsymbol{y}), \qquad \boldsymbol{x}_{2,n}(0) = \boldsymbol{x}_{2n0}, \tag{6.25}$$

$$\hat{\boldsymbol{x}}_{2,m} = \boldsymbol{y}, \tag{6.26}$$

$$\hat{z} = \boldsymbol{C}_z \hat{\boldsymbol{x}}_1, \quad \hat{\boldsymbol{x}} = (\hat{\boldsymbol{x}}_1^T, \boldsymbol{C}_n^T \hat{\boldsymbol{x}}_{2,n} + \boldsymbol{C}^T \boldsymbol{y})^T, \quad \hat{\boldsymbol{x}}_N = \mathcal{J}(\hat{\boldsymbol{x}}), \tag{6.27}$$

$$\boldsymbol{u} = \boldsymbol{\mu}_{lp}(\boldsymbol{x}_1, \boldsymbol{x}_{2,m}, \boldsymbol{x}_{2,n}), \tag{6.28}$$

where

$$\boldsymbol{\mu}_{lp}(\boldsymbol{x}_1, \boldsymbol{x}_{2,m}, \boldsymbol{x}_{2,n}) = -{\boldsymbol{B}_{u,2}^m}^{-1} \left(\boldsymbol{\psi}_m(\hat{\boldsymbol{x}}_1, \hat{\boldsymbol{x}}_{2,m}) + \boldsymbol{K}_c \boldsymbol{y} + \boldsymbol{K}_p \boldsymbol{B}_{2,u}^T \boldsymbol{P}_2 \hat{\boldsymbol{x}}_2 \right).$$

The stability proof of the related nominal closed-loop dynamics as well as the interconnection with parasitic dynamics can be established by using small gain arguments. In original coordinates and considering $\boldsymbol{P}_2 = \omega_k(s_k)$, the LIOF-PWO CES (5.50) is obtained. Again, this fact suggests that there is no difference in the construction process: the same algorithm is obtained following a late or an early lumping approach.

6.4 combining both designs

Making a balance from the two proposed CES, in terms of simplicity, closed-loop performance and robustness, the PIAW-PWO results in a more efficient final product. Nevertheless, the LIOF-PWO has the appealing inventory control term, that accelerates profile convergence by compensating the excess or defect of sensible heat in the distributed heat balance (as industrial inventory control does). Thus, this term is transferred to the PIAW-PWO, to combine the advantages of both designs. In original coordinates an ready for implementation, the Proportional-Integral-Inventory control with Anti Windup scheme-Pointwise Observer (PIIAW-PWO) is:

$$\dot{\hat{\boldsymbol{\chi}}}_1 = \boldsymbol{A}_1 \hat{\boldsymbol{\chi}}_1 + \boldsymbol{B}_{d,1} \bar{\chi}_{1,e} - \boldsymbol{r}(\hat{\boldsymbol{\chi}}_1, \hat{\boldsymbol{\chi}}_2), \qquad \hat{\boldsymbol{\chi}}_1(0) = \hat{\boldsymbol{\chi}}_{10},$$

$$\dot{\hat{\boldsymbol{\chi}}}_{2,n} = \boldsymbol{A}_2^{n,n} \hat{\boldsymbol{\chi}}_{2,n} + \boldsymbol{A}_2^{n,m} \hat{\boldsymbol{\chi}}_{2,m} + \boldsymbol{B}_{d,2}^n \chi_{2,e} + \boldsymbol{r}_n(\hat{\boldsymbol{\chi}}_1, \hat{\boldsymbol{\chi}}_{2,n}) + \boldsymbol{B}_{u,2}^n \boldsymbol{\tau}_c, \quad \hat{\boldsymbol{\chi}}_{2,n}(0) = \hat{\boldsymbol{\chi}}_{2,n,0},$$

$$\hat{\boldsymbol{\chi}}_{2,m} = \boldsymbol{\tau}_m,$$

$$\hat{c}_z = \boldsymbol{C}_1 \hat{\boldsymbol{\chi}}_1, \quad \hat{\boldsymbol{\chi}}_2 = \boldsymbol{C}_n^T \hat{\boldsymbol{\chi}}_{2,n} + \boldsymbol{C}_{y,2}^T \hat{\boldsymbol{\chi}}_{2,m}, \quad \hat{\boldsymbol{\chi}}_N = \boldsymbol{\mathcal{I}}(\hat{\boldsymbol{\chi}}),$$

$$\boldsymbol{\tau}_c = \boldsymbol{\mu}_{s,pi}(\boldsymbol{\tau}_m) = \left[\mathrm{sat}_{\tau_c^-}^{\tau_c^+} \mu_{pii,1}(\tau_{m,1}) \quad \ldots \quad \mathrm{sat}_{\tau_c^-}^{\tau_c^+} \mu_{pi} i, q(\tau_{m,q}) \right]^T,$$

where the entries of the control map $\boldsymbol{\mu}_{s,pi}$ are

$$\mu_{pii,i}(\tau_{m,i}) = \bar{\tau}_{c,i} - k_{p,i}\left((\tau_{m,i} - \bar{\tau}_{m,i}) - t_i^{-1}\int_0^t (\tau_{m,i} - \bar{\tau}_{m,i})\mathrm{d}t\right) - \\ - k_{\mathfrak{z},i}\frac{1}{N_e}\sum_{k=\frac{(i-1)N_e}{q}}^{\frac{iN_e}{q}} \mathrm{e}^{-Pe_h s_k}\left(\hat{\chi}_{2,k} - \bar{\chi}_{2,k}\right) + \\ + t_a^{-1}\int_0^t \left(\mathrm{sat}_{\tau_c^-}^{\tau_c^+}\mu_{pii,i}(\tau_{m,i}) - \mu_{pii,i}(\tau_{m,i})\right)\mathrm{d}t,$$

for $i = 1, \ldots, q$. The PIAW control parameters are given in (4.86g).

To confirm the above mentioned characteristics, the present 3-MIMO PIIAW-PWO is applied to the multi–jacket tubular reactor case study of Section 2.5. The same sensor locations and PIAW parameters determined in Section 4.7.2 are used while $\boldsymbol{K}_{\mathfrak{z}} = 3\boldsymbol{I}_{q\times q}$ is used for the additional control term. Simulation results under the robust testing conditions established in Section 5.6.1, are shown in Figure 6.5a and Figure 6.5b for control and estimation performance. Figure 6.6 shows the related norms which are compared with the 3-MIMO PIAW-PWO CES.

It can be observed that the PIIAW-PWO perform fastest profile regulation compared with the PIAW-PWO. However, the disturbance rejection capability is slightly degraded. The estimation performance is almost the same for both schemes. Thus, the inventory control term accelerates convergence and is more sensible to inlet step disturbances. Thus it might be used in scenarios in which fast profile regulation is mandatory.

6.5 SUMMARY

Methodologically speaking, this chapter closes the theoretical and application-oriented developments of previous chapters by putting the proposed the PIAW-PWO and the LIOF-PWO CES in perspective between them. This is done by first comparing the functioning performance of both schemes, including additional comparisons with an adaptive CES. Then, the extensions and implications of both designs, coming from early or late lumping, are explored in the opposite setting, late or early. Finally, the advantages of both CESs are put together to obtain a new CES which combined both designs.

The simulation-based comparative study done in this chapter compared the two proposed CESs, in robust testing conditions, within them and against another CES composed by an adaptive controller and a pointwise observer was done. It was concluded that the proposed algorithms present better (the PI-based control-estimation system) or similar (the LIOF-PWO CES) than the adaptive counterpart.

After that, an exploratory attempt to: (i) extend the early lumping CE construction methodology of Chapter 4 to its late lumping counterpart, and (ii) vice versa, to translate the late lumping CE methodology used in Chapter 5 to an early lumping

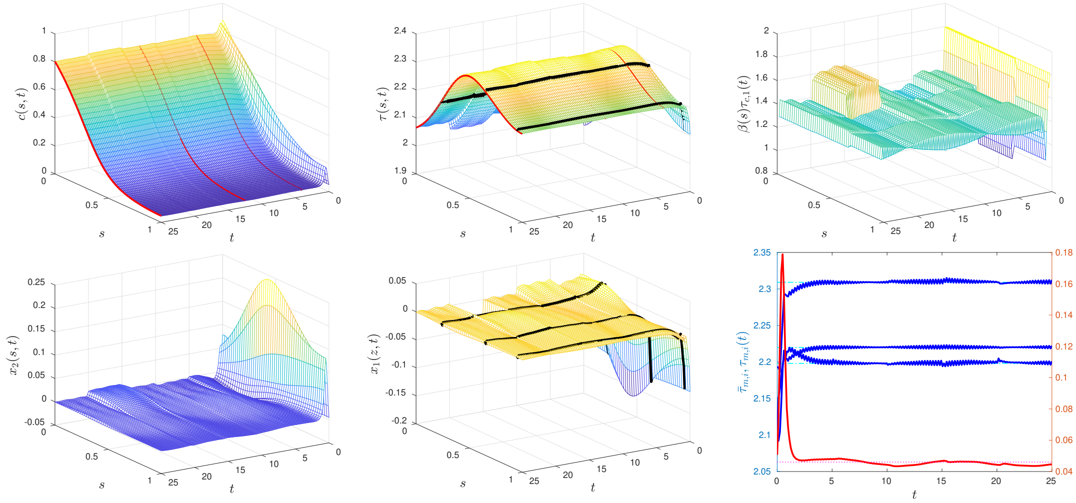

(a) Control functioning. Top left: concentration profile $c(s,t)$. Top center: temperature profile $\tau(s,t)$. Top right: control effort $\sum_{i=1}^{3} \beta_i(s)\tau_{c,i}(t)$. Bottom left: deviated concentration profile $x_1(s,t)$. Bottom center: deviated temperature profile $x_2(s,t)$. Bottom right: measured $\tau_{m,i}(t)$, $i = 1,2,3$ (blue continuous) and regulated $c_o(t)$ (red continuous) outputs and their setpoints (dashed-dotted cyan and dotted magenta, respectively).

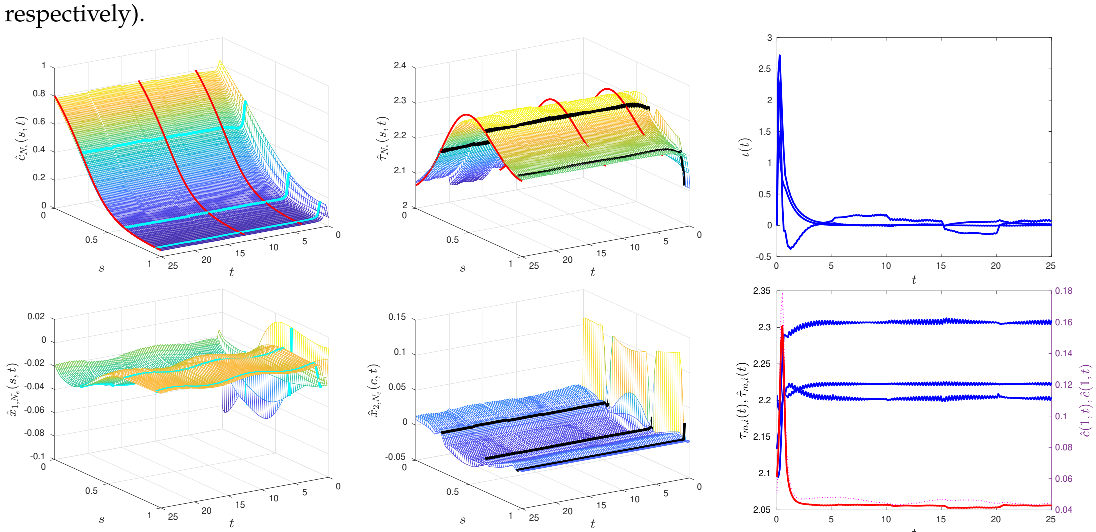

(b) Estimator functioning. Top left: estimated concentration profile $\hat{c}(s,t)$. Top center: estimated temperature profile $\hat{\tau}(s,t)$. Bottom left: estimation error of the concentration profile $\tilde{c}_1(s,t)$. Bottom center: estimation error of the temperature profile $\tilde{\tau}_2(s,t)$. Bottom right: real measured $\tau_{m,i}(t)$, $i = 1,2,3$ (continuous blue) and regulated $c_o(t)$ (dotted magenta) and their estimates $(\hat{\tau}_{m,i}(t), \hat{c}_o(t))$ (continuous blue and red, respectively).

Figure 6.5: Robust closed-loop functioning with the 3-MIMO PIIAW-PWO and PIAW-PWO CESs.

setting. The obtained results suggest that, no matter which approach is followed, early or late, in both cases the final CES is the same. Obviously, depending on the employed

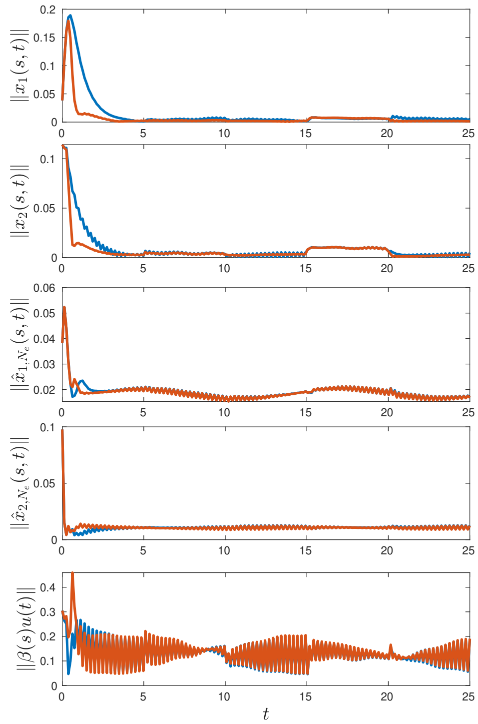

Figure 6.6: Norms of distributed states in deviation, estimation errors and control input for decentralized the 3-MIMO PIIAW-PWO (brown lines) and PIAW-PWO (blue lines) CESs.

setting, early or late, the formal stability proofs may be suited for each case, finite or infinite dimensional.

Finally, as an attempt to take the advantages of the both proposed CES, an additional CE scheme, with the control component constructed as the combination of the PIAW, of the proposed early lumping-based methodology Chapter 4, and an inventory control term, as the one employed in the proposed late lumping-based approach Chapter 5. The resulting PIIAW-PWO has proven to produce, in a simulation-based comparative study, fastest profile regulation in comparison with the PIAW-PWO counterpart.

Part V

CONCLUSIONS

The closing part of the study is composed by a final summary of the whole work, the conclusions and future work.

7 CONCLUSIONS

7.1 GENERAL SUMMARY

The present study tackled the problem of designing Control-Estimation System (CES) for a class of tubular reactors. The designed algorithms must be accompanied with guidelines for the determination of the related actuator and sensor configuration, sensor location criteria and gain tuning guidelines and must ensure robust functioning in the presence of exogenous disturbances and parameter uncertainty.

In the study, two different solution methodologies, within the early and late lumping approaches, are used to construct two different CES: the PI control with AW scheme-Pointwise Observer (PIAW-PWO) and the LIOF-PWO. In both cases, the key cornerstones of the whole theoretical and implantation results are the employment of a constructive control design phylosophy and the efficient modeling approach, all this with an application-oriented aim: improve existent CE algorithms encountered in industry (Proportional-Integral (PI) control and data-driven estimation techniques).

In the first part of the study, within an efficient early lumping approach, a MIMO CES, composed by a set of decentralized PI controllers with Anti-Windup (AW) protection and a pointwise-like observer, was constructed. First, passivity and closed-loop detectability solvability properties, in terms of sensor location and control limits, were identified yielding an advanced CES. Then, with realization theory, the latter scheme is implemented as a set of decentralized PIAW and pointwise-like estimator. Assurance of robust stability is drawn in terms of control gains and limits and sensor locations.

In the second part of the study, within a late lumping approach, an advanced CES composed by the combination of linearizing and inventory-like control terms coupled with pointwise observer was done. This scheme was designed by analyzing the the interplay between the stabilizing and destabilizing properties of the heat transport and generation (sue to reaction) mechanisms, and identifying how could this interplay be modified with feedback control at the appropriate spatial locations. This was done using modal analysis and exploiting the Lur'e structure of the system dynamics. The implementation is done by performing an efficient late lumping based on the efficient modeling approach.

The final part of the study puts both proposed CES in perspective which each other and an adaptive controller coupled with a pointwise estimator. In an exploratory step, the possibilities of extending the results of the proposed early and late lumping approaches to the opposite ones, late or early, are briefly considered.

7.2 MAIN CONTRIBUTIONS AND FUTURE WORK

The present study contributed with important results on the Control-Estimation (CE) problem for a class of distributed tubular reactors. The particular tackled problem has been the design of CESs suited for a class of non-isothermal tubular reactors. Criteria and guidelines to select the related sensor and actuator configuration, in terms of number of jacket sections and sensors and their locations, have been developed for each designed control-estimation system. The proposed designs may have constrained control action and thus are accompanied with a criterion for the selection of control limits. Furthermore, the designs have simple implementation and tuning guidelines, and are constructed on the basis of low computational load models. The main contributions of the study are

- The design of MIMO CES in an integral framework that considers early and late lumping approaches within an application oriented perspective: advanced control and estimation theory for finite and infinite dimensional systems is put together to obtain CES of industrial interest.
- The development of different sensor location criteria from early and late lumping methodologies for the proposed CES.
- Structural and gain tuning guidelines for the selection of actuator and sensor configurations and control gains.
- Efficient implementation with low computational load by employing the efficient modeling approach for tubular reactors.
- An exploratory attempt to assess the implications of the employed, early or late, methodologies in their opposite side, late or early, to conclude, in an informal manner, despite the employed approach, the final implementable algorithm is the same.

As future work, several paths can be followed. A first natural step is the enhancement of the proposed CES with: (i) the addition of a setpoint compensation scheme for disturbance rejection in the inlet concentration, (ii) the addition of derivative control action, and (iii) the consideration of limit rate in the control action.

Other veins that could be taken are: (i) the extension of the approach to more complex transport-reaction processes with different sensor and actuator configurations, such as packed bed and gasification tubular reactors and experimental validation, (ii) the generalization to spatially distributed systems with complex geometries, and (iii) the formalization of the informal results explored in Chapter 6.

Part VI

APPENDIX

a

PROOFS OF ROBUST STABILITY RESULTS

Here, the proofs of the theorems and lemmas presented in Section 3.1 are given.

A.1 PROOF OF LEMMA 3.1

To prove the robust stability of system (3.1a), an estimate of the solution of the perturbed system can be obtained by computing the time derivative of the Lyapunov function, associated to the nominal dynamics, along the trajectories of (3.1a) to get

$$
\begin{aligned}
\dot{V} &= \partial_x V(\boldsymbol{x}) \left[\boldsymbol{f}(\boldsymbol{x}) + \boldsymbol{g}(\boldsymbol{x}, \tilde{\boldsymbol{p}}, \boldsymbol{d}, \boldsymbol{u})\right], \\
&\leq -c_3 \|\boldsymbol{x}\|^2 + \partial_x V(\boldsymbol{x}) \boldsymbol{g}(\boldsymbol{x}, \tilde{\boldsymbol{p}}, \boldsymbol{d}, \boldsymbol{u}), \\
&\leq -c_3 \|\boldsymbol{x}\|^2 + c_4 \|\boldsymbol{x}\| \left(L_x^g \|\boldsymbol{x}\| + L_p^g \|\tilde{\boldsymbol{p}}\| + L_d^g \|\boldsymbol{d}\| + L_u^g \|\boldsymbol{u}\|\right),
\end{aligned}
$$

where the triangle inequality, and the last two inequalities in (3.5a), as well as the Lipschitz condition (3.4c) have been used. Use of the first inequality in (3.5a) and the bounds in (3.2) yield an upper bound for $\dot{V}(\boldsymbol{x})$:

$$
\dot{V}(\boldsymbol{x}) \leq -\left(\frac{c_3}{c_2} - \frac{c_4 L_x^g}{c_1}\right) V^{\frac{1}{2}}(\boldsymbol{x}) + \frac{c_4}{\sqrt{c_1}} V(\boldsymbol{x}) \left(L_p^g \delta_p + L_d^g \varepsilon_d(t) + L_u^g \varepsilon_u(t)\right).
$$

Using the change of variable $v = V^{\frac{1}{2}}$ it follows that

$$
\dot{v} \leq -\frac{1}{2}\left(\frac{c_3}{c_2} - \frac{c_4 L_x^g}{c_1}\right) v + \frac{c_4}{2\sqrt{c_1}} \left(L_p^g \delta_p + L_d^g \varepsilon_d(t) + L_u^g \varepsilon_u(t)\right),
$$

by the comparison lemma [76], $v(t)$ satisfies the inequality

$$
v(t) \leq \mathrm{e}^{-\frac{1}{2}\left(\frac{c_3}{c_2} - \frac{c_4 L_x^g}{c_1}\right) t} v_0 + \frac{c_4}{2\sqrt{c_1}} \int_0^t \mathrm{e}^{-\frac{1}{2}\left(\frac{c_3}{c_2} - \frac{c_4 L_x^g}{c_1}\right)(t - \mathrm{t})} \left[L_p^g \delta_p + L_d^g \varepsilon_d(\mathrm{t}) + L_u^g \varepsilon_u(\mathrm{t})\right] \mathrm{dt}.
$$

The employment of the first inequality in (3.5a) in the above expression yields

$$
\|\boldsymbol{x}(t)\| \leq a_x \mathrm{e}^{-\nu_x t} \|\boldsymbol{x}_0\| + a_x \int_0^t \mathrm{e}^{-\nu_x (t - \mathrm{t})} \left[L_p^g \delta_p + L_d^g \varepsilon_d(\mathrm{t}) + L_u^g \varepsilon_u(\mathrm{t})\right] \mathrm{dt}, \tag{a.2a}
$$

where

$$
\nu_x = \frac{1}{2}\left(\frac{c_3}{c_2} - \frac{c_4 L_1^g}{c_1}\right), \quad a_x = \max\left\{\sqrt{\frac{c_2}{c_1}}, \frac{c_4}{2c_1}\right\}, \quad \frac{a_x}{\nu_x}\left(L_p^g, L_d^g, L_u^g\right) := \left(b_p, b_d, b_u\right).
$$

(a.2b)

Using (3.2) one arrives to (3.3). Assuming that condition (3.6a) is satisfied, then the motion of the perturbed system (3.4) is estimated as

$$\|\boldsymbol{x}(t)\| \leq \max\left\{a_x \|\boldsymbol{x}_0\|, b_p\delta_p + b_d\varepsilon_d^+ + b_u\varepsilon_u^+\right\}.$$

If the above conditions are satisfied in $\mathfrak{X} = \{\boldsymbol{x} \in \mathscr{X} \mid \|\boldsymbol{x}\| \leq r_x\}$, then the domain of attraction or the size of the disturbances need to satisfy (3.6b). Otherwise, if the above conditions are valid for the whole set $\mathscr{X}$, then

$$\|x_0\| \leq \delta_{x0} \to \varepsilon_x := a_x\delta_x + b_p\delta_p + b_d\varepsilon_d^+ + b_u\varepsilon_u^+,$$

where ε_x is the size of the state excursions with respect to the origin.

A.2 PROOFS OF COROLLARY 3.2 AND COROLLARY 3.3

Use the Lyapunov function of the nominal system and the Lipschitz bounds of $\boldsymbol{g}$ to get

$$\begin{aligned}
\dot{V} &= \boldsymbol{x}^T(\boldsymbol{A}^T\boldsymbol{P} + \boldsymbol{P}\boldsymbol{A})\boldsymbol{x} + 2\boldsymbol{x}^T\boldsymbol{P}\boldsymbol{g}(\tilde{\boldsymbol{p}}, \boldsymbol{x}, \boldsymbol{d}, \boldsymbol{u}),\\
&\leq -2\zeta\boldsymbol{x}^T\boldsymbol{P}\boldsymbol{x} + \left\|\boldsymbol{P}\boldsymbol{A})\boldsymbol{x} + 2\boldsymbol{x}^T\boldsymbol{P}\boldsymbol{g}(\tilde{\boldsymbol{p}}, \boldsymbol{x}, \boldsymbol{d}, \boldsymbol{u})\right\|,\\
&\leq -2\zeta V + 2\lambda_P{}^* L_x^g \|\boldsymbol{x}\|^2 + 2\lambda_P{}^* \|\boldsymbol{x}\| \left(L_p^g \|\tilde{\boldsymbol{p}}\| + L_d^g \|\boldsymbol{d}\| + L_u^g \|\boldsymbol{u}\|\right),\\
&\leq -2\zeta V + 2\frac{\lambda_P{}^*}{\lambda_{P*}} L_x^g V + 2\frac{\lambda_P{}^*}{\sqrt{\lambda_{P*}}} V^{\frac{1}{2}} \left(L_p^g \|\tilde{\boldsymbol{p}}\| + L_d^g \|\boldsymbol{d}\| + L_u^g \|\boldsymbol{u}\|\right),\\
&= -2\left(\zeta - \frac{\lambda_P{}^*}{\lambda_{P*}} L_x^g\right) V + 2\frac{\lambda_P{}^*}{\sqrt{\lambda_{P*}}} V^{\frac{1}{2}} \left(L_p^g \|\tilde{\boldsymbol{p}}\| + L_d^g \|\boldsymbol{d}\| + L_u^g \|\boldsymbol{u}\|\right).
\end{aligned}$$

Proceeding as in the previous proof, the following estimate is obtained

$$\|\boldsymbol{x}(t)\| \leq a_x e^{-\nu_x t} \|\boldsymbol{x}_0\| + a_x \int_0^t e^{-\nu_x(t-\mathrm{t})} \left[L_p^g\delta_p + L_d^g\varepsilon_d(\mathrm{t}) + L_u^g\varepsilon_u(\mathrm{t})\right] \mathrm{dt}, \tag{a.4}$$

where ν_x is defined in (3.9). Considering (3.2b), if $\nu_x > 0$ and (3.6b) are met, then the state trajectories are bounded as in (3.3) which implies the local robust stability of the origin. If the preceding conditions are satisfied in the set $\mathscr{X}$, then the result is nonlocal.

The proof of Corollary 3.3 is established by estimating bounds for the solution of the dynamic system in (3.8a). Consider its solution

$$\boldsymbol{x}(t) = e^{\boldsymbol{A}t}\boldsymbol{x}_0 + \int_0^t e^{\boldsymbol{A}(t-\mathrm{t})}\boldsymbol{g}(\boldsymbol{x}, \tilde{\boldsymbol{p}}, \boldsymbol{d}, \boldsymbol{u})\mathrm{dt},$$

take norms on both sides of the equation, use the triangle inequality, substitute (3.4c), apply the Gronwall lemma [76] and integrate by parts to obtain

$$\|\boldsymbol{x}(t)\| \leq a_x \|\boldsymbol{x}_0\| \mathrm{e}^{-\nu_x t} + a_x \int_0^t \mathrm{e}^{-\nu_x (t-\mathrm{t})} \left[L_p^g \delta_p + L_d^g \varepsilon_d(\mathrm{t}) + L_u^g \varepsilon_u(\mathrm{t})\right] \mathrm{dt},$$

with ν_x given in (3.11). Proceeding as in the previous proof it can be shown that the the state trajectories are bounded as in (3.3) which implies the robust stability of the origin in the local sense in $\mathfrak{X}$. If preceding conditions are satisfied in the set $\mathscr{X}$, then the result is nonlocal.

A.3 PROOF OF LEMMA 3.2 AND PROPOSITION 3.1

A.3.1 *Proof of Lemma 3.2*

For the proof of Lemma 3.2, consider (A.2) and define $\Xi_0 = a \|\boldsymbol{x}_0\|$ and the variable $\Xi(t)$ as

$$\Xi(t) = \mathrm{e}^{-\nu_x t} s_0 + a_x \int_0^t \mathrm{e}^{-\nu_x (t-\mathrm{t})} \left[L_p^g \delta_p + L_d^g \varepsilon_d(\mathrm{t}) + L_u^g \varepsilon_u(\mathrm{t})\right] \mathrm{dt},$$

which is written in differential form as

$$\dot{\Xi} = -\nu_x \Xi + a_x \left(L_p^g \delta_p + L_d^g \varepsilon_d(t) + L_u^g \varepsilon_u(t)\right), \; \Xi(0) = a_x \|\boldsymbol{x}_0\|$$

by the definition of $\Xi(t)$ then (3.14a) is implied, using (3.2b) one obtains (3.14b).

A.3.2 *Proof of Proposition 3.1*

Apply Lemma 3.1 to each subsystem to obtain

$$\|\boldsymbol{x}_1(t)\| \leq a_{x_1} \|\boldsymbol{x}_{10}\| \mathrm{e}^{-\nu_{x1} t} + a_{x1} \int_0^t \mathrm{e}^{-\nu_{x1}(t-\mathrm{t})} \left[L_{x_2}^{g_1} \|\boldsymbol{x}_2(\mathrm{t})\| + L_{p_1}^{g_1} \delta_{p1} + L_{d_1}^{g_1} \varepsilon_{d1}(\mathrm{t}) + L_{u_1}^{g_1} \varepsilon_{u1}(\mathrm{t})\right] \mathrm{dt},$$

$$\|\boldsymbol{x}_2(t)\| \leq a_{x_2} \|\boldsymbol{x}_{20}\| \mathrm{e}^{-\nu_{x2} t} + a_{x2} \int_0^t \mathrm{e}^{-\nu_{x2}(t-\mathrm{t})} \left[L_{x_1}^{g_2} \|\boldsymbol{x}_1(\mathrm{t})\| + L_{p_2}^{g_2} \delta_{p2} + L_{d_2}^{g_2} \varepsilon_{d2}(\mathrm{t}) + L_{u_2}^{g_2} \varepsilon_{u2}(\mathrm{t})\right] \mathrm{dt},$$

apply Lemma 3.2 to obtain

$$\|\boldsymbol{x}_1(t)\| \leq \Xi_1(t), \quad \dot{\Xi}_1(t) = -\nu_{x1} \Xi_1 + a_{x1} \left(L_{x_2}^{g_1} \|\boldsymbol{x}_2(t)\| + L_{p1}^{g_1} \delta_{p1} + L_{d_1}^{g_1} \varepsilon_{d1}(t) + L_{u_1}^{g_1} \varepsilon_{u1}(t)\right),$$

$$\|\boldsymbol{x}_2(t)\| \leq \Xi_2(t), \quad \dot{\Xi}_2(t) = -\nu_{x2} \Xi_2 + a_{x2} \left(L_{x_1}^{g_2} \|\boldsymbol{x}_1(t)\| + L_{p_2}^{g_2} \delta_{p2} + L_{d_2}^{g_2} \varepsilon_{d2}(t) + L_{u_2}^{g_2} \varepsilon_{u2}(t)\right),$$

with initial conditions $\Xi_j(0) = a_{xj} \|\boldsymbol{x}_{j0}\|$. Use of the fact that $\|\boldsymbol{x}_j(t)\| \leq \Xi_j(t)$ for $j = 1, 2$ to rewrite the above expression as

$$\|\boldsymbol{x}_1(t)\| \leq \Xi_1(t), \quad \dot{\Xi}_1 \leq -\nu_{x1} \Xi_1 + a_{x1} \left(L_{x_2}^{g_1} \Xi_2(t) + L_{p_1}^{g_1} \delta_{p1} + L_d^{g_1} \varepsilon_d(t) + L_u^{g_1} \varepsilon_u(t)\right),$$

$$\|\boldsymbol{x}_2(t)\| \leq \Xi_2(t), \quad \dot{\Xi}_2 \leq -\nu_{x2} \Xi_2 + a_{x2} \left(L_{x_1}^{g_2} \Xi_1(t) + L_{p_2}^{g_2} \delta_{p2} + L_{d_2}^{g_2} \varepsilon_d(t) + L_{u_2}^{g_2} \varepsilon_{u2}(t)\right),$$

in compact form the inequality in the Ξ_i variables is

$$\dot{\boldsymbol{\Xi}}(t) \leq \boldsymbol{A}_s \boldsymbol{\Xi}(t) + \boldsymbol{B}_p \boldsymbol{\delta}_p + \boldsymbol{B}_d \boldsymbol{\varepsilon}_d(t) + \boldsymbol{B}_u \boldsymbol{\varepsilon}_u(t), \quad \boldsymbol{s}(0) = \boldsymbol{\Xi}_0, \tag{a.5}$$

where $\boldsymbol{\Xi}(t) = \begin{bmatrix} \Xi_1(t) & \Xi_2(t) \end{bmatrix}^T$, $\boldsymbol{\delta}_p = \begin{bmatrix} \delta_{p1} & \delta_{p2} \end{bmatrix}^T$, $\boldsymbol{\varepsilon}_d(t) = \begin{bmatrix} \varepsilon_{d1}(t) & \varepsilon_{d2} t \end{bmatrix}^T$, $\boldsymbol{\varepsilon}_u(t) = \begin{bmatrix} \varepsilon_{u1}(t) & \varepsilon_{u2}(t) \end{bmatrix}^T$, and

$$\boldsymbol{A}_s = \begin{bmatrix} -\nu_{x1} & a_{x1} L_{x_2}^{g_1} \\ a_{x2} L_{x_1}^{g_2} & -\nu_{x2} \end{bmatrix}, \quad \boldsymbol{B}_p = \begin{bmatrix} a_{x1} L_{p_1}^{g_1} & 0 \\ 0 & a_{x2} L_{p_2}^{g_2} \end{bmatrix},$$

$$\boldsymbol{B}_d = \begin{bmatrix} a_{x1} L_{d_1}^{g_1} & 0 \\ 0 & a_{x2} L_{d_2}^{g_2} \end{bmatrix}, \quad \boldsymbol{B}_u = \begin{bmatrix} a_{x1} L_{u_1}^{g_1} & 0 \\ 0 & a_{x2} L_{u_2}^{g_2} \end{bmatrix},$$

The matrix $\boldsymbol{A}_s$ is Hurwitz if conditions (3.15), which implies that the related matrix exponential satisfies

$$\left\| \mathrm{e}^{\boldsymbol{A}_s} t \right\| \leq a_s \mathrm{e}^{-\lambda_s t}, \quad -\lambda_s = \max_{\lambda_j \in \sigma(\boldsymbol{A}_s)} \left\{ \mathrm{Re}(\lambda_j) \right\}. \tag{a.6}$$

Using the comparison lemma, the variable $\boldsymbol{\Xi}(t)$ is bounded by the solution of the Ordinary Differential Equation (ODE) defined by the equality case in (a.5), i. e.,

$$\boldsymbol{\Xi}(t) \leq \mathrm{e}^{\boldsymbol{A}_s t} \Xi_0 + \int_0^t \mathrm{e}^{\boldsymbol{A}_s(t-\mathrm{t})} \left(\boldsymbol{B}_p \boldsymbol{\delta}_p + \boldsymbol{B}_d \boldsymbol{\varepsilon}_d(\mathrm{t}) + \boldsymbol{B}_u \boldsymbol{\varepsilon}_u(\mathrm{t}) \right) \mathrm{dt},$$

taking norms, applying the triangle inequality, using (a.6), and taking the supremums of the exogenous inputs it follows that

$$\| \boldsymbol{\Xi}(t) \| \leq a_s \| \boldsymbol{\Xi}_0 \| \mathrm{e}^{-|\lambda_s| t} + b_{p12} \delta_{p12} + b_{sd} \varepsilon_{d12}^{+} + b_{su} \varepsilon_{d12}^{+},$$

where $\delta_{p12} = \sqrt{\delta_{p1}^2 + \delta_{p2}^2}$, $\varepsilon_{d12} = \sqrt{\varepsilon_{d1}^2 + \varepsilon_{d2}^2}$, and $\varepsilon_{u12} = \sqrt{\varepsilon_{u1}^2 + \varepsilon_{u2}^2}$. Finally, using the definition of $\Xi_i(t)$, $i = 1, 2$ it can be concluded that the state $\boldsymbol{x}(t)$ of the interconnected system (3.12) satisfy (3.3) with

$$\nu_x = \lambda_s, \quad a_x = a_s(a_{1x} + a_{2x}), \quad (b_p, b_d, b_u) = \frac{a_s}{\nu_s} \left(\| \boldsymbol{B}_p \|, \| \boldsymbol{B}_d \|, \| \boldsymbol{B}_u \| \right).$$

If condition (3.15) holds locally in $\mathfrak{X}$ then te result is local, otherwise if the result is valid in the nonlocal sense in $\mathscr{X}$. This completes the proof.

b PARAMETRIC AN DISCRETIZATION ERROR NORMS

The set norm used to assess limit set convergence in (3.24) is given by means of the static parametric error norm defined as

$$\epsilon_d^s(N_{pde}, N) = \sum_{k=1}^{n_s} v_k \sum_{j=1}^{n_p=2} w_j \int_0^1 \left| \chi_{N_{pde},k,j}(s, \boldsymbol{p}) - \chi_{N_{pde},k,j}(s, \boldsymbol{p}) \right| \mathrm{d}s, \tag{b.1a}$$

where n_s is the number of steady-states, n_p is the number of state profiles, and v_k and w_j are weights. If the limit set includes limit cycles, then the following norm must be used

$$\epsilon_d^t(N_{pde}, N) = \sum_{j=1}^{n_p=2} w_j \int_0^{t_f} \left[\int_0^1 \left| \chi_{N,j}(s, t, \boldsymbol{p}) - \chi_{N_{pde},j}(s, t, \boldsymbol{p}) \right| \mathrm{d}s \right] \mathrm{d}t. \tag{b.1b}$$

The computation of the discretization error in (3.29a) must be computed with (b.1b) when the limit sets contains limit cycles, or with (b.1a) when the limit set is composed only with steady-states.

The parametric error for static (or transient) regime are defined as

$$\epsilon_p^s(N_{pde}, \tilde{\boldsymbol{p}}) = \sum_{k=1}^{n_s} v_k \sum_{j=1}^{2} w_j \int_0^1 \left| \chi_{N,k,j}(s, t, \boldsymbol{p} + \tilde{\boldsymbol{p}}) - \chi_{N_{pde},k,j}(s, t, \boldsymbol{p}) \right| \mathrm{d}s, \tag{b.2a}$$

$$\epsilon_p^t(N_{pde}, \tilde{\boldsymbol{p}}) = \sum_{j=1}^{2} w_j \int_0^{t_f} \left[\int_0^1 \left| \chi_{N_{pde},j}(s, t, \boldsymbol{p} + \tilde{\boldsymbol{p}}) - \chi_{N_{pde},j}(s, t, \tilde{\boldsymbol{p}}) \right| \mathrm{d}s \right] \mathrm{d}t. \tag{b.2b}$$

The computation of the parametric error in (3.29b) must be computed with (b.2b) when the limit sets contains limit cycles, or with (b.2a) when the limit is composed only by steady-states.

In all the above definitions: $\chi_{N,k,j}(s)$ and $\chi_{N,j}(s,t)$ (or $\chi_{N_{pde},k,j}(s)$ and $\chi_{N_{pde},j}(s,t)$) are the interpolated solutions of the concentration and temperature profiles of the discretized reactor model (3.22) with discretization order N (or N_{pde}), and t_f is the time window in which a sufficiently rich dynamic transient behavior occur for approximation purposes.

C

HURWITZ MATRICES A_j, $j = 1, 2$

Note that both matrices $\boldsymbol{A}_j$, $j = 1, 2$ in (4.13) are the Finite Differences (FD)-based discretization of the mass and heat transport effects of the Partial Differential Equation (PDE) model (2.7), including the boundary conditions, i. e.,

$$\boldsymbol{A}_j = \boldsymbol{A}_{j,d} + \boldsymbol{B}_{j,b}$$

where $\boldsymbol{A}_{j,d}$ is the discretization of in-domain mass transport, and $\boldsymbol{B}_{j,b}$ together with $\boldsymbol{B}_{d,j} d_j$ accounts for boundary conditions on the mass and heat balances. These matrices are given after (3.19). Note that matrices $\boldsymbol{A}_{j,d}$ are Toeplitz and thus their eigenvalues can be computed as ($i = 1, \ldots, N_e$)

$$\lambda_i(\boldsymbol{A}_{1,d}) = -\frac{2 + Pe_m \Delta s}{Pe_m s^2} - 2\sqrt{\frac{1}{Pe_m \Delta s^2} \frac{1 + Pe_m \Delta_s}{Pe_m \Delta s^2}} \cos(i\pi\Delta s),$$

$$\lambda_i(\boldsymbol{A}_{2,d}) = -\frac{2 + Pe_h \Delta s + v Pe_h \Delta s^2}{Pe_h \Delta s^2} - 2\sqrt{\frac{1}{Pe_h \Delta s^2} \frac{1 + Pe_h \Delta_s}{Pe_h \Delta s^2}} \cos(i\pi\Delta s).$$

From the above formulae, the minimum and maximum eigenvalues are given for the indexes $i = 1$ and $i = N_e$, respectively. Thus, the minimum eigenvalues are given as

$$\lambda_1(\boldsymbol{A}_{1,d}) = -\frac{2 + Pe_m \Delta s}{Pe_m \Delta s^2} - 2\sqrt{\frac{1}{Pe_m \Delta s^2} \frac{1 + Pe_m \Delta_s}{Pe_m \Delta s^2}} \cos(\pi\Delta s),$$

$$\lambda_1(\boldsymbol{A}_{2,d}) = -\frac{2 + Pe_h \Delta s + v Pe_h \Delta s^2}{Pe_h \Delta s^2} - 2\sqrt{\frac{1}{Pe_h \Delta s^2} \frac{1 + Pe_h \Delta_s}{Pe_h \Delta s^2}} \cos(\pi\Delta s),$$

while the maximums are

$$\lambda_{N_e}(\boldsymbol{A}_{1,d}) = -\frac{2 + Pe_m \Delta s}{Pe_m \Delta s^2} - 2\sqrt{\frac{1}{Pe_m \Delta s^2} \frac{1 + Pe_m \Delta_s}{Pe_m \Delta s^2}} \cos(N_e\pi\Delta s),$$

$$\lambda_{N_e}(\boldsymbol{A}_{2,d}) = -\frac{2 + Pe_h \Delta s + v Pe_h \Delta s^2}{Pe_h \Delta s^2} - 2\sqrt{\frac{1}{Pe_h \Delta s^2} \frac{1 + Pe_h \Delta_s}{Pe_h \Delta s^2}} \cos(N_e\pi\Delta s).$$

Consequently, taking the limits as $\Delta s \to 0$ it is possible to characterize the set in which the whole spectrum of both matrices is contained. Accordingly, it can be seen the minimum eigenvalue goes to infinity, i. e.,

$$\lim_{\Delta s \to 0} \lambda_1(\boldsymbol{A}_{1,d}) = -\infty, \quad \lim_{\Delta s \to 0} \lambda_1(\boldsymbol{A}_{2,d}) = -\infty.$$

The maximum eigenvalues can be computed using the change of variable $N_e = \frac{1}{\Delta s} - 1$ and applying the L'Hopital rule twice to obtain

$$\lim_{\Delta s \to 0} \lambda_N(\boldsymbol{A}_{1,d}) = -\left(\frac{\pi^2}{Pe_m} + \frac{Pe_m}{4}\right), \quad \lim_{\Delta s \to 0} \lambda_N(\boldsymbol{A}_{2,d}) = -\left(\frac{\pi^2}{Pe_h} + \frac{Pe_h}{4} + v\right).$$

It can be concluded that all the eigenvalues of the Toeplitz matrices lay in the left of the complex plane, i. e.,

$$\lambda_i(\boldsymbol{A}_{1,d}) \in \left(-\infty, -\left(\frac{\pi^2}{Pe_m} + \frac{Pe_m}{4}\right)\right], \quad \lambda_i(\boldsymbol{A}_{2,d}) \in \left(-\infty, -\left(\frac{\pi^2}{Pe_h} + \frac{Pe_h}{4} + v\right)\right]$$

Applying the Gerschgorin theorem [128], their eigenvalues can be bounded as follows

$$\left|\lambda_1(\boldsymbol{A}_{1,d}) + \frac{2 + Pe_m\Delta s}{Pe_m\Delta s^2}\right| \leq \frac{1}{Pe_m\Delta s^2}, \quad \left|\lambda_1(\boldsymbol{A}_{2,d}) + \frac{2 + Pe_h\Delta s + vPe_h\Delta s^2}{Pe_h\Delta s^2}\right| \leq \frac{1}{Pe_h\Delta s^2}$$

$$\left|\lambda_i(\boldsymbol{A}_{1,d}) + \frac{2 + Pe_m\Delta s}{Pe_m\Delta s^2}\right| \leq \frac{2 + Pe_m\Delta s}{Pe_m\Delta s^2}, \quad \left|\lambda_i(\boldsymbol{A}_{2,d}) + \frac{2 + Pe_h\Delta s + vPe_h\Delta s^2}{Pe_h\Delta s^2}\right| \leq \frac{2 + Pe_h\Delta s}{Pe_h\Delta s^2} \tag{C.1}$$

$$\left|\lambda_N(\boldsymbol{A}_{1,d}) + \frac{2 + Pe_m\Delta s}{Pe_m\Delta s^2}\right| \leq \frac{1 + Pe_m\Delta s}{Pe_m\Delta s^2}, \quad \left|\lambda_N(\boldsymbol{A}_{2,d}) + \frac{2 + Pe_h\Delta s + vPe_h\Delta s^2}{Pe_h\Delta s^2}\right| \leq \frac{1 + Pe_h\Delta s}{Pe_h\Delta s^2},$$

for $2 \leq i \leq N - 1$

Since the eigenvalues are continuous functions of the entries of a matrix, a small change on the entries may produce a small change on the eigenvalues. This means that the matrices $\boldsymbol{B}_{j,b}$, that incorporates the boundary conditions into matrices $\boldsymbol{A}_{j,d}$, move a little the eigenvalues of $\boldsymbol{A}_{j,d}$. As a consequence, the eigenvalues of $\boldsymbol{A}_j$ are located near the eigenvalues of $\boldsymbol{A}_{j,d}$. These eigenvalues can be bounded employing again the Gerschgorin circles theorem [128], which shows that the eigenvalues for $2 \leq i \leq N - 1$ are bounded equally as the ones of $\boldsymbol{A}_{j,d}$ (see (C.1)). For the minimum $\lambda_{A_{j*}}$ and maximum $\lambda_{A_j}{}^*$ eigenvalues of $\boldsymbol{A}_j$ it follows that

$$\left|\lambda_{A_{1*}} + \frac{1 + Pe_m\Delta s}{Pe_m\Delta s^2}\right| \leq \frac{1}{Pe_m\Delta s^2}, \quad \left|\lambda_{A_{2*}} + \frac{1 + Pe_h\Delta s + vPe_h\Delta s^2}{Pe_h\Delta s^2}\right| \leq \frac{1}{Pe_h\Delta s^2},$$

$$\left|\lambda_{A_1}{}^* + \frac{1 + Pe_h\Delta s}{Pe_m\Delta s^2}\right| \leq \frac{1 + Pe_m\Delta s}{Pe_m\Delta s^2}, \quad \left|\lambda_{A_2}{}^* + \frac{1 + Pe_h\Delta s + vPe_h\Delta s^2}{Pe_h\Delta s^2}\right| \leq \frac{1 + Pe_h\Delta s}{Pe_h\Delta s^2},$$

which implies that all the eigenvalues of the matrices $\boldsymbol{A}_j$ lay in the left half of the complex plane, i. e., matrices $\boldsymbol{A}_j$, $j = 1, 2$ are Hurwitz matrices

d

ZERO DYNAMICS STABILITY PROOFS

D.1 PROOF OF PROPOSITION 4.2

Following a similar procedure as in Section 4.2.2.1, it can be established that the first internal state $\boldsymbol{\eta}_1$ satisfy the following expression

$$\|\boldsymbol{\eta}_1(t)\| \leq a_{x1} \|\boldsymbol{\eta}_{10}\| \, \mathrm{e}^{-\nu_{1\eta} t} + a_{x1} \int_0^t \mathrm{e}^{-\nu_{1\eta}(t-\mathrm{t})} \left(\|\boldsymbol{B}_{d,1}\| \, |d_1| + L_{\eta 2}^{\phi_{12}^{\eta}} \|\boldsymbol{\eta}_2\| + L_{\boldsymbol{\xi}}^{\varphi_1^{\xi}} \|\boldsymbol{\xi}\| \right) \mathrm{dt}.$$

locally in $X_{\eta 1}$ and for the bounded inputs $\boldsymbol{d}$ and $\|\boldsymbol{\xi}\| \leq \varepsilon_{\xi}$. Thus, it can be concluded that the dynamics of $\boldsymbol{\eta}_1$ are robustly stable locally in $X_{\eta 1}$ and that satisfies (3.3) with parameters $\nu_{\eta 1} = \zeta_1 + c$, a_{x1} given in (4.17b), and $(b_d, b_{\eta 2}, b_{\xi 1}) = \frac{a_{\eta 1}}{\nu_{\eta 1}} \left(\|\boldsymbol{B}_{d,1}\|, L_{\eta 2}^{\varphi_{12}^{\eta}}, L_{\xi}^{\varphi_1^{\xi}} \right)$.

For the second state, defined in the finite domain $X_{\eta 2}$, apply Lemma 3.1 to obtain

$$\begin{aligned}\|\boldsymbol{\eta}_2(t)\| \leq{} & a_{\eta 2} \|\boldsymbol{\eta}_{20}\| \, \mathrm{e}^{-\nu_{\eta 2} t} + \\ & + a_{\eta 2} \int_0^t \mathrm{e}^{-\nu_{\eta 2}(t-\mathrm{t})} \left(\left\|\boldsymbol{B}_{2,d}^{\eta}\right\| |d_2| + L_{\eta 1}^{\phi_2^{\eta}} \|\boldsymbol{\eta}_1\| + (\left\|\boldsymbol{A}_2^{\eta}\right\| + L_{\xi}^{\varphi_2^{\xi}} \|\boldsymbol{\xi}\| \right) \mathrm{dt}.\end{aligned}$$

and is robustly stable with parameters $\nu_{\eta 2} = (\lambda_{\eta 2}^* - a_{\eta 2} L_{\eta 2}^{\phi_2^{\eta}}$, $a_x = a_{\eta 2}$ and $(b_d, b_{\eta 1}, b_{\xi 2}) = \frac{a_{\eta 2}}{\nu_{\eta 2}} \left(\|\boldsymbol{B}_{d,2}\|, L_{eta_1}^{\phi_2^{\eta}}, \left\|\boldsymbol{A}_2^{\xi}\right\| + L_{\xi}^{\varphi_2^{\xi}} \right)$.

From the application of Proposition 3.1, it follows that the state trajectories of the zero dynamics are bounded as

$$\|\boldsymbol{\eta}(t)\| \leq a_{\eta} \|\boldsymbol{\eta}_0\| \, \mathrm{e}^{-\nu_{\eta} t} + a_{\eta} \int_0^t \mathrm{e}^{-\nu_{\eta}(t-\mathrm{t})} \left(\left\|\boldsymbol{B}_d^{\eta}\right\| \|\boldsymbol{d}\| + \left\|\boldsymbol{B}_{\xi}\right\| \|\boldsymbol{\xi}\| \right) \mathrm{dt},$$

if condition (4.34) is met. This implies the robust stability of the zero dynamics with parameters $\nu_x = \lambda_{\eta}$, $a_x = a_{\eta}(a_{\eta 1} + a_{\eta 2})$, and $(b_d, b_{\xi}) = \frac{a_{\eta}}{\nu_{\eta}} \left(\left\|\boldsymbol{B}_d^{\eta}\right\|, \left\|\boldsymbol{B}_{\xi}\right\| \right)$, where ${\lambda_{\eta}}^*$ is the maximum real part of the eigenvalues of matrix $\boldsymbol{A}_{\eta}$:

$$\boldsymbol{A}_{\eta} = \begin{bmatrix} -\nu_{\eta 1} & a_{\eta 1} L_{\eta 2}^{\varphi_1^{\eta}} \\ a_{\eta 2} L_{\eta 1}^{\phi_2^{\eta}} & -\nu_{\eta 2} \end{bmatrix}, \quad \left\|\boldsymbol{A}_{\mathrm{J}}\right\| \leq a_{\eta} \mathrm{e}^{-\lambda_{\eta} t}, \quad -\lambda_{\eta} = \max_{\lambda_j \in \sigma(A_{\eta})} \{\mathrm{Re}(\lambda_j)\},$$

$$\boldsymbol{B}_d^{\eta} = \begin{bmatrix} a_{\eta 1} \|\boldsymbol{B}_{1,e}\| & 0 \\ 0 & a_{\eta 2} \|\boldsymbol{B}_{2,e}\| \end{bmatrix}, \quad \boldsymbol{B}_{\xi} = \begin{bmatrix} a_{\eta 1} L_{\xi}^{\varphi_1^{\xi}} \\ a_{\eta 2}(\left\|\boldsymbol{A}_2^{\xi}\right\| + L_{\xi}^{\varphi_2^{\xi}}) \end{bmatrix}.$$

This completes the proof.

D.2 PROOF OF PROPOSITION 4.3

Performing a similar procedure as in Section 4.2.2.1, on the stability analysis of the concentration dynamics, it is easy to compute that the state $\boldsymbol{x}_1$ satisfy

$$\|\boldsymbol{x}_1\| \leq a_1 \|\boldsymbol{x}_{10}\| \mathrm{e}^{-\nu_1 t} + a_1 \int_0^t \mathrm{e}^{-\nu_1(t-\mathrm{t})}(L^{\varphi_{n,m}}_{x_{2,n}} \|\boldsymbol{x}_{2,n}\| + L^{\varphi_{n,m}}_{x_{2,m}} \|\boldsymbol{x}_{2,m}\| + \|\boldsymbol{B}_{d,1}\| \, |d_1|)\boldsymbol{d}\mathrm{t},$$

where $\nu_1 = \zeta + c$. For the unmeasured temperature state the application of Lemma 3.1 gives the estimate

$$\begin{aligned}\|\boldsymbol{x}_{2,n}\| \leq\; & a_{2z} \|\boldsymbol{x}_{2,n,0}\| \mathrm{e}^{-\nu_{2z} t} + \\ & + a_{2z} \int_0^t \mathrm{e}^{-\nu_{2z}(t-\mathrm{t})} \left(L^{\psi_z}_{x_1} \|\boldsymbol{x}_1\| + \|\boldsymbol{A}_2^{z,m}\| \, \|\boldsymbol{x}_{2,m}\| + \left\|\boldsymbol{B}^z_{d,2}\right\| |d_2| \right) \mathrm{dt},\end{aligned}$$

with $\nu_{2z} = |\lambda_{A_2^z}{}^*| - a_{2z} L^{\psi_z}_{x_{2,n}}$. The application of Proposition 3.1, establishes that if condition (4.43) is met, then the unmeasured state $\boldsymbol{x}_n = [\boldsymbol{x}_1^T \, \boldsymbol{x}_{2,n}^T]^T$ is robustly stable and satisfies

$$\|\boldsymbol{x}_n(t)\| \leq a_n \|\boldsymbol{x}_{n,0}\| \mathrm{e}^{-\nu_z t} + b_d \varepsilon_d^+ + b_{2m} \varepsilon_{2m}, \tag{d.2}$$

where

$$a_n = a_s(a_1 + a_{2z}),\; \nu_z = \max_{\lambda_j \in \sigma(\boldsymbol{A}_z)} \left\{ \mathrm{Re}(\lambda_j) \right\},\; j = 1, 2, \quad b_d = \frac{a_n \|\boldsymbol{B}_d\|}{\nu_z},\; b_{2m} = \frac{a_n \|\boldsymbol{B}_m\|}{\nu_z},$$

$$\boldsymbol{A}_n = \begin{bmatrix} -(\zeta + \gamma) & a_1 L^{\varphi_{n,m}}_{x_{2,n}} \\ a_{2z} L^{\psi_z}_{x_1} & -(|\lambda_{A_2^z}{}^*| - a_{2z} L^{\psi_z}_{x_{2,n}}) \end{bmatrix}, \quad \boldsymbol{B}_d = \begin{bmatrix} \|\boldsymbol{B}_{d,1}\| & \boldsymbol{0} \\ \boldsymbol{0} & \left\|\boldsymbol{B}^z_{d,2}\right\| \end{bmatrix},$$

$$\boldsymbol{B}^z_m = \begin{bmatrix} L^{\varphi_{n,m}}_{x_{2,m}} \\ \|\boldsymbol{A}_2^{z,m}\| + L^{\psi_z}_{x_{2,m}} \end{bmatrix}.$$

D.3 PROOF OF PROPOSITION 4.4

Recall the reactor model in the normal form (4.30), assume that the conditions of Proposition 4.4 are satisfied. Then the zero dynamics origin is exponentially stable with a Lyapunov function that satisfies (3.5a). The control law

$$\boldsymbol{u} = (\boldsymbol{B}^m_u)^{-1} \left(-\boldsymbol{f}_m(\boldsymbol{x}_1, \boldsymbol{x}_{2,n}, \boldsymbol{x}_{2,m}, d_2) + \left(\partial_\eta V_\eta(\boldsymbol{\eta}) \boldsymbol{F}(\boldsymbol{\eta}, \boldsymbol{\xi})\right)^T + \boldsymbol{v} \right)$$

and the storage function $V(\boldsymbol{\eta}, \boldsymbol{y})$ defined as

$$V = V_\eta(\boldsymbol{\eta}) + \frac{1}{2} \boldsymbol{y}^T \boldsymbol{y}$$

ensure the passivity of the system passive with respect to the new input $\boldsymbol{v}$. This can be proven substituting the above control law in (4.30) and taking the time derivative of V along the trajectories of the system, i. e.,

$$\begin{aligned}\dot{V} &= \partial_\eta V_\eta(\boldsymbol{\eta})\dot{\boldsymbol{\eta}} + \frac{1}{2}\dot{\boldsymbol{y}}^T\boldsymbol{y} + \frac{1}{2}\boldsymbol{y}^T\dot{\boldsymbol{y}},\\ &= \partial_\eta V_\eta(\boldsymbol{\eta})\left(\boldsymbol{f}_\eta(\boldsymbol{\eta}) + \boldsymbol{F}(\boldsymbol{\eta},\boldsymbol{\xi})\boldsymbol{\xi}\right) + \frac{1}{2}\left(\left(\partial_\eta V_\eta(\boldsymbol{\eta})\boldsymbol{F}(\boldsymbol{\eta},\boldsymbol{\xi})\right)^T + \boldsymbol{v}\right)^T\boldsymbol{y} +\\ &\quad + \frac{1}{2}\boldsymbol{y}^T\left(\left(\partial_\eta V_\eta(\boldsymbol{\eta})\boldsymbol{F}(\boldsymbol{\eta},\boldsymbol{\xi})\right)^T + \boldsymbol{v}\right)\\ &= \partial_\eta V_\eta(\boldsymbol{\eta})\boldsymbol{f}_\eta(\boldsymbol{\eta}) + \partial_\eta V_\eta(\boldsymbol{\eta})\boldsymbol{F}(\boldsymbol{\eta},\boldsymbol{\xi})\boldsymbol{y} + \boldsymbol{y}^T\left(\left(\partial_\eta V_\eta(\boldsymbol{\eta})\boldsymbol{F}(\boldsymbol{\eta},\boldsymbol{\xi})\right)^T + \boldsymbol{v}\right),\\ &= \partial_\eta V_\eta(\boldsymbol{\eta})\boldsymbol{f}_\eta(\boldsymbol{\eta}) + \boldsymbol{y}^T\boldsymbol{v}\end{aligned}$$

using

$$\boldsymbol{v} = -\boldsymbol{\kappa}_1(\boldsymbol{\xi}) + \boldsymbol{w}$$

where $\boldsymbol{\kappa}_1$ is a passive static nonlinearity, and the fact that the zero dynamics origin is exponentially stable and its Lyapunov function satisfies (3.5a), then it can be ensured that the system is strictly state passive, i. e.,

$$\dot{V} = -c_\eta \|\boldsymbol{\eta}\|^2 - \boldsymbol{\xi}^T\boldsymbol{\kappa}_1(\boldsymbol{\xi}) + \boldsymbol{y}^T\boldsymbol{w}.$$

The employment of an additional output feedback of a passive static nonlinearity, such as

$$\boldsymbol{w} = -\boldsymbol{\kappa}_2(\boldsymbol{y}),$$

assigns the output convergence. Finally, the feedback control law that renders the system passive is given in (4.50).

e

CLOSED-LOOP STABILITY OF THE CONTROL-ESTIMATION SYSTEM

E.1 FUNCTIONS OF THE ACTUAL CLOSED-LOOP DYNAMICS (4.62)

The functions involved in (4.62) are given as

$$
\begin{aligned}
\boldsymbol{f}_1(\boldsymbol{x}_1, \boldsymbol{x}_{2,n}, \boldsymbol{x}_{2,m}, d_1) &= \boldsymbol{A}_1 \boldsymbol{x}_1 - \boldsymbol{\varphi}_1(\boldsymbol{x}_1) - \boldsymbol{\psi}_{n,m}(\boldsymbol{x}_1, \boldsymbol{x}_{2,n}, \boldsymbol{x}_{2,m}),\\
\boldsymbol{f}^c_{2,n}(\boldsymbol{x}_1, \boldsymbol{x}_{2,n}, \boldsymbol{x}_{2,m}, d_2) &= \boldsymbol{A}_2^{n,n} \boldsymbol{x}_{2,n} + \boldsymbol{A}_2^{m,n} \boldsymbol{x}_{2,m} + \boldsymbol{\psi}_n(\boldsymbol{x}_1, \boldsymbol{x}_{2,n}) + \boldsymbol{B}^n_{u,2} \boldsymbol{\mu}_s(\bar{\boldsymbol{x}}_1, \bar{\boldsymbol{x}}_{2,n}, \boldsymbol{x}_{2,m}),\\
\boldsymbol{f}^c_{2,m}(\boldsymbol{x}_1, \boldsymbol{x}_{2,n}, \boldsymbol{x}_{2,m}, d_2) &= \boldsymbol{A}_2^{m,m} \boldsymbol{x}_{2,m} + \boldsymbol{A}_2^{m,n} \boldsymbol{x}_{2,n} + \boldsymbol{\psi}_m(\boldsymbol{x}_1, \boldsymbol{x}_{2,m}) + \boldsymbol{B}^m_{u,2} \boldsymbol{\mu}_s(\bar{\boldsymbol{x}}_1, \bar{\boldsymbol{x}}_{2,n}, \boldsymbol{x}_{2,m}),\\
\boldsymbol{e}^c_1(\boldsymbol{x}_1, \boldsymbol{x}_{2,n}, \boldsymbol{x}_{2,m}, d_2, \boldsymbol{\pi}, \tilde{\boldsymbol{p}}) &= \boldsymbol{e}_1(\boldsymbol{x}_1, \boldsymbol{x}_{2,n}, \boldsymbol{x}_{2,m}, \boldsymbol{\mu}_s(\boldsymbol{x}_1, \boldsymbol{x}_{2,n}, \boldsymbol{x}_{2,m}, d_2), \boldsymbol{\pi}, \tilde{\boldsymbol{p}}),\\
\boldsymbol{e}^c_{2,n}(\boldsymbol{x}_1, \boldsymbol{x}_{2,n}, \boldsymbol{x}_{2,m}, d_2, \boldsymbol{\pi}, \tilde{\boldsymbol{p}}) &= \boldsymbol{e}_{2,n}(\boldsymbol{x}_1, \boldsymbol{x}_{2,n}, \boldsymbol{x}_{2,m}, \boldsymbol{\mu}_s(\boldsymbol{x}_1, \boldsymbol{x}_{2,n}, \boldsymbol{x}_{2,m}, d_2), \boldsymbol{\pi}, \tilde{\boldsymbol{p}}),\\
\boldsymbol{e}^c_{2,m}(\boldsymbol{x}_1, \boldsymbol{x}_{2,n}, \boldsymbol{x}_{2,m}, d_2, \boldsymbol{\pi}, \tilde{\boldsymbol{p}}) &= \boldsymbol{e}_{2,m}(\boldsymbol{x}_1, \boldsymbol{x}_{2,n}, \boldsymbol{x}_{2,m}, \boldsymbol{\mu}_s(\boldsymbol{x}_1, \boldsymbol{x}_{2,n}, \boldsymbol{x}_{2,m}, d_2), \boldsymbol{\pi}, \tilde{\boldsymbol{p}}),\\
\boldsymbol{\varrho}^c_1(\boldsymbol{x}_1, \boldsymbol{x}_{2,n}, \boldsymbol{x}_{2,m}, \boldsymbol{d}; \boldsymbol{\pi}, \boldsymbol{\nu}) &= \boldsymbol{\varrho}(\boldsymbol{x}_1, \boldsymbol{x}_{2,n}, \boldsymbol{x}_{2,m}, \boldsymbol{d}, \boldsymbol{\mu}_s(\boldsymbol{x}_1, \boldsymbol{x}_{2,n}, \boldsymbol{x}_{2,m}, d_2); \boldsymbol{\pi}, \boldsymbol{\nu}).
\end{aligned}
$$

E.2 CLOSED-LOOP FUNCTIONS OF THE ACTUAL CLOSED-LOOP DYNAMICS (4.70)

The involved functions in the closes-loop system (4.70) are given as

$$
\begin{aligned}
\boldsymbol{\Pi}^c_2(\boldsymbol{x}, \boldsymbol{d}, \tilde{\boldsymbol{x}}_e, \tilde{\boldsymbol{x}}_n; \boldsymbol{\pi}, \boldsymbol{\nu}) &= \boldsymbol{\Pi}(\boldsymbol{x}_1, \boldsymbol{x}_{2,n}, \boldsymbol{x}_{2,m}, \boldsymbol{d}, \boldsymbol{\mu}_{s,e}(\boldsymbol{x}_1 + \tilde{\boldsymbol{x}}_1, \boldsymbol{x}_{2,n} + \tilde{\boldsymbol{x}}_{2,n}, \boldsymbol{x}_2 + \tilde{\boldsymbol{x}}_{2,m}, \boldsymbol{\iota}_y + \tilde{\boldsymbol{\iota}}_y, d_2); \boldsymbol{\pi}, \boldsymbol{\nu}),\\
\tilde{\boldsymbol{f}}_e(\boldsymbol{x}; \boldsymbol{\pi}, \tilde{\boldsymbol{p}}, d_2, \tilde{\boldsymbol{x}}_e, \tilde{\boldsymbol{x}}_n) &= \begin{bmatrix} \tilde{\boldsymbol{f}}_y(\boldsymbol{x}; \boldsymbol{\pi}, \tilde{\boldsymbol{p}}, d_2, \tilde{\boldsymbol{x}}_e, \tilde{\boldsymbol{x}}_n) \\ \tilde{\boldsymbol{f}}_\iota(\boldsymbol{x}; \boldsymbol{\pi}, \tilde{\boldsymbol{p}}, d_2, \tilde{\boldsymbol{x}}_e, \tilde{\boldsymbol{x}}_n) \end{bmatrix}, \quad \boldsymbol{A}_e = \begin{bmatrix} \boldsymbol{K}_y & \boldsymbol{I} \\ \boldsymbol{K}_\iota & \boldsymbol{0} \end{bmatrix},\\
\tilde{\boldsymbol{f}}_y(\boldsymbol{x}; \boldsymbol{\pi}, \tilde{\boldsymbol{p}}, d_2, \tilde{\boldsymbol{x}}_e, \tilde{\boldsymbol{x}}_n) &= \boldsymbol{f}^c_{2,m}(\boldsymbol{x}_1 + \tilde{\boldsymbol{x}}_1 + \boldsymbol{x}_{2,n} + \tilde{\boldsymbol{x}}_{2,n}, \boldsymbol{x}_{2,m} + \tilde{\boldsymbol{x}}_{2,m}, d_2) - \boldsymbol{f}^c_{2,m}(\boldsymbol{x}_1, \boldsymbol{x}_{2,n}, \boldsymbol{x}_{2,m}, d_2) +\\
&\quad + \boldsymbol{B}^m_{u,2} \tilde{\boldsymbol{\mu}}_s(\boldsymbol{x}_1, \boldsymbol{x}_{2,n}, \boldsymbol{x}_{2,m}, \boldsymbol{\iota}_y, d_2, \tilde{\boldsymbol{x}}_1, \tilde{\boldsymbol{x}}_{2,n}, \tilde{\boldsymbol{x}}_{2,m}, \tilde{\boldsymbol{\iota}}_y, \boldsymbol{l}) + \boldsymbol{K}_y \tilde{\boldsymbol{h}}(\boldsymbol{x}_{2,m}),\\
\tilde{\boldsymbol{f}}_\iota(\boldsymbol{x}; \boldsymbol{\pi}, \tilde{\boldsymbol{p}}, d_2, \tilde{\boldsymbol{x}}_e, \tilde{\boldsymbol{x}}_n) &= \boldsymbol{K}_\iota \tilde{\boldsymbol{h}}(\boldsymbol{x}_{2,m}) -\\
&\quad \partial_t \boldsymbol{e}^c_{2,m}(\boldsymbol{x}_1, \boldsymbol{x}_{2,n}, \boldsymbol{x}_{2,m}, \boldsymbol{\mu}_{s,e}(\boldsymbol{x}_1 + \tilde{\boldsymbol{x}}_1, \boldsymbol{x}_{2,n} + \tilde{\boldsymbol{x}}_{2,n}, \boldsymbol{x}_2 + \tilde{\boldsymbol{x}}_{2,m}, \boldsymbol{\iota}_y + \tilde{\boldsymbol{\iota}}_y, d_2), \boldsymbol{\pi}, \tilde{\boldsymbol{p}}),\\
\boldsymbol{f}_n(\tilde{\boldsymbol{x}}_e, \tilde{\boldsymbol{x}}_n, \boldsymbol{d}) &= \begin{bmatrix} \tilde{\boldsymbol{f}}_1(\boldsymbol{x}_1, \boldsymbol{x}_{2,n}, \boldsymbol{x}_{2,m}, d_1; \tilde{\boldsymbol{x}}_1, \tilde{\boldsymbol{x}}_{2,n}, \tilde{\boldsymbol{x}}_{2,m}) \\ \tilde{\boldsymbol{f}}_{2,n}(\boldsymbol{x}_1, \boldsymbol{x}_{2,n}, \boldsymbol{x}_{2,m}, d_2; \tilde{\boldsymbol{x}}_1, \tilde{\boldsymbol{x}}_{2,n}, \tilde{\boldsymbol{x}}_{2,m}) \end{bmatrix},\\
\tilde{\boldsymbol{f}}_1(\boldsymbol{x}_1, \boldsymbol{x}_{2,n}, \boldsymbol{x}_{2,m}, d_1; \tilde{\boldsymbol{x}}_1, \tilde{\boldsymbol{x}}_{2,n}, \tilde{\boldsymbol{x}}_{2,m}) &= \boldsymbol{f}_1(\boldsymbol{x}_1 + \tilde{\boldsymbol{x}}_1, \boldsymbol{x}_{2,n} + \tilde{\boldsymbol{x}}_{2,n}, \boldsymbol{x}_{2,m} + \tilde{\boldsymbol{x}}_{2,m}, d_1) - \boldsymbol{f}_1(\boldsymbol{x}_1, \boldsymbol{x}_{2,n}, \boldsymbol{x}_{2,m}, d_1),\\
\tilde{\boldsymbol{f}}_{2,n}(\boldsymbol{x}_1, \boldsymbol{x}_{2,n}, \boldsymbol{x}_{2,m}, d_2; \tilde{\boldsymbol{x}}_1, \tilde{\boldsymbol{x}}_{2,n}, \tilde{\boldsymbol{x}}_{2,m}) &= \boldsymbol{f}_{2,n}(\boldsymbol{x}_1 + \tilde{\boldsymbol{x}}_1, \boldsymbol{x}_{2,n} + \tilde{\boldsymbol{x}}_{2,n}, \boldsymbol{x}_{2,m} + \tilde{\boldsymbol{x}}_{2,m}, d_2) - \boldsymbol{f}_{2,n}(\boldsymbol{x}_1, \boldsymbol{x}_{2,n}, \boldsymbol{x}_{2,m}, d_2),
\end{aligned}
$$

$$
\begin{aligned}
\mathfrak{e}_n^c(\boldsymbol{x},\boldsymbol{d};\boldsymbol{\pi},\tilde{\boldsymbol{p}},\tilde{\boldsymbol{x}}_e,\tilde{\boldsymbol{x}}_n,\boldsymbol{l}) &= \begin{bmatrix} -\boldsymbol{e}_1^c(\boldsymbol{x}_1,\boldsymbol{x}_{2,n},\boldsymbol{x}_{2,m};d_1\boldsymbol{\pi},\tilde{\boldsymbol{p}},\boldsymbol{l}) \\ -\boldsymbol{e}_{2,n}^c(\boldsymbol{x}_1,\boldsymbol{x}_{2,n},\boldsymbol{x}_{2,m};d_2,\boldsymbol{\pi},\tilde{\boldsymbol{p}},\boldsymbol{l}) \end{bmatrix}, \\
\boldsymbol{f}_c(\boldsymbol{x},\boldsymbol{d}) &= \begin{bmatrix} \boldsymbol{f}_1(\boldsymbol{x}_1,\boldsymbol{x}_{2,n},\boldsymbol{x}_{2,m},d_1) \\ \boldsymbol{f}_{2,n}^c(\boldsymbol{x}_1,\boldsymbol{x}_{2,n},\boldsymbol{x}_{2,m},d_2) \\ \boldsymbol{f}_{2,m}^c(\boldsymbol{x}_1,\boldsymbol{x}_{2,n},\boldsymbol{x}_{2,m},d_2) \end{bmatrix}, \\
\mathfrak{e}^c(\boldsymbol{x},\boldsymbol{d};\boldsymbol{\pi},\tilde{\boldsymbol{p}},\boldsymbol{d},\tilde{\boldsymbol{x}}_e,\tilde{\boldsymbol{x}}_n,\boldsymbol{l}) &= \begin{bmatrix} \boldsymbol{e}_1^c(\boldsymbol{x}_1,\boldsymbol{x}_{2,n},\boldsymbol{x}_{2,m};d_1\boldsymbol{\pi},\tilde{\boldsymbol{p}},\boldsymbol{l}) \\ \boldsymbol{e}_{2,n}^c(\boldsymbol{x}_1,\boldsymbol{x}_{2,n},\boldsymbol{x}_{2,m};d_2,\boldsymbol{\pi},\tilde{\boldsymbol{p}},\boldsymbol{l}) \\ \boldsymbol{e}_{2,m}^c(\boldsymbol{x}_1,\boldsymbol{x}_{2,n},\boldsymbol{x}_{2,m};d_2,\boldsymbol{\pi},\tilde{\boldsymbol{p}},\boldsymbol{l}) \end{bmatrix}, \\
\boldsymbol{e}_1^c(\boldsymbol{x}_1,\boldsymbol{x}_{2,n},\boldsymbol{x}_{2,m},d_2,\boldsymbol{\pi},\tilde{\boldsymbol{p}}) &= \boldsymbol{e}_1\,(\boldsymbol{x}_1,\boldsymbol{x}_{2,n},\boldsymbol{x}_{2,m},\boldsymbol{\mu}(\boldsymbol{x}_1,\boldsymbol{x}_{2,n},\boldsymbol{x}_{2,m},d_2)+ \\
&\qquad +\tilde{\boldsymbol{\mu}}_s(\boldsymbol{x}_1,\boldsymbol{x}_{2,n},\boldsymbol{x}_{2,m},\boldsymbol{\iota}_y,d_2,\tilde{\boldsymbol{x}}_1,\tilde{\boldsymbol{x}}_{2,n},\tilde{\boldsymbol{x}}_{2,m},\tilde{\boldsymbol{\iota}}_y,\boldsymbol{l})), \\
\boldsymbol{e}_{2,n}^c(\boldsymbol{x}_1,\boldsymbol{x}_{2,n},\boldsymbol{x}_{2,m},d_2,\boldsymbol{\pi},\tilde{\boldsymbol{p}}) &= \boldsymbol{e}_{2,n}\,(\boldsymbol{x}_1,\boldsymbol{x}_{2,n},\boldsymbol{x}_{2,m},\mu(\boldsymbol{x}_1,\boldsymbol{x}_{2,n},\boldsymbol{x}_{2,m},d_2)\,+ \\
&\qquad +\tilde{\boldsymbol{\mu}}_s(\boldsymbol{x}_1,\boldsymbol{x}_{2,n},\boldsymbol{x}_{2,m},\boldsymbol{\iota}_y,d_2,\tilde{\boldsymbol{x}}_1,\tilde{\boldsymbol{x}}_{2,n},\tilde{\boldsymbol{x}}_{2,m},\tilde{\boldsymbol{\iota}}_y,\boldsymbol{l})), \\
\boldsymbol{e}_{2,m}^c(\boldsymbol{x}_1,\boldsymbol{x}_{2,n},\boldsymbol{x}_{2,m},d_2,\boldsymbol{\pi},\tilde{\boldsymbol{p}}) &= \boldsymbol{e}_{2,m}\,(\boldsymbol{x}_1,\boldsymbol{x}_{2,n},\boldsymbol{x}_{2,m},\boldsymbol{\mu}(\boldsymbol{x}_1,\boldsymbol{x}_{2,n},\boldsymbol{x}_{2,m},d_2)\,+ \\
&\qquad +\tilde{\boldsymbol{\mu}}_s(\boldsymbol{x}_1,\boldsymbol{x}_{2,n},\boldsymbol{x}_{2,m},\boldsymbol{\iota}_y,d_2,\tilde{\boldsymbol{x}}_1,\tilde{\boldsymbol{x}}_{2,n},\tilde{\boldsymbol{x}}_{2,m},\tilde{\boldsymbol{\iota}}_y,\boldsymbol{l})),
\end{aligned}
$$

$$
\begin{aligned}
\tilde{\boldsymbol{\mu}}_s(\boldsymbol{x}_1,\boldsymbol{x}_{2,n},\boldsymbol{x}_{2,m},\boldsymbol{\iota}_y,d_2,\tilde{\boldsymbol{x}}_1,\tilde{\boldsymbol{x}}_{2,n},\tilde{\boldsymbol{x}}_{2,m},\tilde{\boldsymbol{\iota}}_y,\boldsymbol{l}) &= \boldsymbol{\mu}_{s,e}(\boldsymbol{x}_1+\tilde{\boldsymbol{x}}_1,\boldsymbol{x}_{2,n}+\tilde{\boldsymbol{x}}_{2,n},\boldsymbol{x}_2+\tilde{\boldsymbol{x}}_{2,m},\boldsymbol{\iota}_y+\tilde{\boldsymbol{\iota}}_y,d_2)- \\
&\qquad -\boldsymbol{\mu}_s(\boldsymbol{x}_1,\boldsymbol{x}_{2,n},\boldsymbol{x}_{2,m},d_2), \\
\boldsymbol{l} &= [u^-,u^+]^T-[u^-,u^+]^T.
\end{aligned}
$$

E.3 PROOF OF PROPOSITION 4.7

From the per-subsystem application of Lemma 3.2 , to the fast (4.70a)-(4.70b) and slow (4.70c)-(4.70d) dynamics, it can be established that their closed-loop state motions are bounded as

$$
\begin{aligned}
\|\boldsymbol{\pi}\| &\le \Xi_\pi, & \dot{\Xi}_\pi &= -\lambda_\pi + a_\pi \varepsilon_\nu(t), & \Xi_\pi(0) &= a_\pi\,\|\boldsymbol{\pi}_0\|, \\
\|\tilde{\boldsymbol{x}}_e\| &\le \Xi_e, & \dot{\Xi}_e &= -\lambda_e\Xi_e + a_\psi[L_\pi^{\tilde{f}_e}\Xi_\pi + L_{x_n}^{\tilde{f}_e}\Xi_n + L_x^{\tilde{f}_e}\Xi_x] + \varepsilon_e(t), & \Xi_e(0) &= a_e\,\|\boldsymbol{x}_{e0}\|, \\
\|\tilde{\boldsymbol{x}}_n\| &\le \Xi_n, & \dot{\Xi}_n &= -\lambda_z\Xi_n + a_n[L_\pi^{\mathfrak{e}_c^n}\Xi_\pi + L_e^{\mathfrak{e}_c^n}\Xi_e + L_x^{\mathfrak{e}_c^n}\Xi_x] + \varepsilon_n(t), & \Xi_z(0) &= a_z\,\|\boldsymbol{x}_{n0}\|, \\
\|\boldsymbol{x}\| &\le \Xi_x, & \dot{\Xi}_x &= -\lambda_c\Xi_x + a_x[L_\pi^{\mathfrak{e}_c}\Xi_\pi + L_e^{\mathfrak{e}_c}\Xi_e + L_x^{\mathfrak{e}_c}\Xi_n] + \varepsilon_x(t), & \Xi_x(0) &= a_x\,\|\boldsymbol{x}_0\|
\end{aligned}
$$

$$
\begin{aligned}
&\|\boldsymbol{\nu}(t)\| \le \varepsilon_\nu(t), \quad \varepsilon_p = \|\tilde{\boldsymbol{p}}\|, \quad \|\boldsymbol{d}(t)\| \le \varepsilon_d(t), \quad \varepsilon_e(t) = a_e[L_p^{\tilde{f}_e}\varepsilon_p + L_d^{\tilde{f}_e}\epsilon_d(t)], \\
&\varepsilon_n(t) = a_n[L_p^{\mathfrak{e}_c^n}\varepsilon_p + L_d^{\mathfrak{e}_c}\varepsilon_d(t)], \quad \varepsilon_x(t) = a_x[L_p^{\mathfrak{e}_c}\varepsilon_p + L_d^{\mathfrak{e}}\varepsilon_d(t)],
\end{aligned}
$$

Considering the interconnection between the fast subsystems and applying Proposition 3.1, it is found that:

$$
(\|\boldsymbol{\pi}\|,\|\tilde{\boldsymbol{x}}_e\|) \le \boldsymbol{\Xi}_f(t): \qquad \dot{\boldsymbol{\Xi}}_f = \boldsymbol{A}_f\boldsymbol{\Xi}_f + \boldsymbol{B}_f\boldsymbol{\Xi}_s + \boldsymbol{d}_f(t), \qquad \boldsymbol{\Xi}_f(0) = \boldsymbol{\Xi}_{f0}, \tag{E.1}
$$

$$
(\|\tilde{\boldsymbol{x}}_n\|,\|\boldsymbol{x}\|) \le \boldsymbol{\Xi}_s(t): \qquad \dot{\boldsymbol{\Xi}}_s = \boldsymbol{B}_s\boldsymbol{\Xi}_f + \boldsymbol{A}_s\boldsymbol{\Xi}_s + \boldsymbol{d}_s(t), \qquad \boldsymbol{s}_\Xi(0) = \boldsymbol{\Xi}_{s0}, \tag{E.2}
$$

where

$$\boldsymbol{\Xi}_f = \begin{bmatrix} \Xi_\pi \\ \Xi_\psi \end{bmatrix}, \quad \boldsymbol{A}_f = \begin{bmatrix} -\lambda_\pi & 0 \\ a_e L_\pi^{\tilde{f}_e} & -\nu_e \end{bmatrix}, \quad \boldsymbol{B}_f = \begin{bmatrix} 0 & 0 \\ a_e L_{x_n}^{\tilde{f}_e} & a_e L_x^{\tilde{f}_e} \end{bmatrix}, \quad \boldsymbol{d}_f = \begin{bmatrix} \varepsilon_\nu \\ \varepsilon_e \end{bmatrix},$$

$$\boldsymbol{\Xi}_s = \begin{bmatrix} \Xi_n \\ \Xi_x \end{bmatrix}, \quad \boldsymbol{A}_s = \begin{bmatrix} -\nu_z & a_z L_x^{\mathfrak{e}_c^n} \\ a_x L_{x_n}^{\mathfrak{e}_c} & -\nu_c \end{bmatrix}, \quad \boldsymbol{B}_s = \begin{bmatrix} a_n L_\pi^{\mathfrak{e}_c^n} & a_n L_{x_n}^{\mathfrak{e}_c^n} \\ a_x L_\pi^{\mathfrak{e}_c} & a_x L_e^{\mathfrak{e}_c} \end{bmatrix}, \quad \boldsymbol{d}_f = \begin{bmatrix} \varepsilon_n \\ \varepsilon_x \end{bmatrix},$$

$$\Xi_{f0} = \begin{bmatrix} a_\pi \Xi_{\pi 0} \\ a_\psi \Xi_{e0} \end{bmatrix}, \qquad \Xi_{x0} = \begin{bmatrix} a_n \Xi_{n0} \\ a_x \Xi_{x0} \end{bmatrix}.$$

The above subsystems are robustly stable if: (i) the slow subsystem satisfy conditions in Lemma 4.4, and that the fast subsystem is robustly stable if conditions in Lemma 4.3 are met.

By the application of Proposition 3.1, the state motions of the above system are bounded as

$$\|\boldsymbol{s}_f\| \leq \mathit{\Xi}_f : \quad \dot{\mathit{\Xi}}_f = -\lambda_f \mathit{\Xi}_f + a_f[\|\boldsymbol{B}_f\| \, \mathit{\Xi}_s + \|\boldsymbol{d}_f(t)\|], \quad \mathit{\Xi}_f(0) = a_f \|\boldsymbol{s}_{f0}\|, \tag{e.3}$$

$$\|\boldsymbol{s}_s\| \leq \mathit{\Xi}_s : \quad \dot{\mathit{\Xi}}_s = -\lambda_s \mathit{\Xi}_s + a_s[\|\boldsymbol{B}_s\| \, \mathit{\Xi}_f + \|\boldsymbol{d}_s(t)\|], \quad \mathit{\Xi}_s(0) = a_s \|\boldsymbol{s}_{s0}\|, \tag{e.4}$$

where λ_f is the real part of the dominant eigenvalue of the matrix $\boldsymbol{A}_f$, and λ_s is the real part of the dominant eigenvalue of the matrix of the slow matrix $\boldsymbol{A}_s$. Note that due to the triangular structure of the matrix $\boldsymbol{A}_f$, the dominant eigenvalue is $\lambda_f = \nu_e - \lambda_e(\boldsymbol{K}_y, \boldsymbol{K}_\iota) - L_{x_e}^{\tilde{f}_e}$.

Applying again Proposition 3.1, the following condition for closed-loop stability is obtained

$$\lambda_e(\boldsymbol{K}_y, \boldsymbol{K}_\iota) > L_{x_e}^{\tilde{f}_e}(\boldsymbol{K}_y, \boldsymbol{K}_\iota) + \frac{a_f a_s \|\boldsymbol{B}_f(\boldsymbol{K}_y, \boldsymbol{K}_\iota)\| \, \|\boldsymbol{B}_s\|}{\lambda_s}. \tag{e.5}$$

f

CLOSED-LOOP STABILITY OF THE PIAW-PWO CONTROL-ESTIMATION SYSTEM

F.1 CLOSED-LOOP FUNCTIONS OF THE ACTUAL CLOSED-LOOP DYNAMICS

The involved functions in the closes-loop system (4.79) are given as

$$
\begin{aligned}
\boldsymbol{\Pi}_3^c(\boldsymbol{x},\boldsymbol{d},\tilde{\boldsymbol{\iota}},\tilde{\boldsymbol{x}}_n;\boldsymbol{\pi},\boldsymbol{\nu}) &= \boldsymbol{\Pi}(\boldsymbol{x}_1,\boldsymbol{x}_{2,n},\boldsymbol{x}_{2,m},\boldsymbol{d},\boldsymbol{\mu}_{s,o}(\boldsymbol{y},\tilde{\boldsymbol{\iota}},d_2);\boldsymbol{\pi},\boldsymbol{\nu}),\\
\tilde{\boldsymbol{f}}_\iota^o(\boldsymbol{x};\boldsymbol{\pi},\tilde{\boldsymbol{p}},d_2,\tilde{\boldsymbol{\iota}},\tilde{\boldsymbol{x}}_n) &= -\partial_t \boldsymbol{e}_{2,m}^c(\boldsymbol{x}_1,\boldsymbol{x}_{2,n},\boldsymbol{y},\boldsymbol{\mu}_s^p(\boldsymbol{y},\tilde{\boldsymbol{\iota}}),\boldsymbol{\pi},\tilde{\boldsymbol{p}}),\\
\boldsymbol{f}_n(\tilde{\boldsymbol{x}}_{\iota e},\tilde{\boldsymbol{x}}_n,\boldsymbol{d}) &= \begin{bmatrix}\tilde{\boldsymbol{f}}_1(\boldsymbol{x}_1,\boldsymbol{x}_{2,n},\boldsymbol{y},d_1;\tilde{\boldsymbol{x}}_1,\tilde{\boldsymbol{x}}_{2,n})\\ \tilde{\boldsymbol{f}}_{2,n}(\boldsymbol{x}_1,\boldsymbol{x}_{2,n},\boldsymbol{y},d_2;\tilde{\boldsymbol{x}}_1,\tilde{\boldsymbol{x}}_{2,n})\end{bmatrix},\\
\tilde{\boldsymbol{f}}_1(\boldsymbol{x}_1,\boldsymbol{x}_{2,n},\boldsymbol{y},d_1;\tilde{\boldsymbol{x}}_1,\tilde{\boldsymbol{x}}_{2,n}) &= \boldsymbol{f}_1(\boldsymbol{x}_1+\tilde{\boldsymbol{x}}_1,\boldsymbol{x}_{2,n}+\tilde{\boldsymbol{x}}_{2,n},\boldsymbol{y},d_1)-\boldsymbol{f}_1(\boldsymbol{x}_1,\boldsymbol{x}_{2,n},\boldsymbol{y},d_1),\\
\tilde{\boldsymbol{f}}_{2,n}(\boldsymbol{x}_1,\boldsymbol{x}_{2,n},\boldsymbol{y},d_2;\tilde{\boldsymbol{x}}_1,\tilde{\boldsymbol{x}}_{2,n}) &= \boldsymbol{f}_{2,n}(\boldsymbol{x}_1+\tilde{\boldsymbol{x}}_1,\boldsymbol{x}_{2,n}+\tilde{\boldsymbol{x}}_{2,n},\boldsymbol{y},d_2)-\boldsymbol{f}_{2,n}(\boldsymbol{x}_1,\boldsymbol{x}_{2,n},\boldsymbol{y},d_2),\\
\mathbf{e}_n^o(\boldsymbol{x},\boldsymbol{d};\boldsymbol{\pi},\tilde{\boldsymbol{p}},\tilde{\boldsymbol{x}}_{\iota e},\tilde{\boldsymbol{x}}_n,\boldsymbol{l}) &= \begin{bmatrix}-\boldsymbol{e}_1^o(\boldsymbol{x}_1,\boldsymbol{x}_{2,n},\boldsymbol{x}_{2,m};d_1\boldsymbol{\pi},\tilde{\boldsymbol{p}},\boldsymbol{l})\\ -\boldsymbol{e}_{2,n}^o(\boldsymbol{x}_1,\boldsymbol{x}_{2,n},\boldsymbol{x}_{2,m};d_2,\boldsymbol{\pi},\tilde{\boldsymbol{p}},\boldsymbol{l})\end{bmatrix},\\
\boldsymbol{f}_c(\boldsymbol{x},\boldsymbol{d}) &= \begin{bmatrix}\boldsymbol{f}_1(\boldsymbol{x}_1,\boldsymbol{x}_{2,n},\boldsymbol{x}_{2,m},d_1)\\ \boldsymbol{f}_{2,n}^c(\boldsymbol{x}_1,\boldsymbol{x}_{2,n},\boldsymbol{x}_{2,m},d_2)\\ \boldsymbol{f}_{2,m}^c(\boldsymbol{x}_1,\boldsymbol{x}_{2,n},\boldsymbol{x}_{2,m},d_2)\end{bmatrix},\\
\mathbf{e}^o(\boldsymbol{x},\boldsymbol{d};\boldsymbol{\pi},\tilde{\boldsymbol{p}},\boldsymbol{d},\tilde{\boldsymbol{x}}_{\iota e},\tilde{\boldsymbol{x}}_n,\boldsymbol{l}) &= \begin{bmatrix}\boldsymbol{e}_1^o(\boldsymbol{x}_1,\boldsymbol{x}_{2,n},\boldsymbol{x}_{2,m};d_1\boldsymbol{\pi},\tilde{\boldsymbol{p}},\boldsymbol{l})\\ \boldsymbol{e}_{2,n}^o(\boldsymbol{x}_1,\boldsymbol{x}_{2,n},\boldsymbol{x}_{2,m};d_2,\boldsymbol{\pi},\tilde{\boldsymbol{p}},\boldsymbol{l})\\ \boldsymbol{e}_{2,m}^o(\boldsymbol{x}_1,\boldsymbol{x}_{2,n},\boldsymbol{x}_{2,m};d_2,\boldsymbol{\pi},\tilde{\boldsymbol{p}},\boldsymbol{l})\end{bmatrix},\\
\boldsymbol{e}_1^o(\boldsymbol{x}_1,\boldsymbol{x}_{2,n},\boldsymbol{x}_{2,m},d_2,\boldsymbol{\pi},\tilde{\boldsymbol{p}}) &= \boldsymbol{e}_1\Big(\boldsymbol{x}_1,\boldsymbol{x}_{2,n},\boldsymbol{x}_{2,m},\boldsymbol{\mu}_o(\boldsymbol{x}_1,\boldsymbol{x}_{2,n},\boldsymbol{x}_{2,m},d_2)+\\
&\qquad +\tilde{\boldsymbol{\mu}}_{s,o}(\boldsymbol{x}_1,\boldsymbol{x}_{2,n},\boldsymbol{x}_{2,m},\boldsymbol{\iota}_y,d_2,\tilde{\boldsymbol{x}}_1,\tilde{\boldsymbol{x}}_{2,n},\tilde{\boldsymbol{\iota}}_y,\boldsymbol{l})\Big),\\
\boldsymbol{e}_{2,n}^o(\boldsymbol{x}_1,\boldsymbol{x}_{2,n},\boldsymbol{x}_{2,m},d_2,\boldsymbol{\pi},\tilde{\boldsymbol{p}}) &= \boldsymbol{e}_{2,n}\Big(\boldsymbol{x}_1,\boldsymbol{x}_{2,n},\boldsymbol{x}_{2,m},\boldsymbol{\mu}_o(\boldsymbol{x}_1,\boldsymbol{x}_{2,n},\boldsymbol{x}_{2,m},d_2)+\\
&\qquad +\tilde{\boldsymbol{\mu}}_{s,o}(\boldsymbol{x}_1,\boldsymbol{x}_{2,n},\boldsymbol{x}_{2,m},\boldsymbol{\iota},d_2,\tilde{\boldsymbol{x}}_1,\tilde{\boldsymbol{x}}_{2,n},\tilde{\boldsymbol{\iota}},\boldsymbol{l})\Big),\\
\boldsymbol{e}_{2,m}^o(\boldsymbol{x}_1,\boldsymbol{x}_{2,n},\boldsymbol{x}_{2,m},d_2,\boldsymbol{\pi},\tilde{\boldsymbol{p}}) &= \boldsymbol{e}_{2,m}\Big(\boldsymbol{x}_1,\boldsymbol{x}_{2,n},\boldsymbol{x}_{2,m},\boldsymbol{\mu}_o(\boldsymbol{x}_1,\boldsymbol{x}_{2,n},\boldsymbol{x}_{2,m},d_2)+\\
&\qquad +\tilde{\boldsymbol{\mu}}_{s,o}(\boldsymbol{x}_1,\boldsymbol{x}_{2,n},\boldsymbol{x}_{2,m},\boldsymbol{\iota},d_2,\tilde{\boldsymbol{x}}_1,\tilde{\boldsymbol{x}}_{2,n},\tilde{\boldsymbol{\iota}},\boldsymbol{l})\Big),\\
\tilde{\boldsymbol{\mu}}_{s,o}(\boldsymbol{x}_1,\boldsymbol{x}_{2,n},\boldsymbol{x}_{2,m},\boldsymbol{\iota},d_2,\tilde{\boldsymbol{x}}_1,\tilde{\boldsymbol{x}}_{2,n},\tilde{\boldsymbol{\iota}},\boldsymbol{l}) &= \boldsymbol{\mu}_{s,o}(\boldsymbol{y},\boldsymbol{\iota}+\tilde{\boldsymbol{\iota}})-\boldsymbol{\mu}_o(\boldsymbol{x}_1,\boldsymbol{x}_{2,n},\boldsymbol{x}_{2,m},d_2),\\
\boldsymbol{l} &= [u^-,u^+]^T-[u^-,u^+]^T.
\end{aligned}
$$

F.2 PROOF OF PROPOSITION 4.8

From the of Lemma 3.2 to (4.79), its state motions are bounded as

$$
\begin{aligned}
&(\|\boldsymbol{\pi}\|,\|\tilde{\boldsymbol{\iota}}\|,\|\tilde{\boldsymbol{x}}_n\|,\|\boldsymbol{x}\|) \le (\Xi_\pi,\Xi_\iota,\Xi_z,\Xi_x):\\
&\quad \dot{\Xi}_\pi = -\nu_\pi\Xi_\pi + d_\pi(t), && \Xi_\pi(0) = a_\pi\delta_{\pi 0},\\
&\quad \dot{\Xi}_\psi = -\omega_\iota\Xi_\iota + a_\iota[L_z^{\varpi_\iota}\Xi_z + L_x^{\varpi_\iota}\Xi_x] + d_\iota(t), && \Xi_\iota(0) = a_\iota\delta_{\iota 0},\\
&\quad \dot{\Xi}_z = -\lambda_z\Xi_z + a_z[L_\pi^{\varpi_z}\Xi_\pi + L_\iota^{\varpi_\iota}\Xi_\iota + L_x^{\varpi_z}\Xi_x] + d_z(t), && \Xi_z(0) = a_z\delta_{z0},\\
&\quad \dot{\Xi}_x = -\lambda_c\Xi_x + a_x[L_\pi^{\epsilon_x}\Xi_\pi + L_\iota^{\epsilon_x}\Xi_\iota] + d_x(t), && \Xi_x(0) = a_x\delta_{x0}
\end{aligned}
$$

where

$$
\nu_\pi > 0, \quad \nu_\iota = \omega_\iota - L_\iota^{\varpi_\iota} > 0, \quad \nu_z = \lambda_z - L_z^{\varpi_z} > 0, \quad \nu_x = \lambda_x - L_x^{\varpi_x}.
$$

Each individual subsystem establish stability of the corresponding majorized dynamics. In vector-matrix form, the above system is written as

$$
\begin{aligned}
&(\|\boldsymbol{\pi}\|,\|\boldsymbol{\iota}\|) \le \boldsymbol{\Xi}_f(t), \quad (\|\tilde{\boldsymbol{x}}_z\|,\|\boldsymbol{x}\|) \le \boldsymbol{\Xi}_f(t),\\
&\quad \dot{\boldsymbol{\Xi}}_f = \mathscr{A}_f\boldsymbol{\Xi}_f + \mathscr{B}_f\boldsymbol{\Xi}_s + \boldsymbol{d}_f(t), && \boldsymbol{\Xi}_f(0) = \boldsymbol{\Xi}_{f0},\\
&\quad \dot{\boldsymbol{\Xi}}_s = \mathscr{B}_s\boldsymbol{\Xi}_f + \mathscr{A}_s\boldsymbol{\Xi}_s + \boldsymbol{d}_s(t), && \boldsymbol{\Xi}_s(0) = \boldsymbol{\Xi}_{s0},
\end{aligned}
$$

where

$$
\boldsymbol{\Xi}_f = \begin{bmatrix}\Xi_\pi\\ \Xi_\iota\end{bmatrix}, \quad \mathscr{A}_f = \begin{bmatrix}-\nu_\pi & 0\\ L_\pi^{\varpi_\iota} & -\nu_\iota\end{bmatrix}, \quad \mathscr{B}_f = \begin{bmatrix}0 & 0\\ a_\iota L_z^{\varpi_\iota} & a_\iota L_x^{\varpi_\iota}\end{bmatrix}, \quad \boldsymbol{d}_f = \begin{bmatrix}d_\pi\\ d_\iota\end{bmatrix},
$$

$$
\boldsymbol{\Xi}_s = \begin{bmatrix}\Xi_z\\ \Xi_x\end{bmatrix}, \quad \mathscr{A}_s = \begin{bmatrix}-\nu_z & a_z L_x^{\varpi_z}\\ 0 & -\nu_x\end{bmatrix}, \quad \mathscr{B}_s = \begin{bmatrix}a_z L_\pi^{\varpi_z} & a_z L_\iota^{\varpi_z}\\ a_x L_\pi^{\varpi_x} & a_x L_\iota^{\varpi_x}\end{bmatrix}, \quad \boldsymbol{d}_s = \begin{bmatrix}d_z\\ d_x\end{bmatrix},
$$

$$
\Xi_{f0} = \begin{bmatrix}a_\pi\delta_{\pi 0}\\ a_\iota\delta_{\iota 0}\end{bmatrix}, \quad \Xi_{x0} = \begin{bmatrix}a_x\delta_{x0}\\ a_x\delta_{x0}\end{bmatrix},
$$

and, by Proposition 3.1: (i) the slow subsystem is robustly stable because

$$
\nu_z + \nu_x > 0, \quad \nu_z\nu_x > 0 \Rightarrow \left\|\mathrm{e}^{\mathscr{A}_s t}\right\| \le a_s\mathrm{e}^{-\nu_x t},
$$

and (ii) the fast subsystem is robustly stable if ω_ι is chosen so that condition

$$
\nu_\pi + \nu_\iota > 0, \quad \nu_\pi\nu_\iota > 0 \Rightarrow \left\|\mathrm{e}^{\mathscr{A}_f t}\right\| \le a_f\mathrm{e}^{-\nu_\iota t},
$$

From the per-subsystem application of Lemma 3.2 to the slow a fast interconnections, its state motions are bounded as

$$
\begin{aligned}
&(\|\boldsymbol{s}_f\|,\|\boldsymbol{s}_s\|) \le (\mathit{\Xi}_f,\mathit{\Xi}_s)(t):\\
&\quad \dot{\mathit{\Xi}}_f = -\nu_\iota\mathit{\Xi}_f + a_f[\|\mathscr{B}_f\|\,\mathit{\Xi}_s + \|\boldsymbol{d}_f(t)\|], && \mathit{\Xi}_f(0) = a_f\|\boldsymbol{s}_{f0}\|,\\
&\quad \dot{\mathit{\Xi}}_s = -\nu_c\mathit{\Xi}_s + a_s[\|\mathscr{B}_s\|\,\mathit{\Xi}_f + \|\boldsymbol{d}_s(t)\|], && \mathit{\Xi}_s(0) = a_s\|\boldsymbol{s}_{s0}\|.
\end{aligned}
$$

The application of Proposition 3.1 ensures the robust stability of the above dynamics if the condition (4.80) is satisfied.

9

CLOSED-LOOP STABILITY OF THE LINEAR COMPONENT OF THE DYNAMIC HEAT BALANCE

G.1 PROOF OF LEMMA 5.2

The proof is given in three steps: first, a modal representation for the closed-loop operator $\mathcal{A}_2^c$, in terms of its modal decomposition and the sensor-actuator characteristic functions, then, the eigenvalues of the resulting infinite dimensional matrix are characterized, including the identification of an approximate value of the dominant eigenvalue. Finally, the associated C_0-semigroup is characterized.

G.1.1 *Infinite matrix representation*

Consider the linear system

$$\dot{x}_2 = \mathcal{A}_2^c, x_2 \quad x_2(0) = x_{20}.$$

where $\mathcal{A}_2^c x_2$ is defined in (5.25c). Since the eigenfunctions (5.5c) for the operators $\mathcal{A}_j$, $j = 1, 2$ form an orthogonal basis of the Hilbert space $\mathcal{H}$, the states can be expanded as $x_j = \sum_m a_{j,m}\phi_{j,m}$, $a_{j,m} = \langle x_j, \phi_{j,m}\rangle$, $j = 1, 2$, $m \in 1, 2, \ldots$, where $\sum_m = \sum_{m\in\mathbb{N}}$. Thus, the effect of the closed-loop operator on the first state is given by

$$\begin{aligned}
\mathcal{A}_2^c x_2 &= \mathcal{A}_2 x_2 - \boldsymbol{\mathcal{B}}_{y,2}\boldsymbol{B}_m{}^{-1}\boldsymbol{K}_y\boldsymbol{\mathcal{C}}_{y,2}x_2,\\
\mathcal{A}_2^c x_2 &= \mathcal{A}_2 \sum_m a_{2,m}\phi_{2,m} - \boldsymbol{\mathcal{B}}_u\boldsymbol{B}_m{}^{-1}\boldsymbol{K}_y\boldsymbol{\mathcal{C}}_y \sum_m a_{2,m}\phi_{2,m}.
\end{aligned}$$

Considering the definitions of the input and output operators, the restriction on the matrix gain, and the definition of the matrix $B_m{}^{-1}$, it follows

$$\begin{aligned}
\mathcal{A}_2^c x_2 &= \sum_m \lambda_{2,m}a_{2,m}\phi_{2,m} - v\omega_h \begin{bmatrix}\beta_1 & \ldots & \beta_q\end{bmatrix} \frac{1}{v}\boldsymbol{I}_{q\times q}k_{y,i}\boldsymbol{I}_{q\times q} \begin{bmatrix} \left\langle \gamma_1, \omega_h^{-1}\sum_m a_{2,m}\phi_{2,m}\right\rangle \\ \vdots \\ \left\langle \gamma_q, \omega_h^{-1}\sum_m a_{2,m}\phi_{2,m}\right\rangle \end{bmatrix},\\
&= \sum_m \lambda_{2,m}a_{2,m}\phi_{2,m} - \omega_h \begin{bmatrix}\beta_1 & \ldots & \beta_q\end{bmatrix} k_{y,i}\boldsymbol{I}_{q\times q} \begin{bmatrix} \sum_m a_{2,m}\left\langle \gamma_1, \omega_h^{-1}\phi_{2,m}\right\rangle \\ \vdots \\ \sum_m a_{2,m}\left\langle \gamma_q, \omega_h^{-1}\phi_{2,m}\right\rangle \end{bmatrix},
\end{aligned}$$

$$
\begin{aligned}
&= \sum_m \lambda_{2,m} a_{2,m} \phi_{2,m} - \omega_h \begin{bmatrix} \beta_1 & \dots & \beta_q \end{bmatrix} k_{y,i} \boldsymbol{I}_{q\times q} \begin{bmatrix} \sum_m a_{2,m}\mathfrak{c}_{1,m} \\ \vdots \\ \sum_m a_{2,m}\mathfrak{c}_{q,m} \end{bmatrix}, \\
&= \sum_m \lambda_{2,m} a_{2,m} \phi_{2,m} - \omega_h \sum_{i=1}^{q} \beta_i k_{y,i} \sum_m a_{2,m} \mathfrak{c}_{1,m},
\end{aligned}
$$

where

$$
\mathfrak{c}_{i,m} = \left\langle \gamma_i, \omega_h^{-1} \phi_{2,m} \right\rangle, \quad i = 1, \dots, q, \ m \in \mathbb{N}.
$$

With sensor dependent coefficients $\mathfrak{c}_{i,m}(\varsigma_i)$. Projecting $\mathcal{A}_2^c x_2$ onto the n-th eigenfunction gives

$$
\begin{aligned}
\dot{a}_{1,n} &= \langle \dot{x}_2, \phi_{2,n} \rangle = \langle \mathcal{A}_2^c x_2, \phi_{2,n} \rangle, \\
&= \left\langle \sum_m \lambda_{2,m} a_{2,m} \phi_{2,m} - \omega_h \sum_{i=1}^{q} \beta_i k_{y,i} \sum_m a_{2,m} \mathfrak{c}_{1,m}, \phi_n^1 \right\rangle, \\
&= \sum_m \lambda_{2,m} a_{2,m} \langle \phi_{2,m}, \phi_{2,n} \rangle - \sum_{i=1}^{q} \sum_m a_m^1 \mathfrak{c}_{i,m} \langle \omega_h k_{y,i} \beta_i, \phi_{2,n} \rangle, \\
&= \lambda_{2,n} a_{2,n} - \sum_{i=1}^{q} k_{y,i} \sum_m a_{2,m} \mathfrak{b}_{i,n} \mathfrak{c}_{i,m},
\end{aligned}
$$

with

$$
\mathfrak{b}_{i,n} = \langle \omega_h \beta_i, \phi_{2,n} \rangle, \quad i = 1, \dots, q, \ n \in \mathbb{N}.
$$

In matrix form the above can be rewritten as

$$
\dot{\boldsymbol{a}}_2 = \mathscr{A}_2^c \boldsymbol{a}_2, \quad \boldsymbol{a}_2(0) = \boldsymbol{a}_{20}, \tag{g.1.1}
$$

where $\boldsymbol{a}_2 = [a_{2,n}]_{n\in\mathbb{N}}$ is an infinite dimensional vector and the infinite dimensional matrix

$$
\mathscr{A}_2^c = [\mathfrak{a}_{n,m}(k_{y,1}, \dots, k_{y,q}, \varsigma_1, \dots, \varsigma_q)]_{n,m\in\mathbb{N}}
$$

is defined as

$$
\mathfrak{a}_{n,m} = \begin{cases} \lambda_{2,n} - \sum_{i=1}^{q} k_{y,i} \mathfrak{b}_{i,n} \mathfrak{c}_{i,m}(\varsigma_i) & \text{if } n = m \\ -\sum_{i=1}^{q} k_{y,i} \mathfrak{b}_{i,n} \mathfrak{c}_{i,m}(\varsigma_i) & \text{if } n \neq m \end{cases}, \quad i = 1, \dots, q \tag{g.1.2}
$$

If the conditions in 5.2 are met, then the eigenvalues of $\mathscr{A}_2^c$ are bounded as stated in (5.26c). The proof of this is given below in g.1.2.

G.1.2 *Eigenvalues of infinite matrices*

The infinite dimensional matrix $\mathscr{A}_2^c$ given in (5.25c) is analyzed as the operator $\mathscr{A}_2^c : \mathcal{D}(\mathscr{A}_2^c) \subset l^2 \to l^2$ as $A(\boldsymbol{a}) = \mathscr{A}_2^c \boldsymbol{a}$, $\boldsymbol{a} \in \mathcal{D}(\mathscr{A}_2^c)$, where l^2 is the Banach space of sequences with norm $\|\boldsymbol{a}\|_2 = \left(\sum_{n\in\mathbb{N}} |a_n|^2\right)^{\frac{1}{2}}$. The diagonal dominance property of an infinite matrix is defined in [6, Definition 3] and is adapted here to $\mathscr{A}_2^c$ given in (g.1.2). Denote by $\mathfrak{a}_n = (\mathfrak{a}_{n,m})_{m\in\mathbb{N}}$ the n-th row of matrix $\mathscr{A}_2^c$ and by $\mathfrak{a}_{n,n}$ the n-th diagonal entry.

The infinite matrix $\mathscr{A}_2^c$ is strictly diagonal dominant if and only if the following condition holds

$$\left[\sum_n \left(\frac{r_n(\mathscr{A}_2^c)}{\|\mathfrak{a}_{n,n}\|}\right)^2\right]^{\frac{1}{2}} < 1. \tag{g.1.3}$$

According to [6, Theorem 16(c)] if $\mathscr{A}_2^c$ has pure point spectrum and is diagonally dominant, then the eigenvalues $\lambda_{2,n}^c$, $n \in \mathbb{N}$ of $\mathscr{A}_2^c$ are bounded according to

$$\lambda_{2,n}^c \leq {\lambda_{2,n}^c}^* = \sup_{n\in\mathbb{N}} \left(\mathfrak{a}_{n,n} + R_{\mathscr{A}_2^c}\right), \quad R_{\mathscr{A}_2^c} = \left(\sum_n r_n^2\right)^{\frac{1}{2}} \tag{g.1.4}$$

Note that this is a direct generalization of the classical result of Geršgorin [128].

Applying the above results, from (g.1.2) the spectral radi are given by

$$r_n = \left(\sum_{m\neq n} \left|\sum_{i=1}^{q} k_{y,i} \mathfrak{b}_{i,n} \mathfrak{c}_{i,m}\right|^2\right)^{\frac{1}{2}}.$$

The diagonal sequence $\{\mathfrak{a}_{n,n}\}$ has no accumulation points so the spectrum of $\mathscr{A}_2^c$ coincides with the point spectrum. Accordingly, the condition (g.1.3) for diagonal dominance is equivalent to

$$\left[\sum_{n\in\mathbb{N}} \sum_{m\neq n\in\mathbb{N}} \left|\frac{\mathfrak{a}_{n,m}}{\mathfrak{a}_{n,n}}\right|^2\right]^{\frac{1}{2}} < 1.$$

Given that $\mathfrak{a}_{1,1} = \sup_{n\in\mathbb{N}}\{\mathfrak{a}_{n,n}\}$ and thus $\frac{1}{|\mathfrak{a}_{1,1}|} \geq \frac{1}{|\mathfrak{a}_{n,n}|}$ for all $n \in \mathbb{N}$, the above expression is equivalent to

$$\begin{aligned}
\left[\sum_{n\in\mathbb{N}} \sum_{m\neq n\in\mathbb{N}} \left|\frac{\mathfrak{a}_{n,m}}{\mathfrak{a}_{n,n}}\right|^2\right]^{\frac{1}{2}} &= \left[\sum_{n\in\mathbb{N}} \frac{1}{|\mathfrak{a}_{n,n}|} \sum_{m\neq n\in\mathbb{N}} |\mathfrak{a}_{n,m}|^2\right]^{\frac{1}{2}}, \\
&\leq \frac{1}{|\mathfrak{a}_{1,1}|} \left[\sum_{n\in\mathbb{N}} \sum_{m\neq n\in\mathbb{N}} |\mathfrak{a}_{n,m}|^2\right]^{\frac{1}{2}} \\
&= \frac{R_{\mathscr{A}_2^c}}{|\mathfrak{a}_{1,1}|} < 1,
\end{aligned}$$

with

$$R^2_{\mathscr{A}_2^c} = \sum_n r_n^2(\mathscr{A}_2^c) = \sum_n \sum_{m \neq n} \left| \sum_{i=1}^q k_{y,i} \mathfrak{b}_{i,n} \mathfrak{c}_{i,m} \right|^2 .$$

Since $\sum_{i=1}^q \mathfrak{b}_{i,n} \mathfrak{c}_{i,m}$ is equivalent to the standard inner product in $\mathfrak{R}^q$, the application of the Cauchy–Swartz inequality yields

$$\begin{aligned}
R^2_{\mathscr{A}_2^c} &= \sum_n \sum_{m \neq n} \left| \sum_{i=1}^q k_{y,i} \mathfrak{b}_{i,n} \mathfrak{c}_{i,m} \right|^2 \\
&\leq \sum_n \left[\sum_{m \neq n} \sum_{i=1}^q k_{y,i} \mathfrak{b}_{i,n}^2 \sum_{i=1}^q k_{y,i} \mathfrak{c}_{i,m}^2 \right], \\
&\leq \sum_n \sum_{i=1}^q k_{y,i} \mathfrak{b}_{i,n}^2 \sum_{m \neq n} \sum_{i=1}^q k_{y,i} \mathfrak{c}_{i,m}^2, \\
&\leq \sum_n \sum_{i=1}^q k_{y,i} \mathfrak{b}_{i,n}^2 \sum_m \sum_{i=1}^q k_{y,i} \mathfrak{c}_{i,m}^2, \\
&= \sum_{i=1}^q k_{y,i} \sum_n \mathfrak{b}_{i,n}^2 \sum_{i=1}^q k_{y,i} \sum_m \mathfrak{c}_{i,m}^2.
\end{aligned}$$

Using the Parseval identity it follows that

$$\begin{aligned}
\sum_n \mathfrak{b}_{i,n}^2 &= \sum_n \left\langle \omega_h \beta_{i,n}, \phi^{2,n} \right\rangle^2 = \left\| \omega_h \beta_i \right\|^2, \\
\sum_m \mathfrak{c}_{i,m}^2 &= \sum_m \left\langle \gamma_{i,m}, \omega_h^{-1} \phi_{2,m} \right\rangle^2 = \left\| \omega_h^{-1} \gamma_i \right\|^2,
\end{aligned}$$

and

$$R^2_{\mathscr{A}_2^c} \leq \sum_{i=1}^q k_{y,i} \left\| \omega_h \beta_i \right\|^2 \sum_{i=1}^q k_{y,i} \left\| \omega_h^{-1} \gamma_i \right\|^2 .$$

Thus, the diagonal dominance is ensured if

$$\frac{\left(\sum_{i=1}^q k_{y,i} \left\| \omega_h \beta_i \right\|^2 \sum_{i=1}^q k_{y,i} \left\| \omega_h^{-1} \gamma_i \right\|^2 \right)^{1/2}}{|\mathfrak{a}_{1,1}|} < 1,$$

or equivalently (5.26b) holds true. It follows from (g.1.4) that the eigenvalues are bounded as stated in (5.26c).

G.1.3 *Contraction semigroup property*

Define the Lyapunov function

$$V(\boldsymbol{a}_2) = \boldsymbol{a}_2^T \boldsymbol{a}_2 = \|\boldsymbol{a}_2\|_2^2, \tag{G.1.5}$$

where $\|\cdot\|_2 = \left(\sum_{n\in\mathbb{N}} |a_{1,n}|^2\right)^{\frac{1}{2}}$ denotes the l^2-norm. Evaluating the time derivative of (G.1.5) along the trajectories of (G.1.1) it follows that

$$\begin{aligned}
\dot{V}(\boldsymbol{a}_2) &= \boldsymbol{a}_2^T \left(\mathscr{A}_2^{cT} + \mathscr{A}_2^c\right) \boldsymbol{a}_2, \\
&\leq 2\mathrm{Re}\left\{\lambda_2^{c*}\right\} \boldsymbol{a}_2^T \boldsymbol{a}_2, \\
&= -2\nu_c V(\boldsymbol{a}_2).
\end{aligned}$$

This implies that $V(\boldsymbol{a}_2) \leq V(\boldsymbol{a}_2(0))\mathrm{e}^{-2\nu_c t}$, which in view of (G.1.5) is equivalent to

$$\|\boldsymbol{a}_2(t)\|_2 \leq \|\boldsymbol{a}_2(0)\|_2 \,\mathrm{e}^{-\nu_c t} \Rightarrow \|x_2(t)\| \leq \|x_{20}\| \,\mathrm{e}^{-\nu_c t},$$

given that the l^2-norm of $\boldsymbol{a}_2$ is equivalent to the L^2-norm of x_2 [38]. Accordingly, the operator $\mathcal{A}_2^c$ generates a C_0-semigroup such that $x_2(t) = S_2^c(t)x_{20}$. Taking norms and using the previous result yields

$$\|x_2(t)\| = \|S_2^c(t)\| \, \|x_{20}\| \leq \|x_{20}\| \,\mathrm{e}^{-\nu_c t},$$

implying (5.26d).

h

STABILITY PROOFS OF THE DISTRIBUTED ZERO DYNAMICS

h.1 PROOF OF LEMMA 6.1

Proceed as in [111, Appendix A] an introduce the local coordinate change

$$s_j = \frac{s - \varsigma_{j-1} - \epsilon}{\varsigma_j - \varsigma_{j-1} - 2\epsilon}, \quad j = 1, \ldots, q+1,$$

considering that ϵ is a small number, it can be neglected in the previous expressions to obtain

$$s_j = \frac{s - \varsigma_{j-1}}{\varsigma_j - \varsigma_{j-1}}, \quad j = 1, \ldots, q+1.$$

In this coordinates, the spatial derivatives of the local eigenfunctions $\psi_{2,j,l}(s_j)$, $j = 1, \ldots, q+1$ are given by

$$\partial_s \psi_{2,j,n} = (\partial_{s_j} \psi_{2,j,n}(s_j))(\partial_s s_i) = \frac{1}{\varsigma_i - \varsigma_{i-1}} \partial_{s_i} \psi_{2,j,n}(s_i). \tag{h.1.1}$$

Thus, the related eigenvalue problems are

$$0 = \frac{1}{(\varsigma_i - \varsigma_{i-1})^2} \partial_{s_i}^2 \psi_{2,j,n}(s_i) - \left(\frac{Pe}{4} + v\right) - \lambda_{2,j,n} \psi_{2,j,n}(s_i), \tag{h.1.2}$$

$$\mathbf{0} = \mathscr{B}^z_{n,j} \psi_{2,j,n}, \quad j = 1, \ldots, q+1, \quad n \in \mathbb{N}. \tag{h.1.3}$$

The solution to these problems are the set of eigenfunctions, eigenfrquencies and eigenvalues given in (6.13a), (6.13d), and (6.13g), respectively.

h.2 PROOF OF PROPOSITION 6.1

The proof follows the same procedure as [111]. Since the dynamics of the temperature components $\boldsymbol{x}_{2,n}$ is diagonal, its solutions are given by

$$x_{2,n,j}(t) = S_i(t) x_{2,n,j0} + \int_0^t S_i(t - \mathrm{t}) \rho_{2,z,j}(x_1(\mathrm{t}), x_{2,n,j}(\mathrm{t})) \mathrm{dt},$$

for $j = 1, \ldots, q+1$. Taking norm on both sides of the above expression and using (6.14) and applying the triangle inequality, the temperature components satisfy

$$\left\| x_{2,n,j}(t) \right\| \leq \mathrm{e}^{-\lambda_j^* t} \left\| x_{2,n,j0} \right\| + \int_0^t \mathrm{e}^{-\lambda_j^* (t - \mathrm{t})} \left(L_{x_1}^{\rho_{2,z,j}} \left\| x_1(\mathrm{t}) \right\| + L_{x_{2,n,j}}^{\rho_{2,z,j}} \left\| x_{2,n,j}(\mathrm{t}) \right\| \right) \mathrm{dt}. \tag{h.2.1}$$

Recall (5.11) and the above expression and, proceeding as in the proof of Theorem 3.1, define the right-hand side of the implicated inequalities as

$$\begin{aligned}
\Xi(t) \leq \|x_1(t)\| \leq \mathrm{e}^{-\nu_1 t}\|x_{10}\| + \int_0^t \mathrm{e}^{-\nu_1(t-\mathrm{t})} L_{x_2}^{\mathfrak{r}} \|x_2(\mathrm{t})\|, \\
\Xi_{2,j}(t) \leq \left\|x_{2,n,j}(t)\right\| \leq \mathrm{e}^{-\lambda^*_{2,j}t}\left\|x_{2,n,j0}\right\| + \int_0^t \mathrm{e}^{-\lambda^*_{2,j}(t-\mathrm{t})}\left(L_{x_1}^{\rho_{2,z,j}}\|x_1\| + L_{x_{2,n,j}}^{\rho_{2,z,j}}\left\|x_{2,n,j}\right\|\right)\mathrm{dt},
\end{aligned}$$

for $j = 1, \ldots, 1+1$. In differential, the above expressions are written as

$$\begin{aligned}
\dot{\Xi}_1(t) &\leq -\nu_1 \Xi_1(t) + L_{x_2}^{\mathfrak{r}} \sum_{j=1}^{q+1} L_{x_{2,n,j}}^{\rho_{2,z,j}} \Xi_{2,j}(t), \\
\dot{\Xi}_{2,j}(t) &\leq -\nu_{2,j}\Xi_{2,j}(t) + L_{x_1}^{\rho_{2,z,j}}\Xi_1(t),
\end{aligned}$$

where

$$\nu_{2,j} = |\lambda^*_{2,j}| - L_{x_{2,n,j}}^{\rho_{2,z,j}}.$$

In compact form, the previous expressions are given as

$$\begin{bmatrix} \dot{\Xi}_1(t) \\ \dot{\Xi}_{2,1}(t) \\ \vdots \\ \vdots \\ \dot{\Xi}_{2,q+1}(t) \end{bmatrix} \leq \begin{bmatrix} -\nu_1 & L_{x_1}^{\mathfrak{r}} L_{x_{2,n,1}}^{\rho_{2,z,1}} & \cdots & \cdots & L_{x_1}^{\mathfrak{r}} L_{x_{2,n,q+1}}^{\rho_{2,z,q+1}} \\ L_{x_1}^{\rho_{2,z,1}} & -\nu_{2,1} & 0 & \cdots & 0 \\ \vdots & 0 & \ddots & \ddots & \cdots \\ \vdots & \vdots & \ddots & \ddots & 0 \\ L_{x_1}^{\rho_{2,z,q+1}} & 0 & \cdots & 0 & -\nu_{q+1} \end{bmatrix} \begin{bmatrix} \Xi_1(t) \\ \Xi_{2,1}(t) \\ \vdots \\ \vdots \\ \Xi_{2,q+1}(t) \end{bmatrix}.$$

Application of Schur complement gives the following condition that ensures that the matrix of the above dynamics is Hurwitz

$$\nu_{2,j} > 0,\ j = 1, \ldots, q+1, \quad \nu_1 - \sum_{j=1}^{q+1} \frac{L_{x_1}^{\rho_{2,z,j}} L_{x_{2,n,j}}^{\rho_{2,z,j}}}{\nu_{2,j}} > 0.$$

With the substitution of the maximum eigenvalues $\lambda^*_{2,j}$, according to (6.13g) and the Lipschitz conditions on each $\nu_{2,j}$, and recalling the definition of ν_1 given in (5.12), the expression in (6.16) are obtained. If these conditions are met, then the convergence to zero of $\Xi_1(t)$ and $\Xi_{2,j}(t)$ is ensured and employing their definitions, the following bounds are satisfied

$$\begin{aligned}
\|x_1(t)\| &\leq \Xi_1(t), \\
\left\|x_{2,n,j}(t)\right\| &\leq \Xi_{2,j}(t), \quad j = 1, \ldots, q+1,
\end{aligned}$$

which implies the exponential stability of the zero dynamics origin.

BIBLIOGRAPHY

[1] N. H. El–Farra and Panagiotis D. Christofides. "Bounded robust control of constrained multivariable nonlinear processes." In: *Chemical Engineering Science* 58.13 (2003), pp. 3025–3047. ISSN: 00092509. DOI: 10.1016/S0009--2509(03)00126--X.

[2] Nael H. El–Farra, Antonios Armaou, and Panagiotis D. Christofides. "Analysis and control of parabolic PDE systems with input constraints." In: *Automatica* 39.4 (2003), pp. 715–725. ISSN: 00051098. DOI: 10.1016/S0005--1098(02)00304--7.

[3] Nael H. El–Farra and Panagiotis D. Christofides. "Integrating robustness, optimality and constraints in control of nonlinear processes." In: *Chemical Engineering Science* 56.5 (2001), pp. 1841–1868. ISSN: 00092509. DOI: 10.1016/S0009--2509(00)00530--3.

[4] Nael H. El–Farra and Panagiotis D. Christofides. "Coordinating feedback and switching for control of spatially distributed processes." In: *Computers and Chemical Engineering* 28.1–2 (2004), pp. 111–128. ISSN: 00981354. DOI: 10.1016/S0098--1354(03)00174--1.

[5] Oscar Mauricio Agudelo, Jairo Jose Espinosa, and Bart De Moor. "Control of a tubular chemical reactor by means of POD and predictive control techniques." In: *2007 European Control Conference, ECC 2007* (2007), pp. 1046–1053. DOI: 10.23919/ecc.2007.7068633.

[6] J. Aleksić, V. Kostić, and M. Zihić. "Spectrum localizations for matrix operators on l^p spaces." In: *Applied Mathematics and Comp* 149 (2014), pp. 541–553. DOI: 10.1016/j.amc.2014.10.071. URL: http://dx.doi.org/10.1016/j.amc.2014.10.071.

[7] Antonio A. Alonso, Christos E. Frouzakis, and Ioannis G. Kevrekidis. "Optimal sensor placement for state reconstruction of distributed process systems." In: *AIChE Journal* 50.7 (2004), pp. 1438–1452. ISSN: 00011541. DOI: 10.1002/aic.10121.

[8] Antonio A. Alonso, Ioannis Kevrekidis, Julio R. Banga, and Christos Frouzakis. "Optimal sensor location and reduced order observer design for distributed process systems." In: *Computer Aided Chemical Engineering* 10.C (2002), pp. 415–420. ISSN: 15707946. DOI: 10.1016/S1570--7946(02)80097--9.

[9] Antonio A. Alonso and B. Erik Ydstie. "Stabilization of distributed systems using irreversible thermodynamics." In: *Automatica* 37.11 (2001), pp. 1739–1755. ISSN: 00051098. DOI: 10.1016/S0005--1098(01)00140--6.

[10] Jesús Alvarez, José Alvarez, and Rodolfo Suárez. "Nonlinear bounded control for a class of continuous agitated tank reactors." In: *Chemical Engineering Science* 46.12 (Jan. 1991), pp. 3235–3249. ISSN: 0009–2509. DOI: 10.1016/0009--2509(91)85025--S. URL: https://www.sciencedirect.com/science/article/pii/000925099185025S.

[11] Jesús Alvarez, Rodolfo Suárez, and Arturo Sánchez. "Semiglobal nonlinear control based on complete input–output linearization and its application to the start–up of a continuous polymerization reactor." In: *Chemical Engineering Science* 49.21 (1994), pp. 3617–3630. ISSN: 00092509. DOI: 10.1016/0009--2509(94)00166--9.

[12] José Jesús Alvarez, José Jesús Alvarez, and Rodolfo Suárez. "Nonlinear bounded control for a class of continuous agitated tank reactors." In: *Chemical Engineering Science* 46.12 (1991), pp. 3235–3249. ISSN: 00092509. DOI: 10.1016/0009--2509(91)85025--S.

[13] Jose Alvarez–Ramirez, Jesus Alvarez, and America Morales. "An adaptive cascade control for a class of chemical reactors." In: *International Journal of Adaptive Control and Signal Processing* 16.10 (2002), pp. 681–701. ISSN: 08906327. DOI: 10.1002/acs.717.

[14] H. Amrehn. "Computer control in the polymerization industry." In: *Automatica* 13.5 (Sept. 1977), pp. 533–545. ISSN: 00051098. DOI: 10.1016/0005--1098(77)90073--5. URL: https://www.sciencedirect.com/science/article/pii/0005109877900735.

[15] Neal R Amundson. *Mathematical Understanding Chemical Engineering Systems: Selected Papers of Neal R. Amundson*. Ed. by Rutherford Aris and Arvind Varma. Pergamon Press, 1980. ISBN: 008023836X.

[16] Charalambos Antoniades and Panagiotis D. Christofides. "Computation of optimal actuator locations for nonlinear controllers in transport–reaction processes." In: *Computers and Chemical Engineering* 24.2–7 (2000), pp. 577–583. ISSN: 00981354. DOI: 10.1016/S0098--1354(00)00412--9.

[17] Charalambos Antoniades and Panagiotis D. Christofides. "Non–linear feedback control of parabolic partial differential difference equation systems." In: *International Journal of Control* 73.17 (2000), pp. 1572–1591. ISSN: 00207179. DOI: 10.1080/00207170050197696.

[18] Charalambos Antoniades and Panagiotis D. Christofides. *Studies on nonlinear dynamics and control of a tubular reactor with recycle*. 2001. DOI: 10.1016/S0362--546X(01)00699--X.

[19] Charalambos Antoniades and Panagiotis D. Christofides. “Integrated optimal actuator/sensor placement and robust control of uncertain transport–reaction processes.” In: *Computers and Chemical Engineering* 26.2 (2002), pp. 187–203. ISSN: 00981354. DOI: 10.1016/S0098--1354(01)00740--2.

[20] Charalambos Antoniades and Panagiotis D. Christofides. “Integrating nonlinear output feedback control and optimal actuator/sensor placement for transport–reaction processes.” In: *Chemical Engineering Science* 56.15 (2001), p. 4517. ISSN: 00092509. DOI: 10.1016/s0009--2509(01)00123--3.

[21] Karl J. Astrom and Tore Hagglund. *Advanced PID Control*. 2006. ISBN: 8489925704.

[22] Ulises Badillo–Hernandez, Jesus Alvarez, and Luis Alvarez–Icaza. “Efficient modeling of the nonlinear dynamics of tubular heterogeneous reactors.” In: *Computers and Chemical Engineering* 123 (2019), pp. 389–406. ISSN: 00981354. DOI: 10.1016/j.compchemeng.2019.01.018. URL: https://doi.org/10.1016/j.compchemeng.2019.01.018.

[23] Ulises Badillo–Hernández, Jesús Álvarez, Hugo A. Franco–De los Reyes, and Luis A. Álvarez–Icaza. “Nonlinear output feedback–feedforward control of tubular gasification reactors.” In: *IFAC–PapersOnLine*. Vol. 53. 2. Elsevier B.V., Jan. 2020, pp. 7789–7794. DOI: 10.1016/j.ifacol.2020.12.1869.

[24] Mark J. Balas. “The galerkin method and feedback control of linear distributed parameter systems.” In: *Journal of Mathematical Analysis and Applications* 91.2 (Feb. 1983), pp. 527–546. ISSN: 10960813. DOI: 10.1016/0022--247X(83)90167--1.

[25] Shahid Bashir, Tibor Chován, Bassam J. Masri, Ananya Mukherjee, Alok Pant, Sumit Sen, P. Vijayaraghavan, and József M. Berty. “Thermal Runaway Limit of Tubular Reactors, Defined at the Inflection Point of the Temperature Profile.” In: *Industrial and Engineering Chemistry Research* 31.9 (1992), pp. 2164–2171. ISSN: 15205045. DOI: 10.1021/ie00009a014.

[26] N. Beniich, A. El Bouhtouri, and D. Dochain. “Input constrained adaptive tracking for a nonlinear distributed parameter tubular reactor.” In: *International Journal of Adaptive Control and Signal Processing* 24.February (2010), pp. 249–260. DOI: 10.1002/acs.

[27] N. Beniich, A. El Bouhtouri, and D. Dochain. “ Global Adaptive λ Tracking of a Temperature Profile in Tubular Reactor.” In: *ESAIM: Proceedings and Surveys* 49.February (2015), pp. 11–22. ISSN: 2267–3059. DOI: 10.1051/proc/201549002.

[28] N. Beniich, A. El Bouhtouri, and D. Dochain. “Adaptive local tracking of a temperature profile in tubular reactor with partial measurements.” In: *Journal of Process Control* 50 (Feb. 2017), pp. 29–39. ISSN: 09591524. DOI: 10.1016/j.jprocont.2016.11.006. URL: https://www.sciencedirect.com/science/article/pii/S0959152416301603.

[29] F.W.J. van den Berg, H.C.J. Hoefsloot, H.F.M. Boelens, and A.K. Smilde. "Selection of optimal sensor position in a tubular reactor using robust degree of observability criteria." In: *Chemical Engineering Science* 55.4 (Feb. 2000), pp. 827–837. ISSN: 0009–2509. DOI: 10.1016/S0009--2509(99)00360--7. URL: https://www.sciencedirect.com/science/article/pii/S0009250999003607.

[30] Dejan M. Bošković and Miroslav Krstić. "Backstepping control of chemical tubular reactors." In: *Computers and Chemical Engineering* 26.7–8 (2002), pp. 1077–1085. ISSN: 00981354. DOI: 10.1016/S0098--1354(02)00026--1.

[31] Bernard Brogliato, Rogelio Lozano, Bernhard Maschke, and Olav Egeland. *Dissipative Systems Analysis and Control: Theory and Applications*. Third Edit. Springer, 2020. ISBN: 9783030194192. URL: http://www.springer.com/series/61.

[32] Christopher I. Byrnes, Alberto Isidori, and Jan C. Willems. "Passivity, Feedback Equivalence, and the Global Stabilization of Minimum Phase Nonlinear Systems." In: *IEEE Transactions on Automatic Control* 36.11 (1991), pp. 1228–1240. ISSN: 15582523. DOI: 10.1109/9.100932.

[33] Eduardo Castellanos–Sahagún and Jesús Alvarez. "Synthesis of two–point linear controllers for binary distillation columns." In: *Chemical Engineering Communications* 193.2 (2006), pp. 206–232. ISSN: 00986445. DOI: 10.1080/009864490949071.

[34] Eduardo Castellanos–Sahagún, Jesús Alvarez, Andrea Frau, and Roberto Baratti. "Two–point Lyapunov control of binary distillation columns with four temperature measurements." In: *IFAC Proceedings Volumes (IFAC–PapersOnline)* 9.PART 1 (2010), pp. 55–60. ISSN: 14746670. DOI: 10.3182/20100705--3--BE--2011.00010.

[35] Liang Heng Chen and Hsueh Chia Chang. "Global effects of controller saturation on closed–loop dynamics." In: *Chemical Engineering Science* 40.12 (Jan. 1985), pp. 2191–2205. ISSN: 00092509. DOI: 10.1016/0009--2509(85)85121--6. URL: https://www.sciencedirect.com/science/article/pii/0009250985851216.

[36] Panagiotis D. Christofides. *Nonlinear and Robust Control of PDE Systems: Methods and Applications to Transport–Reaction Processes*. Birkhäuser, 2001.

[37] Panagiotis D. Christofides and James Baker. "Robust output feedback control of quasi–linear parabolic PDE systems." In: *Systems and Control Letters* 36.5 (Apr. 1999), pp. 307–316. ISSN: 01676911. DOI: 10.1016/S0167--6911(98)00103--0.

[38] Ruth Curtain and Hans Zwart. *Introduction to Infinite–Dimensional Systems Theory: A State–Space Approach*. New York: Springer, 2020. ISBN: 9781071605882.

[39] Ruth F. Curtain and Hans Zwart. *An Introduction to infinite–dimentional linear systems thoery*. 1st. New York: Springer–Verlag, 1995.

[40] H. A. Deans and Leon Lapidus. "A computational model for predicting and correlating the behavior of fixed-bed reactors: II. Extension to chemically reactive systems." In: *AIChE Journal* 6.4 (1960), pp. 656–663. ISSN: 15475905. DOI: 10.1002/aic.690060428.

[41] Wolf–Dieter Deckwer. "The backflow cell model—applied to non–isothermal reactors." In: *The Chemical Engineering Journal* 8.2 (Jan. 1974), pp. 135–144. ISSN: 0300–9467. DOI: 10.1016/0300--9467(74)85016--1. URL: https://www.sciencedirect.com/science/article/pii/0300946774850161.

[42] D. Del Vecchio and N. Petit. "Boundary control for an industrial under–actuated tubular chemical reactor." In: *Journal of Process Control* 15.7 (2005), pp. 771–784. ISSN: 09591524. DOI: 10.1016/j.jprocont.2005.03.004.

[43] A. Dhooge, W. Govaerts, and Yu A. Kuznetsov. "MATCONT: A MATLAB package for numerical bifurcation analysis of ODEs." In: *ACM Transactions on Mathematical Software* 29.2 (2003), pp. 141–164. ISSN: 00983500. DOI: 10.1145/779359.779362.

[44] C. Di Blasi and C. Branca. "Modeling a stratified downdraft wood gasifier with primary and secondary air entry." In: *Fuel* 104 (Feb. 2013), pp. 847–860. ISSN: 00162361. DOI: 10.1016/j.fuel.2012.10.014.

[45] D. Dochain. "State Observers for Tubular Reactors with Unknown Kinetics." In: *IFAC Proceedings Volumes* 31.11 (June 1998), pp. 703–708. ISSN: 14746670. DOI: 10.1016/s1474--6670(17)45008--7. URL: http://dx.doi.org/10.1016/S1474--6670(17)45008--7.

[46] D. Dochain. "State observation and adaptive linearizing control for distributed parameter (bio)chemical reactors." In: *International Journal of Adaptive Control and Signal Processing* 15.6 (2001), pp. 633–653. ISSN: 08906327. DOI: 10.1002/acs.691.

[47] Denis Dochain, N. Tali–Maamar, and J. P. Babary. "On modelling, monitoring and control of fixed bed bioreactors." In: *Computers & Chemical Engineering* 21.11 (1997), pp. 1255–1266. ISSN: 18761070. DOI: 10.1016/j.jtice.2010.04.002.

[48] Stevan Dubljevic. "Constraints–driven optimal actuation policies for diffusion–reaction processes with collocated actuators and sensors." In: *Industrial and Engineering Chemistry Research* 47.1 (2008), pp. 105–115. ISSN: 08885885. DOI: 10.1021/ie070546v.

[49] Stevan Dubljevic, Nael H. El–Farra, Prashant Mhaskar, and Panagiotis D. Christofides. "Predictive control of parabolic PDEs with state and control constraints." In: *International Journal of Robust and Nonlinear Control* 16 (2006), pp. 557–5691818749–772. ISSN: 10498923. DOI: 10.1002/rnc. arXiv: arXiv:1505.02595v1. URL: http://onlinelibrary.wiley.com/doi/10.1002/rnc.1553/abstract.

[50] Stevan Dubljevic and Panagiotis D. Christofides. “Predictive output feedback control of parabolic partial differential equations.” In: *Proceedings of the American Control Conference* 45 (2006), pp. 8421–8429. ISSN: 07431619. DOI: 10.1109/acc.2006.1656373.

[51] Carlos Fernandez and Jesus Alvarez. *Geometric estimation of binary distillation columns*. Vol. 7. PART 1. IFAC, 2009, pp. 417–422. ISBN: 9783902661548. DOI: 10.3182/20090712--4--tr--2008.00066. URL: http://dx.doi.org/10.3182/20090712--4--TR--2008.00066.

[52] Carlos Fernandez, Jesus Alvarez, Roberto Baratti, and Andrea Frau. “Estimation structure design for staged systems.” In: *Journal of Process Control* 22.10 (2012), pp. 2038–2056. ISSN: 09591524. DOI: 10.1016/j.jprocont.2012.07.012. URL: http://dx.doi.org/10.1016/j.jprocont.2012.07.012.

[53] Michel Fliess and Cédric Join. “Model–free control.” In: *International Journal of Control* 86.12 (2013), pp. 2228–2252. ISSN: 00207179. DOI: 10.1080/00207179.2013.810345. arXiv: 1305.7085.

[54] Hugo A. Franco–de los Reyes, Alexander Schaum, Thomas Meurer, and Jesús Alvarez. “Nonlinear passive control of a class of coupled partial differential equation models.” In: *Proceedings of the National Conference on Automatic Control, Mexico*. 2019, pp. 477–482.

[55] Hugo A. Franco–de los Reyes, Alexander Schaum, Thomas Meurer, and Jesus Alvarez. “Stabilization of an unstable tubular reactor by nonlinear passive output feedback control.” In: *Journal of Process Control* 93 (2020), pp. 83–96. ISSN: 09591524. DOI: 10.1016/j.jprocont.2020.07.005. URL: https://doi.org/10.1016/j.jprocont.2020.07.005.

[56] Hugo Andrés Franco–de los Reyes and Jesus Alvarez. “Saturated–output feedback control and state estimation of a class of exothermic tubular reactors (in review process), 2021.” In: *Journal of Process Control, submited* ().

[57] Gilbert F. Froment, Kenneth B. Bischoff, and Juray De Wilde. *Chemical Reactor Analysis and Design Fundamentals*. 3rd Edit. John Wiley & Sons, Inc., 2011. ISBN: 9783642253874. DOI: 10.1016/j.ces.2003.12.030.

[58] Pablo González and Jesús Alvarez. “Combined proportional/integral–inventory control of solution homopolymerization reactors.” In: *Industrial and Engineering Chemistry Research* 44.18 (2005), pp. 7147–7163. ISSN: 08885885. DOI: 10.1021/ie040207r.

[59] Michael Grant and Stephen Boyd. “Graph implementations for nonsmooth convex programs.” In: *Recent Advances in Learning and Control*. Ed. by V. Blondel, S. Boyd, and H. Kimura. Lecture Notes in Control and Information Sciences. http://stanford.edu/~boyd/graph_dcp.html. Springer–Verlag Limited, 2008, pp. 95–110.

[60] Michael Grant and Stephen Boyd. *CVX: Matlab Software for Disciplined Convex Programming, version 2.1*. http://cvxr.com/cvx. Mar. 2014.

[61] Gregory Hagen and Igor Mezic. "Spillover Stabilization in Finite–Dimensional Control and Observer Design for Dissipative Evolution Equations." In: *SIAM J. Control and Optimization* 42.2 (2003), pp. 746–768.

[62] T. J. Harris, J. F. Macgregor, and J. D. Wright. "Optimal sensor location with an application to a packed bed tubular reactor." In: *AIChE Journal* 26.6 (1980), pp. 910–916. ISSN: 15475905. DOI: 10.1002/aic.690260605.

[63] Reza Hashemi, Daniel Kohlmann, and Sebastian Engell. "Optimizing Control and State Estimation of a Continuous Polymerization Process in a Tubular Reactor with Multiple Side–Streams." In: *Macromolecular Reaction Engineering* 10.4 (2016), pp. 415–434. ISSN: 18628338. DOI: 10.1002/mren.201500034.

[64] C. van Heerden. "Autothermic Processes." In: *Industrial & Engineering Chemistry* 45.6 (1953), pp. 1242–1247. ISSN: 0019–7866. DOI: 10.1021/ie50522a030.

[65] Charles G. Hill Jr. and Thatcher W. Root. *Introduction to Chemical Engineering Kinetics and Reactor Design*. Second Edi. Wiley, 2014. ISBN: 9783642253874.

[66] Peter Hippe. *Windup in Control Its Effects and Their Prevention*. Springer, 2006. ISBN: 9780857296344. DOI: 10.1007/978--1--4471--4399--4. arXiv: arXiv:1011.1669v3. URL: http://www.springer.com/engineering/control/book/978--0--85729--634--4.

[67] Xiangming Hua and Arthur Jutan. "Nonlinear inferential cascade control of exothermic fixed–bed reactors." In: *AIChE Journal* 46.5 (2000), pp. 980–996. ISSN: 00011541. DOI: 10.1002/aic.690460511.

[68] A. Ichikawa and E. P. Ryan. "Sensor and controller location problems for distributed parameter systems." In: *Automatica* 15.3 (1979), pp. 347–352. ISSN: 00051098. DOI: 10.1016/0005--1098(79)90051--7.

[69] Eugene Isaacson and Herbert Bishop Keller. *Analysis of Numerical Methods*. New York: Dover Publications, Inc., 1994. ISBN: 0486680290. DOI: 10.2307/3614614.

[70] Phisit Jaisathaporn and William L. Luyben. "Dynamic Comparison of Alternative Tubular Reactor Systems." In: *Industrial and Engineering Chemistry Research* 43.4 (2004), pp. 1003–1029. ISSN: 08885885. DOI: 10.1021/ie030434d.

[71] Klavs F. Jensen and W.Harmon Ray. "The bifurcation behavior of tubular reactors." In: *Chemical Engineering Science* 37.2 (Jan. 1982), pp. 199–222. ISSN: 0009–2509. DOI: 10.1016/0009--2509(82)80155--3. URL: https://www.sciencedirect.com/science/article/pii/0009250982801553.

[72] S. B. Jørgensen. "Fixed Bed Reactor Dynamics and Control – a Review." In: *IFAC Control of Distillation Columns and Chemical Reactors*. Bournemouth, UK, 1986, pp. 11–24. DOI: 10.1016/b978--0--08--034917--6.50006--4.

[73] S.B. Jørgensen and N. Jensen. "Dynamics and Control of Chemical Reactors–Selectively Surveyed." In: *IFAC Proceedings Volumes* 22.8 (Aug. 1989), pp. 49–67. ISSN: 14746670. DOI: 10.1016/s1474-6670(17)53338-8.

[74] Preet Joy, Kristina Rossow, Falco Jung, Hans Ulrich Moritz, Werner Pauer, Alexander Mitsos, and Adel Mhamdi. "Model–based control of continuous emulsion co–polymerization in a lab–scale tubular reactor." In: *Journal of Process Control* 75 (Mar. 2019), pp. 59–76. ISSN: 09591524. DOI: 10.1016/j.jprocont.2018.12.014.

[75] Iasson Karafyllis and Miroslav Krstic. *Input–to–State Stability for PDEs*. 2020, pp. 1–4. ISBN: 9783319910109. DOI: 10.1007/978-1-4471-5102-9_100024-1.

[76] H Khalil. *Nonlinear systems*. Third Edition. 2002.

[77] Seyedhamidreza Khatibi, Guilherme Ozorio Cassol, and Stevan Dubljevic. "Linear model predictive control for a coupled cstr and axial dispersion tubular reactor with recycle." In: *Mathematics* 8.5 (2020), pp. 1–17. ISSN: 22277390. DOI: 10.3390/MATH8050711.

[78] Seyedhamidreza Khatibi, Guilherme Ozorio Cassol, and Stevan Dubljevic. "Model predictive control of a non–isothermal axial dispersion tubular reactor with recycle." In: *Computers and Chemical Engineering* 145 (2021), p. 107159. ISSN: 00981354. DOI: 10.1016/j.compchemeng.2020.107159. URL: https://doi.org/10.1016/j.compchemeng.2020.107159.

[79] Yuri A Kuznetsov, Yuri A Kuznetsov, and Y.A. Kuznetzov. "Elements of applied bifurcation theory." In: *Choice Reviews Online* 33.06 (2004). Ed. by J. E. Marsden and L. Sirovich, pp. 33–3370–33–3370. ISSN: 0009–4978. DOI: 10.5860/choice.33-3370.

[80] Joseph La Salle and Solomon Lefschetz. *Stability by Liapunov's Direct Method with Applications*. 1st Editio. New York: Academic Press, 1961.

[81] A. Lafon and H. C. Yee. "Dynamical approach study of spurious steady–state numerical solutions of nonlinear differential equations, part III. The effects of nonlinear source terms in reaction–convection equations." In: *International Journal of Computational Fluid Dynamics* 6.1 (1996), pp. 1–36. ISSN: 10618562. DOI: 10.1080/10618569608940772.

[82] Liangfeng Lao, Matthew Ellis, Panagiotis D. Christofides, Antonios Armaou, and Panagiotis D. Christofides. "Economic model predictive control of parabolic PDE systems: Addressing state estimation and computational efficiency." In: *Proceedings of the IEEE Conference on Decision and Control* 24.February (Apr. 2014), pp. 442–462. ISSN: 07431546. DOI: 10.1109/CDC.2014.7039812. URL: https://www.sciencedirect.com/science/article/pii/S0959152414000316.

[83] Irena Lasiecka. "Control of systems governed by partial differential equations: a historical perspective." In: *Proceedings of the 34th Conference on Decision & control*. New Oreleans, LA, 1995, pp. 2792–2976. ISBN: 9781585443574. DOI: 10.4324/9781315178028--4.

[84] Octave Levenspiel and Kenneth B. Bischoff. "Patterns of Flow in Chemical Process Vessels." In: *Advances in Chemical Engineering* 4.C (Jan. 1964), pp. 95–198. ISSN: 00652377. DOI: 10.1016/S0065--2377(08)60240--9.

[85] Randall J. LeVeque. *Finite Difference Methods for Ordinary and Partial Differential Equations*. Philadelphia: Society for Industrial and Applied Mathematics, 2007. ISBN: 9780898716290. DOI: 10.1137/1.9780898717839.

[86] Randall J. LeVeque. *Finite Difference Methods for Ordinary and Partial Differential Equations: Steady–State and Time–Dependent Equations*. Society for Industrial and Applied Mathamatics, 2007. ISBN: 9780898716290.

[87] Yi Liu and Elling W. Jacobsen. "On the use of reduced order models in bifurcation analysis of distributed parameter systems." In: *Computers and Chemical Engineering*. Vol. 28. 1–2. Elsevier Ltd, Jan. 2004, pp. 161–169. DOI: 10.1016/S0098--1354(03)00183--2.

[88] William L. Luyben. *Process modeling, simulation and control for chemical engineers*. 2nd Ed. McGraw–Hill International Editions, 1989.

[89] William L. Luyben. *Chemical Reactor Design and Control*. Wiley–Interscience, 2010. ISBN: 9780470097700. DOI: 10.1002/cite.201090073.

[90] Anca Maxim, Dana Copot, Cosmin Copot, and Clara M. Ionescu. "The 5w's for control as part of industry 4.0: Why, what, where, who, and when—A PID and MPC control perspective." In: *Inventions* 4.1 (2019). ISSN: 24115134. DOI: 10.3390/inventions4010010.

[91] T. Meurer, J. Becker, and M. Zeitz. "Flatness–based feedback tracking control of a distributed parameter tubular reactor model." In: *European Control Conference, ECC 2003* (2003), pp. 2893–2898. DOI: 10.23919/ecc.2003.7086479.

[92] T. Meurer and M. Zeitz. "Feedforward and feedback tracking control of nonlinear diffusion–convection–reaction systems using summability methods." In: *Industrial and Engineering Chemistry Research* 44.8 (2005), pp. 2532–2548. ISSN: 08885885. DOI: 10.1021/ie0495729.

[93] T. Meurer and M. Zeitz. "Model inversion of boundary controlled parabolic partial differential equations using summability methods." In: *Mathematical and Computer Modelling of Dynamical Systems* 14.3 (2008), pp. 213–230. ISSN: 13873954. DOI: 10.1080/13873950701844873.

[94] Thomas Meurer, Knut Graichen, and Michael Zeitz. "MOTION PLANNING AND FEEDFORWARD CONTROL FOR DISTRIBUTED PARAMETER SYSTEMS UNDER INPUT CONSTRAINTS." In: *IFAC–PapersOnLine*. Vol. 0. 1. 2005, pp. 4–9.

[95] Jarinah Mohd Ali, N. Ha Hoang, M. A. Hussain, and Denis Dochain. "Review and classification of recent observers applied in chemical process systems." In: *Computers and Chemical Engineering* 76 (2015), pp. 27–41. ISSN: 00981354. DOI: 10.1016/j.compchemeng.2015.01.019. URL: http://dx.doi.org/10.1016/j.compchemeng.2015.01.019.

[96] Jaime A. Moreno and Jesús Alvarez. "On the estimation problem of a class of continuous bioreactors with unknown input." In: *Journal of Process Control* 30 (2015), pp. 34–49. ISSN: 09591524. DOI: 10.1016/j.jprocont.2014.12.005. URL: http://dx.doi.org/10.1016/j.jprocont.2014.12.005.

[97] John C. Morud and Sigurd Skogestad. "Analysis of Instability in an Industrial Ammonia Reactor." In: *AIChE Journal* 44.4 (1998), pp. 888–895. ISSN: 00011541. DOI: 10.1002/aic.690440414.

[98] Riccardo Muradore, Fabrizio Bezzo, and Massimiliano Barolo. "Optimal sensor location for distributed–sensor systems using multivariate regression." In: *Computers and Chemical Engineering* 30.3 (2006), pp. 521–534. ISSN: 00981354. DOI: 10.1016/j.compchemeng.2005.10.009.

[99] Isrrael Nájera, Jesús Álvarez, and Roberto Baratti. "Feedforward ouput–feedback control for a class of exothermic tubular reactors." In: *IFAC–PapersOnLine*. Vol. 28. 8. Elsevier, Jan. 2015, pp. 1075–1080. DOI: 10.1016/j.ifacol.2015.09.111. URL: https://www.sciencedirect.com/science/article/pii/S2405896315011921.

[100] Isrrael Nájera, Jesús Álvarez, Roberto Baratti, and Cesar Gutiérrez. "Control of an exothermic packed–bed tubular reactor." In: *IFAC–PapersOnLine* 49.7 (2016), pp. 278–283. ISSN: 24058963. DOI: 10.1016/j.ifacol.2016.07.282.

[101] Isrrael Nájera, Jesús Álvarez, and Cesar Sotrés. "Output–feedback control for a class of exothermic packed bed tubular reactors." In: (), pp. 2–7.

[102] Yuri Orlov and Denis Dochain. "Discontinuous feedback stabilization of minimum–phase semilinear infinite–dimensional systems with application to chemical tubular reactor." In: *IEEE Transactions on Automatic Control* 47.8 (2002), pp. 1293–1304. ISSN: 00189286. DOI: 10.1109/TAC.2002.800737.

[103] Romeo Ortega, Antonio Loría, Per Johan Nicklasson, and Hebertt Sira–Ramírez. *Passivity–vased Control of Euler–Lagrange Systmes: Mechanical, Electrical and ELectromechanical Applications*. London: Springer–Verlag London Ltd., 1998. ISBN: 9781849968522. URL: http://marefateadyan.nashriyat.ir/node/150.

[104] Radhakant Padhi and Sk Faruque Ali. "An account of chronological developments in control of distributed parameter systems." In: *Annual Reviews in Control* 33.1 (Apr. 2009), pp. 59–68. ISSN: 13675788. DOI: 10.1016/j.arcontrol.2009.01.003.

[105] T. M. Pell and Rutherford Aris. "Problems in Chemical Reactor Analysis with Stochastic Features: Control of Linearized Distributed System on Discrete and Corrupted Observations." In: *I & EC Fundamentals* 9.1 (1970), pp. 15–20.

[106] Marcella Porru, Jesus Alvarez, and Roberto Baratti. "A distillate composition estimator for an industrial multicomponent IC4–NC4 splitter with experimental temperature measurements." In: *IFAC Proceedings Volumes (IFAC–PapersOnline)* 10.PART 1 (2013), pp. 391–396. ISSN: 14746670. DOI: 10.3182/20131218--3--IN--2045.00028.

[107] Davood Babaei Pourkargar and Antonios Armaou. "Low–dimensional adaptive output feedback controller design for transport–reaction processes." In: *2015 European Control Conference, ECC 2015* (2015), pp. 885–890. DOI: 10.1109/ECC.2015.7330654.

[108] Carlos Eduardo Ramirez–Castelan, Jazael Moguel–Castañeda, Hector Puebla, and Eliseo Hernandez–Martinez. "A study of temperature sensor location based on fractal analysis for cascade control schemes in tubular reactors." In: *Chemical Engineering Science* 141 (2016), pp. 195–204. ISSN: 00092509. DOI: 10.1016/j.ces.2015.10.036. URL: http://dx.doi.org/10.1016/j.ces.2015.10.036.

[109] W. H. Ray. "Some recent applications of distributed parameter systems theory–A survey." In: *Automatica* 14.3 (1978), pp. 281–287. ISSN: 00051098. DOI: 10.1016/0005--1098(78)90092--4.

[110] Martin Ruszkowski, Vianey Garcia–Osorio, and B. Erik Ydstie. "Passivity based control of transport reaction systems." In: *AIChE Journal* 51.12 (2005), pp. 3147–3166. ISSN: 00011541. DOI: 10.1002/aic.10543.

[111] A. Schaum, J. Alvarez, T. Meurer, and J. A. Moreno. "State–estimation for a class of tubular reactors using a pointwise innovation scheme." In: *Journal of Process Control* 60 (2017), pp. 104–114. ISSN: 09591524. DOI: 10.1016/j.jprocont.2017.05.013. URL: http://dx.doi.org/10.1016/j.jprocont.2017.05.013.

[112] A. Schaum, J. P. Garcia–Sandoval, J. Alvarez, and V. Gonzalez–Alvarez. *Saturated output–feedback control of continuous anaerobic digestors*. Vol. 45. 15 PART 1. IFAC, 2012, pp. 573–578. ISBN: 9783902823052. DOI: 10.3182/20120710--4--SG--2026.00026. URL: http://dx.doi.org/10.3182/20120710--4--SG--2026.00026.

[113] Alexander Schaum, Jesus Alvarez, Juan P. Garcia–Sandoval, and Victor M. Gonzalez–Alvarez. “On the dynamics and control of a class of continuous digesters.” In: *Journal of Process Control* 34.October (2015), pp. 82–96. ISSN: 09591524. DOI: 10.1016/j.jprocont.2015.07.004.

[114] Alexander Schaum, Jesus Alvarez, and Teresa Lopez–Arenas. “Saturated linear dynamic output–feedback control for a class of three–state continuous bioreactors with inhibited kinetics.” In: *Journal of Process Control* 23.3 (2013), pp. 332–350. ISSN: 09591524. DOI: 10.1016/j.jprocont.2012.11.010. URL: http://dx.doi.org/10.1016/j.jprocont.2012.11.010.

[115] Alexander Schaum, Thomas Meurer, and Jaime A. Moreno. “Dissipative observers for coupled diffusion–convection–reaction systems.” In: *Automatica* 94 (2018), pp. 307–314. ISSN: 00051098. DOI: 10.1016/j.automatica.2018.04.041. URL: https://doi.org/10.1016/j.automatica.2018.04.041.

[116] Panos Seferlis and Michael C. Georgiadis, eds. *The Integration of Process Design and Control*. 2004.

[117] Peter Seibert. “Reduction theorems for stability of systems in general spaces.” In: *Nonlinear Analysis, Theory, Methods and Applications* 30.7 (1997), pp. 4675–4681. ISSN: 0362546X. DOI: 10.1016/S0362--546X(97)00192--2.

[118] R. Sepulchre, M. Janoković, and Petar Kokotović. *Constructive Nonlinear Control*. Springer Science & Business Media., 2012. ISBN: 9783642253874.

[119] F. G. Shinskey. *Process Control Systems: Application, Design, and Tuning*. Fourth Ed. McGraw–Hill, 1996.

[120] Abhay K. Singh and Juergen Hahn. “Determining optimal sensor locations for state and parameter estimation for stable nonlinear systems.” In: *Industrial and Engineering Chemistry Research* 44.15 (2005), pp. 5645–5659. ISSN: 08885885. DOI: 10.1021/ie040212v.

[121] Sadanand Singh, Shivangi Lal, and Nitin Kaistha. “Case study on tubular reactor hot–spot temperature control for throughput maximization.” In: *Industrial and Engineering Chemistry Research* 47.19 (Aug. 2008), pp. 7257–7263. ISSN: 08885885. DOI: 10.1021/ie071287c.

[122] R. E. Skelton. *Dynamic systems control: linear systems analysis and synthesis*. 1988. ISBN: 0080325750. DOI: 10.1016/c2009--0--00310--9.

[123] R. E. Skelton. “Model error concepts in control design.” In: *International Journal of Control* 49.5 (1989), pp. 1725–1753. ISSN: 13665820. DOI: 10.1080/00207178908559735.

[124] Andrey Smyshlyaev and Miroslav Krstic. “Backstepping observers for a class of parabolic PDEs.” In: *Systems and Control Letters* 54.7 (2005), pp. 613–625. ISSN: 01676911. DOI: 10.1016/j.sysconle.2004.11.001.

[125] Eduardo D. Sontag. "The ISS philosophy as a unifying framework for stability–like behavior." In: *Nonlinear control in the year 2000 volume 2* 0 (2007), pp. 443–467. DOI: 10.1007/bfb0110320.

[126] Arjan Van Der Schaft. *Communications and Control Engineering L2–Gain and Passivity Techniques in Nonlinear Control*. 2017. ISBN: 9783319499918. URL: http://www.springer.com/series/61.

[127] Alain Vande Wouwer, Nicolas Point, Stéphanie Porteman, and Marcel Remy. "Approach to the selection of optimal sensor locations in distributed parameter systems." In: *Journal of Process Control* 10.4 (2000), pp. 291–300. ISSN: 09591524. DOI: 10.1016/S0959--1524(99)00048--7.

[128] Richard S. Varga. *Gershgorin and his circles*. 2004, p. 226. ISBN: 3540211004.

[129] Arvind Varma and Neal R. Amundson. "Some Problems Concerning the Non–Adiabatic Tubular Reactor: A–Priori Bounds, Qualitative Behavior, Preliminary Uniqueness and Stability Considerations." In: *The Canadian Journal of Chemical Engineering* 50.August (1972), pp. 470–485.

[130] Arvind Varma and Neal R. Amundson. "Some observations on uniqueness and multiplicity of steady states in non-adiabatic chemically reacting systems." In: *The Canadian Journal of Chemical Engineering* 51.2 (1973), pp. 206–226. ISSN: 1939019X. DOI: 10.1002/cjce.5450510211.

[131] Arvind Varma and Neal R. Amundson. "The non-adiabatic tubular reactor: Stability considerations." In: *The Canadian Journal of Chemical Engineering* 51.4 (1973), pp. 459–467. ISSN: 1939019X. DOI: 10.1002/cjce.5450510411.

[132] Antonio Visioli. *Practical PID Control*. Springer–Verlag, 2006, p. 332. ISBN: 1846285860. URL: http://books.google.com/books?id=ymyAY01bEe0C%7B%5C&%7Dpgis=1.

[133] Walter Waldraff, Denis Dochain, Sylvie Bourrel, and Alphonse Magnus. "On the use of observability measures for sensor location in tubular reactor." In: *Journal of Process Control* 8.5–6 (1998), pp. 497–505. ISSN: 09591524. DOI: 10.1016/s1474--6670(17)43163--6.

[134] Larry C. Windes and W. Harmon Ray. "A control scheme for packed bed reactors having a changing catalyst activity profile. I: On–line parameter estimation and feedback control." In: *Journal of Process Control* 2.1 (1992), pp. 23–42. ISSN: 09591524. DOI: 10.1016/0959--1524(92)80015--P.

[135] Larry C. Windes and W. Harmon Ray. "A control scheme for packed bed reactors having a changing catalyst activity profile. II: On–line optimizing control." In: *Journal of Process Control* 2.1 (1992), pp. 23–42. ISSN: 09591524. DOI: 10.1016/0959--1524(92)80015--P.

[136] Joseph J. Winkin, Denis Dochain, and Philippe Ligarius. "Dynamical analysis of distributed parameter tubular reactors." In: *Automatica* 36.3 (2000), pp. 349–361. ISSN: 00051098. DOI: 10.1016/S0005--1098(99)00170--3.

[137] Wei Wu. "Finite difference output feedback control of a class of distributed parameter processes." In: *Industrial and Engineering Chemistry Research* 39.11 (2000), pp. 4250–4259. ISSN: 08885885. DOI: 10.1021/ie9908783.

[138] Wei Wu and Chao Wei Chen. "Measurement–based optimization and predictive control for an exothermic tubular reactor system." In: *Industrial and Engineering Chemistry Research* 46.7 (2007), pp. 2064–2076. ISSN: 08885885. DOI: 10.1021/ie0611296.

[139] Lu Zhang, Junyao Xie, Charles Robert Koch, and Stevan Dubljevic. "Model Predictive Control of Jacket Tubular Reactors with a Reversible Exothermic Reaction." In: *Industrial & Engineering Chemistry Research* 59.42 (2020), pp. 18921–18936. ISSN: 15205045. DOI: 10.1021/acs.iecr.0c02500.

[140] W. Zhou, B. Hamroun, Y. Le Gorrec, and F. Couenne. "Availability based stabilization of tubular chemical reactors." In: *IFAC Proceedings Volumes (IFAC–PapersOnline)* 46.14 PART 1 (2013), pp. 96–101. ISSN: 14746670. DOI: 10.3182/20130714--3--FR--4040.00014. URL: http://dx.doi.org/10.3182/20130714--3--FR--4040.00014.

[141] W. Zhou, B. Hamroun, Y. Le Gorrec, and F. Couenne. "Infinite dimensional port hamiltonian representation of reaction diffusion processes." In: *IFAC–PapersOnLine* 28.1 (2015), pp. 476–481. ISSN: 24058963. DOI: 10.1016/j.ifacol.2015.05.119.

[142] W. Zhou, B. Hamroun, Y. Le Gorrec, and F. Couenne. "Lyapunov based nonlinear control of tubular chemical reactors." In: *IFAC–PapersOnLine* 28.8 (2015), pp. 1045–1050. ISSN: 24058963. DOI: 10.1016/j.ifacol.2015.09.106.

DECLARATION

Put your declaration here.

CDMX, Septiembre 2021

Hugo Andrés Franco de los Reyes

COLOPHON

This document was typeset using the typographical look-and-feel `classicthesis` developed by André Miede and Ivo Pletikosić. The style was inspired by Robert Bringhurst's seminal book on typography "*The Elements of Typographic Style*". `classicthesis` is available for both LaTeX and LyX:

https://bitbucket.org/amiede/classicthesis/

Happy users of `classicthesis` usually send a real postcard to the author, a collection of postcards received so far is featured here:

http://postcards.miede.de/

Thank you very much for your feedback and contribution.

Final Version as of February 11, 2022 (classicthesis v4.6).